Developing an integrated approach to seaweed resource assessment

Thomas Rossiter

A thesis submitted for the degree of Doctor of Philosophy

Supervisor: Dr. Dagmar B. Stengel

Co-supervisors: Mr. Thomas Furey[1], Dr. Timothy McCarthy[2]

[1]INFOMAR, Marine Institute, Rinville, Co. Galway

[2]National Centre for Geocomputation, National University of Ireland Maynooth, Co. Kildare

Botany and Plant Science

School of Natural Science

National University of Ireland Galway

Ireland

February 2020

This Cullen Fellowship research (Grant-Aid Agreement No. CF/15/02) was supported by the Marine Institute and INFOMAR and funded under the Marine Research Sub-programme by the Irish Government.

Contents

For Gramps. He would have loved this.

To my unborn son. I hope you grow up to be a nerd (like your parents).

Acknowledgements

I start by extending my sincere gratitude to Dr. Dagmar Stengel who has supported me throughout these past four years, always providing patient and sage counsel over the various predicaments I seemed to always find myself in and for insisting that I did, indeed, know more about macroalgal biology than I claimed. I am thankful too for the guidance provided to me by Tommy Furey who opened my eyes to the bigger picture in which this research sits, for facilitating many remote sensing surveys and making me feel part of the INFOMAR team. Dr. Tim McCarthy was fantastic in helping to connect me with some of the great researchers in Maynooth and for providing valuable technical feedback on my work. To the three of you, I am very grateful for the opportunity that you provided to me, I have learnt a lot and almost had fun doing it. I also thank Dr. Zoë Popper for her helpful advice, both inside and outside of my GRC and also to Dr. Dara Stanley, Dr. Rachel Cave and Dr. Karen Bacon for their invaluable GRC help too along with Síle for all her help over the past four years.

It is unfortunate that academia is such a transient line of work. Many good friends have long since moved on in search of pastures new, yet I fondly remember the good times shared. Freddy, Alex, Pedro and Dara helped to provide many of my most memorable office moments, particularly our coffee mornings, and each helped greatly with many aspects of my work. Fortunately, some still remain, Claudia, Betty, Mane and Keelan have all been a pleasure to work alongside. I wish them all the very best.

Working alongside INFOMAR friends has been an immensely rewarding experience and has provided me with many great opportunities that I may not have otherwise had. David, Linda, Eimear, Fergal, Oisin, Kevin, Janine, Nicola, Vera, Dee, Julie and Mike were all very supportive of my work, minus the seaweed jokes. However, I must single out my favourite Italian, Fabio, who has been incredibly supportive of my work and my professional development and to whom I owe a great deal of gratitude. I have also had the pleasure of working with many talented individuals who have been instrumental to the outcome of this research. I must first thank the team at GeoAerospace, Fearghus, Daire, Aidan and Sean, without whose equipment and expertise the drone and plane surveys would never have happened. To all those in the GSI who facilitated the acoustic remote sensing survey, particularly Ronan, Sean, Eoin, Felim and Peter, here is your shout out.

My family have, of course, been very supportive and understanding. I am pleased too that they have had the chance to visit and fall in love with the west of Ireland.

I must lastly thank my wife Kate. Without her support I could not have done any of this.

List of figures

List of tables

Technical support:

The following people were involved in providing logistical and technical support for the research conducted in the following chapters.

Chapter 2

Dr. Gema Casal and Dr. Tiit Kutser provided technical and theoretical support on the application of the TriOS RAMSES radiometer for sampling macroalgal reflectance spectra.

Chapter 3

Fearghus Foyle, Aidan Magee, Sean Mannion and Daire Walsh conducted the hyperspectral drone survey. Aidan Magee was instrumental in processing the data outputs and Fearghus Foyle provided flight plan data.

Chapter 4

Fearghus Foyle, Aidan Magee, Sean Mannion and Daire Walsh conducted the aerial and drone multispectral surveys. Aidan Magee processed the multispectral and RGB data. Fearghus Foyle provided flight plan data.

Chapter 6

Eoin MacCraith and Ronan O'Toole facilitated vessel time. Eoin MacCraith was party chief and organised local operations. Peter Cullen skippered the RV Lir and Felim O'Toole was the hydrographic surveyor. Fabio Sacchetti, Oisin McManus and Mike Arrigan provided technical support for data processing and analysis.

Abbreviations

BRDF	Bi-directional Reflectance Distribution Function
BVLOS	Beyond Visual Line of Site
CART	Classification and Regression Tree
CDD	Charged Couple Device
CMOS	Complementary Metal-Oxide Semiconductor
DSM	Digital Surface Model
EM	Electromagnetic
EMR	Electromagnetic Radiation
FOV	Field of View
GCP	Ground Control Point
GFOV	Ground Field of View
GMT	Greenwich Meantime
GNSS	Global Navigation Satellite System
GPS	Global Positioning System
GSD	Ground Sampling Distance
ILS	Incident Light Sensor
IMU	Inertial Measurement Unit
ITM	Irish Transverse Mercator
LiDAR	Light Detection and Radar
MBES	Multibeam Echosounder
MLC	Maximum Likelihood Classification
MSI	Multispectral Instrument
NDVI	Normalised Difference Vegetation Index
NDWI	Normalised Difference Water Index
NIR	Near Infrared
OA	Overall Accuracy
OBIA	Object-based Image Analysis
PA	Producer Accuracy
PPK	Post Processing Kinematic
RGB	Red, Green, Blue
ROMS	Regional Ocean Modelling System
ROV	Remotely Operated Vehicle
RTK	Realtime Kinematic
SAC	Special Area of Conservation
SAM	Spectral Angle Mapper
SAV	Submerged Aquatic Vegetation
SBES	Singlebeam Echosounder
SfM	Structure-from-Motion
SSS	Sidescan Sonar
SVP	Sound Velocity Profile
TSS	True Skills Statistic
UA	User Accuracy
UAV	Unoccupied Aerial Vehicle
UTM	Universal Transverse Mercator
UV	Ultraviolet
VI	Vegetation Indices
VTOL	Vertical Take-off and Landing

Abstract

Increasing interest in the sustainable management of Irish macroalgal resources requires the development of a cost-effective and efficient methodology for quantifying the distribution of key species. Remote sensing provides a mapping solution that allows for large areas to be covered and is increasingly being applied to a range of macroalgal mapping research questions. Of interest to this research were the commercially and ecologically important intertidal brown fucoid, *Ascophyllum nodosum* and subtidal kelp communities (often dominated by *Laminaria hyperborea*).

Using a spectroradiometer, the spectral reflectance signatures of common canopy-forming intertidal macroalgae were sampled across four seasons during 2018. Classification and regression tree (CART) analysis showed that it was possible to discriminate between the three macroalgal groups and also between all sampled spectrally similar brown species in all seasons, aside from in winter. Intra-specific variation in spectral response of *A. nodosum* thalli was observed across the seasons and should potentially be accounted for in the creation of a spectral library.

A pushbroom hyperspectral drone survey showed that, using a Maximum Likelihood Classifier (MLC), it was possible to accurately map *A. nodosum* distribution ((Overall Accuracy (OA) 94.7 %) along with other dominant canopy-forming species. The accurate mapping of multiple species corroborated the results found using the spectroradiometer and highlighted the potential of this technology for intertidal resource mapping. Further work was undertaken at a separate site to compare the ability of two multispectral remote sensing platforms (drone and plane) to accurately map *A. nodosum*. Using MLC, the drone was found to produce a more accurate (OA 92 %) and higher taxonomic resolution map than the plane (OA 78.9 %) which could only identify a mixed *A. nodosum* and fucoid class. Experience gained from this research contributed to the creation of a comprehensive guide for using drones to map intertidal macroalgae which detailed the current technology and key challenges associated with mapping within the intertidal zone.

Vessel-mounted multibeam sonar was used to map a subtidal kelp bed. Three different acoustic frequencies (200, 300, 400 kHz), each logging water column data, were used to determine whether there was an optimum frequency for the accurate estimation of canopy height and extent. Each of the three frequencies provided slightly different estimates of canopy height and extent. A drop-down camera validated the presence of the kelp bed (dominated by *L. hyperborea*) but further research is required to determine the source of the variation between the three survey frequencies.

Chapter 1: General introduction

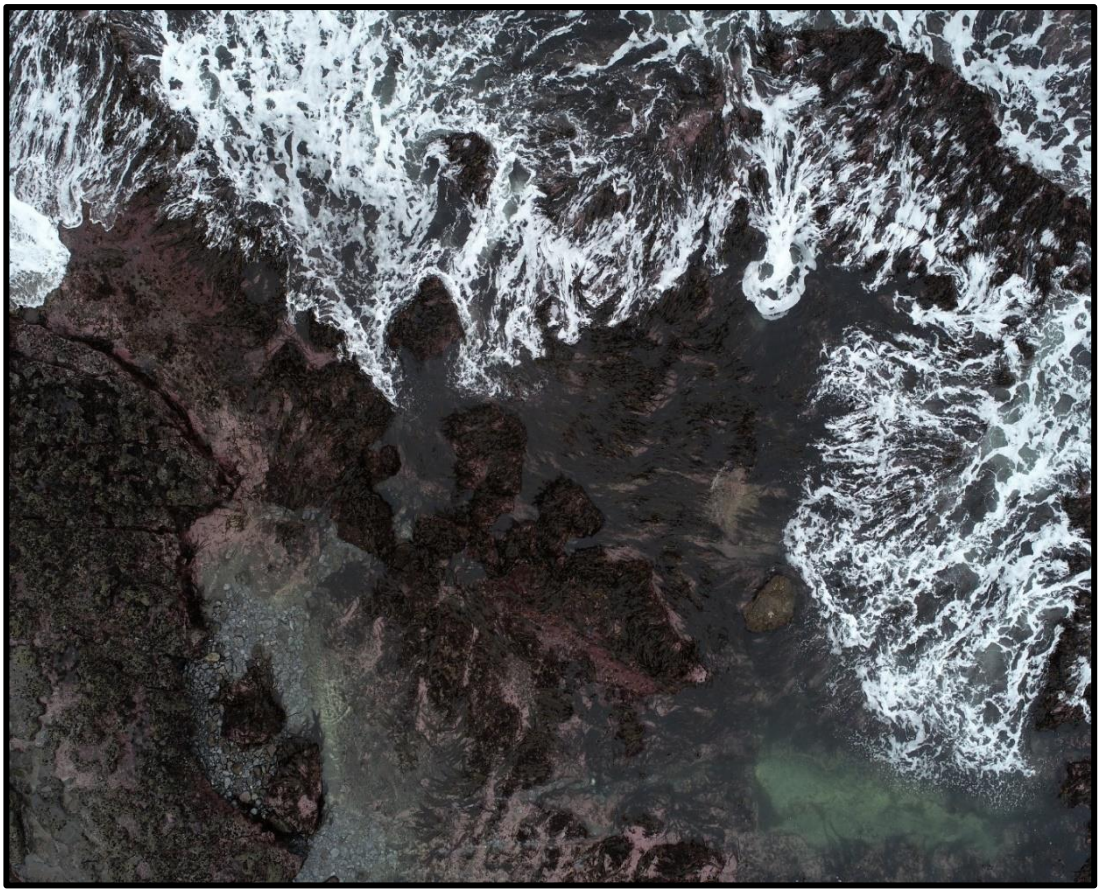

Drone image of waves breaking over intertidal macroalgae at Black Head (Co. Clare).

1.1. What are marine macroalgae?

The term macroalgae (or seaweed) refers to large, multicellular marine algae (Hurd *et al*., 2014) including the red algae (Rhodophyta), green algae (Chlorophyta) and brown algae (Phaeophyceae). Each of these groups can trace their origins back 1.5 billion years to a single endosymbiotic event where a heterotrophic eukaryotic host cell captured a cyanobacteria creating an ancestral primary plastid (Leliaert *et al*., 2012). Evolution and diversification of this ancestral plastid gave rise to Chlorophyta (green algae), Rhodophyta (red algae) and the cyanelles of glaucophytes (Le Corguillé *et al*., 2009), which are part of the monophyletic eukaryotic group Archaeplastida (Popper *et al*., 2011). Brown algae are part of the 'super group' known as Chromalveolates (Palmer *et al*., 2004) and evolved later than green and red algae through secondary endosymbiosis with red algae (Reyes-Prieto *et al*., 2007), and are subsequently only distantly related to the red and green algae. Secondary endosymbiosis now represents a significant driver of known eukaryotic diversity (Keeling, 2010). Each of the three macroalgae groups can be characterised by variations in pigment content and composition which can often, but not always, lead to clear colour differences between the three groups, aiding in their identification.

Both unicellular and multicellular algae can be found in terrestrial, marine or freshwater environments, but macroalgae are almost exclusively marine, with comparatively few freshwater species, and they have a wide distribution across all coastal latitudes (including free-floating variants). Macroalgae can range in size from the towering giant kelp (*Macrocystis pyrifera* (Linnaeus) C.Agardh) to small encrusting morphologies and each species' respective microscopic stages within their life history (Tirichine & Bowler, 2011). Variation in the morphology of macroalgal thalli leads to a greater diversity than observed in vascular plants (Hurd *et al*., 2014) and this morphology is directly related to physiological functions such as photosynthetic performance (Littler, 1979).

In temperate coastal regions, areas of hard substratum are dominated by algae of the orders Laminariales and Fucales (Dayton, 1985). Shallow, rocky coastal waters provide access to substratum and light which is required by macroalgae. These are foundation species and serve to create the structural elements of the system. Such species increase the heterogeneity of the environment providing spatial refuge from environmental or predation stress and enhance the settlement of species through spatial availability (Bruno & Bertness, 2002). The waters around Britain and Ireland are especially rich in macroalgal diversity, containing around 7% of the world's seaweeds, making them of international importance (Bunker *et al*., 2017).

1.2. Macroalgal community ecology

Since this study focuses on mapping macroalgae, it is prudent to provide an overview of the ecological importance of macroalgae and those factors, both abiotic and biotic, that control macroalgal distribution. Benthic macroalgal assemblages provide important environmental and economic services. They are essential for many faunal species, including commercially important ones, as they provide habitats, nursery and mating grounds (Casal *et al*., 2011). They also make an important contribution to primary production (De Oliveira *et al*., 2006) along with protecting the coastline from storm surges and flooding (Madsen *et al*., 2001). Owing to the anticipated increase in commercial applications of macroalgal species, for cosmetic, pharmaceutical and human nutrition uses (Mac Monagail & Morrison, 2020), it is important that effective management decisions are underpinned by accurate ecological monitoring data collection methodologies. The two species studied in this thesis are both economically and ecologically important in Ireland, yet there is a paucity of biological information with which to support informed decision making for the development of management plans (Roberts & Upham, 2012).

1.2.1. Zonation

Macroalgae grow in distinct vertical bands from the intertidal down to the subtidal (Lubchenco, 1980) and factors influencing these distributions are listed in the next section. **Fig. 1.1** shows the different biological zones (representative of south-west Britain) in intertidal and subtidal environments. Stephenson & Stephenson (1949) provide broad descriptions of each of these zones which are applicable, globally, to intertidal rocky shores.

The littoral, or intertidal, zone is comprised of the supralittoral and eulittoral zones. The supralittoral, described by Stephenson & Stephenson (1949) as 'an arid zone, subject to transitional conditions between land and sea', is commonly referred to as the splash zone and supports limited floral and faunal assemblages, with the notable exception of lichen species such as *Verrucaria maura* Wahlenberg. The eulittoral zone is dominated by dense fucoid assemblages including *Ascophyllum nodosum* (Linnaeus) Le Jolis, *Fucus vesiculosus* Linnaeus and *Fucus serratus* Linnaeus whilst also supporting greater faunal abundances than the supralittoral zone. The margin between the littoral and sublittoral is known as the sublittoral fringe which experiences reduced emersion times compared to the rest of the intertidal. This zone is characterised by *F. serratus, Laminaria digitata* (Hudson) J.V. Lamouroux and dense, mixed red macroalgal communities.

The sublittoral is divided into the infralittoral and the circalittoral (Connor *et al*., 2004) with the location of the boundary between them being defined by light availability. The

circalittoral is typically dominated by faunal species with the infralittoral dominated by macroalgae (Hurd *et al*., 2014). Around Britain and Ireland *Laminaria hyperborea* (Gunnerus) Foslie is the dominant subtidal macroalgal species with other opportunistic kelps including *Sacchoriza polyschides* (Lightfoot) Batters and *Saccharina latissima* (Linnaeus) C.E. Lane also being present and *Laminaria ochroleuca* Bachelot de la Pylaie being recently described in Ireland for the first time (Schoenrock *et al*., 2019).

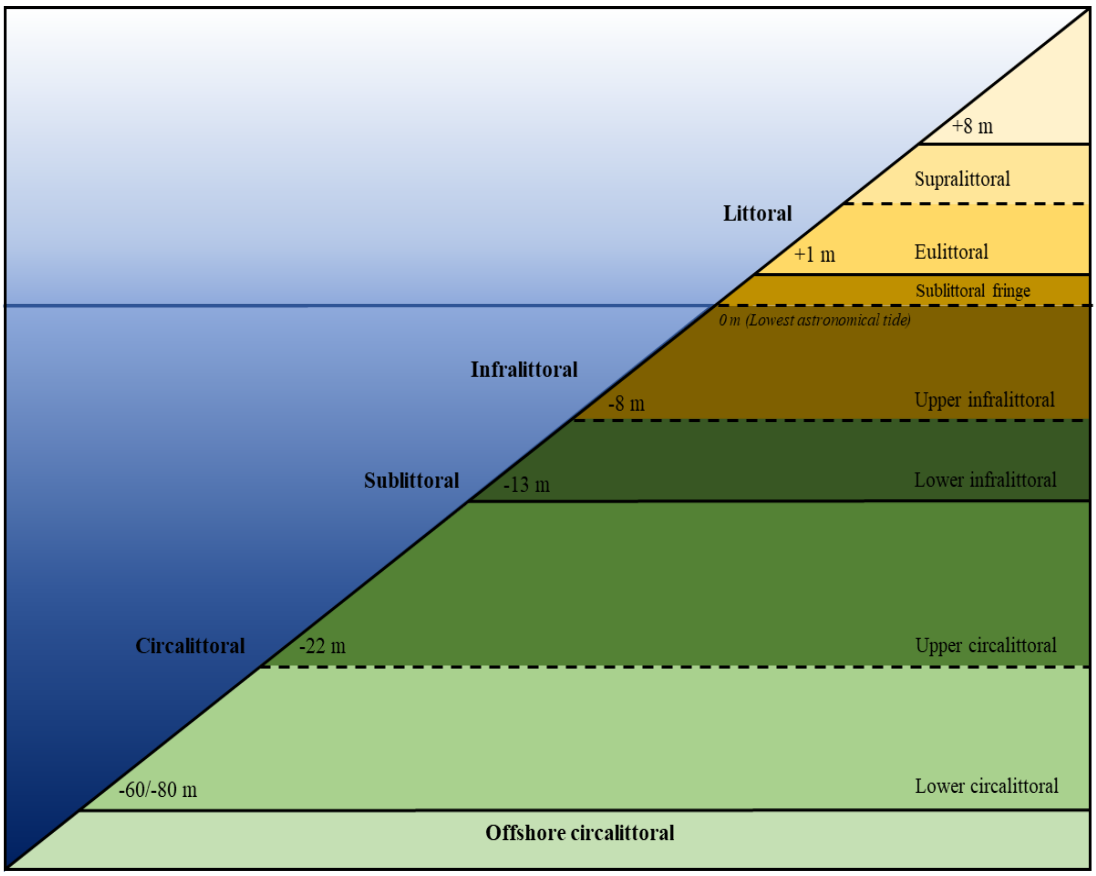

Fig. 1.1. Pictorial representation of a typical vertical zonation pattern for a rocky shoreline. Adapted from Connor *et al*. (2004).

1.2.2. Intertidal macroalgal community ecology

A hardy subset of macroalgal species choose life on the very margins of the marine realm where they grow in distinctive vertical or horizontal bands along strong environmental gradients across rocky intertidal zones (Hurd *et al*., 2014) where they are exposed to fluctuations and sometimes extreme temperatures (Helmuth & Hofmann, 2001). In Ireland and the UK, rocky shores are dominated by large multicellular brown macroalgal species, competing for space and light in dynamic and complex environments. It is important to note

that the strong zonation bands of individual species can often overlap causing mixtures of two or more species which, as will be discussed later in this thesis, can make accurately mapping them challenging. Removal of competitors allows some species, such as *F. vesiculosus* and *F. serratus* to extend their distribution up or down the shore, highlighting the importance of competition in zonation patterns (Hawkins & Harkin, 1985). Patterns of zonation along a rocky shore, and the species present, are strongly influenced by the geologic and topographic nature of the coastline. Location and orientation will determine site exposure levels, altering the species that may be found there, depending on their wave exposure tolerances. The upper intertidal zone, where emersion times are greater, the small, shrubby species *Pelvetia canaliculata* (Linnaeus) Decaisne & Thuret and *F. spiralis* often dominate. These species are able to tolerate long periods of desiccation-stress and then return to their normal state once rehydrated (Schonbeck & Norton, 1979). Below this zone, overlapping assemblages of *A. nodosum* and *F. vesiculosus* can often occur, with the latter being more tolerant of exposed conditions, albeit with a decrease in size and branching (Kalvas & Kautsky, 1993). *Himanthalia elongata* (Linnaeus) S.F. Gray, in the west of Ireland, typically occurs between *F. serratus* and *L. digitata* on semi-exposed shores (Stengel *et al*., 1999). *L. digitata* is able, due to its flexible stipe, to occupy a unique niche on the margins of the intertidal and subtidal zone (Lüning & Dring, 1979), being easily accessible during spring tides.

1.2.3. Subtidal macroalgal community ecology

Kelps are large brown alga of the order Laminariales (Phaeophyceae) and dominate the rocky, sublittoral coastal zone throughout global temperate environments (Yesson *et al*., 2015). In Ireland, rocky subtidal communities are dominated by kelps which are habitat forming foundation species (Bruno & Bertness, 2001) and are a major structuring component through temperate and polar latitudes (Pehlke & Bartsch, 2008). Kelp provide important habitat for a range of species including those of commercial value such as juvenile cod (Cote *et al*., 2003). Depending on the height of their fronds, kelps can be classified into three categories. The fronds of canopy forming kelps (not present in Ireland) float high in the water column due to the presence of pneumatocysts (gas-filled bladders), stipate kelps are usually smaller and consist of a rigid stipe and prostrate kelps have flexible stipes and tend to sit closer to the seafloor (Krumhansl & Scheibling, 2012) and each of these provides unique habitat structures for associate flora and fauna (Steneck *et al*., 2002). Species present in Ireland and the UK include *Alaria esculenta* (Linnaeus) Greville, *L. digitata, L. hyperborea, L. ochroleuca, S. latissima, S. polyschides* and *Undaria pinnatifida* (Harvey) Suringar (Smale *et al*., 2013, Yesson *et al*., 2015). Major canopy-forming species tend to be *L. hyperborea, L. digitata* and *L. ochroleuca* (the latter in the UK) but these can be

outcompeted, for example in wave-exposed conditions where *A. esculenta* can dominate (Hawkins & Harkin, 1985). Most of these species are long-lived, with *L. hyperborea* having a lifespan of up to 18 years (Kain 1971) and only two (*S. polyschides* and *U. pinnatifida*) being short-lived, annual species. *Sacchoriza polyschides* is a common opportunistic species, tolerant of a range of exposure conditions and able to attach to both solid (bedrock) and loose (pebbles and cobbles) substratum (Norton, 1969). It can replace *L. hyperborea* in the wake of storm events (Hennequart *et al*., 2006). Worldwide, kelp communities are experiencing a loss of biomass through climate change and direct anthropogenic impacts such as harvesting (Krumhansl & Scheibling, 2012). As previously mentioned, *L. digitata* occurs at the sublittoral fringe but is quickly succeeded by *L. hyperborea* at depths of ~2.5 m LAT (Kitching, 1941) which can, under the right conditions (in the UK), reach maximum depths of ~20 m (Kain, 1962).

1.3. Study species

1.3.1. *Ascophyllum nodosum*

Ascophyllum nodosum (**Fig. 1.2**) is an intertidal brown foundation (Olsen *et al*., 2010) species of the order Fucales which inhabits the mid-shore along sheltered coastlines in the North Atlantic (Stengel & Dring, 1997). *Ascophyllum nodosum* is widely distributed across the North Atlantic, from Arctic Canada, Greenland, Iceland and Norway down south through to Portugal (Seeley & Schlesinger, 2012). In some sheltered locations it can form almost monospecific coverage of the mid-shore region (Jenkins *et al*., 2004).

It is a relatively long-lived species, having a short reproductive season in the spring, with some individuals reaching around fifty years old (Davies *et al*., 2007). Differences in maximum age can exist between different shore levels. Stengel & Dring (1997) reported the maximum age of unbroken fronds on the lower shore as reaching 17 years and 6 for the upper shore from Strangford Lough in Northern Ireland. The plant forms long fronds, of up to 150cm, with bladders, and is also relatively resilient as new fronds can be generated when larger fronds are damaged. The fronds are branched in an irregular, forked manner and attached to the substrate via a holdfast (Bunker *et al*., 2017). The thallus grows by apical growth, branching dichotomously once a year with a single oval-shaped air bladder being formed each year of grow after the first (David, 1943). *Ascophyllum nodosum* exhibits seasonal growth patterns with the lowest rates in the winter period and highest in late spring and early summer (David, 1943, Stengel & Dring, 1997). Reproductive structures (receptacle and supporting structures) appear in June, reaching their largest size in May the following year when the gametes have been released, and are subsequently shed (Åberg,

1996). This may, however, vary between sites. In western Ireland, *A. nodosum* is morphologically distinct from co-occurring macroalgal species, particularly *F. vesiculosus* and *F. serratus*. *Fucus vesiculosus* is identifiable through its flattened fronds, with a midrib and pairs of air bladders either side. It can grow up to 90 cm long. *Fucus serratus* also has flattened fronds and a midrib but lacks the air bladders and is instead easily recognised by the serrated edges of the fronds (Bunker *et al*., 2017).

The fronds of *A. nodosum* can create three different types of complex habitat, wrack, drifting mats and attached plants which, in North America, can support thirty-four species of fish and upwards of one hundred invertebrate species (Seeley & Schlesinger, 2012). *Ascophyllum nodosum* not only provides important habitat but also nitrogen and carbon storage services highlighting its ecological importance (Schmidt *et al*., 2011). The branching structure of *A. nodosum* provides habitat and shelter from predation for a range of different faunal species as documented by Colman (1940) whilst also providing shelter for larger benthic species. The epiphytic alga *Polysiphonia lanosa* (Linnaeus) Tandy is synonymous with *A. nodosum* across its geographic range, apart from Sweden where it has not been observed (Åberg, 1996). *Polysiphonia lanosa* itself also provides habitat for small faunal species, such as ostracods and copepods (Colman, 1940). The loss of canopy cover, either through direct harvesting impacts or storm events negatively impacts on the sub-tidal canopy. Jenkins *et al*. (2004) reported that in a twelve-year period following the experimental removal of the *A. nodosum* canopy the sub-canopy community did not return to its original state. This community was previously characterised by a delicate balance between red algae and limpets but bleaching of the red algae post canopy removal led to an increase in grazing pressure, inhibiting red algal regrowth. Increases in limpet densities can cause a loss of *A. nodosum* through direct grazing pressure and Davies *et al*. (2007) observed that this was preventing *A. nodosum* growth in Strangford Lough.

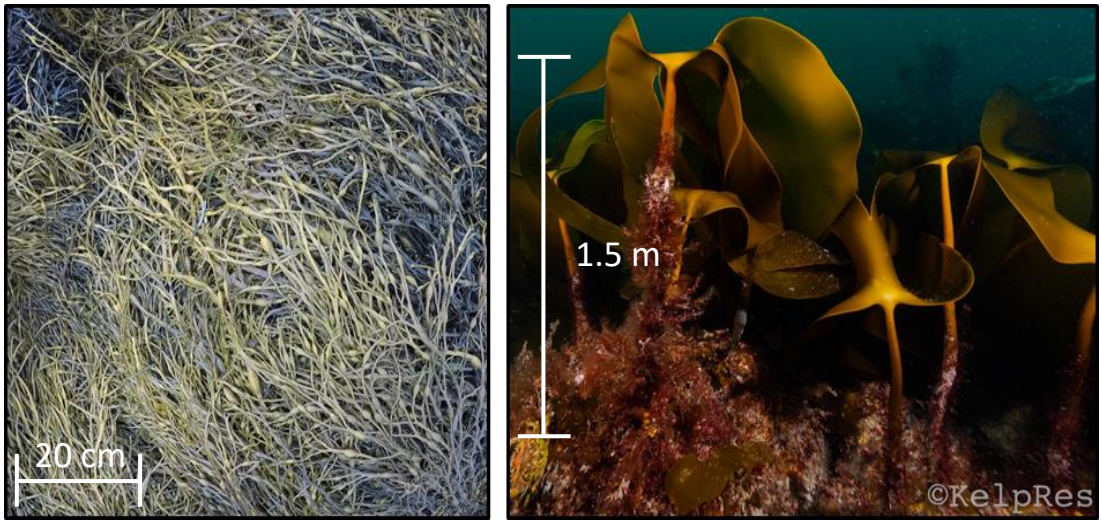

Fig. 1.2. *Ascophyllum nodosum* (left) and *Laminaria hyperborea* (right). Image credit: Tom Rossiter (*A. nodosum*) & Kenan Chan (KelpRes) (*L. hyperborea*).

1.3.2. *Laminaria hyperborea*

Laminaria hyperborea is often the dominant subtidal kelp species in the UK (Kain, 1962) and possibly also in Ireland. It has a wide latitudinal geographic distribution from Norway to Portugal (Kain, 1971) where suitable substratum and environmental conditions exist. Found in clear water in depths of ~30 m, *L. hyperborea* grows attached to solid rock or boulders that are large enough not to be frequently disturbed by wave action and storm events (Kain, 1971). *Laminaria hyperborea* is tolerant of strong water movement and currents, but in areas of more extreme exposure it is often replaced by *A. esculenta* (Kain, 1971).

Laminaria hyperborea, reaching lengths of 1.5–2 m (Kain, 1963), is characterised by a rigid, rough stipe that is often colonised by a high diversity of epiphytic red algal species (Christie *et al*., 2003). This rough stipe is not found on other Irish kelp species and is the primary diagnostic character of *L. hyperborea* (Bunker *et al*., 2017). Both stipe and frond growth occur at the meristem. Stipe growth occurs year-round but is fastest in from January to June. Fronds grow rapidly between January and May with a period of slower growth producing a small amount of frond tissue, forming a narrow base at the old frond. When further fast growth occurs, a new frond is produced, joined to the old growth by this narrow base until the old frond is shed in April/May (Kain, 1963). Reproductive tissue appears on *L. hyperborea* during winter with a peak in January and the gametophytes are able to survive and grow in low irradiance conditions, potentially finding more bare rock surfaces to settle on due to increased storminess during winter (Kain, 1975). Pedersen *et al*. (2012) observe an increase in the density, individual size and biomass with increased exposure levels.

Traditional morphological adaptations for increased exposure levels in kelps include a larger holdfast, thicker and occasionally shorter stipe and smaller, more streamlined blades. *Laminaria hyperborea* differs somewhat as individuals become much larger, increasing in biomass.

Laminaria hyperborea hosts a diverse array of species owing to the distinct habitats provided by the holdfast, stipe and lamina. In a study on *L. hyperborea* populations in Norway Christie *et al*. (2003) found 238 different species of macrofauna living on 56 *L. hyperborea* individuals. The study observed differences in species composition between the three distinct habitats. Holdfasts were found to contain the most diverse community; stipes had the highest abundance (likely due to the additional habitat provided by epiphytic red algal species) and the lamina had both the lowest diversity and abundance. The habitat created by *L. hyperborea* can also support a diverse range of fish species. Norderhaug *et al*. (2005) recorded 21 different species of fish occurring within a Norwegian *L. hyperborea* forest and found that stomach contents were dominated by invertebrate species that live on kelp individuals. Associated macroalgal communities can also be diverse within *L. hyperborea* forests. Leclerc *et al*. (2015) identified 65 macroalgal taxa occurring both on kelp individuals and the surrounding substrate along with 279 macrofauna taxa within *L. hyperborea* forests along the coast of Brittany.

1.4. Controls on macroalgal distribution

1.4.1. Abiotic controls

Tides are a result of the gravitational attractions of the sun and the moon, the latter exerting a stronger gravitational pull being much closer to the Earth (Dawes, 1998). Many coastlines, including Ireland, experience semidiurnal tides and when the Earth, moon and sun align their combined gravitational pull causes extreme tides known as spring tides. When the sun and the moon are at right angles to each other more moderate neap tides occur. Tides exert an important control on intertidal zonation, for example the coincidence of a spring tide and hot, dry weather can lead to mortality and bleaching events (Dawes, 1998). During summer, desiccation, UV and rockpool water salinity stress increase when low tides occur during the day (Hurd *et al*., 2017). Tides in Ireland occur semi-diurnally and are a result of the gravitational attraction between the sun and the moon and the shape of ocean basins can increase or reduce the gravitational effects of the sun and moon, influencing the tide type and amplitude (Dawes, 1998). In Ireland tidal predictions are a result of the analysis of a series of tide gauges located around the coastline and in some locations, predictions can be made from the Marine Institute Regional Ocean Modelling System (ROMS).

As light is essential for photosynthesis, it is thus the most important factor in affecting the distribution of seaweeds (Hurd *et al*., 2014). Factors such as water turbidity, depth and current velocity can affect the available light levels (Madsen *et al*., 2011) and light levels will affect the depth distribution of seaweeds (Dawes, 1998). Terrestrial inputs of sediment, such as river outputs, as well as anthropogenic sources, increase sedimentation in coastal regions, decreasing the available light for benthic macroalgae (Hurd *et al*., 2014). Kelp can survive so long as the light reaching them is greater than 1% of the surface light, below this level kelp is absent (Blight *et al*., 2011). Although Lüning & Dring (1979) reported that 0.5 - 1% was the lower light limit for kelps from their study in Helgioland (Germany). Light availability in the intertidal zone can influence the concentration of pigments within a species with shaded thallus regions having higher concentrations of photosynthetic pigments than thalli exposed to sunlight (Sampath-Wiley *et al*., 2008).

Nitrogen is the most important nutrient for seaweed growth (Hurd *et al*., 2014) and water motion is the main provider of nutrients. There are four main elements important for algae growth, oxygen, carbon, nitrogen and phosphorus (Dawes, 1998). Gagne *et al* (1982) showed how the difference in availability of nitrogen led to differences in the growth strategy for *Laminaria longicuris* Bachelot de la Pylaie. In the site where nitrogen was not limited (due to an upwelling) kelp growth followed the seasonal pattern of light. At the other site, growth was greatest during the winter, when nitrogen was abundant, and continued through into the summer using stored nitrogen. Nitrogen is often limiting during the summer months, where the algae grows slower whilst using stored reserves and higher during winter, when the algae builds up its internal reserves (Hatcher *et al*., 1977). In the intertidal zone, nitrogen can also be a limiting factor as emersion means that the nutrients provided by the seawater are unavailable (Davison & Pearson, 1996).

Temperature is a major factor in controlling seaweed distribution. Temperature may restrict a species' distribution through limitations to either survival or reproductive ability (Hurd *et al*., 2014). For kelps, increasing ocean temperatures are stressful and can lead to a decrease in their abundance (Wernberg *et al*., 2010). A study conducted in Australia by Wernberg *et al.* (2011) showed, using historical records, how continued warming of the oceans is likely to drive many macroalgal species towards the edge of the Australian continent and beyond the limits of available habitat. Potential climate change scenarios (IPCC A2, A1B and B1) indicate a potential northwards shift of three foundational intertidal macroalgal species, including *A. nodosum*, and a contraction of their southern range (Jueterbock *et al*., 2013). Within the intertidal zone there are a plethora of microhabitats that can affect the local temperature, rocks can provide shading and rockpools provide a degree of protection from solar insolation (Hurd *et al*., 2014). Desiccation is a major stress factor for intertidal species

whereby they start to lose water, becoming dehydrated. Often species compensate for this by developing morphological adaptations (i.e. *F. spiralis* and *P. canaliculata*) or by being protected by their micro-habitats (Hurd *et al*., 2014). It is also accepted that species higher up the shore have a greater tolerance to desiccation (Davison & Pearson, 1996).

Water motion directly affects nutrient availability, light penetration and salinity and acts as a physical force, through wave action, causing the removal of species from the rock which are then replaced by fast growing, opportunistic species (Hurd *et al*., 2014). Wave action can determine the survival and persistence of a species (Jonsson *et al*., 2006) and currents can increase the re-suspension of sediment reducing the available light (Madsen *et al*., 2001). Upwellings can also increase the amount of nutrients available and provide a supply of cooler water enabling species to survive beyond their biogeographical distribution (Gagné *et al*., 1982). Variations in rocky shore wave exposure levels can alter the species composition of macroalgal assemblages. Ballantine (1961) observed variations in macroalgal community composition in relation to wave exposure, finding that species such as *A. nodosum* are absent from highly exposed coastlines (species like *F. vesiculosus* and *F. serratus* are more tolerant of exposed conditions), becoming progressively more abundant as wave exposure levels decrease. *Laminaria hyperborea* is found in high abundance in wave-exposed areas, with abundance significantly decreasing in more wave-sheltered areas. Increased wave action may facilitate the growth of light-limited kelps occurring in deeper water as increased movement of kelp fronds maximises the amount of light captured by the fronds whilst also preventing excessive epiphytic fouling (Bekkby *et al*., 2019).

Variations in salinity levels have a major influence in the determinations of species presence and distribution (Scherner *et al*., 2013). Certain marine species are tolerant to a specific range of salinities and can accommodate slight variations. However, a species can experience stress once salinity thresholds are reached (Wilkinson *et al*., 2007). Inputs of freshwater also act to decrease salinity, for example in rockpools during low-tide (Hurd *et al*., 2014) and in coastal areas in the vicinity of estuaries. Increased rainfall in coastal regions, as a result of climate change, could likely lead to higher freshwater inputs through rivers and a decrease in coastal salinity (Scherner *et al*., 2013).

1.4.2. Biotic controls

Foundation species are those that modify their surrounding environmental conditions providing suitable habitat for other species to settle (Hurd *et al*., 2014). Both kelps (Pehlke & Bartsch, 2008) and fucoids (Olsen *et al*., 2010; Davies *et al*., 2007) are considered as foundation species. Foundation species assist the growth and development of other species by increasing propagule retention and resources (Bruno & Bertness, 2001). These species

can also provide protection from grazing, ultraviolet (UV) light and damaging wave forces (Wernberg, 2005). Facilitation species are those which have a positive impact on their surrounding community through their actions (Bruno & Bertness, 2001). Choi & Norton (2005) found that under desiccation, *F. vesiculosus* enhanced the survival of *A. nodosum* at the early germling stage, an example of facilitation.

Competition between species is based on access to a common resource, in many temperate coastal environments access to rock substratum is a limiting resource (Hurd *et al*., 2014). Access to light is another major limiting factor as dense seaweed canopies restrict the amount of light passing through them to juvenile species, meaning that to survive these new recruits need to be able to grow quickly (Worm & Chapman, 1996).

Grazing by faunal species is significant in controlling species presence and physiological condition. High levels of grazing can prevent the establishment of macroalgal species (Hawkins *et al*., 2008). Davies *et al.* (2007) found that in Strangford Lough the densities of limpets were preventing the growth of *A. nodosum* through grazing. Outbreaks of sea urchins can destroy kelp forests and maintain a post-kelp barren community dominated by crustose coralline algae, whilst reductions in grazing pressure can lead to a resurgence in kelp forest growth (Hagen, 1995). A study by Poore *et al.* (2012) observed that on a global scale consumer impacts on primary producers reduced, on average, abundance by 60%, confirming that consumers exert a strong control over primary producers. Kelp is almost exclusively grazed upon by sea urchins (Dayton, 1985) and whilst kelp deforestation can happen as a result of disease and physiological stress sea urchins are, at mid-latitudes, the most common driver of kelp deforestation (Steneck *et al*., 2002). There have been no reports of significant over-grazing of kelp in Ireland.

One cannot delve further into the mapping of macroalgal communities without first knowing their importance to humans. Providing the necessary context to this relationship helps to address the core factors underpinning this research. The state of macroalgal harvesting in Ireland and the attitudes of various stakeholders towards macroalgal management are important in considering the impact this research may have in Ireland. Without knowing the historical context of Irish macroalgae and understanding the strong cultural and societal importance (Delaney *et al*., 2016), for many coastal communities in the west of Ireland, it would be difficult to develop an effective and sensitive methodology for the assessment of macroalgal resources within Ireland as support from local communities will be required to facilitate surveys.

1.5. Humanity's historical relationship with macroalgae

Humans have long had an affinity with the sea and have been exploiting the resources found within the coastal zone for thousands of years (Steneck *et al*., 2002). The earliest record of human exploitation of the coastal zone comes from Pinnacle Point in South Africa, where shellfish remains indicate the addition of a new type of food to the traditional terrestrial diet of early humans (Marean *et al*., 2007). Evidence from Monte Verde in Chile suggests that macroalgae was being used by humans as early as 12,500 BC (Dillehay *et al*., 2008). In Japan, remains of *Sargassum* have been found in middens dating back to the early-to-mid Jōmon Period, around 6,000 BC, and was even used to feed the armies of feudal lords during the Age of Civil War (Nisizawa *et al*., 1987). Seaweed has historically been part of the Hawaiian diet and is still added to taro and rice-based dishes for flavour (Abbott, 1978). Closer to home, Bronze-Age middens from Shetland attest to the use of fucoid species for crop fertilisation, highlighting the ability of the Neolithic community to fully exploit all available resources and the importance of macroalgae to these societies (Dockrill & Bond, 2009). There is also evidence of the seasonal presence of macroalgae in the diet of Orkney sheep during the Neolithic and Iron Age periods, suggesting that it was used as fodder during times of resource scarcity (Balasse *et al*., 2009).

Much of the evidence for early human occupation of the coastal zone, along with its importance to us, may well have been lost to changing sea levels (Allen *et al*., 1988., Garrod *et al*., 1928., Erlandson, 2002), yet enough archaeological evidence remains to show the importance of coastal and aquatic environments for the development of early human society. The presence of marine resources, including macroalgae, helped to contradict a previously held belief that these environments were more of a hinderance than a help to early humans (Erlandson, 2002). Further importance is highlighted by the 'Kelp Highway Hypothesis', which posits that the productive nearshore kelp forests stretching from Japan to Baja California facilitated the movement of coastal humans and allowed the settlement of the Americas via the Beringia land bridge approximately 18,000–13,000 years ago (Erlandson *et al*., 2007).

There appears to be scant archaeological evidence for the collection of macroalgae during the Mesolithic period in Ireland (Warren, 2015). Instead, shell assemblages can be used a proxy for its presence, as shown by Murray (2007) who documented the presence of species such as periwinkles, blue-rayed limpets and whelks at sites in Ireland ranging from the Mesolithic through to the early Christian period. These species are directly associated with macroalgal communities and indicate that macroalgae was either harvested directly or foraged within.

One of the earliest recorded instances of macroalgae harvesting in Ireland comes from a poem, dating to the 12th Century, describing monks harvesting *Palmaria palmata* (Linnaeus) F. Weber and D. Mohr (referred to as dillisk) and distributing it to the poor (Guiry, 2010). By the time of the 18th Century, dillisk, or dulse, was being used as chewing tobacco and as medicine and, over the centuries, different types of macroalgae were used in a range of applications from fertiliser, aquaculture feed, glazing pottery and the production of glass (Guiry, 2010). Kelp was also being burned in order to produce iodine, valuable for medicine and also to create silver iodide for cameras, this was often a seasonal occupation for many (Harper, 1974). The depletion of suitable woodland, from which alkali was previously made, in post-medieval Ireland gave rise to the burning of kelp which, despite its low alkali content relative to alternatives, produced useful by-products such as salt and manure (Forsythe, 2006). Early records of the use of kelp for industry come from the early 17th Century where it was involved in the manufacturing of glass (Westropp, 1920). Evidence for the growth of the Irish macroalgal harvesting industry can be found in J.C. Curwen's 'State of Ireland' (1813) where the annual average export of kelp during the years 1702-1809 was recorded. In 1702, 118 tons was exported, in 1752 it was 742 tons and by 1809 it had reached 5,410 tons (Harper, 1974). However, come 1880, significant declines in kelp production were recorded, for example in the district of Kilkieran the total price paid for kelp fell from £15,000 per annum in 1875 to £3,000 (Irish Pound) in 1880. This was attributed to the discovery of 'some other compound' in South America, likely 'Chile saltpeter' (Delaney *et al*., 2016), reducing both the 'demand and the price' of kelp (Anon. 1880).

Scientific research on Irish marine algae began with the work of Henry Harvey (1811-1866) where he was involved in describing algae for the *British Flora* (Webb, 1966).

1.5.1. Irish macroalgal industry

The modern Irish macroalgal industry is primarily associated with the Gaeltacht areas of Ireland (Anon, 2015a) and macroalgae are used for a range of different commercial applications. The main uses of Irish macroalgae are as animal feed, plant supplements and specialist fertilisers which are high volume, low value products (Anon, 2015a). A smaller proportion (approximately 1%) of macroalgae is used in higher value products, such as foods, cosmetics and therapies, and is responsible for 30% of the value generated by the Irish seaweed industry (Anon, 2015a). The value of the industry is estimated at €18 million per annum (Morrissey *et al*., 2011), €6 million of which is associated with the export industry (Walsh & Watson, 2011). As of 2011, the Irish macroalgal industry produced 36,000 tonnes of wild macroalgae annually and employed 185 full time equivalents (Walsh & Watson, 2011).

Almost all the macroalgae harvested in Ireland are wild, the majority of this is collected manually, with over 75% of this being *A. nodosum*, and there is very little in the way of macroalgal cultivation occurring (Anon, 2015a). Whilst foreshore licenses are required to harvest seaweed, those individuals or families who have traditional access rights to the foreshore do not require any license and manage their plots individually (Mac Monagail & Morrison, 2020). The majority of firms operating in this industry are micro enterprises, each employing fewer than five people (Anon, 2015a). With increased commercial interest, the demand for high value species, such as *L. hyperborea*, is likely to increase. Whilst there is currently no extensive commercial harvesting of *L. hyperborea* in Ireland, licensing applications are underway for the mechanical harvesting of kelp in Bantry Bay (Baker, 2019). The paucity of baseline ecological data on such habitats (Schoenrock *et al*., 2019) makes the ecological consequences of increased mechanical harvesting difficult to quantify. The increasing number of companies operating in the Irish seaweed market, alongside increased research and the development of novel applications, is creating new demand for macroalgal products, seeking higher value species for food and cosmetic applications. Such renewed commercial interest could, if left to develop unchecked, lead to extensive degradation of Irish macroalgal resources (Mac Monagail & Morrison, 2020). The study species for this research represent both the present (*A. nodosum*) and likely future (*L. hyperborea*) of the Irish seaweed industry. Developing an accurate and cost-effective method for assessing their populations will support the sustainable management of Ireland's macroalgal resource.

The above passage offers a mere glimpse into the historical, and more recent, relationships between humankind and macroalgae. It is clear, however, that macroalgae has likely been a valuable resource for the spread and development of human society and most probably for far longer than records suggest. This understanding helps one to appreciate the importance effectively managing this resource as it has, is and always will be of great value to humanity.

1.6. Macroalgal mapping methods

1.6.1. The importance of mapping macroalgae

Intertidal macroalgal communities face an increasing range of anthropogenic (Godet *et al*., 2009) and environmental pressures (Brodie *et al*., 2014) which underscores the importance of monitoring these communities and developing ecological baselines. Climate change effects on the ocean, including warmer waters, increased storminess and changing chemistry, are likely to impact macroalgal ecophysiology and distribution, affecting associated faunal communities (Harley *et al*., 2012) and, consequently, industries that rely

on these resources. Increasing human development along many of the world's coastlines is a direct threat to marine and coastal ecosystems, especially macroalgal communities. This brings not only direct physical destruction but also increased pollution from run-off, contamination from organic matter and increased turbidity from sediment loading (Coelho *et al*., 2000; Walker & Kendrick, 1998). Invasive species can be a major contributor to the degradation of coastal marine ecosystems, and the spread of invasive species is often facilitated by greater levels of human activity in these environments (Grosholz, 2002). *Sargassum muticum* (Yendo) Fensholt is the 'poster-child' for invasive macroalgal species in Europe where it can often dominate in disturbed habitats, outcompeting native species (Sánchez & Fernández, 2005) but is not established in Ireland to the point where it forms nuisance monospecific stands (Baer & Stengel, 2010).

The concept of 'shifting-baselines' in ecology (Pauly, 1995) has now expanded beyond fisheries science and has come to encapsulate the idea that what is viewed as 'normal' (ecologically speaking) today must be considered in a historical context. In some cases, this may mean that the 'normal' of today is the 'degraded' of yesterday, an important caveat for the establishment of baseline monitoring studies.

Traditionally, macroalgal surveys have, and still are (Burrows *et al*., 2010), carried out by the means of detailed field surveying. This is considered the most accurate habitat mapping methodology (Simms, 2003; Stevens *et al*., 2004), particularly regarding taxonomic resolution, as it allows for the collection of data over the finest of spatial resolutions and often allows for the quantification associated floral and faunal species. This complexity can, however, limit the scale of field surveys, making surveying large areas time-consuming and costly (Oppelt *et al*., 2012; Casal *et al*., 2013; Brodie *et al*., 2018) and they can suffer from standardisation issues if multiple surveying organisations are involved (MacAlister & Mahaxay, 2009). Similar constraints also apply to a wide range of terrestrial and marine mapping applications and there has, over the past three decades, been a concerted effort to develop accurate remote sensing assessment methodologies (Goetz, 2009). For the effective implementation of management and conservation strategies such data needs to be collected in a cost-effective and efficient way (Nagendra, 2001).

Remote sensing can broadly be defined as the science of monitoring the Earth from a distance. For this research project, and for the sake of simplicity, remote sensing can be split into two subdivisions, optical and acoustic. The former is the initial focus. Smith (2012) defines optical remote sensing as the 'science of obtaining and interpreting information from a distance, usually through the means of either aerial, satellite or spacecraft observations'. Acoustic remote sensing can be similarly defined, where the limited penetrating of

electromagnetic radiation (EMR) through water requires that boats and acoustic sensors be used instead of aerial, satellites or spacecraft (Brown *et al*., 2019). This technology allows for some of the limitations with traditional field-surveying to be addressed, chief of which being the limited spatial extent covered. Depending on the platform used, remote sensing can cover much larger tracts of the Earth's surface than on-foot methods, in the same amount of time (Gray *et al*., 2018). Data can be collected over a wide range of spatial resolutions and across the entirety of the electromagnetic spectrum providing information on a cornucopia of Earth system processes that would be immensely difficult to quantify on foot.

1.7. Optical remote sensing

1.7.1. History and development of optical remote sensing

An appreciation for the historical context in which modern optical remote sensing sits is required to understand how the technology has developed over the past century and how current remote sensing capabilities differ greatly in the types of data collected and the spatial and spectral resolutions that can be achieved with modern technology.

Soon after the development of practical photography techniques in the late 1830's, interest grew in their use for capturing images from high-vantage points. Balloons and kites were the initial method of choice for attaining such images and the first document case is that of Gaspard Félix Tournachon (known as 'Nadar') who, in 1858 successfully used a balloon-mounted camera to capture the cityscape of Paris (Amad, 2012). Unfortunately, none of Nadar's photographs exist today but other notable pioneers include James Wallace Black who, using a balloon, took the first extant aerial image over Boston in 1860 (**Fig. 1.3**) (Skoog, 2008) and the infamous Eadweard Muybridge who, whilst famed for his work on photographic studies of motion, created the world's first panoramic image, of San Francisco in 1877 (Amad, 2012). Soon the idea of mounting cameras on rockets was being championed by Alfred Nobel and in 1897, the year after his death, the first successful images were supposedly captured, although doubt has been cast on whether the images were captured from a hill instead (Skoog, 2008).

Fig. 1.3. First aerial image of Boston, taken in 1860 by James Wallace Black using the 'Queen of the Air' hot-air balloon. Credit: James Wallace Black (CC).

The invention and development of aircraft opened a whole new avenue of potential applications for aerial imagery, none better encapsulated then their pioneering use in WWI. From 1915 onwards, both the Allies and the Central Powers extensively used aerial photography to reconnoitre and observe enemy defences (Gheyle *et al*., 2016). So extensive are the archives of these images, that they are still being used today to understand and preserve the war's heritage (Note *et al*., 2018). WWII saw the further development of aerial imagery acquisition, interpretation and use of the non-visible EM spectrum. The skillset developed by those involved was, after the war, transferred to civilian occupations and helped to drive the continued development of remote sensing (Campbell, 2002). Since then, planes have been a reliable platform from which to conduct remote sensing surveys.

The first images taken where the Earth's curvature was visible were in 1935 from the Explorer II stratospheric balloon, piloted by Captain Albert Stevens, which took images from around 20 km in height (Briggs, 1935). Some of the earliest images taken from space were from captured V2 rockets followed by Viking rockets launched from New Mexico from 1946 – 1955 (Bird & Morrison, 1964). Initially these images were taken from a height of about 100 – 200 km, but by 1959 the Atlas rocket, launched from Cape Kennedy, took images from 1400 km above Earth (Bird & Morrison, 1964). Soon after followed the first manned orbital and suborbital flights of the Project Mercury mission where photographs were taken by the astronauts (Bird & Morrison, 1964). This coincided with the launch of the first TIROS satellite, designed for climatological and meteorological observations, (TIROS-1) in 1960, with a subsequent seven launched by 1964 (Bird & Morrison, 1964). These satellites were the proving ground for satellite Earth observation and their success in monitoring global weather patterns paved the way for future satellites (NASA, 2016). In 1972 the first civilian Earth observation multispectral satellite, Landsat 1, was launched (Goetz, 2009), in part due to the development of microprocessors (Cohen & Goward, 2004). As of 2013, there have been eight Landsat missions, with the ninth planned for 2020 (USGS, 2019). Each satellite improved upon the capabilities of the last, particularly with respect to increased spatial and spectral resolution (Markham *et al*., 2004). Landsat data has been used in a vast number of scientific studies, covering a wide range of scientific disciplines (*e.g.* South *et al*., 2004; Yang *et al*., 2003; MacAlister & Mahaxay, 2009; Petropoulos *et al*., 2010). Since 1972 many Earth observation satellites have been launched and, as of 2008, there were more than 150 in orbit (Tatem *et al*., 2009). Research into hyperspectral sensor technology began in the 1980's (Campbell, 2002), yet the number of hyperspectral satellites remains limited owing to difficulties with obtaining sufficient spatial resolution, power requirements, data storage limitations and cost (Transon *et al*., 2018). Most current and future Earth observation satellites are multispectral.

Aircraft and satellites supported the development of optical remote sensing and Earth observation throughout the 20th, and into the 21st, century. The development of drone technology has a long and complicated history focused on their use in military applications and it is recommended, for those interested, to read Keane & Carr (2013) for a detailed historical account. Drones are now increasingly being used in a range of different environmental monitoring studies and evolution of drone technology over the past ten years has turned them into a cost-effective and accurate mapping platform for researchers (Johnston, 2019), yet their application for macroalgal mapping studies is limited but growing. These three platforms remain the most popular for the acquisition of remote

sensing data and the decision on which to use often depends on research objectives as they each offer unique mapping capabilities, primarily focused on their survey height (**Fig. 1.4**).

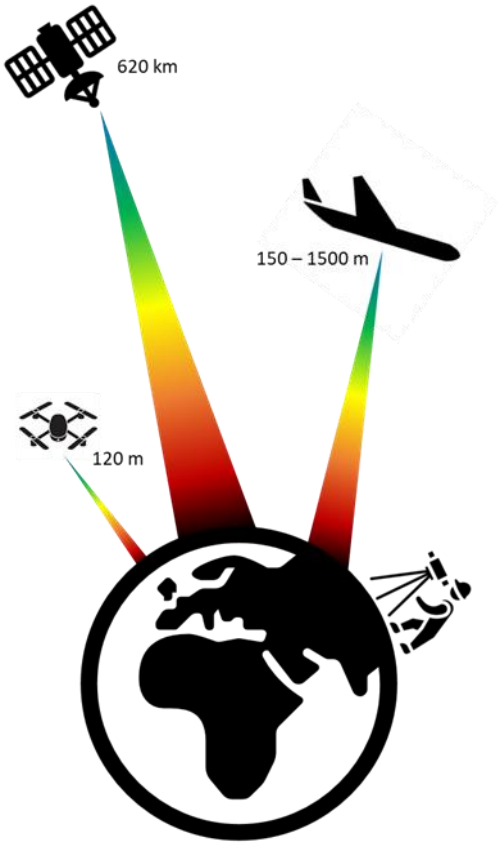

Fig. 1.4. Representation of the three main platforms used to collect remote sensing data and their operational ranges. Different ground field of views (GFOV) are highlighted. Satellites cover the largest areas, followed by aircraft, drones and then on-foot surveys. Adapted from Johnston (2019).

1.7.2. Optical remote sensing theory

Optical remote sensors can typically either be passive or active. Passive sensors depend on an external energy source, such as the sun, and measure how this energy interacts with a feature. Active sensors produce their own energy and radiate it onto a feature, measuring the returning energy (Richards & Jia, 2006). Active sensors are not used in this research and shall not be discussed further. Good examples, however, include Radar (radio waves) and Light Detection and Ranging (LiDAR) which uses pulsed lasers. Thermal remote sensing technology will also not be discussed as it is not used in this research. This research focused on the use of RGB, multispectral and hyperspectral passive remote sensors and the theory behind them and their development are discussed in the following sections.

Nucleic reactions within the sun produce a full spectrum of electromagnetic radiation (EMR), which travels, relatively unaltered, through space until it reaches the atmosphere of Earth. At this point, certain wavelengths are scattered or absorbed by particles within the atmosphere with the remainder eventually reaching and interacting with features on the Earth's surface (Milton, 2004). EMR is combined of visible, radio, thermal, ultra-violet and x-rays and radiates in accordance with basic wave theory, which describes the energy as travelling in a sinusoidal way, at the speed of light (Lillesand *et al*., 2004). This is represented by the following equation:

$$c = \lambda v$$

Where c represents the velocity of light, which is constant (3×10^8m/sec), frequency (v) and wavelength (λ).

The sum of all energy reaching a feature on the Earth's surface is known as incident energy, at this point, five fundamental interactions take place. EMR is either absorbed, reflected, scattered, refracted or transmitted, and it is variations in these three interactions that create unique spectral signatures enabling different objects to be spectrally distinguished from one another (Govender *et al*., 2007). Incident energy can be described as follows:

$$E_I(\lambda) = E_R(\lambda) + E_A(\Lambda) + E_T(\lambda)$$

Where incident energy (E_I) is the sum of the interactions between reflected energy (E_R), absorbed energy (E_A) and transmitted energy (E_T).

There are three major, arbitrarily, defined regions of the EM spectrum. Regions below 400 nm, which includes gamma rays, x-rays and ultraviolet, are typically not considered useful for remote sensing applications (Campbell, 2002). The visible region contains the blue (400-500 nm), green (500-600 nm) and red (600-700 nm) light, which are the wavelengths recorded in three-band RGB sensors. Beyond this is the infrared region of the EM spectrum which covers from ~700 nm to 1500 nm and can be sub-divided into the near-infrared (NIR) (750-100 nm) and thermal wavelength regions (1000-1500 nm). NIR behaves in a manner consistent with visible light and can therefore be captured using similar sensors (Campbell, 2002).

Optical remote sensors are designed to record the ways in which incident light interacts with features of interest, usually in the form of reflectance. This is the ratio of incident-to-reflected radiant flux measured from a feature over specific wavelengths (Peddle *et al*., 2001) and is represented by the following:

$$E_R(\lambda) = E_I(\lambda) - [E_A(\lambda) + E_T(\lambda)]$$

Reflected energy is equal to incident energy minus the energy that is absorbed or transmitted upon contact with an object leaving a surface without a change in frequency (Nicodemus *et al*., 1977). Sensors measure the radiance of an object which provides information on how much energy is being reflected or emitted but this needs to be displayed as a percentage of incident radiation. This is because spectral reflectance is an inherent property of an object and is independent of location, time, atmospheric or weather conditions (Peddle *et al*., 2001). The nature of this reflection depends upon the size of object surface irregularities, essentially how rough or smooth they are, in relation to the wavelength of radiation (Campbell, 2002). A perfectly smooth surface, such as a mirror, will produce a specular reflection where the angle of incidence is equal to the angle of reflection and almost all the energy is reflected in a single direction (Campbell, 2002). A uniformly rough surface (at a scale equivalent to the wavelength), referred to as a Lambertian surface, will produce a diffuse reflection where energy is scattered equally in all directions providing equal brightness when viewed from any angle (Campbell, 2002). Many objects fall somewhere in between specular and diffuse reflectors and this behaviour is described by the bidirectional reflectance distribution function (BRDF) with respect to angles of illumination and observation (Nicodemus *et al*., 1977; Mac Arthur *et al*., 2012).

Three characteristics of a remote sensor define the type of data it can collect, its spatial, spectral and radiometric resolution. The level of detail that can be depicted in an image is defined as the spatial resolution. Each detector in a remote sensor measures a finite area on the ground, the smaller the individual areas, the higher the spatial resolution (Govender *et al*., 2007). The spatial resolution is affected by the design of the sensor and the height that it is flown or orbits at. Wider field of views (FOV) can lead to decreased spatial resolution caused by the lower pixel densities. A sensor with the same native resolution, but narrower FOV, would likely have a finer spatial resolution, but would on capture a smaller area. Some sensor manufacturers offer different lenses to suit client needs (Headwall, 2020). Spectral resolution refers to the ability of the sensor to capture bands within the EM spectrum, a sensor that can capture many small bands within the spectrum would have a high resolution. A higher spectral resolution (*i.e.* hyperspectral sensor) increases the chances of being able to differentiate between two objects which may have a similar spectral signature as these spectral differences are often narrow (Kutser *et al*., 2006b). Radiometric resolution is the ability of a sensor to measure the signal strength of objects, the higher the radiometric resolution the more sensitive the sensor is to detecting small differences in reflected energy (Butler, 2014). The energy recorded is represented by bits (used to code numbers in binary format) and the maximum number of brightness levels depends on the number of bits used. One bit would be a sensor that could only distinguish black and white, whereas eight-bit

sensors can distinguish 255 different shades making them better capable of observing more differences in surface feature reflection (Smith, 2012). There is a trade-off between spatial resolution, spectral resolution and radiometric resolution which results in spatial resolution being decreased when spectral resolution is enhanced (Eismann & Hardie, 2005).

1.7.3. Optical remote sensing of macroalgae

Multispectral remote sensors, such as Landsat and SPOT (Satellite Pour l'Observation de la Terre), collect images with a few relatively broad wavelength bands from the visible and near-infrared regions of the EM spectrum (Smith, 2012). The fine spectral resolution of multispectral sensors means that they may not be suitable for discriminating between macroalgae at a species level (Oppelt *et al*., 2012), but can achieve accurate results when looking at broader taxonomic groups (Brodie *et al*., 2018). Their use is mostly restricted to areas with low spatial heterogeneity and a few optically distinct species, which form monospecific stands (Knudby *et al*., 2011). Several studies have had success using multispectral imagery in such environments. Stekoll *et al*. (2006) found good correlations between remote sensing data and ground truth data for kelp biomass estimates in Alaska. Cavanaugh *et al*. (2010) combined multispectral imagery and dive-based surveys to assess changes in *M. pyrifera* canopy cover and biomass in California, finding a strong correlation between *in-situ* measurements and remote sensing data. Casal *et al*. (2011) used data from the SPOT-4 satellite to map subtidal kelp in turbid waters, noting that whilst challenges arising from working in turbid water affected some of the results, there was still correlation to be found between remote sensing and field data. The method was unable to identify different species, however.

Intertidal macroalgal communities can often be spatially and spectrally heterogeneous (Tait *et al*., 2019), as spectrally similar species can often be found in mixed assemblages, requiring remote sensing technology with both high spatial and spectral resolutions (Vis *et al*., 2003). The use of hyperspectral sensors has grown in the past decade. Hyperspectral sensors collect ten to hundreds of narrow contiguous spectral bands across the EM spectrum whilst, depending on the type, also having high spatial resolutions (Pe'eri *et al*., 2008). This enables more accurate discrimination between spectral signatures of target features (*i.e.* macroalgal species). Hyperspectral sensors can be mounted on a range of platforms including satellites, planes and drones. To date, and to the best of our knowledge, there have been no studies which have applied drone-mounted hyperspectral remote sensing for intertidal macroalgal habitat mapping. Relatively few studies have used hyperspectral sensors, on any platform, for this type of work. Oppelt *et al*. (2012) successfully used a motorised glider and AISAeagle+ hyperspectral sensor to map the intertidal zone at

Heligoland (German Bight) but found discriminating to species level was difficult as for some brown macroalgal classes, only mixtures could be identified. This may have been a result of low spatial resolution not being able to observe the complexities of mixed macroalgal assemblages. Hennig *et al*. (2007) used the ROSIS airborne hyperspectral sensor to map intertidal macroalgae (only to group level) and zonation in Heligoland. They were able to identify these broad macroalgal groups along with mussel beds and observed that it was not possible to achieve species level discrimination. The authors do not offer an explanation for this, perhaps the spatial resolution of the ROSIS sensor (GSD 0.84 m/pixel) was not suitable for visualising complex intertidal spatial assemblages. The high spectral resolution of hyperspectral sensors is considered particularly important for accurately discriminating between spectrally similar macroalgal species (Oppelt *et al*., 2012). Combined with the fine spatial resolution that can be achieved using drones, hyperspectral remote sensing potentially allows for fine spatial patterns to also be observed (Lucieer *et al*., 2014).

1.7.4. Spectral library data collection

The most important consideration prior to conducting a remote sensing survey is how to collect accurate training and reference data. A common and effective method of achieving this is through the creation of a spectral library of key species features present within a study site (Kutser *et al*., 2003). Spectroscopy is the study of light that is reflected and emitted from material, and its variation in energy and wavelength (Lillesand *et al*., 2004). A spectral library can be used to identify materials as seen by the hyperspectral imager (Dekker *et al*., 2003) to train image analysis and classification software to verify the information extracted from the hyperspectral imagery (Lillesand *et al*., 2004). Reflectance spectroscopy requires a source of illumination (of sufficient intensity across wavelengths of interest), a means of measurement, a method to direct the illumination on to the same and a means of analysis (Milton, 2004). The collection of spectral library information can be collected either in the field, under natural illumination conditions, or under artificial conditions in a laboratory. Measurements collected in a laboratory may not be suitable for classifying remote sensing data and are useful for conducting more detailed investigations into the spectral properties of macroalgae under controlled conditions (Uhl *et al*., 2013). For some species, such as canopy forming ones, it may be necessary to sample a sufficiently extensive area of the surface to be representative (Milton, 2004), although for in the case of macroalgae, Kotta *et al*. (2014) observe how variation in canopy geometry and properties do not significantly change reflectance values. Spectral libraries also need to account for spatial and temporal variations in reflectance spectra. Seasonal changes in environmental conditions lead to variations in macroalgal pigment concentrations (Stengel & Dring, 1997) which, intern, affect reflectance

properties. It is, depending on research objectives, important to design spectral sampling surveys to account for this and also to determine the spatial variation in the reflectance spectra of macroalgal species (Kotta *et al*., 2014).

1.7.5. Macroalgal spectral characteristics

There are three main groups of macroalgae, each having characteristic pigments with different optical properties giving them their unique colouration, these are Chlorophyta (green), Rhodophyta (red) and Phaeophyceae (brown) (**Tab. 1.1**). Light harvesting pigments are found either within, or on, the thylakoid membrane of chloroplasts and concentrated in cortical cells of macroalgal species. The presence and concentration of these pigments is what makes it possible to spectrally discriminate between groups and, to some extent, species (Dekker *et al*., 2003). All three groups contain chlorophyll-*a*, but it is the presence of the other chlorophylls and pigments which varies (Hedley & Mumby, 2002). Other pigments include carotenoids and phycobilins which are also responsible for the variation in reflectance within the visible wavelengths, particularly for red and brown macroalgal species. (Pe'eri *et al*., 2008). The chlorophylls are all tetrapyrrole rings surrounding Mg^{2+} (Fischer, 1936) and chlorophyll *a* and *b* have a fatty acid tail which is lacking in chlorophyll *c* (Hurd *et al*., 2014). The carotenoids, split into carotenes and xanthophylls, provide additional photoprotective services under high irradiance. Both are C_{40} tetraterpenes with carotene being a hydrocarbon and xanthophylls containing at least one oxygen molecule (Hurd *et al*., 2014). Phycobiliproteins are water-soluble accessory light-harvesting pigment molecules serving as the photosynthetic apparatus in some eukaryotic algae. They are comprised of proteins bound by chromophores called phycobilins which are usually either phycoerythrobilin or phycocyanobilin and these can further be divided into three classes depending on the wavelength absorption region and number of phycobilin molecules present within their polypeptide chains (Hurd *et al*. 2014). Absorption of EM radiation is thus, owing to the presence of pigments, greatest in visible wavelengths. Chlorophyll, for example, strongly absorbs in the blue and red spectral regions (Campbell, 2002) which, for green macroalgal species, contributes to a distinctive spectral profile in the visible region. which creates distinctive reflectance troughs. Spectral reflectance in the near infrared (NIR) is controlled, not by pigments, but by the internal cellular structure of macroalgae (Campbell, 2002). This can vary greatly owing to stresses such as water limitation (Smith, 2012) or even subtle variations in the localised hydrodynamic and climate conditions within a single site and, as highlighted by Uhl *et al*. (2013), can be difficult to quantify, especially for brown macroalgal species. Temporal variation in pigment concentrations occur due to differing light regimes, and this can lead to intraspecific variation in thalli colour along with variation within a thalli of an individual. This can be seen for *A. nodosum* in **Fig 2.4**

(Chapter 2). The presence of water also affects the spectral signature in NIR wavelengths as absorption of insolation is high, which is why water appears black in NIR images. This can make the analysis of spectral signatures within the NIR wavelengths difficult and explains why many spectral studies to date have focused on the visible (400-700 nm) wavelength range where spectral response is controlled pigment presence and concentration.

Tab.1.1. Main pigments associated with each of the three macroalgal groups. Adapted from Hedley & Mumby, (2002).

Pigments	Absorption Peaks (nm)	Chlorophyta	Phaeophyceae	Rhodophyta
Chlorophylls				
Chl-*a*[1]	435, 670-680	x	x	x
Chl-*b*[1]	480, 650	x		
Chl-*c*[1]	645		x	
Carotenoids				
α[2]	423, 444, 473			x
β[2]	427, 449, 475	x	x	x
Xanthophylls				
Zeaxanthin[2]	428, 450, 478	x		x
Neoxanthin[2]	415, 438, 467	x	x	
Lutein[2]	422, 445, 474	x		x
Violaxanthan[2]	417, 440, 469	x	x	
Fucoxanthin[2]	426, 449, 465		x	
Diotoxanthin[2]	425, 449, 475		x	
Diadinoxanthin[2]	424, 445, 474		x	
Siphonxanthin[2]	540	x		
Phycobilins				
Phycocyanin[1]	618			x
Phycoerythrin[1]	490, 546, 576			x
Allophycocyanin[1]	654			x

[1]*in vivo*, [2]*in-vitro*

1.7.6. Remote sensing of biomass

The effective conservation and management of macroalgal resources requires the ability to conduct biomass, along with distribution assessments. *In-situ* biomass surveys are usually time consuming, costly and require logistical support, which is why Stekoll *et al.* (2006) observe how it is important to find a morphometric measurement that is correlated with biomass and that can also be easily measured in the field. The use of remote sensing technologies potentially allows spatial coverage and biomass estimates to be provided for much larger sites than were previously available when using field-based survey techniques. These technologies also offer the prospect of a reduced need for extensive field-based biomass surveys if relationships can be developed between morphometric data and biomass, which can then enable biomass to be determined from remote sensing data (Gevaert *et al*., 2008). To the best of our knowledge, only one recent study has attempted to use remote sensing technology to assess the biomass of intertidal macroalgal species. Remote sensing of

biomass requires being able to quantify the volumetric properties of macroalgae and the development of linear relationships between biomass and either volume or height (Cunliffe *et al*., 2016). What research that has been done on the remote sensing of macroalgal biomass has been conducted on subtidal species (*e.g.* kelps and seagrasses) using acoustic remote sensing. This has proven difficult for intertidal macroalgae as, when emersed, morphometric properties that can be correlated with biomass, such as length, cannot be measured. In an attempt to address this, Webster *et al*. (2019) used LiDAR to measure the height of the *A. nodosum* canopy in Nova Scotia by surveying at low and high tide. By identifying the waveform response of *A. nodosum* and the seabed they calculated the height of the canopy at high tide and, using biomass to height relationships developed during field-sampling, they were able to derive biomass estimates for the site. Potential relationships between vegetation biomass and vegetation indices, such as normalised difference vegetation index (NDVI), have been developed for homogenous saltmarsh communities (Doughty & Cavanaugh, 2019). Such relationships may also exist for macroalgae but will require the ability to first identify different species within a community, otherwise it would not be possible to determine whether variations in NDVI were related to biomass or different species.

Blight *et al*. (2011) collected measurements from kelp plants and found a strong relationship between stipe length and biomass. This meant that acoustic data could then be used to obtain kelp canopy height which can then be used to estimate biomass for the wider area. The ability of acoustic sensors to observe the height of the kelp canopy above the seabed was also explored by Mac Craith & Hardy (2015) who created a kelp height map and noted the potential of this method for creating biomass maps. Quintino *et al*. (2010) found that SBES, with a 200 kHz frequency, was able to distinguish areas of different macroalgal biomass and that it would be possible to model the biomass of *Caulerpa prolifera* (Forsskål) J.V. Lammouroux. Minami *et al.* (2010) also had success in using SBES to measure the thickness of the kelp canopy, further highlighting the potential for a synergy between morphometric data and remote sensing. Lefebvre *et al*. (2009) were also able to use SBES to delineate the canopy height of seagrass in the Solent (UK).

Several studies choose to use remote sensing data to assess the spatial distribution of a target species and then scale up field-based biomass assessments to the wider study area. Stekoll *et al.* (2006) found a good correlation between multispectral imagery and biomass data collected from field surveys. The study used estimated biomasses from sampling sites to calibrate the multispectral imagery where relationships between biomass and density enabled a biomass map to be produced. They also found that the best predictor of plant biomass was the weight of the blade. Andréfouët *et al*. (2004) used IKONOS satellite data to determine the spatial extent of two invasive brown seaweeds. They used field and laboratory

measurements to provide percentage cover versus biomass estimate for the sampling site and then scaled this value up to represent the species cover throughout the study site. Simms (2005) conducted a kelp biomass assessment using CASI. The study conducted a traditional field-based biomass survey and then used the following equation to estimate biomass for the study area.

$$B = AW$$

Where **B** is the total biomass for the site (kg), **A** is the total area of kelp classified using the remote sensing data and **W** is the median biomass from the survey (kg/m^2). The study notes that although this is an effective method for quantifying biomass the high heterogeneity of the coastal environment leads to high variability in biomass estimates. Riegl *et al.* (2005) used acoustic remote sensing to define three species categories, seagrass, spare algae and dense algae. Biomass estimates were then calculated for each of these categories and then extrapolated to the wider site by counting the colour coded pixels assigned to each category.

Biomass assessments are usually a destructive process (Gevaert *et al*., 2008) as they require the removal of macroalgal species from the substratum. Both subtidal and intertidal kelp biomass assessments rely on a quadrat methodology where plants are removed in order to be weighed (Andréfouët *et al*., 2004; Bajjouk *et al*., 2015; Gorman *et al*., 2013; Quintino *et al*., 2010; Simms, 2003; Vadas *et al*., 2004). Subtidal biomass surveys are usually conducted by Scuba divers whereas intertidal surveys are conducted on foot or by boat if areas are inaccessible. As water levels in plants can vary on a daily basis obtaining the dry weight of a plant is more accurate than the fresh, or wet, weight. Studies appear to use of mix of both wet (Fyfe *et al*., 1999; Simms, 2003; Reigl *et al*., 2005; Stekoll *et al*., 2006) and dry weight (Andréfouët *et al*., 2004; Barillé *et al*., 2010; Quintino *et al*., 2010) biomass measurements. Wet weight can either be obtained in the field or in the laboratory and involves cleaning the samples of any sediment or epiphytes before weighing (Vadas *et al*., 2004). To obtain the dry weight samples need to be transported to the laboratory, cleaned and then dried before weighing (Quintino *et al*., 2010).

1.7.7. Challenges of subtidal optical remote sensing

The presence of water can severely limit the effectiveness of optical remote sensing technology and the attenuation of light becomes greater with increasing depth and turbidity (Bajjouk *et al*., 2015). Water is a strongly absorbing medium for solar energy (Bushing, 2000) and the degree of absorption is mostly dependent on wavelength (Lillesand *et al*., 2004). Absorption is much stronger in the near-to-mid infrared region of the EM spectrum and varies for the visible region depending on water body properties (Campbell, 2002). In

coastal waters, light is also scattered and absorbed by suspended organic/inorganic material, phytoplankton and dissolved organic substances contributing to a decrease in the spectral reflectance of submerged benthic macroalgae (Casal *et al*., 2012). This strong attenuation of light by water limits the depth at which benthic macroalgae can be identified (Kotta *et al*., 2013). Often, emergent species, such as canopy forming kelps, have higher average reflectance values than submerged species due to the lack of interference from water (Oppelt *et al*., 2012) and these have been the subject of several remote sensing studies (Stekoll *et al*., 2006; Cavanaugh *et al*., 2010). Within the visible wavelengths the green band is considered the most useful for identifying submerged macroalgae, followed by the red and red-edge regions (Silva *et al*., 2008). Blue wavelengths penetrate the water well, but are scattered and reflected, giving water its characteristic blue colour (Campbell, 2002). The main challenge in subtidal remote sensing is to isolate the feature-of-interest signal from water column interference (Casal *et al*., 2013). These challenges make it more straightforward to conducting remote sensing surveys during low tide, despite the time constraints this creates. Depth limitations of light penetration would mean that optical remote sensing surveys of subtidal macroalgae would not provide a complete picture and this is where acoustic remote sensing technology can potentially provide an effective mapping solution.

1.8. Acoustic remote sensing

1.8.1. History and development of acoustic remote sensing

For almost four thousand years, up to the 1900's, the primary method for measuring the depth of the seafloor was the lead line. The earliest evidence for seafloor mapping comes from a model boat found in tomb of Meket-re (buried in Thebes ca. 2000 BC) showing a lead line being used to measure depth (Mayer, 2006). Merchants in the Mediterranean used this method to develop some of the first known maps of the seafloor during the 13th century (Brown *et al*., 2011). With the development and eventual acceptance of the echosounder, post WWII, the ability to create maps of the seafloor was greatly enhanced (Mayer, 2006). Along with developing an understanding of the bathymetry of the seafloor came the need to understand its biological and geological nature. In the 19th century, such studies were rudimentary and involved the use of simple dredges and grab techniques (Brown *et al*., 2011). The development of sidescan sonar systems in the 1940's provided the first, low-resolution, images of the nature of the seafloor (Kenny *et al*., 2003) and modern multibeam systems (MBES), developed in the 1970's (Renard & Allenou, 1979), can record high resolution data on bathymetry and backscatter, making them invaluable for seafloor and benthic habitat mapping studies.

1.8.2. Principles of acoustic remote sensing

Acoustic remote sensing technologies are not constrained by the same physical factors as optical remote sensing technology and, as such, can operate in both deep oceanic and shallow coastal waters. Acoustic remote sensing technologies allow for the quick and precise acquisition of data over large spatial scales (Kruss *et al*., 2006), making them the tool of choice for seafloor habitat mapping. Acoustic remote sensors work by transmitting, from a transducer attached to the hull of a vessel, a pulse of sound through the water to the seabed and then listening for the returning echo (Stanton, 2012). There are two types of information gathered from these systems, bathymetric and backscatter. By measuring the time it takes for the acoustic wave to be transmitted to, and reflected from, the seabed one can assess its depth (Blight *et al*., 2011). Bathymetric data, however, only provides information on the profile and depth of the seafloor and not any information on seafloor characteristic such as bottom type (de Moustier, 1985). Backscatter data enables bottom roughness and substrate type to be inferred as different sediments and rock types cause fluctuations in the scattering of the acoustic signal. Harder surfaces such as bedrock will cause a higher return of the sound energy, providing a stronger signal, whereas softer sediments absorb more of the sound energy producing a weaker return signal. The level of detail afforded by some sensors can create almost photo-realistic imagery of the seabed (Kenny *et al*., 2003).

1.8.3. Acoustic remote sensing technologies

1.8.3.1. Sidescan sonar (SSS)

Sidescan devices usually consist of a towfish, transmission cable and topside processing unit. The SSS transducer transmits sound and analyses the return signal to build a relatively high-resolution image of the seafloor (Mayer, 2006). The sound is emitted perpendicular to the two fish, meaning that the area directly below is not isonified by the sound waves (**Fig. 1.5**). Given the need to deploy the towfish below the vessel, SSS systems are difficult to use in shallow water environments (Komatsu *et al*., 2003). The inability of such a system to provide measurements of canopy height makes it unsuitable for use in subtidal macroalgal mapping surveys, although they are capable of detecting the lateral distribution of, for example, seagrass beds (Lefebvre *et al*., 2009). Being close to the seabed allows SSS to create ultra-high spatial resolution images of the seabed. Their application, then, may depend on research requirements and may be suitable if information on canopy height is not required.

1.8.3.2. Singlebeam Echosounders (SBES)

The principle function of SBES systems is to calculate the water depth immediately below the vessel (Colbo *et al*., 2014). The backscatter signal can also be analysed. SBES emits a pulse of sound directed vertically below the vessel and the analysis of this echo contains information about the water column and seabed (Blight *et al*., 2011). These systems are popular because they are simple to use and prevalent on nearly all vessels (Kruss *et al*., 2008). Having only a single beam, these systems are unable to cover large area, only isonifying a small area directly beneath the vessel (**Fig. 1.5**). Studies using SBES to map the spatial distribution of habitats have concluded that while SBES allows for the discrimination of habitats, the use of MBES would offer enhanced resolution and greater spatial coverage (Jordan *et al*., 2005; Kruss *et al*., 2017). These systems are also unsuitable for mapping the spatial extent of species with patchy distributions as their limited seabed coverage would make it inefficient (Komatsu *et al*., 2003). Most of the studies, to date, which used acoustic remote sensing to successfully map benthic macroalgal and macrophytic communities have used SBES systems (Riegl *et al*., 2005; Noel *et al*., 2008; Lefebvre *et al*., 2009; Minami *et al*., 2010; Blight *et al*., 2011; Kruss *et al*., 2017). The prevalence of SBES on many vessels and their relative simplicity make them a useful tool for subtidal habitat mapping but, owing to their limited ability to survey large areas would not be able to provide a complete picture of the feature of interest meaning that, depending on the research question, important details, such as variation in canopy height (*e.g.* seagrass or kelp) could be lost.

1.8.3.3. Multibeam Echosounders (MBES)

MBES systems transmit several beams (into the hundreds for some systems) in a fan shape, covering a wide swath either side of the vessel (**Fig. 1.5**) (Brown & Blondel, 2009). It is the ability of the MBES to gather data on bathymetry and backscatter across a wide area that makes it so useful. Each beam can also be analysed for simultaneous depth measurements across the width of the swath (Lurton, 2002). MBES systems offer a high vertical and horizontal resolution and there are variants which can operate at a range of water depths, from deep ocean to shallow coastal waters (Colbo *et al*., 2014). Until recently, the backscatter collected using SSS systems was of greater detail, but developments in data collection and processing has vastly improved the resolution of MBES data (Le Bas & Huvenne, 2009). Whilst MBES systems provide much greater spatial coverage, analysis of their data output is not as straightforward as it is for SBES systems (Blight *et al*., 2011).

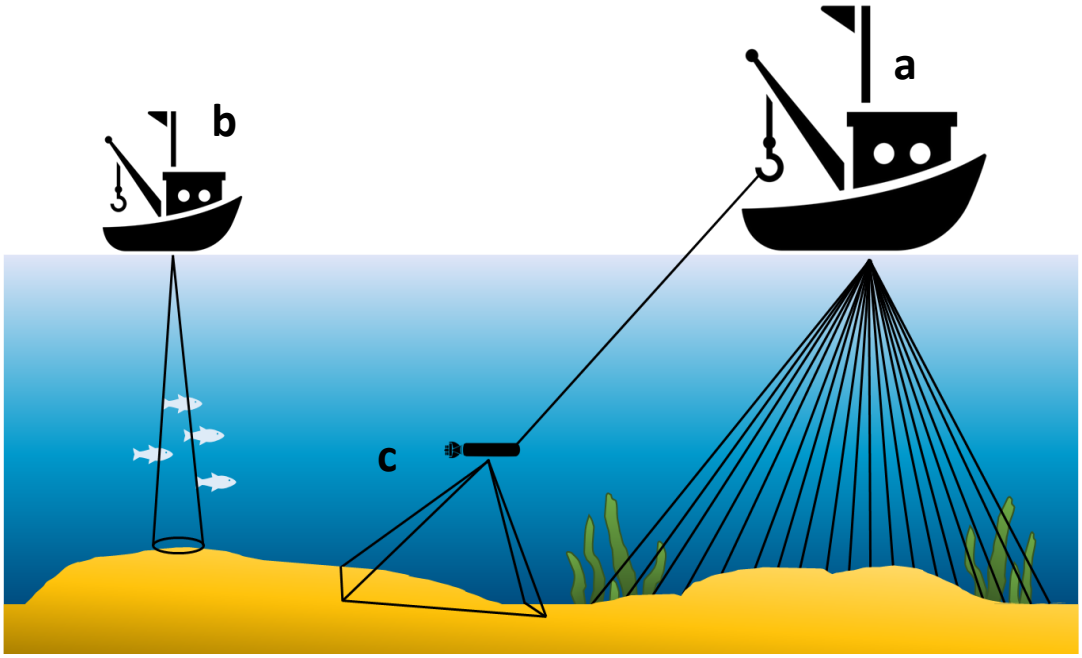

Fig. 1.5. Pictorial representation of the data collection methods for three acoustic remote sensing devices, MBES (**a**), SBES (**b**) and SSS (**c**).

1.8.4. Application of acoustic remote sensing in the marine environment

The most common application of acoustic remote sensing technologies is for seabed mapping and bathymetric surveys (Renard & Allenou, 1979; Ierodiaconou *et al*., 2007; Preston, 2009). Interest is growing in the acoustic returns that can be detected from objects in the water column which act to scatter sound waves (Freitas *et al*., 2008). Given the commercial value of fish, it is not surprising that SBES data have been used in fisheries management since the last 1940s (Cushing, 1962). The use of acoustic data enables estimates of fish volume, morphology and allows behaviour to be studied (Weber *et al*., 2009) and aids in locating target species. The majority of effort in the water column application of acoustic remote sensing has gone into fisheries and applications of the study of benthic habitats are still in their infancy (Colbo *et al*., 2014). Several studies succeeded in using acoustic data to map benthic habitats that have strong geophysical signatures, for example, scallops (Kostylev *et al*., 2003) and biogenic Rhodolith (Corallinales, Rhodophyta) beds (Falace *et al*., 2014). Technological advancements mean that the limitations surrounding the extraction of water column data are now being overcome (Brown & Blondel, 2009).

Several studies have had success in using acoustic remote sensing to map the distribution of seagrass beds. Komatsu *et al.* (2003) used MBES to map seagrass beds in Japan, finding it

possible to assess the distribution, volume and biomass of the seagrass beds, something that was likely facilitated by their homogenous distribution in the study site. Biomass estimations were calculated by extrapolating m^2 biomass of seagrass to the area covered by seagrass (as determined during the survey). Lefebvre *et al.* (2009) showed that it was possible to predict seagrass abundance and canopy height using acoustic sensors supported by video surveys and Sabol *et al*. (2002) showed good agreement between acoustic estimates of seagrass canopy height and ground truth data.

1.8.5. Acoustic remote sensing of macroalgae

The majority of the sound energy emitted from the sensor head is reflected from the seafloor and this is used to determine its depth (Blight *et al*., 2011). The presence of fish and macroalgae above the seabed can interfere with the acoustic energy, through scattering and absorption, producing a weaker return signal, allowing for their detection. Ierodiaconou *et al*. (2007) combined MBES and video transects to accurately identify dominant substratum and biota classes, including seagrass and macroalgae dominated communities. Kruss *et al*. (2008), in a preliminary study, used both SBES and MBES, supported by direct sampling and observation, to identify the presence of macroalgal species, but did not describe the species present. SBES was also used by Riegl *et al*. (2005) to differentiate between different substrates and also between seagrass and macroalgae using 50 khz and 200 khz frequencies. The successful mapping of laminarians was demonstrated by McGonigle *et al*. (2011) who used MBES and two different techniques, one based on the software QTC-Multiview, and the other based on the extraction of water column data. The acoustic data correlated well with ground truth data collected using drop down video. Studies have noted that using higher frequency SBES channels created less backscatter in the water column, making them more suitable for delineating macroalgal canopies (Blight *et al*., 2011; Mac Craith & Hardy, 2015). Wilson *et al*. (2013) highlights that, whilst acoustic methods have emerged as a useful tool for mapping subtidal macroalgal communities, they remain unable to directly assess biomass, density and physiological condition. However, the ability to define canopy height and distribution can allow for the calculation of volume (Abukawa *et al*., 2012) which may allow for estimations of biomass.

1.8.6. Acoustic properties of macroalgae

The presence of macrophytes is usually discernible by their backscatter signature, which is weaker than the seabed and stronger than the ambient noise in the water column (Lefebvre *et al*., 2009) and, under the right frequencies, can be distinguished from the seafloor (McGonigle *et al*., 2011). The acoustic impedance of macroalgae is thought to result primarily from the gas within them, with more buoyant species being more acoustically

reflective (Sabol *et al*., 2002). Wilson *et al.* (2013) found it more difficult to detect kelp without pneumatocysts using acoustic methods and that the acoustic signatures of kelp species appeared to be biomass dependent and that future work should focus on the relationship between kelp biomass and backscatter intensity, which will vary depending on the species. Kruss *et al*. (2017) successfully used SBES to map macroalgal communities in Kongsfjorden (including kelp species such as *A. esculenta* and *S. latissima*) and were able, after interpolation, to derive area estimations. The study noted that variations in the backscatter intensity of the macroalgal layer may indicate different species as macroalgal morphology and density may influence the signal, concluding that more work is required to verify this. Several studies have reported strong backscatter from dense seagrass canopies (Lefebvre *et al*. 2009; Parnum *et al*., 2012) and for kelp (Mac Craith & Hardy, 2015), suggesting that canopy size and density influences the amount of energy reflected back to the receiver. Bennion *et al*. (2017) used backscatter intensity to predict the presence of kelp (species not defined) off the coast of Dorset. Training data was used to verify the presence of kelp and bare substratum and this data was inputted into a Species Distribution Model (SDM) to predict the distribution of kelp based on the backscatter.

1.8.7. Challenges of using acoustic remote sensing to map macroalgae

The use of MBES and water column analysis for subtidal macroalgal mapping is an emerging field which has traditionally been focused on the detection of fish in the water column (McGonigle *et al*., 2011). The slow development of using MBES to collect water column data was due to the large data storage requirements and that many MBES devices did not permit the digital logging of water column returns (Colbo *et al*., 2014). These limitations are now being overcome through technological developments in software and hardware (Brown *et al*., 2009). A primary limitation of acoustic remote sensing technologies, for macroalgal mapping, is their inability to differentiate between species with similar morphological characteristics. Blight *et al*. (2011) found that they could no differentiate between *L. hyperborea* and *L. digitata* and were unable to identify the transition zone between the species without the use of dive surveys. Bajjouk *et al*. (2015) highlight how difficulties in identifying species will likely make accurate biomass assessments incredibly challenging until methods for acoustically discriminating between species are developed. Lefebvre *et al*. (2009) found that the correct calculation of canopy presence and height was reliant on the accurate computation of seabed depth, a particularly dense canopy could lead to the higher backscatter values being found on the canopy causing it to be potentially misclassified as seabed. Within shallow water environments, MBES experience a decrease in efficiency as the swath widths shorten, requiring more track lines to be undertaken and increasing the cost (Costa *et al*., 2009).

1.9. Research aims

With increased interest in Ireland's macroalgal resource, there is a need to develop accurate, efficient and cost-effective baseline resource assessment methodologies for ecologically and economically important macroalgal species. The use of remote sensing technologies allows for larger areas to be surveyed than would be possible using traditional survey methods. This research sought to understand how these technologies could be applied for the assessment of macroalgae and what challenges and limitations were associated with this novel application.

The core of this research (**Chapters 2, 3, 4, 6**) focused on the use of optical remote sensing technologies to map *A. nodosum*, whilst **Chapter 5** explored the application of acoustic remote sensing technology for the mapping of subtidal kelp species. The challenges of spectrally discriminating between macroalgal species has previously been highlighted (Kotta *et al.*, 2014). In **Chapter 2** it was first necessary to quantify the spectral reflectance properties of common intertidal canopy forming macroalgal species through the creation of a spectral library. Further to this, seasonal sampling of reflectance spectra was conducted to determine whether there was an optimum time of year in which to conduct optical remote sensing survey based upon intra and inter-specific spectral variation. Seasonal variations in pigment concentrations within macroalgal species may lead to variations in the spectral response, potentially making different species more, or less, spectrally separable from one another. Ultimately, a set of hierarchical classification rules were created using classification and regression tree (CART) models to define a suitable subset of wavelengths that would allow for accurate discrimination between all sampled species for each season.

UAV-mounted hyperspectral remote sensing was then used (**Chapter 3**) to map the distribution of *A. nodosum* at a spatially and spectrally complex intertidal site. The high spectral and spatial resolution of these sensors provided the best opportunity to identify subtle spectral variations between species, allowing for their identification. Two supervised classification methods, Maximum Likelihood Classifier (MLC) and Spectral Angle Mapper (SAM), were used, one training using a spectral library and the other using image-derived spectra. The accuracy of drone-mounted hyperspectral remote sensing, and the two classifiers used to analyse the data, was assessed along with the effectiveness and accuracy of utilising high-resolution RGB imagery for the collection of training and reference data.

The technical complexity of hyperspectral sensors, for operation, processing and analysis, and their high cost made it prudent to explore the mapping capabilities of more affordable technology. Many commercially available multispectral sensors are lightweight, affordable and often easily integrated with UAVs and software, making them an accessible mapping solution. **Chapter 4** sought to compare the mapping capabilities, for *A. nodosum*, of

multispectral sensors mounted on a satellite, airplane and UAV, each offering distinct advantages and disadvantages. Like **Chapter 3**, high-resolution RGB imagery was also used to efficiently collect training and reference data.

Chapter 5 evaluates the applicability of applying acoustic remote sensing technologies to map the distribution of subtidal kelp species, which is often dominated by *L. hyperborea*. The ability of acoustic sonar to penetrate the water column much more effectively than optical remote sensing allows, in theory, a more accurate distribution map to be created which is not depth limited. Water column data have been highlighted as a useful method for accurate delineation of subtidal macroalgal canopies (McGonigle *et al*., 2011). Multiple frequencies of water column data were collected over a small kelp bed and ground-truthing was carried out using a drop-down camera to verify the presence and species composition of the kelp beds. The extraction of water column data should allow for the accurate area and height of the kelp bed to be determined, allowing the calculation of volume and, pending the establishment of linear relationships, biomass.

The application of UAV mapping techniques for intertidal macroalgal research is still in its infancy. The knowledge acquired in the previous chapters, combined with a detailed review of existing literature were integrated into **Chapter 6** where we sought to develop a comprehensive guide, not only on the most recent UAV and sensor technology but also how they can be applied to intertidal mapping. Specific focus was put on the unique characteristics of intertidal macroalgal assemblages and how these would influence the choice of UAV, sensor and operational parameters.

Publications

Rossiter, T., Furey, T., McCarthy, T., Stengel, D. (2020). UAV-mounted hyperspectral mapping of intertidal macroalgae, *Estuarine, Coastal and Shelf Science*, *242*, 1–16. **(Chapter 3 – unmodified from article)**

Rossiter, T., Furey, T., McCarthy, T., Stengel, D. (2020). Application of multi-platform, multispectral remote sensors for mapping intertidal macroalgae: a comparative approach, *Aquatic Conservation: Marine and Freshwater Ecosystems.* **(Chapter 4 – unmodified from article)**

Chapter 2: Temporal inter and intra-specific variation in spectral properties of intertidal brown macroalgal species

Drone image of *A. nodosum*, *H. elongata* and mixed fucoids during low tide in An Cheathrú Rua (Co. Galway)

Abstract

Monitoring intertidal macroalgal communities using optical remote sensing technologies will support their sustainable management over medium-to-large spatial scales. The effectiveness of optical remote sensors will depend, in-part, on developing a detailed understanding of the inter and intra-specific reflectance properties of macroalgal species, within and across seasons, to quantify their spectral separability from one another and identify temporal variation within these relationships. This study visited a single site in the west of Ireland and sampled the reflectance spectra of common canopy-forming intertidal macroalgal species across four seasons during 2018 and sought to distinguish, not only between macroalgal groups, but also between different brown species. A TriOS RAMSES spectroradiometer was used to record reflectance spectra over a wavelength range of 320 – 950 nm. For each season, the statistical separability between each species sampled during each season were quantified using a Classification and Regression Tree (CART) approach to define an optimal subset of wavelengths which enable spectral separation. Results show that it is possible to distinguish between the three macroalgal groups, and that for spring, summer and autumn it is possible to spectrally distinguish between the majority of common intertidal macroalgal species. Winter showed poor spectral separability between a number of common species. This study showed that seasonal variation in reflectance properties affected both the inter and intra-specific spectral relationships, thus highlighting the importance of the collection of concurrent spectral profiles and remote sensing data. Overall, the most suitable wavelength for discrimination between species, across all four seasons, was 500 – 575 nm.

2.1. Introduction

Macroalgae communities are some of the most productive and important systems on Earth (Dawes, 1998; Harley *et al*., 2012) and provide habitats for a diverse range of fish and invertebrate species (Bruno & Bertness, 2001; Davies *et al*., 2007; Mineur *et al*., 2015). They modify local hydrodynamic regimes, such as through dampening of water motion (Bunker *et al*., 2017) whilst providing coastal protection services (Løvås & Tørum, 2001). Intertidal macroalgal communities occupy the uppermost reaches of the marine realm and, by virtue of their location, face a raft of ever-increasing anthropogenic pressures (Mineur *et al*., 2015), including direct harvesting impacts. The effective management of these ecosystems requires a detailed understanding of their distribution through the collection of accurate, current, baseline data (Dekker *et al*., 2003). Traditional field survey methods, whilst highly accurate, are often time-consuming, intensive and limited in the spatial extent that can be efficiently covered (Kerr & Ostrovsky, 2003; Hamylton, 2017). This is often

compounded by the occurrence of species in spatially heterogenous and fine-scale communities, combined with difficulties in accessing and traversing the intertidal zone. Macroalgal communities within the Irish intertidal zone are structured by defined bands of vertical zonation and dominated by large brown macroalgal species of the order Fucales.

Remote sensing provides the ability to survey large, inaccessible areas and is more efficient, in terms of survey hours versus area covered, than on-foot methods (Gray *et al*., 2017). Remote sensing surveys have been used for macroalgal mapping for several decades and primarily used satellites (Cavanaugh *et al*., 2010; Casal *et al*., 2011; Bell *et al*., 2015) and planes (Bajjouk *et al*., 1996; Dekker *et al*., 2003; Pe'eri *et al*., 2008; Oppelt *et al*., 2012; Uhl *et al*., 2016) as the remote sensing platform. Recently, and despite several decades of use for military and agricultural applications (Watts *et al*., 2012), unoccupied aerial vehicles (UAVs) are now seeing increased uses as seagrass (Duffy *et al*., 2017) and macroalgal (Murfitt *et al*., 2017; Kellaris *et al*., 2019; Taddia *et al*., 2019) remote sensing platforms.

The chief challenge of using remote sensing technology for mapping macroalgal communities is to determine the best method for identifying species, in what are often spatially and spectrally complex environments (Cruzan *et al*., 2016), with intertidal macroalgal communities are often found in mixed assemblages. When found in mixed assemblages, this complexity can be measured in centimetres, with fronds from one species can be overlapping another or where a mosaic of different species occur, up to metres where homogenous stands of one species is interspersed by small aggregations of another (Webster *et al*., 2019). RGB sensors are a popular, low-cost way to conduct surveys (Buters *et al*., 2019), but their low spectral resolution makes discriminating between spectrally similar species difficult. Increasing the spectral resolution of sensors, and consequently the price (i.e. multispectral and hyperspectral), allows identification of distinctive spectral features (reflectance peaks and troughs), controlled principally, in visible wavelengths, by pigment composition and concentrations (Slaton *et al*., 2001). By recording the spectral reflectance properties of different macroalgal species, across the visible and non-visible electromagnetic (EM) spectrum, spectral libraries can be created, which can then be used to train supervised classification workflows to identify target species within a study site (O'Neill *et al*., 2011). It is important to try and mitigate potential source of variation in reflectance spectra. Structural variation within a sample, such as orientation of thalli and roughness, the reflectance properties of which are defined by bidirectional reflectance distribution function (BDRF), often require replicate sampling. The presence of water could also after spectral response, especially in the near-infrared (NIR) and there should be a process in place to ensure excess water is removed (Kotta *et al*., 2014). Diffuse illumination, a result of atmospheric (e.g.

solar angle) and terrain conditions (e.g. slope) should be recorded for different surveys if they are to be directly compared between (Schaepman-Strub *et al*., 2006).

Spectral sampling should include all features (i.e. macroalgae, substratum etc.) that are likely to be observable from a remote sensing platform. Strong seasonal variation within the pigment composition of intertidal macroalgae (Schmid *et al*., 2017) means that it is important to record the inter and intra-specific spectral relationships across seasons, identifying any season-specific variation in reflectance spectra, to support the provision of representative spectral training data for the habitat classification workflow. Inter-thallus variation in pigment content was observed by Stengel & Dring (1998) with shading resulting higher pigment content in the base of *Ascophyllum nodosum* individuals leading to it being darker in appearance compared to the tips, which experience more light. This inter-thallus variation could influence spectral response leading to potential misclassification if not properly accounted for in the creation of a spectral library.

The spectral properties of the three major macroalgal groups (**Fig. 2.1**), green (Chlorophyta), brown (Phaeophyceae) and red (Rhodophyta) have been well documented in the literature (Bajjouk *et al*., 1996; Vahtmäe *et al.*,2006; Uhl *et al*., 2013; Kotta *et al*., 2014) and are considered to be relatively simple to spectrally discriminate between (Kutser *et al*., 2006; Chao Rodríguez *et al*., 2017). All three groups contain chlorophyll-*a*, but variations in other chlorophylls, chlorophyll-*b* in green and chlorophyll-*c* in brown for example (Hurd *et al*., 2014), and accessory pigments such as carotenoids and phycobilins (Kotta *et al*., 2014), influence their unique spectral responses. Questions over the extent to which species within each group are spectrally separable from one another have been highlighted by previous studies (Kutser *et al*., 2006b; Casal *et al*., 2013).

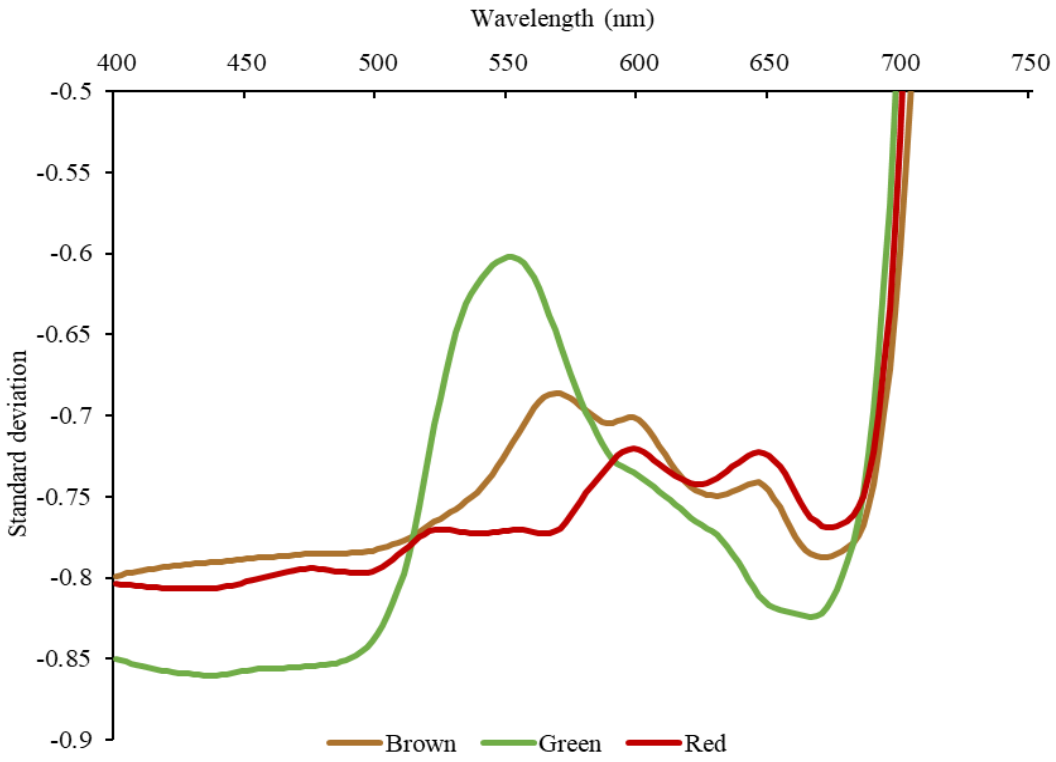

Fig. 2.1 Averaged spectral profiles for brown (*A. nodosum*), green (*Ulva* spp.) and red (*C. crisp*) macroalgal groups showing their characteristic spectral profiles. Spectra collected May 2018 from Carraroe.

Along North-eastern Atlantic rocky coastlines, many of the dominant canopy forming macroalgal species are brown (Lubchenco, 1980), which is also the case for the UK and Ireland (Stephenson & Stephenson, 1949), and this spectral similarity presents a challenge to remote sensing technology. To support the accurate mapping of these resources using remote sensing it is imperative that, not only are the spectral profiles of species within these environments recorded, but that the unique temporal spectral relationships between, and within, macroalgal groups are understood in detail and their spectral separability from one another determined. Understanding temporal variability in spectral response will allow for conclusions to be made on the suitability of different seasons for conducting mapping surveys. To achieve this, the following questions were addressed:

i. To what extent are canopy-forming brown macroalgal (shown in **Tab. 2.2**) species spectrally separable from one another across every season?
ii. What are the temporal impacts on the spectral separability between different macroalgal species?

iii. What are the implications of the spectral separability results for the planning of remote sensing surveys?

2.2. Methodology

2.2.1. Study Site

Reflectance measurements of macroalgal species were taken at Doleen Pier, near An Cheathrú Rua (Carraroe) (53°15’08’’N, 009°37’51’’W) which lies within Kilkieran Bay (Co. Galway), western Ireland (**Fig. 2.2**). Kilkieran Bay and Islands is designated as a Special Area of Conservation (SAC) due to the presence of mudflats and sandflats not covered by seawater at low tide and large shallow inlets, bays and reefs (Anon, 2015b). The primary underlying bedrock of the bay is granite (Könnecker & Keegan, 1983) and the low relief shoreline is dominated by rocky substrate which yields to muddy sediment in shallow waters (Sides *et al*., 1994). Water depths are shallow in the bay, ranging from 2–10 m inland to around 25 m at the entrance to the bay, with salinity ranging from 30–35 ppt (O’Donohoe *et al*., 2000). The entrance to the bay is exposed to the Atlantic Ocean and the prevailing southwest winds cause significant turbulence during stormy periods (Tully & O’Ceidigh, 1989).

There is a high abundance of *A. nodosum* and general high diversity of other canopy forming intertidal macroalgal species including *Pelvetia canaliculata*, *Fucus spiralis, F. vesiculosus*, *F. serratus* and *Himanthalia elongata* (all Phaeophyceae). Owing to its moderately exposed location in the mouth of the bay, and the presence of suitable substrata, the kelp species *Laminaria digitata* (Phaeophyceae, Ochrophyta) is present in the sublittoral zone. Red (rhodophyte) species, including *Chondrus crispus* and *Mastocarpus stellatus* are common in the canopy understory but do not form dense canopies that would be visible to a remote sensing platform. *Ulva* spp. (Chlorophyta) are occasionally found in small patches atop of the macroalgal canopy.

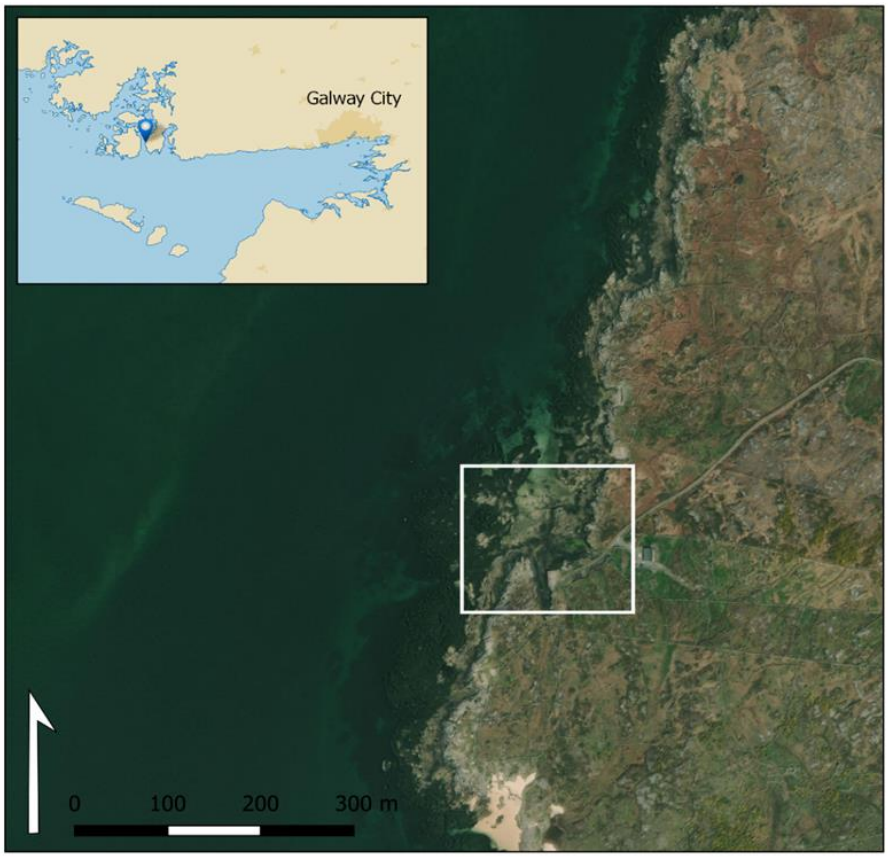

Fig. 2.2 Location of the sampling site at Doleen Pier in the context of Galway Bay (Co. Galway).

2.2.2. Spectroradiometer sampling

A spectroradiometer was used to record the spectral reflectance of dominant canopy forming intertidal macroalgal species and substratum *in-situ*. All reflectance measurements were carried out during low tide over a two-day period for each of the four sampling seasons (**Tab. 2.1**). A TriOS RAMSES Hyperspectral Radiance and Irradiance Sensor (TriOS Optical Sensors, Rastede, Germany) was used to collect spectral measurements from dominant intertidal macroalgal species (**Fig. 2.3**). Species were chosen if they represented a dominant canopy-forming species within the study site and these were all brown species. Representative species representing red and green macroalgal groups were also chosen to allow for a simple comparison between the reflectance spectra of the three macroalgal groups. The setup comprised of two sensors. The radiance sensor had a 7 ° field of view (FOV) recording 256 channels in the range of 320-950 nm, with a wavelength accuracy of 0.3 nm. The irradiance sensor had a cosine response with a 180 ° FOV and measures across the same wavelength range as the radiance sensor. The sensors were mounted on a frame, the irradiance sensor facing vertically upwards and the radiance sensor facing nadir, supplied by the company and was approximately 20 cm above the ground, providing a ground field of view (GFOV) of 4.8 cm^2. The sensors were connected to a control box (TriOS Optical

Sensors, Rastede, Germany), which was powered by a 12 V battery (Enersys, Reading, Pennsylvania). A HP Pavilion laptop (HP, Palo Alto, USA) was used to operate the proprietary MSDA_XE software which controls the sensors. All measurements were conducted on a wooden surface painted with ultra-black paint (Culture Hustle, London, UK) to reduce background noise (Dekker *et al*., 2003) and to reduce the impact of variation caused by different slope angles and terrain effects (Schaepman-Strub *et al*., 2006).

Tab. 2.1 Data of seasonal spectral sampling surveys. Time represents time of first measurement.

Season	Date	Time (GMT)	Solar angle zenith (deg)	Cloud cover (%)
Spring	28/05/2018	11:00	31	65
Summer	10/08/2018	11:30	52	27
Autumn	24/11/2018	14:00	82	71
Winter	05/02/2019	13:00	72	61

The limited portability of the radiometer meant that we could not measure samples *in-situ*, therefore target species were collected from the intertidal and brought to the pier in a bucket of seawater for measurement. Samples were collected at random from the easiest areas of the intertidal to access to ensure rapid collection. Samples were first shaken to remove excess water and then placed beneath the radiance sensor so that they covered the entire GFOV (Fyfe, 2003). Integration time was left set to automatic to account for slight variations in insolation. Our primary focus for spectral sampling was brown macroalgal species, as these represented the dominant canopy forming species present in the intertidal. Knowledge of the spectral separability of these dominant species is essential for supporting accurate remote sensing surveys. At our site green macroalgal species were not present year-round and, when present, often occurred in small patches. Red macroalgal species were almost exclusively sub-canopy, but we wanted to include spectra from both representative red and green species to corroborate, with existing literature, the spectral relationships between the three macroalgal groups. Only visually healthy specimens were collected that represented the general site condition for each species (Jiménez & Díaz-Delgado, 2015). For large species, such as *A. nodosum*, *F. vesiculosus* and *F. serratus*, one individual (comprised of multiple fronds) sufficiently covered the GFOV, but for smaller species such as *C. crispus* and *Ulva* spp., multiple thalli of individuals were combined during the measurements to ensure enough coverage. Ten replicate individuals were measured for each species and each of these was replicated three times, finally a single irradiance measurement was taken for each of the 10 replicates and this was carried out under constant light conditions. All

measurements were hemispherical-conical due to contributions from both direct and diffuse irradiance components (Schaepman-Strub *et al*., 2006). If there was significant intra-thallus colour variation, these were recorded as separate spectra, i.e. light and dark *A. nodosum* (typically the base and tips of the thalli which are exposed to different light regimes affecting their pigment composition). This may have importance implications for fine spatial resolution surveys as not properly accounting for this within-thallus colour variation could reduce the accuracy of the final classification as darker or light thalli sections could be misclassified as a different class. **Tab. 2.2** shows the different species measured in each sampling season. Herein, species will also refer to 'light' and 'dark' variants of a species along with its traditional definition. Species codes are shown in **Tab. 2.3**.

Prior to calculating reflectance, the raw radiance and irradiance (**Tab. 2.4**) spectra were linearly interpolated to a 2 nm step using a formula in Excel (Microsoft, Redmond, USA) (**Fig. S2.1**). This aligns the wavelengths, accounting for the slight differences in the wavelengths observed by each sensor, of the two sensors and addresses potential artefacts in the spectra associated with sharp change in signal, such as the oxygen absorption peak at 760 nm (Kutser, Pers. Comm.). Raw radiance was then converted into reflectance by dividing each radiance measurement by the corresponding irradiance measurement:

$$p\lambda = \frac{P(\lambda)}{P0(\lambda)}$$

Where *P* (λ) is radiance of the macroalgal sample and *P0* (λ) is downwelling irradiance.

Tab. 2.2 Species sampled during each season. Dark (D) and light (L) colour variants were sampled when species displayed strong intra-specific colour variation.

Spring	**Summer**	**Autumn**	**Winter**
Ascophyllum nodosum (D)	*Ascophyllum nodosum* (D)	*Ascophyllum nodosum* (D)	*Ascophyllum nodosum* (D)
Ascophyllum nodosum (L)	*Ascophyllum nodosum* (L)	*Ascophyllum nodosum* (L)	*Ascophyllum nodosum* (L)
Chondrus crispus	*Chondrus crispus*	*Chondrus crispus*	*Chondrus crispus*
Fucus serratus	*Fucus serratus*	*Fucus serratus*	*Fucus serratus*
Fucus spiralis	*Fucus spiralis*	*Fucus spiralis*	*Fucus spiralis*
Fucus vesiculosus	*Fucus vesiculosus* (D)	*Fucus vesiculosus*	*Fucus vesiculosus*
Himanthalia elongata	*Fucus vesiculosus* (L)	*Himanthalia elongata*	*Himanthalia elongata*
Laminaria digitata	*Himanthalia elongata*	*Laminaria digitata*	*Laminaria digitata*
Pelvetia canaliculata	*Laminaria digitata*	*Pelvetia canaliculata*	*Pelvetia canaliculata*
Sargassum muticum	*Pelvetia canaliculata*		*Ulva* spp.
Ulva spp.			

Tab. 2.3 Species codes used in Chapter 2 to refer to sampled species.

Species	Code
Ascophyllum nodosum (light variant)	ANL
Ascophyllum nodosum (dark variant)	AND
Chondrus crispus	C.crisp
Fucus serratus	Fserr
Fucus spiralis	Fspi
Fucus vesiculosus (light variant)	FVL
Fucus vesiculosus (dark variant)	FVD
Himanthalia elongata	Him
Laminaria digitata	Ldig
Pelvetia canaliculata	PelC
Sargassum muticum	Sarg
Ulva spp.	Ulva

Tab. 2.4 SI units used to define feature surface reflectance quantities.

	Units	**Description**
Radiant exitance	(M [W m^{-2}])	Radiant flux emitted by a surface per unit area.
Radiance	L [W m^{-2} sr^{-1}]	Radiant flux emitted, reflected, transmitted or received by a surface, per unit solid angle per unit projected area.
Irradiance	(E [W m^{-2}])	Radiant flux received by a surface per unit area.
Reflectance	$P(S_i, S_r, \lambda)$	Angular distribution of incident (S_i) and reflected (S_r) radiance.

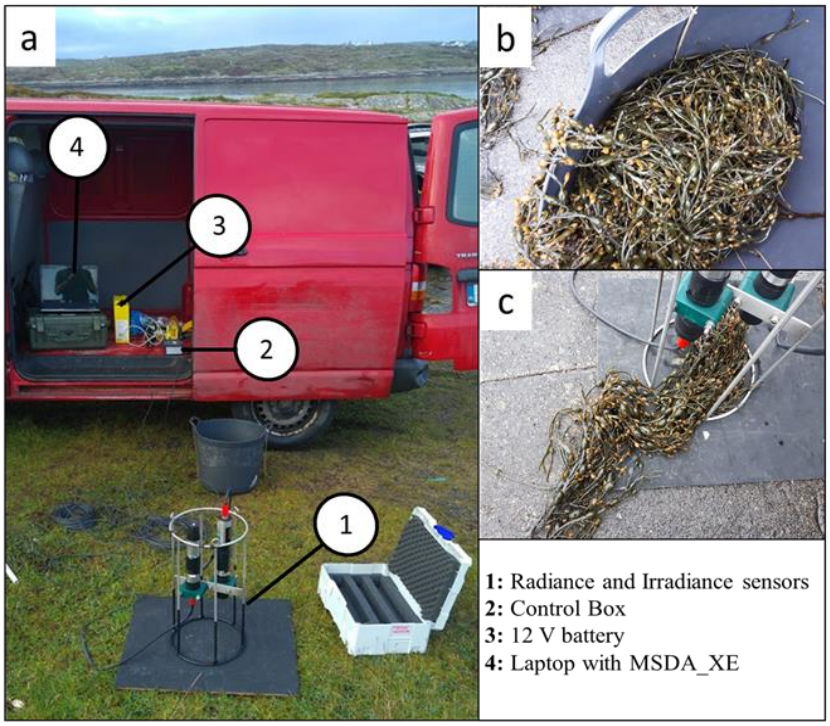

Fig. 2.3 The typical setup of the TriOS RAMSES Hyperspectral radiometer mounted on a frame supplied by the manufacturer (**a**). Samples are cut and placed in a bucket with water (**b**), brought to the pier immediately and measured, ensuring that the ground field of view (GFOV) of the sensor is fully covered (**c**).

2.2.3. Spectral Discrimination Statistics

To spectrally separate between the different common intertidal macroalgal species we followed the method developed by Kotta *et al.* (2014) to discriminate between macroalgal groups, which was also applied by Chao Rodríguez *et al.* (2017), also looking at macroalgal groups. Reflectance spectra were first standardised through subtracting the mean of all wavelengths from each individual spectrum and then dividing by the standard deviation of all wavelengths. Reflectance at each wavelength was treated as a distribution, meaning standardisation allows for the comparison of the relative differences in spectral variability and between different spectral profiles, as opposed to potential variation in intensity caused by slight changes in sun angle (which could occur during the survey) and canopy orientation (Dymond *et al*., 2001) for example, and is represented by the standard deviation of the original wavelength values (Kotta *et al*., 2014). In addition, Kotta *et al*. (2014) used standardisation to enable direct comparisons between submerged and emerged species reflectance data. In this case, the presence of water can dampen the reflectance spectra and it was important to determine that the reflectance profile of samples removed from *in-situ* submerged conditions for measurement were representative of *in-situ* reflectance. Through

standardisation we also hoped to account for variation in the amount of water present on the samples (despite shaking), which could have altered the true spectral signature of the sample.

Next, the optimal discriminatory boundaries between all pairs of species were identified. A Mann-Whitney U test was applied to identify those wavelengths, between species, that were statistically different from one another ($p < 0.05$). For those wavelengths where differences were identified, an optimal separating boundary was calculated using the True Skills Statistic (TSS) test, calculated using Spatial Data Calculator (SDC), developed by Remm & Kelviste (2014). TSS, traditionally used to assess the accuracy of weather forecasts, reports on the sensitivity, or the proportion of observed presences correctly observed as present, and the specificity, the proportion of observed absences correctly predicted as absent (McPherson *et al*., 2004). In this case, sensitivity refers to the proportion of one species being above the threshold and specificity for the proportion of the second species lying below the threshold (Chao Rodríguez *et al*., 2017):

$$\text{TSS} = \text{Sensitivity} + \text{Specificity} - 1$$

TSS ranges from -1 to +1 with the latter representing a perfect agreement, indicating good separability at the chosen wavelength (Allouche *et al*., 2006), and 0 or less for random decisions (Kotta *et al*., 2014). TSS also outputs the optimum discriminatory boundary between two sets of reflectance spectra where the mean proportion of false classification results for both sets of spectra is minimal (Kotta *et al*., 2014).

To identify suitable wavelengths that could allow for accurate discrimination between all sampled species (including light and dark *A. nodosum* and *F. vesiculosus*) ($p < 0.05$) the non-parametric Kruskal-Wallis test was used (in SDC). Perfect distinction between all species, as observed by Kotta *et al* (2014), was only achieved for some wavelengths, meaning that suitable wavelength ranges are chosen based upon their overall ability to discriminate between the species (i.e. are most species spectrally separable from one another within a chosen range?). Classification and Regression Tree (CART) models were then used, in Salford Predictive Modeler (SPM) (Minitab LLC, Pennsylvania, USA), to derive an optimal subset of bands, creating a set of rules for discrimination between target species. These decision-tree learning algorithms are flowcharts where each node represents a test on an attribute, in this case individual wavelengths, each branch represents the outcome of the test and each leaf is a class prediction (Han *et al*., 2012), i.e. species. CART models can be sensitive to noise which is why the Kruskal-Wallis was first performed to reduce the number of input bands (Han *et al*., 2012; Kotta *et al*., 2014). Owing to a relatively small sample size,

cross-validation was used for testing as it does not require setting aside data, rather it grows multiple replicate trees which each use 90 % of the data for model training and the remaining 10 % for testing, these separate error percentages are combined into a single test statistic. For each season, both full and subset CART models were created. Full models utilised all wavelengths within the investigated spectral range (400–750 nm) whereas subset models used wavelengths identified by the Kruskal-Wallis. Subset models that still allowed the same levels of discrimination between species were preferred over the full models. If required, models (full and subset) were simplified by pruning them to help prevent overfitting (Krzywinski & Altman, 2017).

2.3. Results

2.3.1. Spectral properties

For all four seasons, spectral measurements were recorded for brown, and a single red (*C. crispus*), macroalgal species, with green species only recorded in spring and winter (**Fig. 2.5**). *Sargassum muticum* was only sampled during spring (the only season it was observed). Across all seasons, brown macroalgal species showed a series of reflectance peaks around 580, 600 and 650 nm, with distinctive reflectance troughs present at 630 and 675 nm (**Fig. 2.5**). The chlorophyll-*a* absorption trough for *L. digitata* (Ldig), across all seasons, showed slightly increased variability, often occurring between 660–670nm (**Fig. S2.2**). *Chondrus crispus* (C.crisp) was characterised by two reflectance peaks around 600 and 650 nm, along with a reflectance trough at 675 nm (**Fig. 2.5**). Another trough at 580 nm helped to distinguish *C. crispus* from brown macroalgal species. In summer, *C. crispus* had a shoulder between 520–570 nm and a minimal trough at 580 nm. In spring and winter *Ulva* spp. was easily recognisable owing to a single reflectance peak centred on 550 nm, helping to distinguish it from both brown and red macroalgal species (**Fig. 2.5**). Whilst in spring, the chlorophyll-*a* absorption trough for *Ulva* spp. occurred between 670–675 nm, in winter it is centred around 655 (**Fig. S2.2**).

2.3.2. Seasonal spectral discrimination

CART model results provided a hierarchical set of rules to determine those wavelengths most suitable for spectrally discriminating between commonly found intertidal macroalgal species. Subset CART models were used for each season and were based on the results of the Kruskall-Wallis tests, which determined at which wavelengths each species was statistically different ($p < 0.05$) from all other species. Summer and autumn models could discriminate between all species sampled, with spring and winter unable to discriminate

between some brown macroalgal species (**Fig. 2.6**). **Fig. 2.4** shows the changes in colour, across the seasons for *A. nodosum* and *F. vesiculosus*.

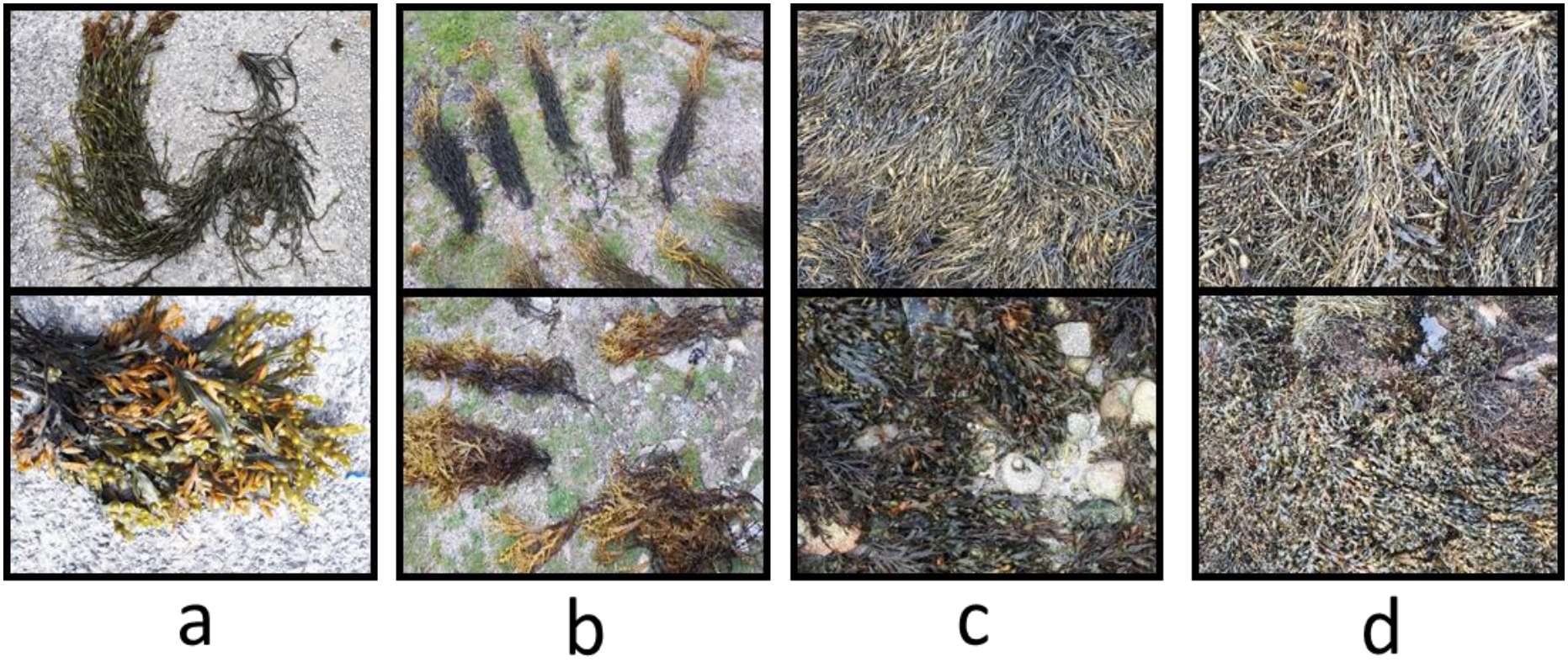

Fig. 2.4. Images showing the variation in colour for *A. nodosum* (top row) and *F. vesiculosus* (bottom row) across **a** Spring (May 2018), **b** Summer (August 2018), **c** Autumn (November 2018) and **d** Winter (February 2019).

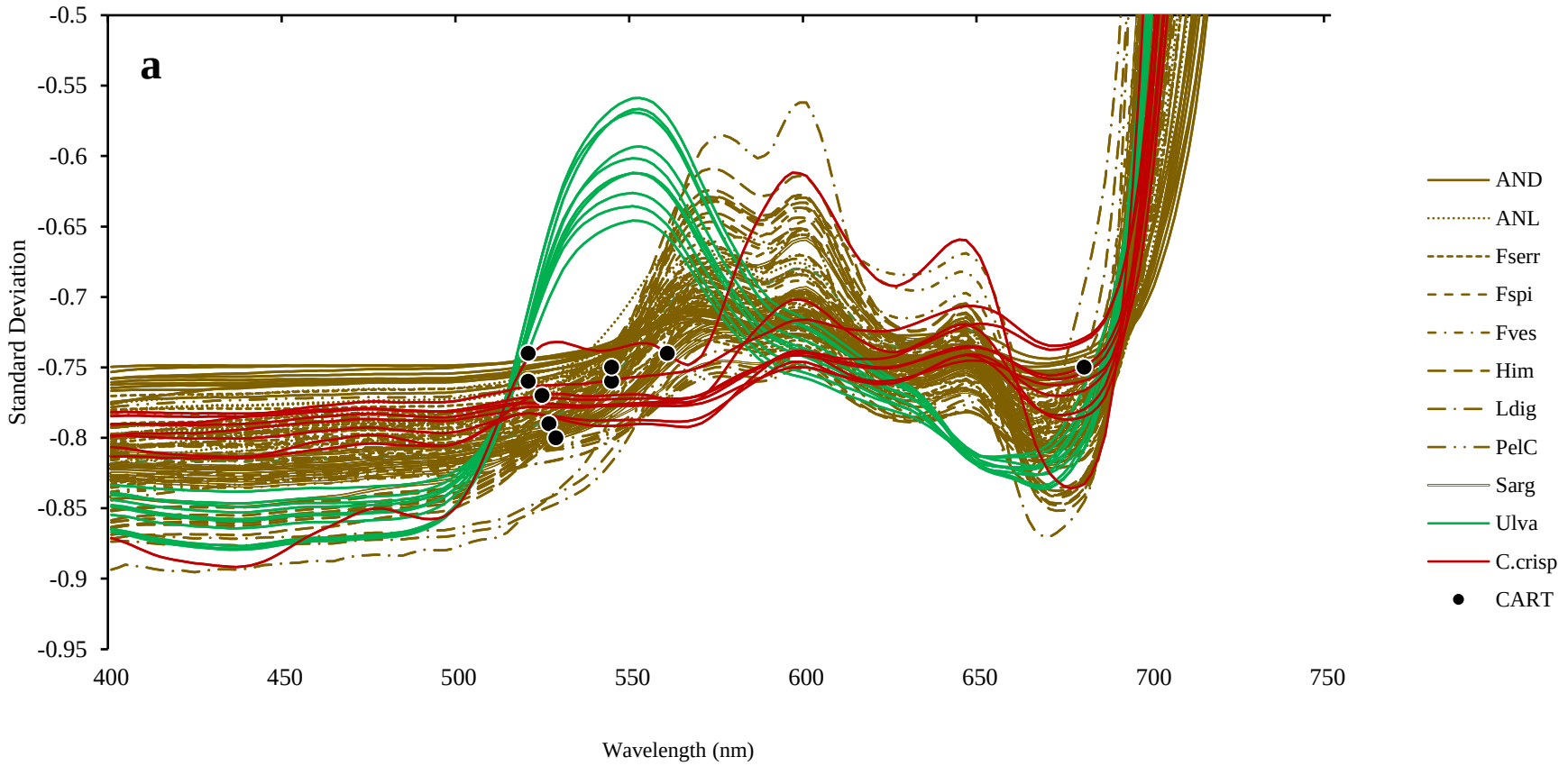

Fig. 2.5 Combined spectral profiles for all species (including replicates) across spring (**a**), summer (**b**), autumn (**c**) and winter (**d**). Black dots represent suitable separability wavelengths determined by CART models. Codes represent the following species; *A. nodosum* dark/light ('AND'/'ANL'), *Fucus* serratus ('Fserr'), *Fucus spiralis* ('Fspi'), *Fucus vesiculosus* ('Fves'), *Fucus vesiculosus* light/dark ('FVL'/'FVD'), *Himanthalia elongata* ('Him'), *Laminaria digitata* ('Ldig'), *Pelvetia canaliculata* ('PelC'), *Sargassum muticum* ('Sarg'), *Ulva* sp. ('Ulva'), *Chondrus crispus* ('C. crisp').

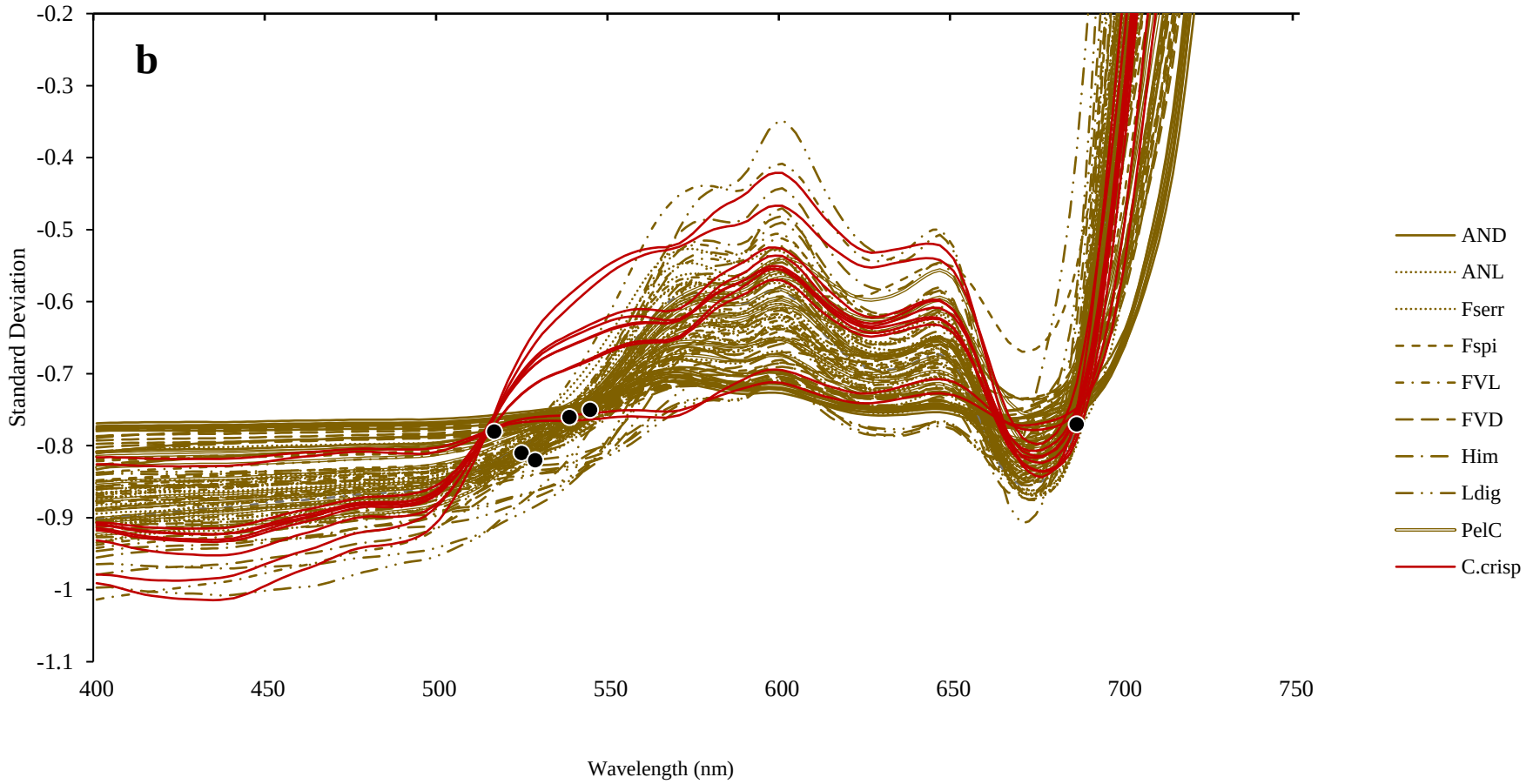

Fig. 2.5 (Continued) Combined spectral profiles for all species (including replicates) across spring (**a**), summer (**b**), autumn (**c**) and winter (**d**). Black dots represent suitable separability wavelengths determined by CART models. Codes represent the following species; *A. nodosum* dark/light ('AND'/'ANL'), *Fucus* serratus ('Fserr'), *Fucus spiralis* ('Fspi'), *Fucus vesiculosus* ('Fves'), *Fucus vesiculosus* light/dark ('FVL'/'FVD'), *Himanthalia elongata* ('Him'), *Laminaria digitata* ('Ldig'), *Pelvetia canaliculata* ('PelC'), *Sargassum muticum* ('Sarg'), *Ulva* sp. ('Ulva'), *Chondrus crispus* ('C. crisp').

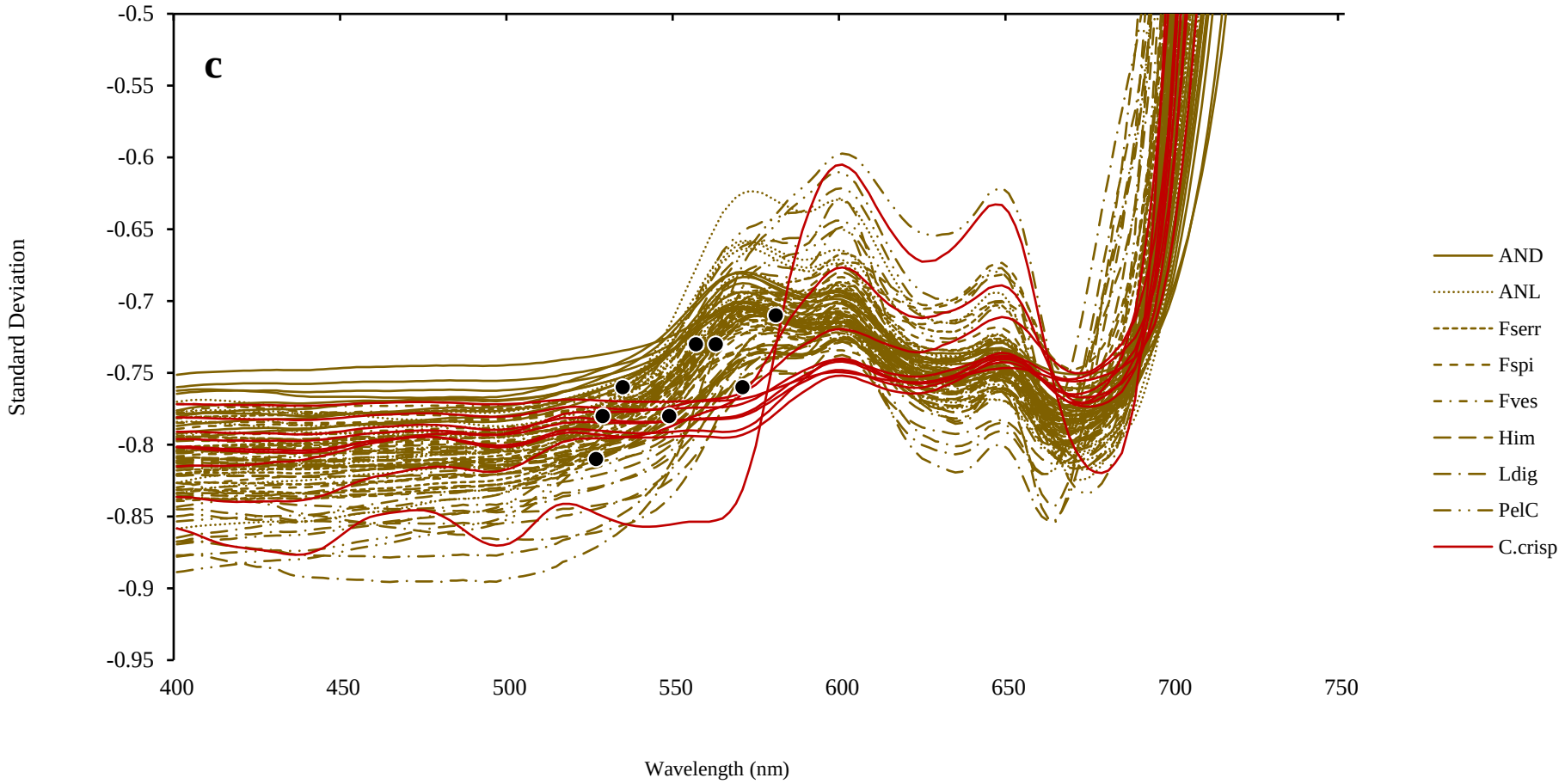

Fig. 2.5 (Continued) Combined spectral profiles for all species (including replicates) across spring (**a**), summer (**b**), autumn (**c**) and winter (**d**). Black dots represent suitable separability wavelengths determined by CART models. Codes represent the following species; *A. nodosum* dark/light ('AND'/'ANL'), *Fucus* serratus ('Fserr'), *Fucus spiralis* ('Fspi'), *Fucus vesiculosus* ('Fves'), *Fucus vesiculosus* light/dark ('FVL'/'FVD'), *Himanthalia elongata* ('Him'), *Laminaria digitata* ('Ldig'), *Pelvetia canaliculata* ('PelC'), *Sargassum muticum* ('Sarg'), *Ulva* sp. ('Ulva'), *Chondrus crispus* ('C. crisp').

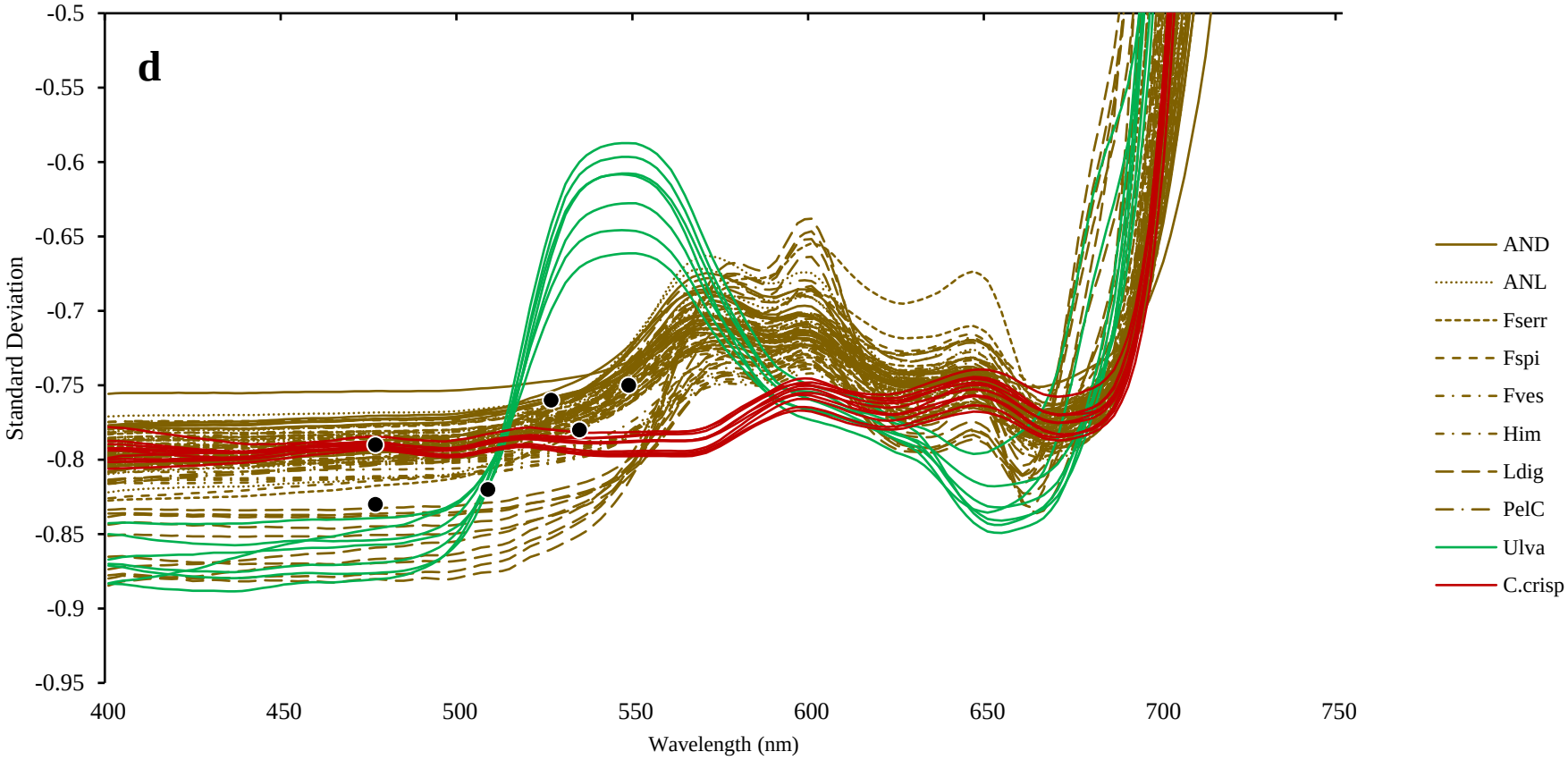

Fig. 2.5 (Continued) Combined spectral profiles for all species (including replicates) across spring (**a**), summer (**b**), autumn (**c**) and winter (**d**). Black dots represent suitable separability wavelengths determined by CART models. Codes represent the following species; *A. nodosum* dark/light ('AND'/'ANL'), *Fucus* serratus ('Fserr'), *Fucus spiralis* ('Fspi'), *Fucus vesiculosus* ('Fves'), *Fucus vesiculosus* light/dark ('FVL'/'FVD'), *Himanthalia elongata* ('Him'), *Laminaria digitata* ('Ldig'), *Pelvetia canaliculata* ('PelC'), *Sargassum muticum* ('Sarg'), *Ulva* sp. ('Ulva'), *Chondrus crispus* ('C. crisp').

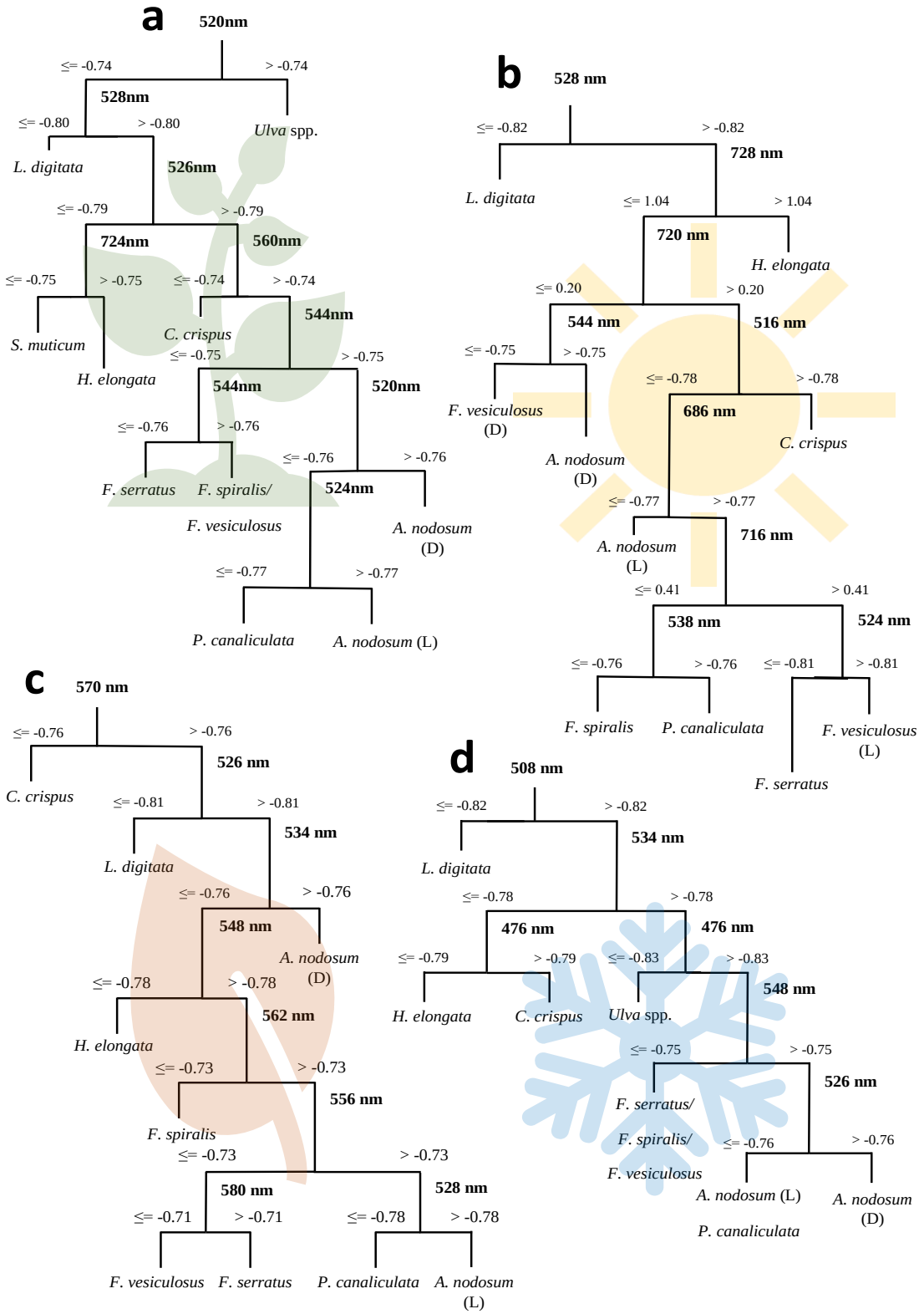

Fig. 2.6 Classification and Regression Tree (CART) models showing an optimum subset of wavelengths for discrimination between sampled species during spring (**a**), summer (**b**), autumn (**c**) and winter (**d**).

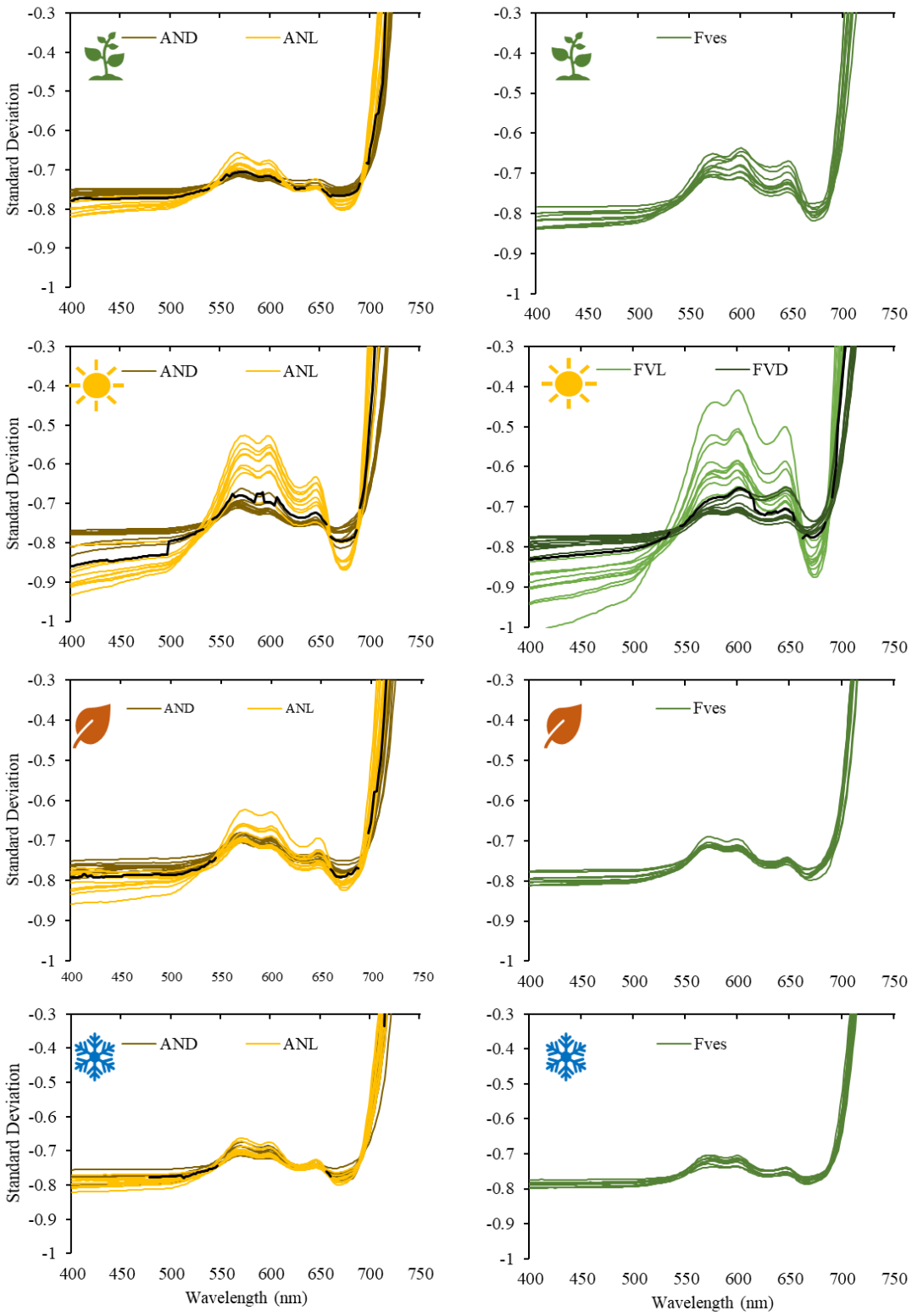

Fig. 2.7 Seasonal intra-specific variation for *Ascophyllum nodosum* light/dark (ANL/AND), *Fucus vesiculosus* (Fves) and *Fucus vesiculosus* light/dark (FVL/FVD) across spring (**a**), summer (**b**), autumn (**c**) and winter (**d**). The black line represents the optimum discriminatory boundaries between two samples as determined by TSS.

2.3.2.1. Spectral discrimination of spring-collected thalli

The subset spring model was used which showed good separation between most species sampled (**Fig. 2.6a)**. *Fucus spiralis* ('Fspi') and *F. vesiculosus* ('Fves') were the only two species not distinguishable from one another. Pairwise spectral separability results support this by showing these two species to only be separable over a very small wavelength range. Dark and light *A. nodosum* variants ('AND' & 'ANL') were separable over most wavelengths with notable features, for ANL, including a deeper reflectance trough at 675 nm and increased reflectance in over the 550–625 nm range (**Fig. 2.7a**). Wavelengths suitable for discrimination between most species were clustered within the 520–560 nm range.

2.3.2.2. Spectral discrimination of summer-collected thalli

All species were spectrally separable from one another using the subset CART summer model (**Fig. 2.6b**). Dark and light *A. nodosum* could be differentiated over most wavelengths with *A. nodosum* (light) ('ANL') showing increased reflectance over the 550–650 nm wavelength range (**Fig. 2.7b**). Dark and light *F. vesiculosus* variants ('FVD' & 'FVL') also showed the same separability pattern (**Fig. 2.6f**). Wavelengths that could be used to distinguish between different species were clustered into two groups of wavelengths, 520–550 nm and 680–730nm.

2.3.2.3. Spectral discrimination of autumn-collected thalli

The autumn subset CART model showed that all species were spectrally separable from one another (**Fig. 2.6c)**. *Ascophyllum nodosum* (dark) ('AND') and *A. nodosum* (light) ('ANL') could not be differentiated in the 550–650 nm wavelength range but could in the 400–550 nm range, whilst the characteristic deep reflectance trough at 675 nm remained for *A. nodosum* (light) ('ANL') (**Fig. 2.7c**). *Chondrus crispus* ('C. crisp') was easily separable from all brown macroalgal spectral signatures at 570 nm, corresponding to decreased reflectance in this region. Suitable spectral wavelength for separation between all species, as defined by CART, were clustered between 520–580 nm.

2.3.2.4. Spectral discrimination of winter-collected thalli

The pruned winter subset CART model was not able to discriminate between all species (**Fig. 2.6d**). There were two distinct groups, within which species could not be distinguished and these relationships were confirmed by the pairwise spectral separability tests. The first comprises *F. serratus* ('Fserr'), *F. spiralis* ('Fspi') and *F. vesiculosus* ('Fves') and the second, *A. nodosum* (light) ('ANL') and *P. canaliculata* (PelC). *Chondrus crispus* ('*C.*

crisp') and *Ulva* spp. were both distinguishable from each other and all other species at 476 nm. Dark *A. nodosum* ('AND') and light *A. nodosum* ('ANL') were separable from one another in the 475–550 nm range but not between 550–650 nm (**Fig. 2.7d**). Suitable wavelengths that allowed for separation between most species, excluding those discussed above, occurred between 475–550 nm.

2.4. Discussion

This study used a spectroradiometer to conduct temporal sampling of the spectral reflectance for dominant canopy-forming intertidal species (including colour variants observed in *A. nodosum* and *F. vesiculosus*). Understanding temporal and inter and intra-specific spectral variation is an important prerequisite for remote sensing surveys of intertidal macroalgal habitats. Knowledge of inter and intra-specific spectral relationships can help to determine the optimum time of year for surveying and help to inform the choice of classes (i.e. species or colour variants) to include within a spectral library. This study successfully applied a spectral separability methodology, developed by Kotta *et al*. (2014) who only looked at distinguishing between macroalgal groups, to identify, across four seasons, a suitable subset of wavelengths which enabled the discrimination between common intertidal macroalgal species, including within, and between, macroalgal groups. We demonstrate how distinguishing features within each species spectral profiles were characteristic of known pigment absorption wavelengths (Bajjouk *et al*., 1996; Dawes, 1998) and how these profiles corresponded to existing macroalgal profiles (Kutser *et al*., 2006; Uhl *et al*., 2013; Kotta *et al*., 2014). Further to this, we demonstrated that species within a macroalgal group (brown) could be successfully discriminated between in three out of the four sampling seasons, suggesting that it may be possible to do so during remote sensing surveys. However, as sampling was only conducted at a single site, we were unable to evaluate the impact of spatial variation (within a season) on our ability to spectrally discriminate between macroalgal species.

2.4.1. Spectral separability of brown macroalgal species

Our findings represent the first detailed investigation into the spectral separability of different brown macroalgal species and shows that it is possible to discriminate between them across three of the four seasons. Previous studies have highlighted the difficulties of spectrally discriminating between brown macroalgal species, both during reflectance spectra analysis (Kutser *et al*., 2006; Kotta *et al*., 2014) and during remote sensing surveys (Hennig *et al*., 2007) where species' spectral reflectance properties were considered too similar to

allow for discrimination. Perhaps our results should not come as too much of a surprise when considering the work of Fyfe (2003), who identified clear spectral differences between different species of seagrasses and Ullah *et al.* (2000), who achieved this for aquatic macrophytes (stands of *Typha*, *Phragmites* and *Scirpus*). The optimal wavelength range, observable in all seasons, for discriminating between all the sampled brown macroalgal species was between 500–575 nm, which was where fucoxanthin causes strong absorption. Variations in fucoxanthin content can be caused by temperature and light availability (Nomura *et al*., 2013) and fucoxanthin concentrations can also vary significantly between brown macroalgal species (Schmid & Stengel, 2015). Whilst the location of pigment absorption features varied little between the sampled brown species, and across seasons, it is apparent that varying concentration of accessory pigments, particularly fucoxanthin, may have been responsible for our success in spectrally distinguishing between them. As to what causes this variation in the first place, there could be a multitude of reasons, from thallus morphology (Hurd *et al*., 2014), localised hydrodynamic, temperature and light regimes to variations in emersion regimes (Ramus *et al*., 1976). The sometimes-mixed and fine-scale nature of intertidal macroalgal assemblages makes being able to accurately discriminate between species important for the accuracy of the resulting classification map. Such knowledge is also important when planning surveys as a desired taxonomic resolution needs to first be decided upon and knowledge of spectral relationships between species will help to determine both sensor and platform model and the desired spatial and spectral resolution required to identify features of interest.

2.4.1.1. Intra-thallus spectral variation

Two dominant canopy forming species displayed clear intra-thallus colour differences that varied between the seasons, *A. nodosum* and *F. vesiculosus*. These differences were sometimes visually striking when observed *in-situ* and quantifying their spectral separability would better help remote sensing surveys, especially those that collect high-spatial resolution data, such as UAV surveys.

Visually, there was variation in the colour of many species within, and across seasons. *Ascophyllum nodosum* showed a constant colour gradient from the tip (lighter) of the fronds to the base (darker) across all seasons and could always be spectrally distinguished from each other. The base of the thallus experiences less exposure to irradiance, owing to shading, than the tips, and the increased pigment concentrations increases absorption, leading to a darker appearance for the base (Stengel & Dring, 1998). In spring, individuals were green in colour and the difference between the tips and base was subdued whereas in summer, there

was a much stronger gradient with the tips yellow and the base a dark olive brown. The response to these varying light regimes was evident in the spectral profiles where light *A. nodosum* displayed significantly higher reflectance values across the 550–650 nm range in summer than in winter. In autumn there was still a strong colour gradient between the tips and base, but the tips were a much duller yellow than in summer. However, in winter the colour gradient was not readily apparent with the entire thallus and fronds a light olive brown colour. Yet, despite this the tips and base were still separable from one another in the 500–550 nm range. Across all seasons, apart from winter, light *A. nodosum* (lighter thalli) exhibited a lower reflectance trough at 675 nm than darker *A. nodosum* (darker thalli) indicating greater levels of absorption by chlorophyll-*a* (Kotta *et al*., 2014).

In spring, *F. vesiculosus* was a consistent olive brown and although there were yellower fronds, these were randomly located and there was no clear colour change gradient. In summer, as with *A. nodosum*, there was a strong colour gradient from lighter (upper thalli) to darker (lower thalli) and both colour variants were clearly separable across almost the entire visible wavelength range. The lighter upper thalli had consistently higher reflectance over the 550-650 nm wavelength range and a deeper chlorophyll-*a* reflectance trough at 675 nm compared to the darker, basal thalli. In autumn, *F. vesiculosus* was a consistent dark olive brown and was even darker in winter, and there was no obvious colour gradient in either of these seasons.

Identifying these intra-thallus spectral differences, and the seasons in which they occur, clearly indicates the need for season specific spectral profiles and may influence the choice of survey season. Both of these species are, in Ireland, common along intertidal rocky coastlines and knowledge about their unique intra-thallus seasonal spectral variation will likely improve the accuracy of remote sensing surveys. One may wish to choose a season where intra-thallus variation is minimal or non-existent to avoid potentially classification errors during a remote sensing survey. High-resolution imagery, such as that collected by UAVs, will increase the spatial and spectral complexity of the dataset (Adão *et al* (2017) by potentially making these spectral variations visible, leading to increased classification errors if they are not accounted for in the spectral library (Fyfe, 2003).

2.4.1.2. Spectral separability of macroalgal groups

Previous studies have demonstrated the spectral separability of the three macroalgal groups (Bajjouk *et al*., 1996; Kutser *et al*., 2006; Kotta *et al*., 2014) and our findings support their results. Several remote sensing studies have successfully applied this knowledge when mapping macroalgal communities at relatively broad taxonomic levels (Casal *et al*., 2012;

Oppelt *et al*., 2012; Brodie *et al*., 2018). In the visible wavelength region, the reflectance properties of macroalgae are determined, principally by the presence of photosynthetic pigments (Slaton *et al*., 2001). The three macroalgal groups are visually distinct from one another and it is the presence of different pigments that causes differences in their spectral profiles. Chlorophyll-*a* is present in the three macroalgal groups sampled and has two strong absorption peaks at ~435 nm and ~675 nm (Bajjouk *et al*., 1996). Chlorophyll-*b* is only found in green macroalgae (Dawes, 1998) and has *in vivo* absorption peaks at 480 nm and 650 nm, with the latter observable as a small dip in reflectance just before the main chlorophyll-*a* reflectance trough. With strong absorption occurring in the red and blue parts of the spectrum it is the broad reflectance peak, centring on 550 nm, which distinguished green macroalgal spectra from brown and red. The presence of the carotenoid fucoxanthin in brown macroalgae causes high *in vivo* absorption in the 500–560 nm range (Passaquet *et al*., 1991) and this enabled clear distinction from green macroalgae. The three reflectance peaks of brown species (570, 590 and 650 nm) were interspersed with a series of troughs which were attributed to absorption effects of fucoxanthin and chlorophyll-*c* (Uhl *et al*., 2013). Red macroalgae displayed a distinctive reflectance trough at ~570 nm, caused by phycoerythrin (Dawes, 1998), separating it from the green and brown groups. This feature was not apparent in the summer spectral profile where there is a steep shoulder instead which could be attributed to the bleached nature of many of the samples of *C. crispus* during this sampling season. Bleached *C. crispus* appeared significantly paler in colour through the loss of photosynthetic pigments such a chlorophyll due to oxidative stress (Bischof *et al*., 2003).

2.4.2. Optimal survey seasons

The remote sensing of vegetation communities requires consideration of the phenology of the different constituent species and how seasonal variations in this, alongside intra-specific variation, may determine the times of the year when the most accurate results can be obtained. Butera. (1978) found, that for coastal marsh vegetation, June and September were the best months for remote sensing surveys. This was due to differences in growth, for example, flowering and fruiting in September helped to distinguish between species. Li *et al*. (2019) determined April-May and December-February to be the best months for accurately mapping on-year and off-year Moso bamboo in China, which are characterised by different leaf and stem colours. In this study, for macroalgae, summer, autumn and, to a slightly lesser extent spring, appear to be the most suitable survey seasons regarding being able to spectrally discriminate between common intertidal species. Terrestrial studies have observed transition seasons, such as spring and autumn, as providing the best separation between broad-leaf tree species, however, winter can be useful for classifying evergreen tree species

(van Deventer *et al*., 2019). Winter appears to be the least suitable season in which to conduct habitat mapping of intertidal macroalgal communities. In winter, *Ascophyllum nodosum* (light) could not be distinguished from *P. canaliculata* at any wavelength. This could severely impact the classification accuracy of potential remote sensing surveys by misclassifying between a class that often dominates in the mid-intertidal zone (*A. nodosum*) and one that often occupies a thin horizontal band in the upper intertidal (*P. canaliculata*). During summer, variation in pigment concentrations between the tips of *A. nodosum* and *P. canaliculata* could be explained by different light regimes owing to higher levels of irradiance (Stengel & Dring, 1998), by virtue of increased emersion times, for species occupying higher zones. However, in winter, decreased irradiance levels and increased water turbidity would lead to both species having similar, higher, pigment concentrations owing to experiencing more similar irradiance conditions due to light limitation (Stengel & Dring, 1998). The presence of receptacles on *A. nodosum* may also have contributed towards the similarity. Pigment concentration for five intertidal macroalgal species, in Ireland, were shown to be at their greatest in winter, and lowest during the summer (Schmid *et al*., 2017). Spectral separation was, in winter, also not possible between *F. vesiculosus, F. serratus* and *F. spiralis*. Despite their different vertical distributions within the intertidal zone (Knight & Park, 1950), during winter these three species may experience more similar, lower irradiance regimes than in the other seasons, leading to more similar pigment concentrations compared to the rest of the year. *Fucus serratus* samples were collected further down the shore from *F. vesiculosus* ones and this may explain why differences are observed in spring through autumn, but not in winter as different light regimes may have affected pigment composition of the two species.

2.4.3. Implications for remote sensing surveys

Our results highlight the potential need for the creation of season specific spectral libraries and awareness of spatial influences on spectral response. Schmid *et al*. (2017) showed that the concentration and composition of pigments, in macroalgae, varied according to location and that there appeared to be spatial trend, suggesting that varying light and temperature conditions may have been responsible for the observed pigment variations. Whether separate spectral libraries should be created for distinct regions or a single spectral library can be created using multiple species replicates from different locations (Kotta *et al*., 2014) will depend on research objectives and must be the subject of further research. Future spectral library sampling should better account for atmospheric variation (e.g. cloud cover and solar angle) through standardisation of sampling conditions and should also consider the potential impacts of sensor inter-calibration. The mismatch of wavelengths between the radiance and

irradiance sensor, although partly corrected here through linear interpolation, may still create artefacts in the resulting reflectance profiles and intercalibration will allow for generation of absolute reflectance values (Anderson *et al*., 2006). Inter-calibration is also important if looking to directly compare reflectance spectra collected using different sensor models and can be done through comparing reflectance measurements of surfaces with known reflectance properties (Vabson *et al*., 2019). The creation of a spectral library serves a single objective, to support the collection of remote sensing data by under pinning supervised classification methodologies. The safety and effectiveness of remote sensing surveys requires other operational factors to be considered, chief of which being the weather (depending on geographic location). In temperate coastal regions unsuitable weather (wind, rain etc.) and storms can restrict the number of survey days, reducing survey efficiency (Duffy *et al*., 2017). Operationally, it would be more efficient to survey during those seasons where weather conditions are more suitable. Unpredictable, or changing weather conditions in the coastal zone can increase the risk of equipment damage or injury. In summary, the combination of poor spectral separability and inclement weather makes winter a potentially unsuitable season for the mapping of intertidal macroalgal communities.

2.5. Conclusions

Spectral libraries are a well-established source of training data for remote sensing surveys. The collection of spectral library data must be supported by an understanding of the relationship between, and within, species across seasons and how their pigment composition can vary owing to the seasonal variation in light conditions. In this study, spectral investigations concluded that it is possible, across most seasons, to discriminate not only between, but also within, macroalgal groups. Seasonal variations in the spectral response of species can affect interspecific spectral relationships which, in this study, meant that during winter it was not possible to distinguish between key canopy forming species.

This study has demonstrated the need for development of season-specific spectral libraries for intertidal macroalgal species. Data collection was limited to a single site, meaning that it was not possible to draw conclusions on the effects of spatial variation on spectral response. For remote sensing surveys over relatively small geographic areas (i.e. using a UAV) it may only be necessary to account for temporal, rather than spatial, spectral variation. Future research should explore both the spatial and temporal spectral response of macroalgal species, to confidently support large-scale remote sensing surveys.

Chapter 3: UAV-mounted hyperspectral mapping of intertidal macroalgae

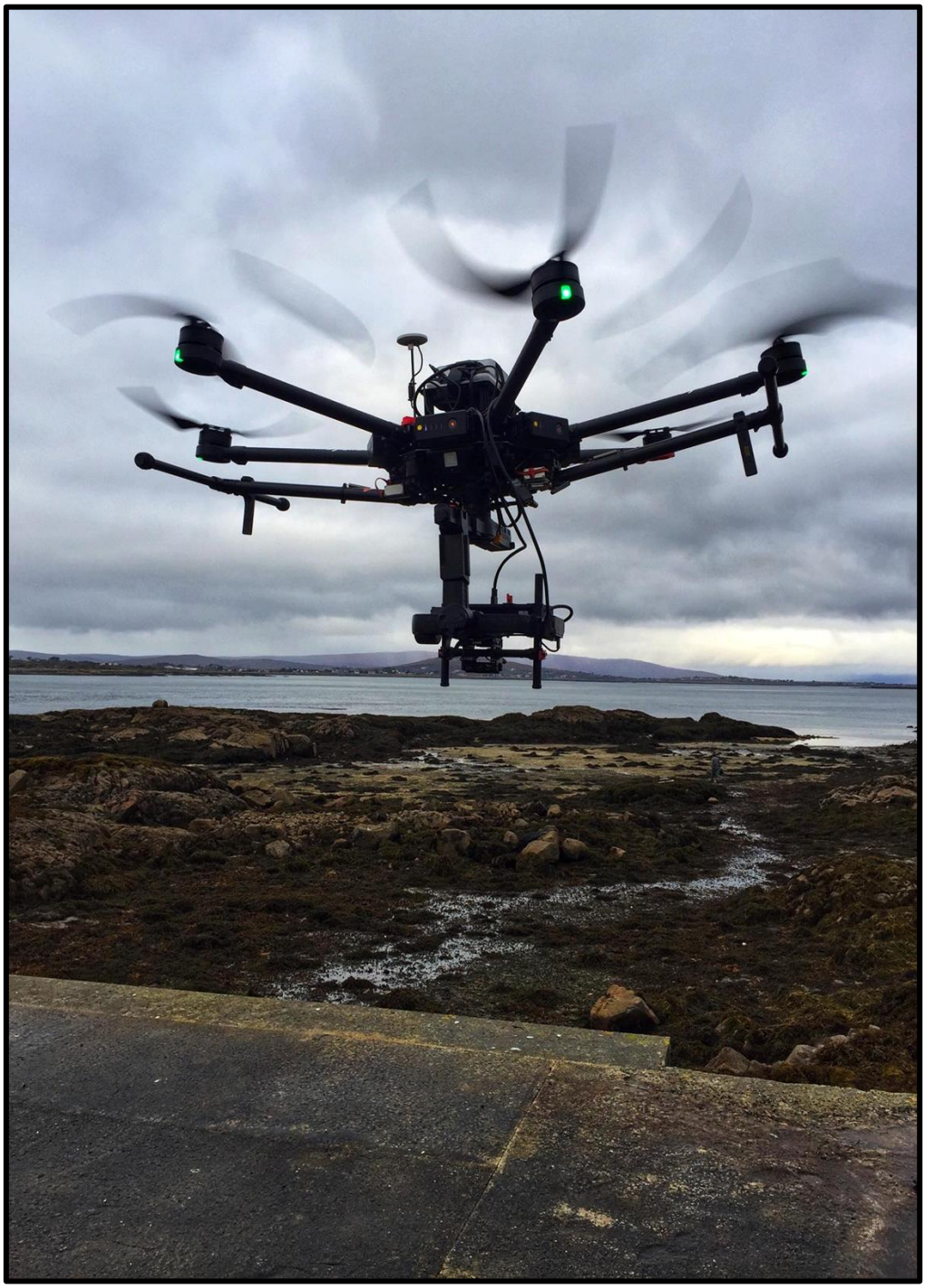

DJI Matrice 600 Pro carrying the BaySpec hyperspectral sensor during the December 2017 survey at An Cheathrú Rua (Co. Galway).

This chapter (unmodified) was published in the *Journal of Estuarine Coastal and Shelf Science*, 242, https://doi.org/10.1016/j.ecss.2020.106789

Author contributions

Thomas Rossiter, Dagmar Stengel, Thomas Furey and Tim McCarthy developed the research idea. Thomas Rossiter drafted the manuscript and all authors contributed to data collection and interpretation along with providing feedback on the manuscript.

Abstract

Intertidal macroalgal communities mark the boundary of the marine realm and are faced with many direct and indirect anthropogenic pressures. The effective and sustainable management of these resources must be underpinned by accurate, efficient and cost-effective environmental data collection. Traditional field survey methods, whilst accurate, are time-consuming and limited in the area that can be covered. Remote sensing permits large areas to be rapidly surveyed but the effectiveness of satellites and aircraft for mapping fine-scale intertidal macroalgal mapping is limited by their coarse spatial resolution and restricted operational flexibility. The rapid development of unoccupied aerial vehicle (UAV) and sensor technology can address these issues and provide a potential alternative to established remote sensing platforms. Here, a detailed methodology is presented for the assessment of the commercially and ecologically important intertidal brown macroalgae *Ascophyllum nodosum* using a multirotor UAV and pushbroom hyperspectral sensor. Two different classifiers, Maximum Likelihood Classifier (MLC) and Spectral Angle Mapper (SAM), were compared along with two different sources of spectral libraries, one collected *in-situ* with a spectroradiometer and the other derived from hyperspectral imagery. Of the classifiers compared, both trained using image-derived spectra, MLC more accurately classified *A. nodosum*, and other common intertidal species and substratum (Overall Accuracy (OA) 94.7 %) than SAM (OA 81.1 %). In addition, SAM, trained using *in-situ* spectra, was the least accurate of the three classifier workflows used (OA 71.4 %). The low accuracy of the spectroradiometer approach was likely due to high levels of noise present in the hyperspectral data, a result of the relative instability of the UAV platform causing vibration. The accurate mapping of non-target species also highlights the applicability of this methodology for a broader range of intertidal species and communities. This research clearly demonstrates the potential of UAV-mounted hyperspectral remote sensing for mapping the spatially and spectral complex macroalgal habitats found within the intertidal zone.

3.1. Introduction

Remote sensing allows for the monitoring of the Earth's surfaces and processes at a wide range of spatial, spectral and temporal scales, enabling patterns and relationships, once unobservable from the ground, to be studied (Kerr & Ostrovksy, 2003; Thenkabail, 2016). Monitoring environmental interactions, change and trends is increasingly important due to rising anthropogenic pressures (Bartholomé & Belward, 2005; Hennig *et al*., 2007). The intertidal zone occupies a unique location on the confluence of the marine and terrestrial realms for which a variety of monitoring techniques have been established (Chust *et al*., 2010; Leon *et al*., 2013). The intertidal zone offers a range of challenges for mapping activities with tides offering a limited time window in which to survey (Hamylton, 2017).

Intertidal macroalgal communities are important primary producers (Harley *et al*., 2012) providing habitat for a diverse range of ecologically and commercially important fish and invertebrate species (Bruno & Bertness, 2001; Vadas *et al*., 2004; Davies *et al*., 2007). With increasing anthropogenic pressures on coastal environments (Mineur *et al*., 2015), quantifying their distribution and the development of baseline data collection methods is important for the effective management of these ecosystems (Dekker *et al*., 2003). Many intertidal macroalgal communities, particularly along temperate rocky shores, are spatially and spectrally complex with species occurring in mixtures over fine spatial scales. This can make traditional field surveys costly, time-consuming and limited in the areal extent that can be efficiently covered (Kerr & Ostrovsky, 2003; Hennig *et al*., 2007).

Remote sensing can cover large and inaccessible areas, and often allows for repeat, standardised surveys of the same site (Casal *et al*., 2012; Thenkabail, 2016). The type of remote sensing platform used in habitat mapping is pursuant to research needs. Satellites are considered to have too coarse a spatial resolution to be effective in the intertidal zone (Costa *et al*; 2007; Oppelt *et al*., 2012; Brodie *et al*., 2018) although success has been achieved when mapping broad-scale, homogeneous canopy forming species such as kelp (Cavanaugh *et al*., 2010; Casal *et al*., 2011). Light aircraft are a common platform for intertidal mapping surveys as they afford higher spatial resolutions than satellites (Anderson & Gaston, 2013). Still, the relatively low spatial resolutions (~ $\geqslant$ 1 m^2) of these surveys (**Tab. S3.1**) means species discrimination has been difficult. Successful spectral separation between macroalgal groups has been achieved (Hennig *et al*., 2007) and homogeneous cover species have been accurately mapped (Pe'eri *et al*., 2008), yet identification to species level, particularly within groups, has not been achieved (Oppelt *et al*., 2012).

The rapid development of unoccupied aerial vehicle (UAV) technology, bringing decreasing costs, longer battery life and higher spatial resolutions (Colefax *et al*., 2017), could potentially make them a more cost-effective alternative to aircraft for habitat mapping (Johnston, 2019). Inexpensive UAVs have demonstrated their ability to assess the distribution of homogeneous cover species like intertidal seagrass (Duffy *et al*., 2018) and macroalgae (Murfitt *et al*., 2017). RGB-based classification techniques, such as object-based image analysis (OBIA), have also been used for mapping distinctive coastal habitats (Ventura *et al*., 2018), something made possible by the high spatial resolution of UAVs. The spatial and spectral complexity of intertidal macroalgal communities will require higher spectral resolutions than available with RGB sensors (Adão *et al*., 2017). This is an ideal environment to deploy hyperspectral remote sensors which, with their ability to record a narrow, contiguous spectrum for each pixel (Goetz, 2009), can greatly improve the spectral discrimination of different species.

To date, there are no published studies assessing intertidal macroalgal communities with UAV-mounted hyperspectral sensors. As of 2014, there were relatively few research groups actively deploying this technology in any capacity (Lucieer *et al*., 2014; Adão *et al*., 2017). The high-power consumption of hyperspectral sensors and their weight makes integration with UAVs difficult (Jakob *et al*., 2017) perhaps explaining the limited amount of research to date. Hyperspectral sensors also create huge volumes of data (Adão *et al*., 2017) requiring higher capacity compression (Herrero *et al*., 2015) or hardware solutions. The high spatial and spectral resolutions created with UAV-mounted hyperspectral remote sensing have been used to assess the health and vigour of Antarctic mosses which occur over highly fragmented, fine scales (Lucieer *et al.*, 2014), like those found in the north-east Atlantic intertidal zone. Full-frame hyperspectral sensors have been used for geological surveys (Jakob *et al.*, 2017), for feature classifications within mango orchards (Ishida *et al*., 2018) and to monitor acid mine drainage minerals (Jackisch *et al*., 2018).

Here, a UAV-mounted pushbroom hyperspectral remote sensor was deployed, supported by high-resolution RGB imagery, to assess the distribution of *Ascophyllum nodosum*, an ecologically and economically important intertidal brown macroalgal species found on moderately exposed to sheltered rocky coastlines (Åberg, 1992; Stengel & Dring, 1997). To support future, large-scale UAV surveys and resource management decision making, the following questions were addressed:

i. How effective is high-resolution, UAV-mounted RGB imagery for the collection of training and ground-truth data?
ii. Is there a supervised classification method that provides the most accurate result?

iii. Are supervised classifiers that utilise image-derived spectra more accurate than those using spectral library datasets?

iv. Can a UAV-mounted hyperspectral sensor distinguish *A. nodosum* from other common canopy forming intertidal macroalgal species?

This case study was undertaken at a site in western Ireland, considered both spatially and spectrally complex, with a high diversity of intertidal macroalgal species. Two different sources of spectral endmember data were applied to train supervised classifiers aiming to classify intertidal canopy-forming macroalgae. Two comparative investigations were conducted. The first, using a single source of spectral endmember data, sought to compare the ability of two common supervised classification methods to most accurately classify intertidal canopy-forming macroalgae. The second aimed to compare, using the same supervised classification method, two different source of spectral endmember data.

3.2. Methods

3.2.1. Study site

The study was carried out at Doleen Pier, near An Cheathrú Rua, (53°15'08''N, 009°37'51''W) which lies within Kilkieran Bay (Co. Galway), western Ireland (**Fig. 3.1**). Kilkieran Bay and Islands is designated as a Special Area of Conservation (SAC) due to the presence of mudflats and sand flats not covered by seawater at low tide and large shallow inlets, bays and reefs (Anon, 2015b). The Habitats Directive, under which SACs are designated, aims 'to maintain or restore the favourable conservation status of habitats and species of community interest' (NPWS, 2014). The primary underlying bedrock is granite (Könnecker & Keegan, 1983) and the low relief shoreline is dominated by rocky substrate yielding to muddy sediment in shallow waters (Sides *et al*, 1994). Water depths are generally quite shallow, ranging from 2-10 m inland to around 25 m at the entrance to the bay, with salinity ranging from 30-35 ppt (O'Donohoe *et al*., 2000). The entrance to the bay is exposed to the Atlantic Ocean and the prevailing southwest winds cause significant turbulence during stormy periods (Tully & O'Ceidigh, 1989).

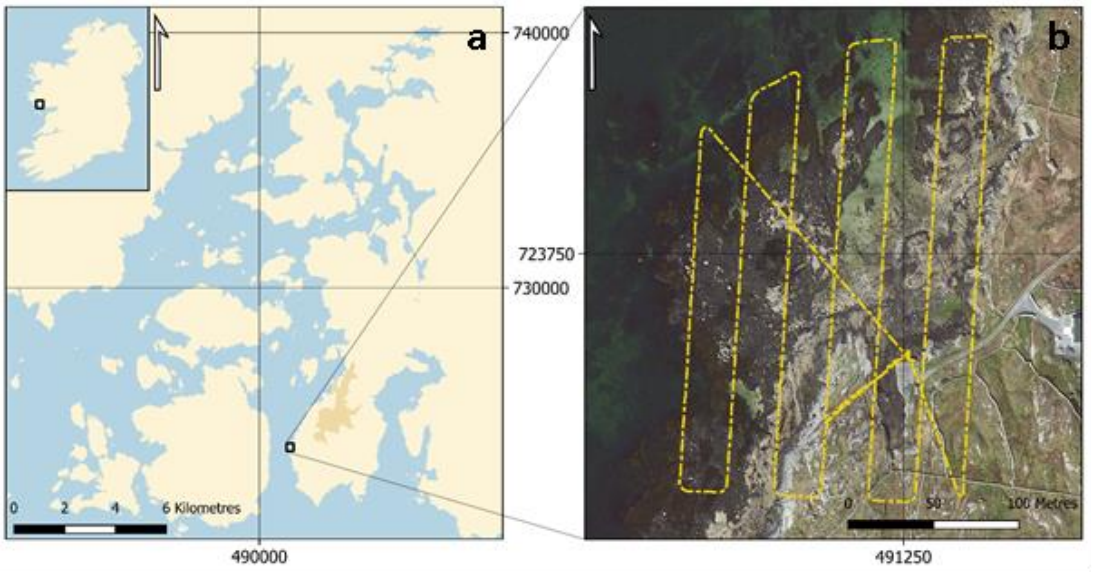

Fig. 3.1. Location of the study site at Doleen Pier in the context of Kilkieran Bay and Ireland (**a**). The yellow line marks the flight path of the RGB drone survey which covered a similar area as the hyperspectral survey (**b**). The total intertidal area shown in **b** is ~38,000 m^2. Coordinates are in Irish Transverse Mercator (ITM).

The study site was chosen because of the high abundance of *A. nodosum* and the general high diversity of other intertidal macroalgal species. Owing to its moderately exposed location in the mouth of the bay, and the presence of suitable substrata, the kelp species *L. digitata* (Phaeophyceae, Ochrophyta) is present in the sublittoral zone. The site is topographically complex, being dominated by granite bedrock with areas of mixed, sandy substrate. Common canopy forming species occurring at the site include; *Pelvetia canaliculata*, *Fucus spiralis*, *F. vesiculosus*, *F. serratus* and *Himanthalia elongata* (all Phaeophyceae) with red (Rhodophyta) species, including *Chondrus crispus* and *Mastocarpus stellatus*, being common in the understory. *Ulva* spp. (Chlorophyta) are occasionally found in small patches atop of the macroalgal canopy.

3.2.2. Remote sensing data

The UAV-mounted hyperspectral remote sensing survey was conducted on December 6th, 2017. Weather conditions were calm and dry with low wind (~13.5 km/h) and moderate cloud cover (67 %). A lightweight, pushbroom BaySpec OCI^{TM}-F Ultra Compact Hyperspectral Imager (BaySpec Inc. San Jose, USA) was used which collects data within a spectral range of 400-1000 nm, containing 124 bands and having a spectral bandwidth of ~4 nm. The sensor has a 21° field of view (FOV) and weighs ~570 g. There was no built-in irradiance sensor to correct for variations in insolation during the flight and calibration was

performed prior to each flight, first using a white standard to adjust for exposure and then dark reference by covering the lens. Integration time was set to ~2 milliseconds as there was moderate cloud cover. The sensor was mounted, using a custom three-axis gimbal mount, on a DJI Matrice 600 Pro (DJI, Shenzhen, China), which has a maximum unladen flight time of ~30 min when using the TB47S Intelligent Flight Batteries (DJI, Shenzhen, China). The sensor was connected to an Intel NUC (Intel Corporation, Santa Clara, USA), mounted atop of the UAV. Whilst on the ground this was connected to a laptop containing the proprietary SpecGrabber software allowing data recording parameters to be modified. DJI Go software (v.3.1.23) was used to plan and control the flight plan which was designed to cover a subsection of the site (~30,000 m^2) in order to balance out limitations of data storage and variation in cloud cover and insolation. Flight height was set to 60 m with a velocity of ~15 km/h (to ensure high overlap between scanlines), resulting in a ground sampling distance (GSD) of ~1.8 cm/pixel. Image overlap was set at 90 % for the side (each parallel flight line). Despite moderate passing cloud cover, surveys were conducted only during windows of constant light conditions. To maximise the spatial resolution of the resulting data, 60 m was the minimum flight height that still allowed for the desired survey area to be covered. As there were passing clouds, the survey only took place during periods of clear sky to avoid shading. Approximately 21,500 m^2 was covered in 10 flight lines.

A DJI Inspire 1 (DJI, Shenzhen, China), flown within 30 min of the hyperspectral survey, was used to collect high-resolution RGB imagery with a built-in 12-megapixel Zenmuse X3 camera which has a 94° FOV. This UAV has a maximum flight time of 18 min and was controlled using MapPilot (v.2.7.0) (Drones Made Easy, San Diego, USA). The survey was also conducted at 60 m, using a 70 % side and front overlap, resulting in a GSD of 2.6 cm/pixel and a total of 95 images taken. At 60 m flight altitude, an area 72,000 m^2 was surveyed.

Nine ground control points (GCPs) were deployed to accurately geo-reference the data. Each GCP consisted of a 50 x 50 cm black board with a white cross and a centre point easily visible from the air, the coordinates of the centre point were recorded using a Trimble R8 post processing kinematic (PPK) global navigation satellite system (GNSS) unit (Trimble, Sunnyvale, USA). GCPs were spaced evenly throughout the site with one in each corner of the survey area and the others spaced to reflect topographical (i.e. vertical) variation. GCPs were post-processed using Trimble Business Centre (v. 5.00, Trimble, Sunnyvale, USA).

3.2.3. Data processing

RGB imagery was processed using Pix4D Mapper (Pix4D, Lausanne, Switzerland) and GCPs were imported in to enhance georeferencing accuracy and avoid layer co-registration errors (Bentoutou *et al*., 2005) which was important for operating in a fine scale spatially heterogenous environment. An average root mean square (RMS) error of 0.017 m was achieved.

BaySpec's CubeCreator (BaySpec Inc. San Jose, USA) software was used to process the raw hyperspectral imagery into hyperspectral cubes. To aid with the processing workflow data were processed in sections, with each section containing the data from individual survey flight lines. Light and dark calibration standards were used to convert at sensor radiance values to reflectance using the empirical line approach (Smith & Milton, 1999). The relationship between digital numbers (DN), which is the format that the sensor records data in, and at-sensor radiance is assumed to be linear. This allows for the accurate conversion to reflectance values, the accuracy of which can, however, be influenced by the quality of calibration targets (Barreto *et al*., 2019). The hyperspectral cubes created by CubeCreator (BaySpec Inc. San Jose, USA) had no geographic information as the sensor contained no GPS, thus they required georectification, which was achieved through image-to-image georectification using the orthorectified RGB imagery as, owing to noise present in the data, it was not possible to clearly observe any of the nine GCPs deployed on site. Georectification was conducted manually using the Georeferencer tool available in QGIS (v.3.4.1). Preliminary examination of the data revealed that there was a significant degree of noise present in the hyperspectral dataset. This noise is a function of the pushbroom hyperspectral such as scanline errors (Hruska *et al*., 2012), slight variations in irradiance levels and the instability of the UAV platform (Rasti *et al*., 2018). The impact of this noise was most pronounced near the edge of each hyperspectral strip. For this reason, the edges of each strip were first removed using a 0.5 m buffer and strips were then resampled, using bilinear interpolation, to a coarser resolution (6.5 cm^2/pixel) to compensate for noise within the remaining image. This resolution was chosen as it appeared to best alleviate the impact of the noise present whilst providing a spatial resolution that would capture the fine spatial scales present within the intertidal zone. Coarser spatial resolutions may have increased to risk of the spectral mixing of signatures within individual pixels, without providing further noise alleviation. Resampling to coarser resolutions will also reduce file size, addressing issues arising from limited computer processing power (Grohmann, 2015). Finally, data strips were then mosaicked together into a single raster layer using Image Composite Editor (ICE) (Microsoft, Redmond, USA). A miscalculation of the hyperspectral sensor FOV, or

the incorrect FOV value being entered, led to gaps occurring between the data strips, as the desired overlap was not achieved, meaning full site coverage was not obtained.

3.2.4. Hyperspectral classification

3.2.4.1. *In-situ* spectral profiles

The classification workflow is highlighted in **Fig. 3.2**. Reflectance measurements of intertidal macroalgae and substratum were carried out using a TriOS RAMSES Hyperspectral Radiance and Irradiance Sensor (TriOS Optical Sensors, Rastede, Germany). The radiance sensor has a 7° FOV, recording 256 channels between 320-950 nm with a wavelength accuracy of 0.3 nm. The irradiance sensor had a cosine response with a 180° FOV and measures across the same wavelength range as the radiance sensor. Both sensors were mounted on a frame supplied by the company, and the radiance sensor was approximately 20 cm above the ground giving a ground field of view (GFOV) of 4.7 cm^2. The irradiance sensor was mounted facing upwards and so that the tip was just above the frame, minimising the risk of shading. The sensors were connected to a control box (TriOS Optical Sensors, Rastede, Germany), which was powered by a 20 kg, 12V battery (Enersys, Reading, Pennsylvania). A HP Pavillion laptop (HP, Palo Alto, USA) was used to operate the proprietary MSDA_XE software controlling the sensor. All measurements were conducted on a wooden surface painted with ultra-black paint, which has extremely low reflectance in the visible wavelength range, to reduce background noise (Dekker *et al*., 2003). Seven common intertidal macroalgal species and one substratum type were sampled (**Tab. 3.1**). **Fig. S3.1** shows the setup of the spectroradiometers.

For each monospecific collection, ten individual seaweed samples were measured, and each measurement was replicated three times to mitigate slight variations in insolation and morphological variations within samples (Dekker *et al*., 2003). A single irradiance measurement was taken for each of the ten samples. Each replicate was placed below the radiance sensor ensuring that it covered an area larger than the GFOV (Fyfe, 2003). Integration time was set to automatic to account for slight variations in insolation. Raw radiance was converted into reflectance by dividing each radiance measurement by the corresponding irradiance measurement (Kotta *et al*., 2014). The ten spectral profiles (each consisting of three replicates) for each species were then averaged to create a single species spectrum. Individual spectra were then formatted in a .csv file to be imported into the spectral library builder and each averaged spectrum was resampled to the wavelength range and scale of the hyperspectral imagery using ENVI 5.4 (Harris Geospatial Solutions, Boulder, USA).

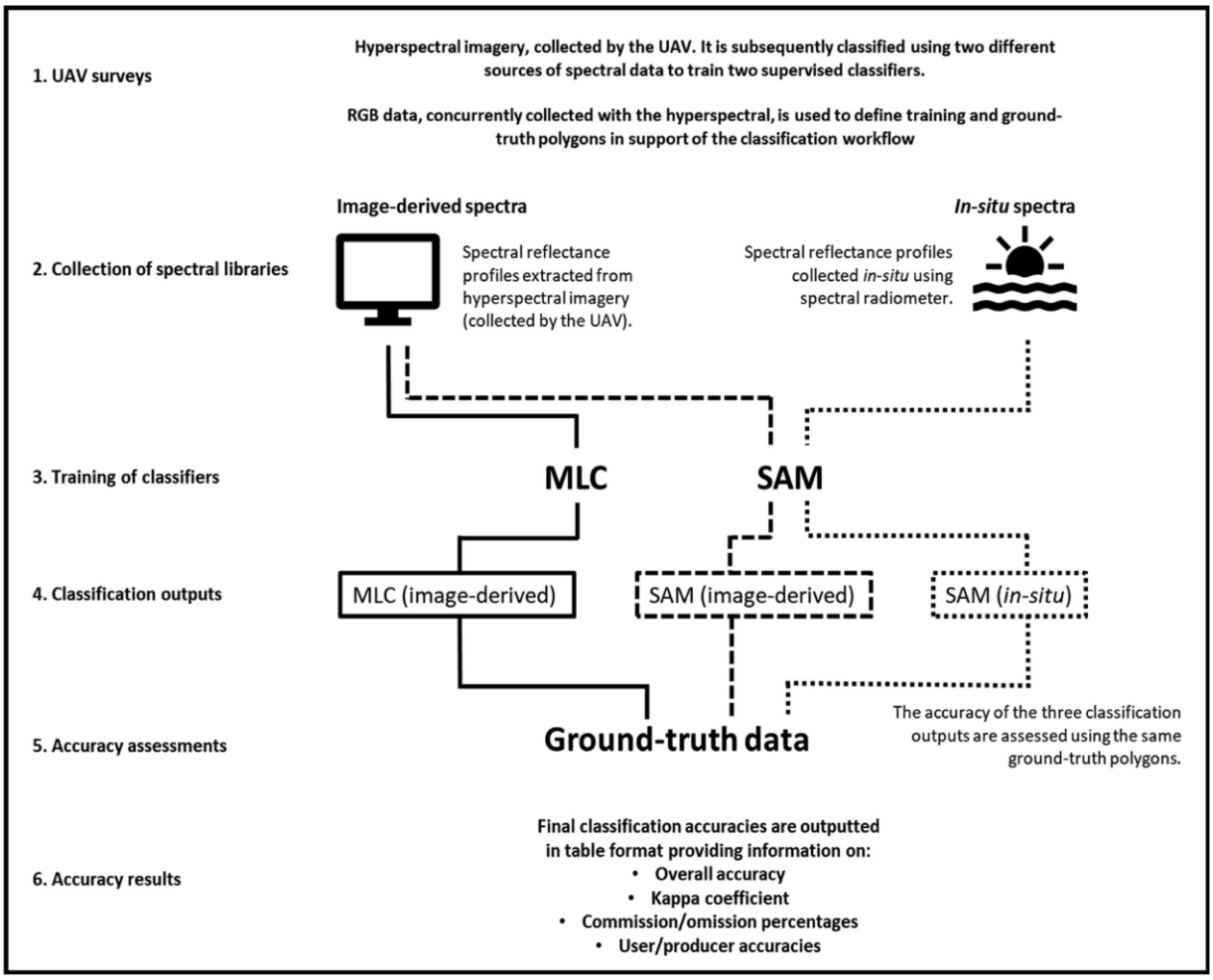

Fig. 3.2. Diagram showing hyperspectral classification workflow once the UAV data has been collected and processed.

Tab. 3.1. Spectral endmember classes collected using the hyperspectral image data and spectral library approaches. Habitat classes are listed under Class Code**.** *Fucus vesiculosus*, *Fucus spiralis* and *Fucus serratus* were combined into a single category '*Fucus* spp.'.

Image-Derived	Spectral Library	Class Code
Ascophyllum nodosum	*Ascophyllum nodosum*	Asco
Fucus vesiculosus	*Fucus vesiculosus*	-
Fucus spiralis	*Fucus spiralis*	*Fucus* spp.
Fucus serratus	*Fucus serratus*	-
Pelvetia canaliculata	*Pelvetia canaliculata*	PelC
Himanthalia elongata	*Himanthalia elongata*	Him
Laminaria digitata	*Laminaria digitata*	Kelp
Substratum	Substratum	Substratum
Submerged	-	Submerged
Ulva spp.	-	Green

The weight of the sensor and associated components (the battery weighed 20 kg) made it impractical to measure reflectance spectra *in-situ*, so samples were cut and then immediately brought to the radiometer measurement area. They were carried in a container filled with seawater and were then shaken, prior to measurement, to remove excess water yet ensure that samples remained hydrated. The removal of samples (i.e. not *in-situ*) for spectral reflectance sampling is a common method that has been used to derive representative macroalgal spectral profiles for spectral library comparison studies (Kutser *et al*., 2006b; Uhl *et al*., 2013; Kotta *et al*., 2014; Chao Rodríquez *et al*., 2017) and for the training of hyperspectral remote sensing classifiers (Dekker *et al*., 2003; Barillé *et al*., 2010; Casal *et al*., 2013; Dierssen *et al*., 2015). To better understand the effects of sample removal on changes (or lack thereof) in spectral response a small pilot study was conducted to compare the spectral properties of *A. nodosum* that was first measured *in-situ* before being cut and then taken to the measurement area, following an analytical method developed by Kotta *et al*. (2014). *In-situ* sampling was conducted first. The radiometer was setup in close proximity to dense assemblages of *A. nodosum* and a 25 m radius was established around the radiometer (determined by cable length from sensor to control unit). Within this 25 m zone, five one m^2 quadrats were randomly placed and ten spectral measurements (each replicated three times) were taken of the *A. nodosum* canopy in each quadrat. After *in-situ* sampling was completed, *A. nodosum* individuals, corresponding to the locations of the first, fifth and tenth i*n-situ* measurement for each quadrat, were removed from the five sampled quadrats and brought to the measurement area where three replicates of each were sampled using the same steps highlighted in section ***2.4.1***. The statistical workflow, described in detail by Kotta *et al* (2014), showed there to be only minor variation in the spectral response of *A. nodosum* for the measurement methods (**Fig. S3.2.**). Where small differences were observed, True Skills Statistic (TSS) indicated a far from perfect separation between the two classes. This demonstrated that the removal of individuals did not significantly affect their spectral response and that their spectral signatures could be considered representative of those found *in-situ*.

3.2.4.2. Image-derived spectral profiles

Image-derived endmember spectra were obtained by using the RGB as a reference dataset, with ENVI 5.4 (Harris Geospatial Solutions, Boulder, USA), allowing for the identification of different species before extracting spectral information from the aligned hyperspectral layer. The usefulness of this approach was noted by van Iersel *et al*. (2018), especially when accounting for species not easily observable in the field. This method is also advantageous over utilising field mapping techniques to create training areas when considering scaling up

of data collection to larger areas. It is less time consuming and costly, allowing much larger areas to be covered than possible on-foot during the same period of time (Gray *et al*., 2018). Training area polygons were created for areas where individual classes were easily identifiable such as dense stands of *A. nodosum* (Class code = 'Asco') which were clearly recognisable through their yellow/pale green colour and the distinctive pattern created by the fronds, resembling a field of long grass blown flat by the wind (**Fig. 3.3**). The number of training polygons per class was dependent on the observable area of that class and the area of each training polygon depended on the extent of homogeneous class cover Larger and more homogeneous cover classes had more numerous, larger training areas than smaller or less frequently occurring classes (**Fig. S3.3**). Areas that provided a 'pure' spectral signature were preferred over mixed assemblage areas. *F. vesiculosus, F. serratus* and *F. spiralis* were combined into a single class, '*Fucus* spp'. These species were also combined in the spectral *in-situ* spectral library dataset. The similar, 'shrubby' nature of these species leads to a mottled appearance in the RGB (**Fig. 3.3**) and it was hard to confidently discern between them. *Laminaria digitata* and *H. elongata* were visually distinct from all other intertidal features and thus, were also included as separate classes ('Kelp' & 'Him'). The spectral properties of the varying site substrates (rock, sand & mixed sediments) are relatively similar to one another and sufficiently distinct from macroalgae that they are combined into the 'Substratum' class (**Fig. S3.5)**. Water was not present in the hyperspectral data aside from a few large rockpools which contained submerged macroalgae. Since visual identification of the macroalgae was difficult and the presence of water would likely distort the signal (Zoffoli *et al.*, 2014) it was decided to include a 'Submerged' macroalgal class (this class was not present in the spectral library and no attempt was made to identify species) in order to separate it from identifiable intertidal macroalgal classes. In total, eight classes were identified (**Tab. 3.1**).

The spectral separability of endmember classes was determined prior to running a supervised classification algorithm. An assessment of the mathematical separability of the classes was performed to assess whether sufficient and representative training data have been selected (Richards & Jia, 2006). Training data were checked for class separability using the Jeffries-Matusita Distance (Carrasco-Escobar *et al*., 2019). The values of the resulting output between each pair of classes range from 0 to 2 with values greater than 1.9 indicating almost perfect separability between them (Richards & Jia, 2006). Good class separability would indicate that sufficient training areas have been selected, whereas values approaching zero would indicate either the need for more training areas or that two classes were inherently similar in their spectral properties. This could then indicate that the two classes could potentially be combined (Thomas *et al*., 2003).

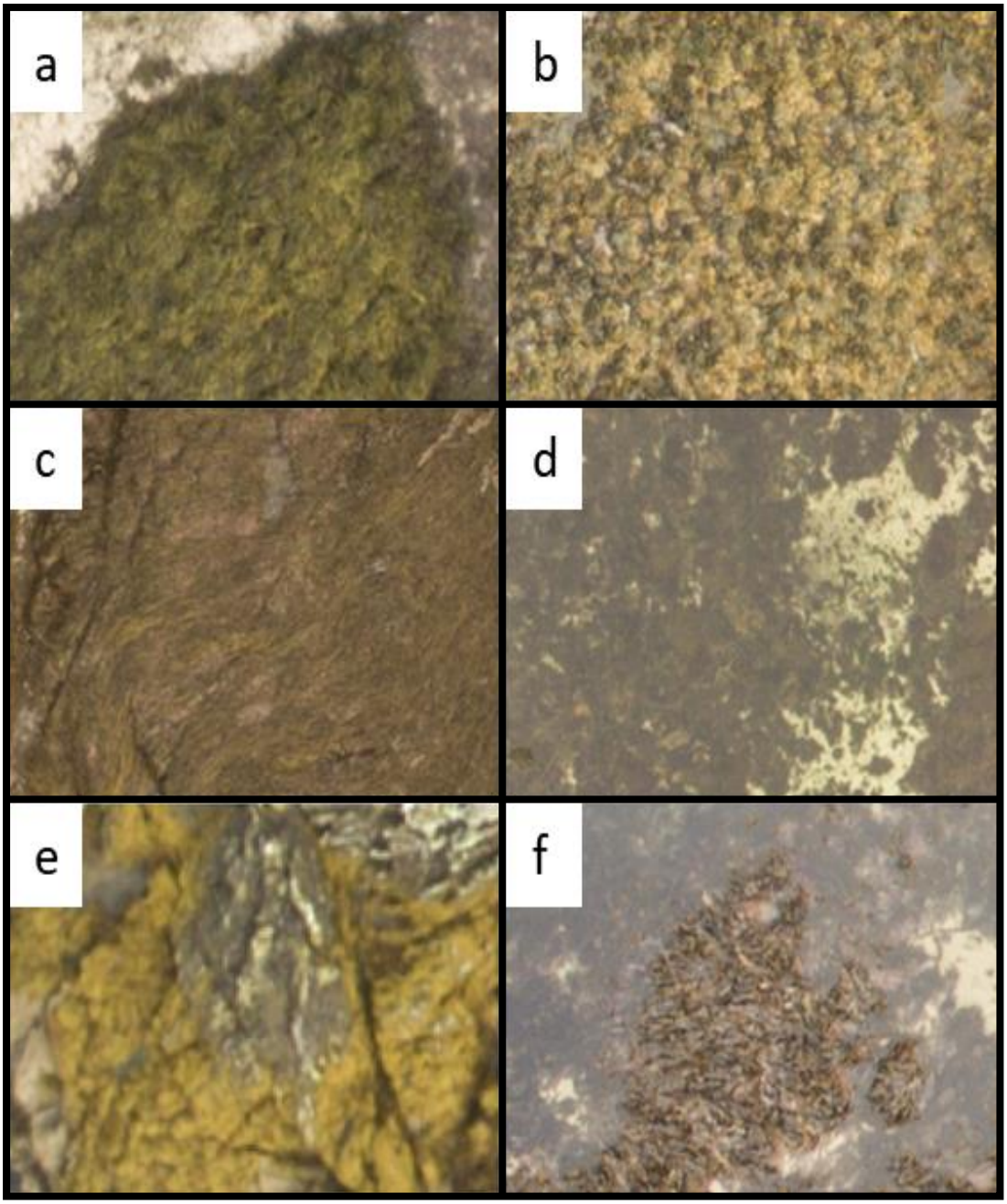

Fig. 3.3. Sections of high-resolution RGB drone imagery showing *Ascophyllum nodosum* (**a**), *Fucus* spp (**b**), *Himanthalia elongata* (**c**), Submerged macroalgae (**d**), *Pelvetia canaliculata* (**e**), *Laminaria digitata* (**f**). The distinctive morphological properties of each species were used to identify each of them from the RGB drone imagery.

3.2.4.3. Supervised classification workflows

Two supervised classification methods were used in ENVI 5.4 (Harris Geospatial Solutions, Boulder, USA), Maximum Likelihood Classification (MLC) and Spectral Angle Mapper (SAM). MLC is a popular classifier (Paola & Schowengerdt, 1995) which calculates the probability that an individual pixel belongs to a specific class and is based on an estimated

probability density function derived from the defined reference classes (Foody *et al.*, 1992). The MLC classifier assumes a Gaussian distribution for each of the inputted training classes (Jia & Richards, 1994) and can be expressed by the following equation:

$$g_i(x) = \ln p(\omega_i) - \frac{1}{2}\ln|\sum_i| - \frac{1}{2}(x - m_i)t\,\Sigma_i^{-1}(x - m_i)$$

Where *i* is class, *x* equals *n*-dimensional data, $p(\omega_i)$ is the probability that class ω_i occurs in the image and is assumed the same for all classes, $|\sum_i|$ is the determinant of the covariance matrix of the data in class ω_i, Σ_i^{-1} is the inverse matrix and m_i is the mean vector.

SAM identifies the spectral similarity of a pixel's spectrum to that of a reference spectrum which can either be collected using a radiometer or taken from an image (Kruse *et al.*, 1993). This technique seeks to reduce the dimensionality of the hyperspectral data by ignoring the magnitude of pixel vectors in hyperspectral space and instead classify using their angular orientations (Yang *et al*., 2008). Each pair (reference and classification) of spectra is treated as a vector in n-dimensional space meaning that their similarities can be compared regardless of differences in brightness (Yuhas *et al.*, 1992). SAM is expressed by the following equation, taken from Kruse *et al.* (1993):

$$\alpha = \cos^{-1}\left[\frac{\sum_{i=1}^{nb} t_i r_i}{(\sum_{i=1}^{nb} t_i r_i)^{\frac{1}{2}}(\sum_{i=1}^{nb} t_i r_i)^{\frac{1}{2}}}\right]$$

Where *t* is the spectra for a pixel, *r* is for the reference spectrum pixel, α is the spectral angle between *t* and *r* (measured in radians or degrees) and n is the number of bands.

The classification accuracy of the two classifiers was first compared using the image-derived spectra (**Tab. 3.1)** as inputs for both MLC and SAM. Average spectral reflectance curves first had to be extracted from the image-derived training data as SAM requires endmember spectra, unlike MLC, which calculates covariance and probabilities from training polygons. No thresholds were selected so that all pixels would be classified, and spectral separability results were used to determine whether sufficient training areas had been selected to be representative of features present at the site (Richards & Jia, 2006).

After the accuracy of two different classifiers, both using the same training spectra, were compared, the two different sources of training data, image-derived and *in-situ* spectral library (**Tab. 3.1)**, were compared using SAM. The image-derived spectra were processed in the same manner as in the previous comparison. Spectra for green and submerged macroalgae were not collected for the *in-situ* spectral library and were not used in the

classification workflow. No thresholds were applied so that every pixel was classified, and direct comparisons could be made between the two classification outputs.

3.2.4.4. Accuracy assessment

Ground-truth, or reference, data were derived from the high-resolution RGB imagery utilising the same rationale as for the training data collected for the MLC (**Fig. S3.4**). The accuracy of this approach was noted by Lechner *et al.* (2012) and was also found to be more reliable and accurate than GPS-based validation methods, primarily owing to GPS error (Laliberte & Rango, 2011). Reference data collected from *in-situ* field observations are considered the most accurate, however this can be time consuming meaning that data derived from imagery are more common (McDermid *et al*., 2005; McRoberts *et al*., 2018). Polygons were created for each of the eight (MLC) and six (SAM) classes and this was carried out independently of those used to create the training areas using ENVI 5.4 (Harris Geospatial Solutions, Boulder, USA). Polygons were created so that they covered as much of each class as possible and only in areas where homogeneous class coverage could be confidently identified. The accuracy assessment tool was used to create the confusion matrix and derive quantitative measures of accuracy (i.e. kappa, user/producer accuracy, errors of commission/omission).

3.3. Results

3.3.1. Spectral properties of macroalgal species

For both image derived spectral and spectral library reflectance spectra there were similar key characteristics present (**Fig. 3.4**). Image derived spectra appear to be heavily affected by noise when compared to spectral library profiles. All brown macroalgal species contain three characteristic peaks (580, 600, 650 nm) as well as a trough at 675 nm. The 'Green' spectral profile (image-derived only) had a single peak at 550 nm which was visible despite the noise present in the profile. 'PelC' had a very distinctive profile in both sets of reflectance spectra where its reflectance was higher than that of other brown macroalgae. 'Kelp' was also distinct as the chlorophyll-*a* absorption trough occurred around 665/670 nm in contrast to 675 nm for the other species. 'Submerged' and 'Kelp' had very similar profiles in the imaged-derived spectra with 'Submerged' having higher reflectance across the entire spectrum. The relationship between 'Asco' '*Fucus* spp' and 'Him' varied between both sets of spectra. The spectral library revealed 'Asco' and '*Fucus* spp' to be more similar and 'Him' relatively distinct, whereas the image derived data shows 'Asco' to be more distinct and '*Fucus* spp' and 'Him' to be more similar.

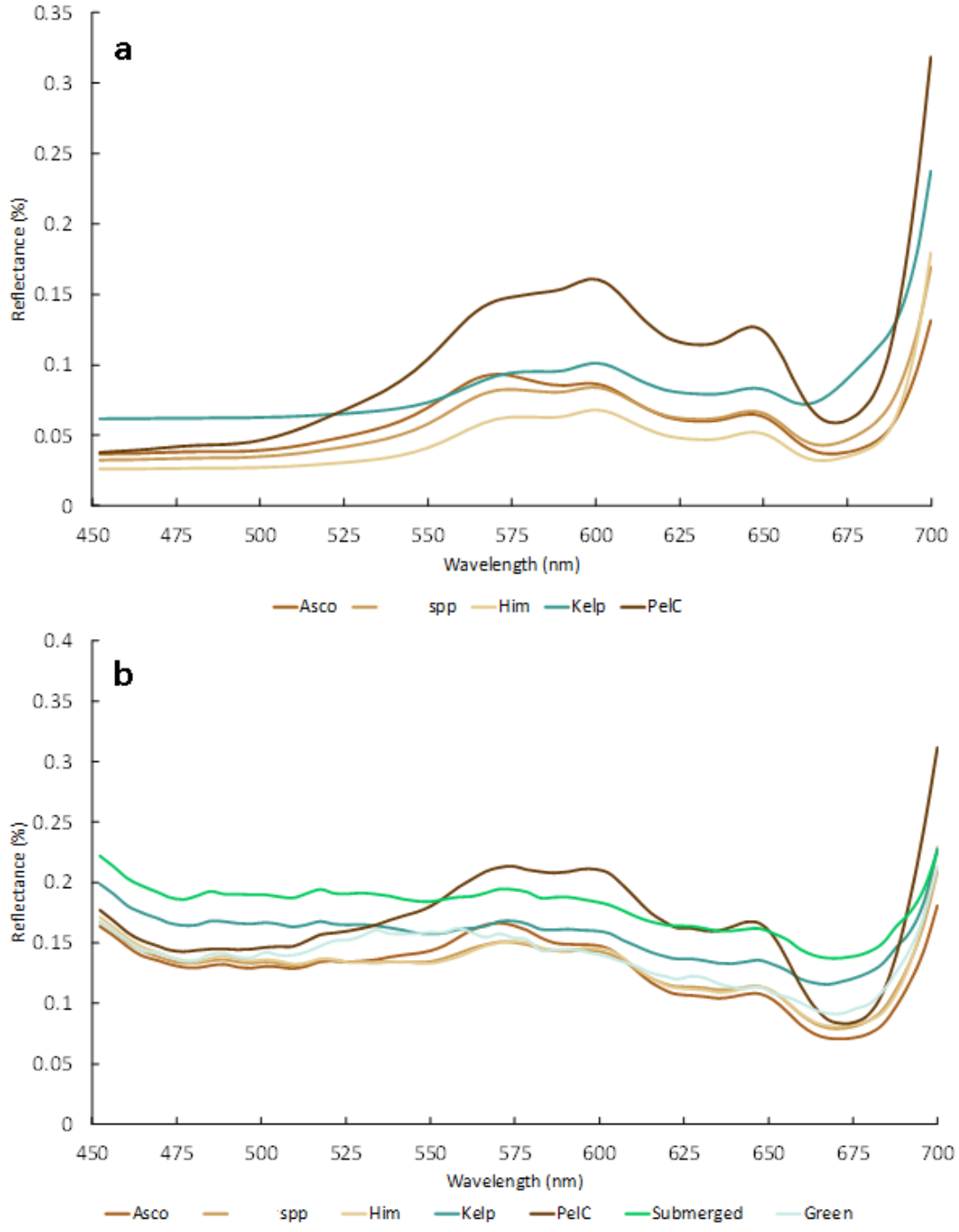

Fig. 3.4. Spectral profiles of species derived from the Spectral Library (**a**) and Image-derived Spectra (**b**). The wavelength range was chosen to highlight key spectral properties present within the visible portion of the electromagnetic spectrum. Class codes represent the following species. *Ascophllum nodosum* (Asco), mixed fucoids (*Fucus* spp.), *Himanthalia elongata* (Him), *Laminaria digitata* (Kelp), *Pelvetia canaliculata* (PelC), submerged macroalgae (Submerged) and unidentified green macroalgal species (Green).

3.3.2. Supervised classification results

3.3.2.1. MLC image-derived results

The results of the class separability test, for image-derived spectra, showed that all class pairs, apart from 'Kelp' and 'Submerged', had values greater than 1.9 indicating good class separation (Marçal *et al*., 2005). 'Kelp' and 'Submerged' had a value of 1.78 (**Tab. S3.2)** but were retained as their poor spectral separability reflects their inherent spectral similarities, significantly, it could not be guaranteed that the 'Submerged' class was comprised of *L. digitata*.

The MLC classifier, trained using image-derived spectra, revealed a dense covering of intertidal brown macroalgal species. The upper intertidal was dominated by a thin ribbon of *P. canaliculata* with the mid-intertidal dominated by either dense beds of *A. nodosum* or mixed assemblages of *F. vesiculosus* and *F. serratus.* The lower intertidal was characterised by the presence of *H. elongata* and partially emersed stands of *L. digitata* (**Fig. 3.5**). The 'Substratum' class, whilst classified alongside macroalgal cover classes, has been excluded from the figures to improve the clarity and interpretability of the maps. As no thresholds were set, all pixels were classified, and all 'blank' pixels thus represent the 'Substratum' class. MLC resulted in an overall classification accuracy of 94.7 % and a Kappa Coefficient of 0.9290. The 'Asco' and '*Fucus* spp' classes showed the highest producer/user accuracies but there was some misclassification between these two classes and also between the 'Asco' and 'PelC' classes, highlighting their similar spectral properties (**Tab. 3.2 & 3.3**). Aside from 'Green', which was not classified at all, 'Kelp' was the least accurately classified class, having the lowest producer/user accuracy, with significant misclassification occurring with 'Him' and 'Submerged'. The total area classified as *A. nodosum* by MLC was 4,447 m^2 out of a total classified macroalgal area of ~13,114 m^2 (**Fig. 3.5**).

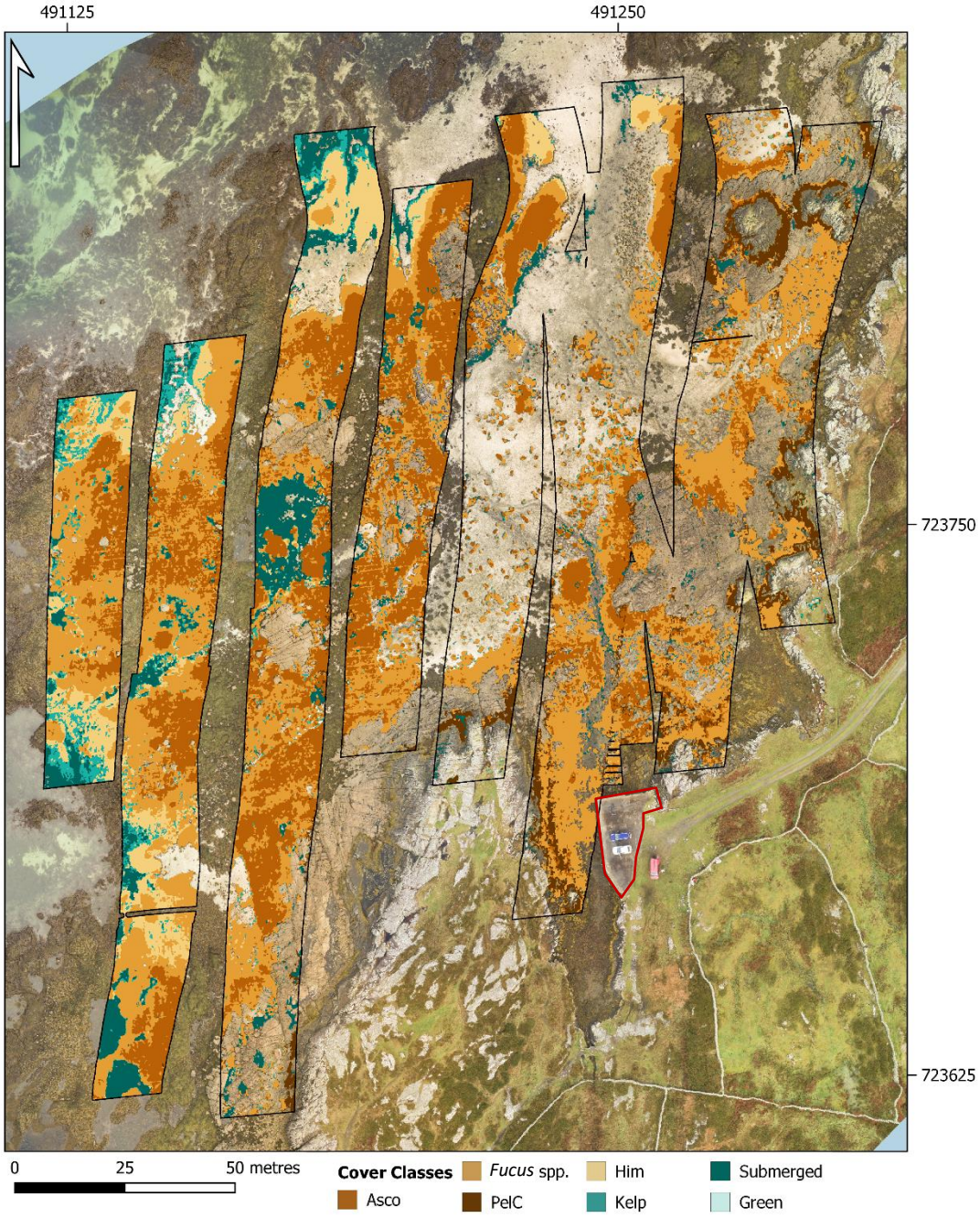

Fig. 3.5. Maximum Likelihood Classification (MLC) result from the hyperspectral drone survey in Carraroe. Seven macroalgal cover classes are displayed over the drone RGB imagery, 'Substratum' was not included. Black lines mark the footprint of the hyperspectral data strips. The pier, used for deployment, is marked by a red line. Coordinates are in Irish Transverse Mercator (ITM). Class codes represent the following species. *Ascophyllum nodosum* (Asco), mixed fucoids (*Fucus* spp.), *Himanthalia elongata* (Him), *Laminaria digitata* (Kelp), *Pelvetia canaliculata* (PelC), submerged macroalgae (Submerged) and unidentified green macroalgal species (Green).

Tab. 3.2. Maximum Likelihood Classification (MLC) confusion matrix, calculated, using ENVI 5.4, by comparing pixels of known class locations to those predicted by the classification workflow, for each of the eight cover classes, results are recorded as percentage of pixels assigned, correctly or incorrectly, to each class.

Class	*Fucus* spp.	Asco	Him	Kelp	PelC	Submerged	Substratum	Green	Total
Unclassified	0	0	0	0.01	0	0	0	0	0
***Fucus* spp.**	**94.66**	3.35	1.71	2.09	2.47	3.45	0.16	17.43	21.61
Asco	2.33	**94.54**	0	0.13	5.1	0.38	0.01	0	20.21
Him	0.98	0.01	**87.62**	10.16	0	1.26	0	11.53	7.19
Kelp	0.29	0.02	6.72	**61.53**	0	4.17	0.04	21.72	2.32
PelC	0.46	1.88	0.02	0	**87.4**	0.07	0.07	27.35	2.05
Submerged	0.27	0.11	3.89	25.75	0	**89.82**	0.32	0.27	7.08
Substratum	1	0.09	0.03	0.33	5.03	0.85	**99.4**	21.72	39.54
Green	0	0	0	0	0	0	0	**0**	0
Total	100	100	100	100	100	100	100	100	**100**

Tab. 3.3. Maximum Likelihood Classifier (MLC) User (probability of correct class assignment, calculated by dividing the number of correctly classified pixels by the total number of pixels in a class) and Producer (correctly classified reference pixels, calculated by dividing the number of correctly classified pixels by the total number of pixels that should be in a class) accuracies for each of the eight cover classes computed using ENVI 5.4.

Class	User Acc (Percent)	Prod Acc (Percent)	User Acc (Pixels)	Prod Acc (Pixels)
***Fucus* spp.**	94.38	94.66	247445/262179	247445/261392
Asco	96.92	94.54	237681/245234	237681/251405
Him	92.51	87.62	80697/87228	80697/92100
Kelp	62.29	61.53	17542/28162	17542/28508
PelC	74.02	87.4	18446/24919	18446/21106
Submerged	84.35	89.82	72516/85968	72516/80737
Substratum	99	99.4	475024/479807	475024/477888
Green	0	0	0/0	0/373

3.3.2.2. SAM *image-derived results*

The SAM classifier, trained using image-derived spectra, showed a similarly dense covering of intertidal brown macroalgal species as the MLC, dominated, in the mid-intertidal, by *A. nodosum* ('Asco') and mixed fucoids '(*Fucus* spp'). In contrast to MLC, both upper and lower intertidal macroalgal communities were poorly classified (**Fig. 3.6**). SAM produced a lower overall classification accuracy of 81.1 % and a Kappa Coefficient of 0.7552. The confusion matrix and user/producer accuracies are shown in **Tab. 3.4 & 3.5**. Both 'Asco' and '*Fucus* spp' show the highest producer/user accuracies and, as with the MLC, there was some misclassification between them with 6.2 % of '*Fucus* spp' pixels misclassified as 'Asco' and only 2.76 % of 'Asco' pixels misclassified as '*Fucus* spp'. Aside from 'Substratum' the remaining cover classes had low classification accuracies. A significant number of pixels were misclassified as 'Green', most notably along the margins of the data strips and in the immediate vicinity of the pier. A lot of this misclassification came from 17 % of reference 'Him' pixels being incorrectly assigned as 'Green' and, as 'Him' was a much larger class; this significantly inflated the area estimations for 'Green' leading to a UA of almost zero. 'PelC' was relatively accurately defined using MLC, yet was poorly classified using SAM, with ~69 % of pixels classified as 'PelC' belonging to other classes and 49 % of pixels that should have been classified as 'PelC' being classified as other classes. A significant amount of this misclassification was from 'Substratum' pixels being incorrectly classified as 'PelC'. As expected, there was significant misclassification between the 'Kelp' and 'Submerged' classes. The total area classified as *A. nodosum* by MLC was 4,120 m^2 out of a total classified macroalgal area of ~15,213 m^2 (**Fig. 3.6**).

Fig. 3.6. Spectral Angle Mapper (SAM) classification result, trained using image-derived spectra, from the hyperspectral drone survey in Carraroe. Seven macroalgal cover classes are displayed over the drone RGB imagery. The 'Substratum' class is represented by unclassified pixels. Black lines mark the footprint of the hyperspectral data strips. The pier, used for deployment, is marked by a red line. Coordinates are in Irish Transverse Mercator (ITM). Class codes represent the following species. *Ascophyllum nodosum* (Asco), mixed fucoids (*Fucus* spp), *Himanthalia elongata* (Him), *Laminaria digitata* (Kelp), *Pelvetia canaliculata* (PelC), submerged macroalgae (Submerged) and unidentified green macroalgal species (Green).

Tab. 3.4. Spectral Angle Mapper (SAM) (image-derived) confusion matrix calculated, using ENVI 5.4, by comparing pixels of known class locations to those predicted by the classification workflow, for each of the eight cover classes, results are recorded as percentage of pixels assigned, correctly or incorrectly, to each class.

Class	*Fucus* spp	Asco	Him	Kelp	Submerged	Substratum	PelC	Green	Total
Unclassified	0	0	0	0.01	0	0	0	0	0
***Fucus* spp**	**82.86**	2.76	1.47	1.17	2	0.05	3.06	2.14	18.77
Asco	6.2	**86.98**	0.45	0.52	0.56	0.01	5.6	0	19.54
Him	3.51	5.6	**70.83**	28.71	1.89	0	22.43	1.61	8.48
Kelp	0.25	0.05	6.57	**22.68**	19.32	3.61	1.14	0	3.82
Submerged	0.13	0.02	2.01	41.51	**72.41**	7.99	2.65	0.54	9.17
Substratum	0.47	0.03	0	0	0.69	**85.36**	4.23	0	33.84
PelC	1.3	1.82	1.65	0.72	1.56	2.81	**50.4**	31.9	2.9
Green	5.27	2.74	17.03	4.68	1.57	0.17	10.49	**63.81**	3.48
Total	100	100	100	100	100	100	100	100	**100**

Tab. 3.5. Spectral Angle Mapper (SAM) (image-derived) User (probability of correct class assignment, calculated by dividing the number of correctly classified pixels by the total number of pixels in a class) and Producer (correctly classified reference pixels, calculated by dividing the number of correctly classified pixels by the total number of pixels that should be in a class) accuracies for each of the eight cover classes computed using ENVI 5.4.

Class	User Acc *(Percent)*	Prod Acc *(Percent)*	User Acc *(Pixels)*	Prod Acc *(Pixels)*
***Fucus* spp**	95.12	82.86	216600/227715	216600/261392
Asco	92.23	86.98	218673/237107	218673/251405
Him	63.36	70.83	65230/102949	65230/92100
Kelp	13.94	22.68	6466/46393	6466/28508
Submerged	52.53	72.41	58460/111286	58460/80737
Substratum	99.33	85.36	407909/410660	407909/477888
PelC	30.27	50.4	10638/35148	10638/21106
Green	0.56	63.81	238/42236	238/373

3.3.2.2. SAM image-derived results

SAM, trained using the *in-situ* spectral profiles, identified a similar mid-intertidal distribution of A. nodosum (Asco) and mixed fucoids (*Fucus* spp) as the previous two classification workflows. The upper and lower intertidal regions were very poorly classified using this method (**Fig. 3.7**). With an overall classification accuracy of 71.4 % and a kappa coefficient of 0.62, the lowest classification accuracies of the three methods were recorded. The confusion matrix and user/producer accuracies are shown in **Tab. 3.6 & 3.7**. The two dominant macroalgal cover classes, 'Asco' and '*Fucus* spp' remained the two most accurately classified classes with approximately 13 % of reference 'Asco' pixels being misclassified as '*Fucus* spp', but only 1.6 % of '*Fucus* spp' pixels were misclassified as 'Asco'. *Laminaria digitata* (Kelp) would usually occupy the upper-subtidal zone but were classified across the entire intertidal, up to its upper limits. The 'Kelp' class had the lowest UA (6.5 %) and there are a significant number of pixels classified as being 'Kelp' that actually belonged to other classes, most notably of which being 27 % of reference 'Substratum' pixels, vastly increasing the area covered by 'Kelp'. A further source of classification error were from ~60 % of 'Him' reference pixels being misclassified as 'PelC'. As with the previous classification workflows, this misclassification led to a significant inflation of the area occupied by 'PelC' which normally occupies a thin band in the upper intertidal zone. Instead, in this classification, 'PelC' was classified in the lower intertidal zone where it should not occur. The total area classified as *A. nodosum* by MLC was 2,114 m^2 out of a total classified macroalgal area of ~13,170 m^2 (**Fig. 3.7**).

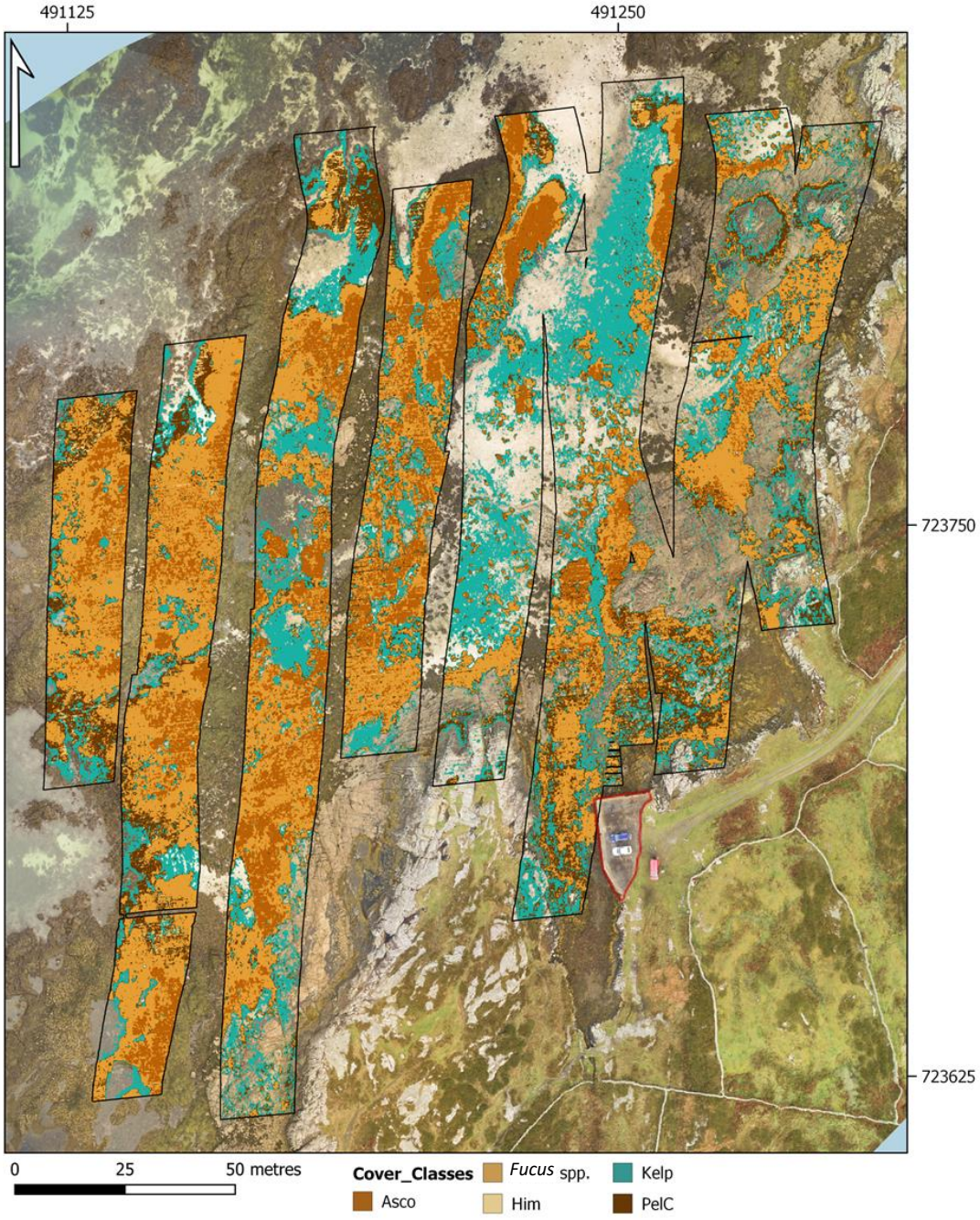

Fig. 3.7. Spectral Angle Mapper (SAM) classification result, trained using *in-situ* spectral library spectra, from the hyperspectral drone survey in Carraroe. Five macroalgal cover classes are displayed over the drone RGB imagery. The 'Substratum' class is represented by unclassified pixels. Black lines mark the footprint of the hyperspectral data strips. The pier, used for deployment, is marked by a red line. Coordinates are in Irish Transverse Mercator (ITM). Class codes represent the following species. *Ascophyllum nodosum* (Asco), mixed fucoids (*Fucus* spp), *Himanthalia elongata* (Him), *Laminaria digitata* (Kelp) and *Pelvetia canaliculata* (PelC).

Tab. 3.6. Spectral Angle Mapper (SAM) (*in-situ*) confusion matrix calculated, using ENVI 5.4, by comparing pixels of known class locations to those predicted by the classification workflow, for each of the six cover classes, results are recorded as percentage of pixels assigned, correctly or incorrectly, to each class.

Class	*Fucus* spp	Asco	Him	Kelp	PelC	Substratum	Total
Unclassified	0	0	0	0.01	0	0	0
***Fucus* spp**	**90.01**	13.53	10.57	2.85	7.41	0.09	24.89
Asco	1.63	**76.37**	0.02	0.15	1.3	0	17.36
Him	0.31	1.35	**15.85**	7.06	0.1	0	1.84
Kelp	1.47	1.34	12.87	**38.33**	30.45	27.6	14.86
PelC	6.4	7.39	59.26	16.77	**56.67**	0.31	9.55
Substratum	0.18	0.02	1.44	34.83	4.07	**72**	31.5
Total	100	100	100	100	100	100	**100**

Tab. 3.7. Spectral Angle Mapper (SAM) (*in-situ*) User (probability of correct class assignment, calculated by dividing the number of correctly classified pixels by the total number of pixels in a class) and Producer (correctly classified reference pixels, calculated by dividing the number of correctly classified pixels by the total number of pixels that should be in a class) accuracies for each of the eight cover classes computed using ENVI 5.4.

Class	User Acc *(Percent)*	Prod Acc *(Percent)*	User Acc *(Pixels)*	Prod Acc *(Pixels)*
***Fucus* spp**	83.48	90.01	235266/281811	235266/261392
Asco	97.66	76.37	192001/196611	192001/251405
Him	70.07	15.85	14595/20829	14595/92100
Kelp	6.49	38.33	10928/168327	10928/28508
PelC	11.06	56.67	11960/108110	11960/21106
Substratum	96.46	72	344066/356706	344066/477888

3.4. Discussion

Whilst there is a need for the development of faster and more efficient intertidal macroalgal monitoring methods, the spatial and spectral complexity of coastal environments can impede the application of remote sensing technologies for accurate baseline resource assessments. Species level identification is essential for the quantification of *A. nodosum* distribution and this can only be achieved using high spatial and spectral resolutions (Oppelt *et al*., 2012). This case study, using a UAV-mounted hyperspectral pushbroom sensor, represents the successful first attempt towards developing a methodology for the assessment of *A. nodosum* populations in Ireland and demonstrates its potential application for assessing a broader range of intertidal macroalgal species.

The methods employed allowed the accurate spectral distinction of *A. nodosum* from other surrounding macroalgal species and non-vegetated surfaces. Of the three combinations of classification method and training data used, MLC (image-derived) was found to be the most accurate, followed by SAM (image-derived) and SAM (*in-situ*). The latter of the three seemingly heavily affected by the presence of noise in the hyperspectral imagery (**Fig. 3.3b**) and both SAM classification workflows are potentially unsuitable for distinguishing between numerous spectrally similar species (Shafri *et al*., 2007). MLC was also able to more accurately map other selected classes, making it well suited towards a wider range of intertidal mapping applications. The classification accuracy for SAM (*in-situ*) could be improved by using a full-frame hyperspectral sensor. This may provide better quality data than the current pushbroom sensor which was affected by the movement of the UAV (Ringaby *et al*., 2010). High-resolution RGB imagery has previously been used for cover class identification (Lechner *et al*., 2012; Duffy *et al*., 2018) and emerged as an effective tool for the collection of both training and ground-truth data. Species could be confidently identified owing to their distinctive morphologies and colouration, and this was further improved by having prior site knowledge and appropriate macroalgal identification skills.

3.4.1. Discrimination of *Ascophyllum nodosum*

MLC (image-derived) produced the highest classification accuracies for ‘Asco’ (UA = 96 %, PA = 94 %), SAM (image-derived) achieved reasonable levels of accuracy (UA = 92 %, PA = 86.9 %) whilst SAM (*in-situ*) achieved the lowest accuracies (UA = 97.6 %, PA = 76.4 %). These levels of accuracy were somewhat surprising owing to the similar spectral properties between brown macroalgal species (Kutser *et al*., 2006b; Uhl *et al*., 2013). Visually, *A. nodosum* at Carraroe was easily distinguishable from all other classes and its propensity for forming homogenous stands has likely helped in distinguishing it. Both of the

classifiers trained using image-derived spectra produced similar area estimations for *A. nodosum* of ~ 4,300 m^2 whilst SAM, trained using *in-situ* spectra, estimated a significantly lower area, suffering from high percentages of omission, in particular with mixed fucoids, subsequently lowering confidence in its accurate representation of *A. nodosum* area. Gaps between the hyperspectral data strips meant that the total area covered by *A. nodosum* at the site could not be established.

The high classification accuracies observed for 'Asco' do not necessarily account for the spatial bias of error (Pontius & Millones, 2011). MLC showed a small amount of misclassification occurring between 'Asco' and 'PelC' which primarily occured towards the pier and along the margins of data strips. This spatial aspect to classification error is important to recognise when interpreting a finished map (Foody, 2002). In this case the misclassification of 'Asco' pixels as 'PelC' did not significantly affect the total area estimations for 'Asco', it did, however, inflate the classified 'PelC' extent, owing to the small area of this class to begin with. It is important to note that although a very small percentage of 'Asco' pixels were incorrectly misclassified as 'PelC', the fact that this was concentrated in one small area of the site highlights the importance of not solely relying on a single value, like kappa, when assessing accuracy. *Ascophyllum nodosum* close to the pier area appeared much yellower than in the rest of the site and visual analysis of endmember spectral profiles indicated that it was closer to *P. canaliculata* than lower-shore *A. nodosum* (**Fig. S3.6**). This could be as a result of increased emersion times or stressors associated with localised inputs of fresh water (Hurd *et al*., 2014) and may help to explain the observed misclassification. Factoring in intraspecific variation to survey design was noted by Clark *et al.* (2005) and could be accounted for by the creation of 'subclasses' representing observed spectral variations. Towards the pier, both SAM classifiers poorly predicted the distribution of *A. nodosum*. SAM (image-derived) misclassified *A. nodosum* as either *P. canaliculata*, green macroalgae or *H. elongata*, a species that isn't found in the upper intertidal (Stengel *et al*., 1999). SAM (*in-situ*) misclassified much of the *A. nodosum* in the pier region as either *L. digitata* or *P. canaliculata*, the former of which, again would not be present in the upper intertidal.

Field surveys confirmed the presence of mixed fucoid assemblages and these were responsible for the misclassification between 'Asco' and '*Fucus* spp' seen in the three classification workflows. It is evident that this misclassification was spread across the site, rather than concentrated in one area, likely reflecting the heterogenous nature of these assemblages. Mixed fucoid assemblages were spatially and spectrally complex, challenging the discriminatory ability of both classifiers. These assemblages have previously proven

difficult to assess (Hennig *et al*., 2007) and whilst some authors have defined the species present within those assemblages, creating specific mixed classes (Oppelt *et al*., 2012), it was felt that this approach would be difficult to collect data for through visual analysis of the RGB imagery as species identification was difficult in mixed areas. There was little misclassification between 'Asco' and the remaining classes for MLC indicating that, whilst spectrally similar to 'PelC' (upper shore) and '*Fucus* spp', 'Asco' was sufficiently distinct from other brown macroalgal species. Both SAM workflows followed this trend, with the exception of some notable misclassification of 'Asco' as 'Him' for the image-derived SAM. *Laminaria digitata* and *F. serratus* dominated communities were spectrally separable in Heligoland (Oppelt *et al*., 2012), supporting our findings and demonstrating that whilst difficult, spectral separation within (brown) macroalgal groups is possible. It is important to be critical of the final classification and avoid the temptation to rely solely on the Kappa coefficient as a measure for accuracy. Understanding the spatial aspect of error has allowed us to place a few caveats upon the Kappa score, helping to paint a better picture of overall classification accuracy and to understand areas within the site where estimates of *A. nodosum* distribution may be inaccurate.

3.4.2. High resolution reference imagery

The ability to use high-resolution RGB imagery to collect both training and ground-truth data is currently only possible because of the high spatial resolution afforded by UAVs. The time saved by utilising UAVs in surveys would otherwise be lost if detailed supporting field surveys were required and this would also be an obstacle to the scaling up of surveys. Gray *et al*. (2018) demonstrated that UAVs were able to collect data covering an entire site (4,325,000 m^2) in the same time it took them to conduct transect surveys throughout a subsection (186,000 m^2). Having a trained observer with strong macroalgal identification skills is vital for the accurate identification of cover classes in remote sensing (Lechner *et al*., 2012; Vahtmäe & Kutser, 2013) and, when combined with high spatial resolution, can be a reliable assessment method (Ventura *et al*., 2018). Central to the accurate analysis of RGB imagery is to heed the advice of Foody (2002) who cautioned against simply assuming the reference datasets are accurate. To this end, we sought to mitigate potential sources of error where possible. Confidence in the assignment of classes is required to prevent incorrect class assignment (Olofsson *et al*., 2014) and the slight misalignment between the hyperspectral and RGB layers meant that the collection of data using GPS would have been potentially problematic, with GPS error and fine spatial scales compounding this (Laliberte & Rango, 2011). This further justifies our decision not to create a mixed species class (of *A. nodosum* and other fucoids) as we could not confidently identify whether a mixed assemblage was

indeed so and why we endeavoured not to create polygons at class boundaries where classification errors are common (Radoux & Bogaert, 2017). The visual analysis also permitted the acquisition of more data than could possibly have been achieved through the collection of GPS point data and helped to account for classes that were not observed or recorded during *in-situ* data collection.

3.4.3. Spectral profile sampling

Spectral libraries have been successfully used in many remote sensing studies (Kutser *et al*., 2006a; Casal *et al*., 2013; Bareth *et al*., 2015; Dierssen *et al*., 2015) and have been identified as an efficient and accurate methodology for training supervised classification methodologies. The spectral profiles obtained *in-situ* corresponded to other macroalgal spectral measurements reported in the literature, with brown macroalgae displaying characteristic reflectance peaks around 580, 600 and 650 nm (Kutser *et al*., 2006b; Uhl *et al*., 2013; Kotta *et al*., 2014; Chao Rodríguez *et al*., 2017). Arroyo-Mora *et al* (2019) found good agreement between spectral library and image-derived spectra, of calibration panels, using a pushbroom sensor, showing that this technology can achieve accurate results. In our case, the noise present in the hyperspectral dataset, an effect of UAV platform instability on the pushbroom sensor (Saari *et al*., 2011; Jaud *et al*., 2018), limited the effectiveness of the *in-situ* spectral sampling approach. One approach to mitigate this noise may have been to better determine an optimal flight speed prior to surveying. We flew at ~15 km/h, yet Arroyo-Mora *et al* (2019), using a µCASI pushbroom device, determined 9.7 km/h to be the optimal speed for their system. This speed ensured minimal roll and pitch whilst still allowing the chosen study are to be surveyed. Optimum flight parameters may vary depending on the sensor make and model along with prevailing wind conditions and should be factored into survey design. Integrating an inertial measurement unit (IMU) and GPS with the hyperspectral sensor has also been shown to minimise noise present in the imagery and improve its spatial accuracy (Arroyo-Mora *et al*., 2019), avoiding the need for manual georectification. However, these can be expensive, and many integrated devices do not log high accuracy GPS/IMU data (Aasen *et al*., 2018).

3.4.4. Implications for resource management and conservation

The ability to accurately assess a resource is crucial for establishing an environmental baseline with which to inform future management decisions (Connell *et al*., 2008). Maps of coastal environments are essential for management planning (Mumby *et al*., 1999) and need to balance the needs of humanity whilst preventing the degradation of ecosystem function, goods and services (Crain *et al*., 2009). We have demonstrated that accurate area estimations

of *A. nodosum* can be achieved which could lead to the development of more efficient and cost-effective resource assessment methodologies. Our results further highlight that other canopy-forming species can be accurately mapped (i.e. *H. elongata* and *P. canaliculata*), outlining the potential application of this technology for mapping a wider range of species than present in this study. Such data can potentially be used by various interested stakeholders, allowing for informed decision making on how best to sustainably manage intertidal resources.

The development of full-frame hyperspectral sensors will improve the efficiency and accuracy of UAV-based data collection (i.e. Senop HSC-2 https://senop.fi/en/optronics-hyperspectral). Georeferencing is simpler as standard photogrammetry methods can be used (Honkavaara *et al*., 2016; Aasen *et al*., 2018) and noise is easier to correct for than with pushbroom sensors (Hagen & Kudenov, 2013). With fixed-wing UAVs now achieving flight times up to 180 min (i.e. C-Astral Bramor http://www.c-astral.com/en/unmanned-systems) they provide the opportunity to conduct large-scale, low-cost surveys of intertidal communities but data storage limitations may still constrain flight times (Arroyo-Mora *et al*., 2019). Also, in many countries, regulations restrict the height and range of UAVs (Baena *et al*., 2017), limiting their potential. The development and granting of beyond visual line of site (BVLOS) permissions to companies and individuals who meet specified national aviation authority guidelines will allow the scaling up of UAV surveys to the point where they may offer a more cost-effective mapping alternative to aircraft.

3.5. Conclusions

With the likely increase in anthropogenic pressures upon intertidal communities there is a need for an assessment methodology to complement field-based surveys, one that can cover large areas accurately. Despite a growing trend towards using UAVs in nearshore/intertidal environments (Valle *et al*., 2015; Murfitt *et al*., 2017; Duffy *et al*., 2018; Ventura *et al*., 2018) there is a conspicuous absence of recent studies using hyperspectral remote sensors. This study has demonstrated how these two technologies can be utilised for intertidal macroalgal resource assessment through the accurate quantification of *A. nodosum* distribution and extent. High resolution RGB imagery has facilitated the rapid and accurate collection of both training and reference data and this method is likely to prove valuable if remote sensing surveys were to be scaled up. The three classification workflows used in this study each achieved good mapping accuracies for *A. nodosum*. Yet, MLC, trained using image-derived spectra, was the most accurate at classifying *A. nodosum*, but also other canopy-forming intertidal species, potentially making it more suitable for a broader range of

intertidal mapping objectives. Although we caution that these results should be considered with respect to the season (late autumn) and distinct region in which they occurred, the technology used has produced accurate classification results in a spectrally complex environment. Further work is still needed to explore the effects of variations in location and season on macroalgal spectral properties and on the ability of UAV-mounted hyperspectral remote sensors to accurately discriminate between canopy-forming intertidal macroalgae.

Acknowledgements

The authors greatly appreciate the invaluable help provided by Fearghus Foyle, Aidan Magee, Daire Walsh and Sean Mannion (GeoAerospace) with the collection and processing of UAV imagery. This Cullen Fellowship research (Grant-Aid Agreement No. CF/15/02) was carried out with the support of the Marine Institute and INFOMAR and funded under the Marine Research Sub-programme by the Irish Government.

Chapter 4: Application of multiplatform, multispectral remote sensors for mapping intertidal macroalgae: a comparative approach

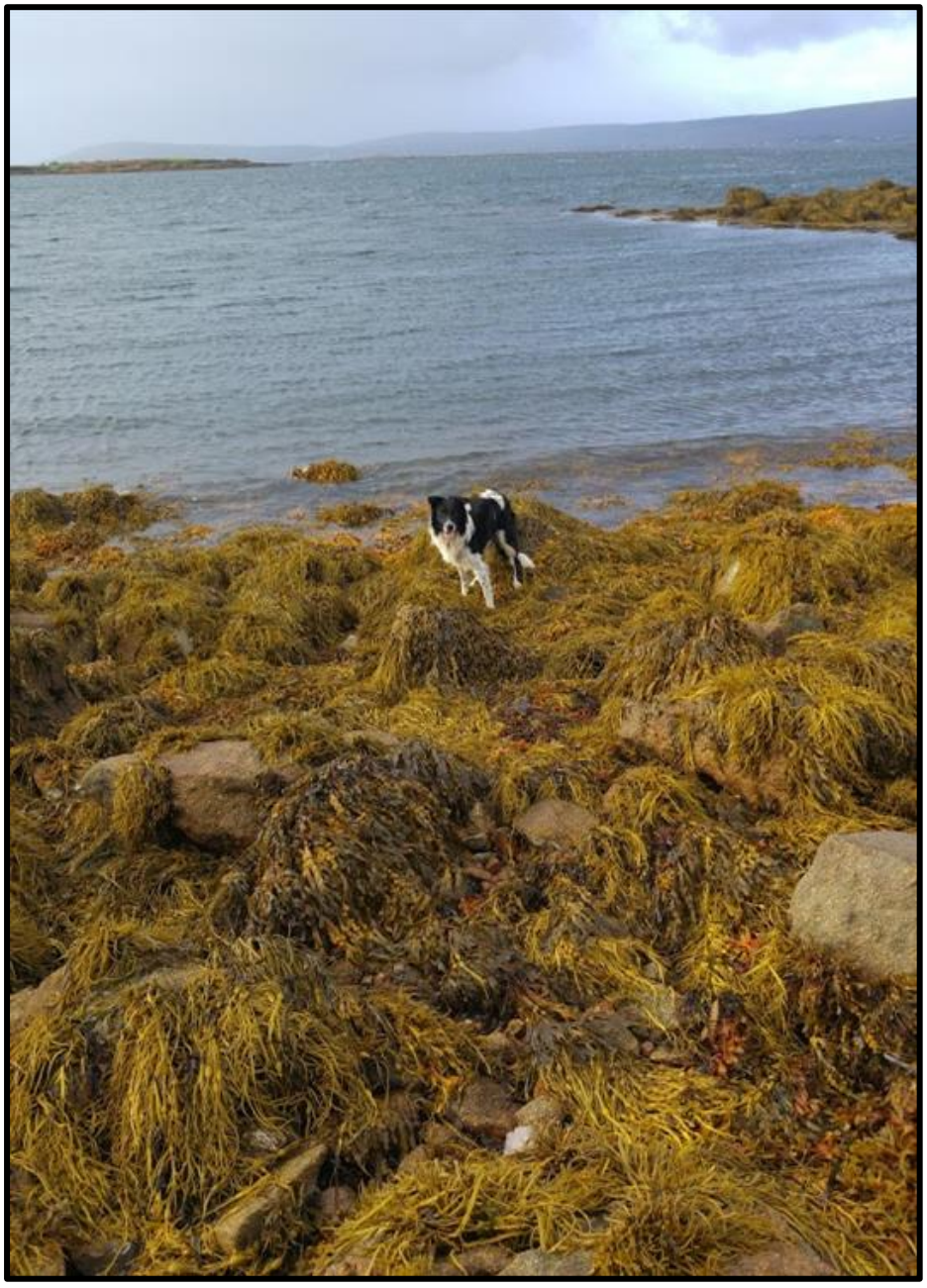

Sailor the dog. Always present and always annoying (Béal an Daingin).

The following chapter (unmodified) has been accepted (pending revisions) in the *Journal of Aquatic Conservation: Marine and Freshwater Ecosystems* (27/01/2020).

Author contributions

Thomas Rossiter, Dagmar Stengel, Thomas Furey and Tim McCarthy developed the research idea. Thomas Rossiter and Dagmar Stengel were present during the data collection. Thomas Rossiter drafted the manuscript and all authors contributed to data interpretation along with providing feedback on the manuscript.

Abstract

Intertidal macroalgal communities are economically and ecologically important and, with a likely increase in anthropogenic pressures, there is growing need to evaluate and monitor these diverse and complex environments. Efforts to conserve and sustainably manage need to be underpinned by accurate, cost-effective and efficient data collection methods. The high spatial and temporal resolution of unoccupied aerial vehicles (UAVs), compared to satellites and aircraft, combined with the development of lightweight sensors, provides researchers with a valuable set of tools to conduct research on intertidal macroalgal communities. We compared the ability of multispectral sensors, mounted on a satellite, aircraft and UAV, to identify and accurately map the intertidal brown fucoid *Ascophyllum nodosum* (Fucales, Ochrophyta) at a single site with a relatively low species diversity of canopy-forming macroalgae. Visual analysis confirmed that the spatial resolution of satellite imagery (Sentinel-2) was too coarse to map intertidal macroalgae as the resolution could not capture the fine spatial patterns of the macroalgal community. Concurrent high-resolution RGB imagery was taken during the aircraft and UAV surveys and this was used to collect training and reference data through the visual identification and digital delineation of species and classes. Classes were determined based on the level of taxonomic detail that could be observed, with higher levels of taxonomic detail observed in the UAV over the aircraft imagery and the data from both was used to train a Maximum Likelihood Classifier (MLC). UAV imagery was able to more accurately classify a distinct *A. nodosum* class, along with other macroalgal and substratum classes (Overall Accuracy (OA) 92 %), than aerial imagery, which could only identify a lower taxonomic resolution mixed *A. nodosum* and fucoid class, achieving a lower OA (78.9 %). This study has demonstrated that in a coastal site with relatively low macroalgal species diversity, and despite the spectral similarity of the brown species present, UAV-mounted multispectral sensors provided the most accurate tool for focused assessments of individual canopy-forming species.

4.1. Introduction

Temperate rocky shorelines are typically dominated by dense communities of macroalgal (seaweed) primary producers, providing habitat for a diverse range of other biota (Bruno & Bertness, 2000; Vadas *et al*., 2004; Davies *et al*., 2007). With increasing anthropogenic pressures on intertidal communities (Mineur *et al*., 2015), an understanding of their distribution and the development of baseline data collection methods is important for their effective conservation and management (Dekker *et al*., 2003). Traditional field surveys, whilst collecting highly detailed and accurate information, are time consuming and restricted in scale (Kerr & Ostrovsky, 2003; Hennig *et al*., 2007; Oppelt *et al*., 2012). On the other hand, remote sensing can capture larger areas, often allowing for standardised, repeat surveys of the same site (Casal *et al*., 2012; Thenkabail, 2015), and potentially offering alternative survey methodologies for intertidal data collection.

Traditionally, aircraft have been the dominant remote sensing platform for macroalgal mapping studies (Bajjouk *et al*., 1996; Dekker *et al*., 2003; Garono *et al*., 2004; Stekoll *et al*., 2006; Casal *et al*., 2012; Oppelt *et al*., 2012), primarily owing to their greater operational flexibility and spatial resolution when compared to satellites (Brodie *et al*., 2018). Satellite-based technologies have also been useful for assessing the extent of broad-scale canopy-forming species (Cavanaugh *et al*., 2010; Casal *et al*., 2011), but for intertidal mapping, the acquisition of satellite images that coincide with suitable tidal and atmospheric conditions is challenging (Bell *et al*., 2015). The relatively coarse spatial resolution of aircraft has made identification to species level difficult (Oppelt *et al*., 2012; Cruzan *et al*., 2016), although success has been had when discriminating between spectrally distinct macroalgal groups (Hennig *et al*., 2007; Casal *et al*., 2012) and when mapping homogenous cover species (Pe'eri *et al*., 2008; Dierssen *et al*., 2015).

The recent and rapid proliferation of affordable unmanned aerial vehicles (UAVs) (Colefax *et al*., 2018) has created a promising remote sensing alternative to aircraft and satellites. UAVs can capture the highest spatial resolution imagery and have the greatest levels of operational flexibility, making them well-suited to operating in dynamic environments (Jensen *et al*., 2011), including the intertidal zone. They are currently the most cost-effective solution over small areas (Matese *et al*., 2015), with continued technological development and improvements in battery life and payload capacity (Colefax *et al*., 2018) likely to increase their application for larger areas, for example, some fixed-wing models (Quantum Tron F90+ https://www.quantum-systems.com/project/tron-f90/) can cover up to 7500 ha (at 1000 m flight altitude). UAVs have been successfully used in a wide range of environments including riparian wetlands (Jensen *et al*., 2011), intertidal seagrass meadows

(Duffy *et al*., 2017), intertidal reefs (Murfitt *et al*., 2017), coastal habitats (Ventura *et al*., 2018) and wetlands (Doughty and Cavanaugh, 2019). There are now a range of lightweight sensors that can be UAV-mounted (Colomina and Molina, 2014), further increasing their potential applications.

Intertidal macroalgal communities can be spatially and spectrally complex, with species occurring in mixtures over fine scales, requiring high spatial and spectral resolutions to accurately identify species present. Whilst hyperspectral sensors have both high spatial and spectral resolutions, they are currently prohibitively expensive (Manfreda *et al*., 2018), which can act as a barrier to research groups and organizations. It is therefore important to develop remote sensing methodologies that cover different technologies and budgets. Multispectral sensors typically contain three-or-more spectral bands (Burns and Berns, 1996) with many current models ranging from five to 12 (Adão *et al*., 2017). This lower spectral resolution makes them less suited to spectrally complex environments, but they are significantly cheaper and less complex to operate, process and analyse than hyperspectral sensors (Marshall and Thenkabail, 2015). To date, for UAVs, multispectral sensors have primarily been used for precision agriculture, where different band combinations allow for the identification of weeds (Barrero *et al*., 2018), measuring grass crop quality (Askari *et al*., 2019) and the monitoring of vegetation health is improving yields and harvest efficiency (Candiago *et al*., 2015; Kazantsev *et al*., 2018). Decreasing costs are now seeing them applied to broader environmental questions, with recent uses including the mapping of malaria vector larval habitat (Carrasco-Escobar *et al*., 2019) and for use in forestry management (Dash *et al*., 2018). Two very recent studies successfully applied UAV-mounted multispectral remote sensing to macroalgal habitats. Taddia *et al*. (2019) characterised the presence of submerged green macroalgae but did not identify the species and Tait *et al*. (2019) managed to discriminate between spectrally distinct intertidal species.

Here, the spectral discriminatory ability of multispectral sensors, mounted on a satellite, airplane and UAV, to accurately map the intertidal fucoid *Ascophyllum nodosum* (Ochropyta, Phaeophyceae), a commercially and ecologically important brown macroalgal species common on moderately exposed to sheltered rocky coasts (Stengel and Dring, 1997) was evaluated. An accurate, affordable methodology was developed to support resource management decision making, addressing the following specific challenges:

i. How accurately can multispectral sensors map the distribution of *A. nodosum* within a spatially and spectrally complex intertidal environment?
ii. Which platform(s) achieve the most accurate mapping of *A. nodosum*?

iii. Can high-resolution RGB imagery be used for the collection of training and validation spectral information?

We provide a novel methodology, presenting details of data collection, processing and analysis workflows used, and compare the ability of the three remote sensing platforms to accurately quantify *A. nodosum* distribution.

4.2. Methods

4.2.1. Study site

This study was carried out near Béal an Daingin (53°19'19.7"N, 9°37'16.8"W) which lies within the inner reaches of Kilkieran Bay in Co. Galway, Ireland (**Fig. 4.1**). The bay itself is characterised by a range of habitats including, mudflats, coastal lagoons, shallow inlets and bays, reefs, saltmarshes and machair (NPWS, 2014). The primary underlying bedrock is granite (Könnecker & Keegan, 1983) and the shoreline is dominated by rocky substrate giving way to muddy sediment in shallow waters (Sides *et al*., 1994). The site was characterised by a relatively narrow intertidal zone which drops abruptly into muddy sediments and abuts onto steep granite cliffs and was chosen due to the high abundance of *A. nodosum* and the relatively low species diversity of canopy-forming macroalgae. Vertical zonation is, in-part, controlled by the gentle sloping nature of the intertidal zone, *Pelvetia canaliculata* and *Fucus spiralis* dominate the upper littoral, followed by pure or mixed beds of *A. nodosum* and *F. vesiculosus* and finally, *F. serratus* and patchy *Himanthalia elongata* (all Phaeophyceae). There are areas dominated by boulders in the south of the site that support dense, homogeneous patches of *A. nodosum*. Access to the site was provided by a narrow track.

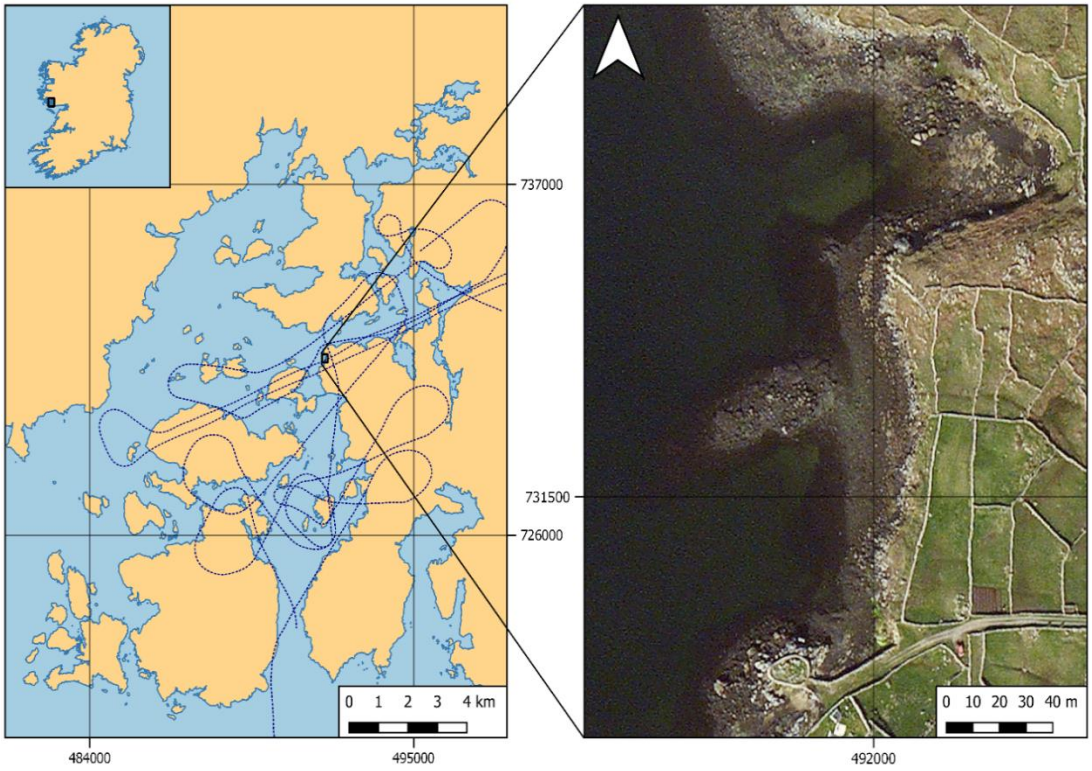

Fig. 4.1. Location of the study site at Béal an Daingin in relation to Kilkieran Bay and Ireland. The dotted blue line marks the flight path of the aerial survey. Coordinates are in Irish Transverse Mercator (ITM).

4.2.2. Multispectral acquisition

We sought to collect remote sensing data from the same time of year (June/July), endeavouring to ensure that the three datasets covered the same site (**Fig. 4.2**). The datasets were collected over a three-year period, from 2016 to 2018.

4.2.2.1. Satellite imagery

The Sentinel-2 satellite mission comprises two polar-orbiting satellites, each mounted with a high-resolution Multispectral Instrument (MSI). Each MSI can capture 13 bands over a wavelength range of 440 to 2200 nm. Four bands had a spatial resolution of 10 m, six of 20 m and three of 60 m (Clevers and Gitelson, 2013). Bandwidths range from 15 – 180 nm and are listed in **Tab. S4.1**. A cloud-free Sentinel-2 multispectral image taken on June 16th, 2018 at 11:43 GMT was acquired over the Kilkieran Bay area (**Fig. 4.2**). The timestamp shows that the image was taken ~1 ½ hours before low tide (0.7 m) which was at 13:49 GMT, indicating a tide height of approximately 1 m.

4.2.2.2. Aerial imagery

An aerial survey was conducted by AirSurvey in July 2016 during clear weather conditions to coincide with low tide at 12:00 GMT (0.8 m) and the survey was planned so that the plane was over Kilkieran Bay approximately 30 min before this time.

A Cessna-172 (Cessna, Wichita, USA) mounted with an AIRINOV AgroSensor (Parrot SA, Paris, France) was used to collect multispectral data for the intertidal zone in Kilkieran Bay. The sensor, operating as a global shutter, contained four bands; green (550 nm), red (660 nm), red-edge (735 nm) and near-infrared (NIR (790 nm)). The green, red and NIR bands have a bandwidth of 20 nm and the red-edge is narrower at 10 nm. There was no integrated light sensor (ILS) so calibration targets were recorded before take-off. However, atmospheric conditions were likely different over the study area than at the airfield (~135 km away) meaning radiometric calibration may not be accurate for localized atmospheric conditions. The flight lasted approximately 90 min (not including transit) and, at an average altitude of 600 m, providing a ground sampling distance (GSD) of 60 cm/pixel, was tasked with covering as much of the intertidal zone in Kilkieran Bay as possible. A Nikon D800E (Nikon, Tokyo, Japan) camera was mounted on the plane to collect high resolution RGB imagery (6 cm/pixel). No GPS data were collected for the multispectral imagery and only photo centre coordinates were available for the RGB (which were not stored in the image tile metadata). The scale of the aircraft survey meant that it was not practical to deploy ground control points (GCPs).

4.2.2.3. UAV imagery

A UAV survey was conducted in July 2017 by GeoAeroSpace. Weather conditions were moderately calm and there was significant passing cloud cover. The survey was planned to coincide with the low tide at 12:45 GMT (1 m).

A DJI Inspire V1 (DJI, Shenzhen, China) was used to conduct a multispectral and RGB survey and had a maximum flight time of ~18 min depending on wind speed. RGB imagery was captured using the inbuilt 12 MP X3 camera and a Parrot Sequoia (Parrot SA, Paris, France) sensor was used to collect multispectral data. This four-band sensor records in the green (530 nm), red (660 nm), red-edge (735 nm) and near-infrared (NIR) (790 nm) with a 20 nm band width. The Parrot Sequoia operated a global shutter for the multispectral bands allowing the entire scene to be captured simultaneously. There was a separate four-band integrated light sensor (ILS) with an inbuilt GPS sensor. AIRINOV calibration targets were used to calibrate the sensor pre-flight. Map Pilot (v.2.7.0) (Drones Made Easy, San Diego, USA) was used to plan the flight. The sensor was not connected to the controller and was set

to take an image every 2 s based on an average flight speed of 3 m/s. The UAV flew at an altitude of 50 m, for ~12 min, achieving a GSD of 2.2 cm/pixel (RGB) and ~5 cm/pixel (Multispectral) (**Fig. 4.2**) and covered a total area of 2.09 ha. Image overlap was set at 70 % for the RGB and 65 % for the multispectral (side and frontal).

Nine ground control points (GCPs) were deployed to accurately geo-reference the data. Each GCP consisted of a 50 cm x 50 cm black board with a white cross and a centre point easily visible from the air, the coordinates of the centre point were recorded using a Trimble R8 post processing kinematic (PPK) global navigation satellite system (GNSS) unit (Trimble, Sunnyvale, USA). GCPs were spaced evenly throughout the site with one in each corner of the survey area and the others spaced to reflect topographical (i.e. vertical) variation. GCPs were post-processed using Trimble Business Centre (v. 5.00, Trimble, Sunnyvale, USA).

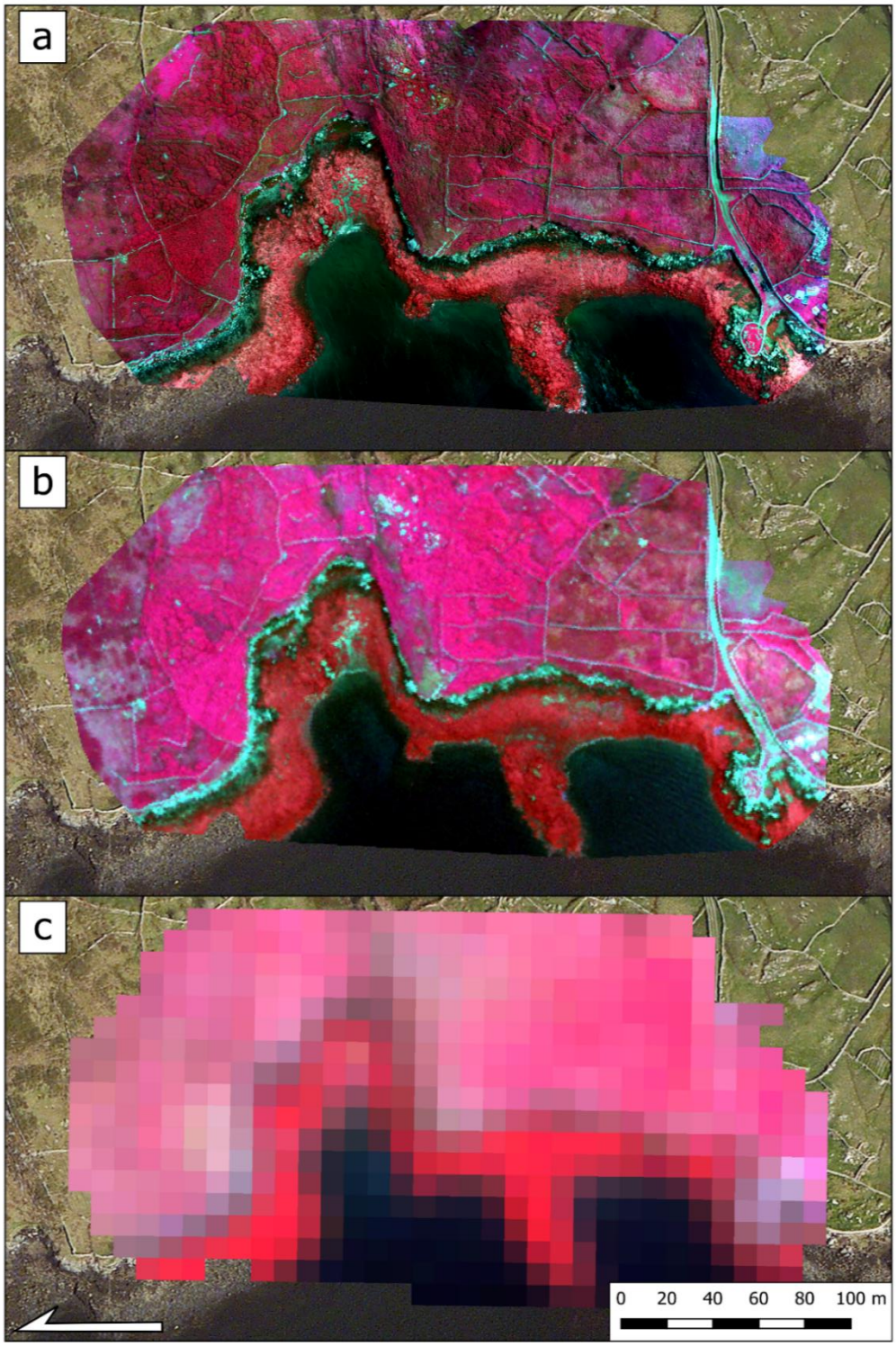

Fig. 4.2. Comparison of the multispectral ground sampling distance (GSD) from each of the three platforms. UAV = 5 cm/pixel (**a**), aircraft = 60 cm/pixel (**b**) and Satellite = 10 m/pixel (**c**). Layers were clipped to the extent of the UAV imagery.

4.2.3. Image processing

4.2.3.1. Aerial image processing

Aerial RGB imagery were processed using Microsoft Image Composite Editor (ICE) (Microsoft, Redmond, USA) and ArcGIS (v.10.3.1) (ESRI, Redlands, USA). The lack of associated GPS data required a more 'manual' approach to data processing. Suitable RGB tiles were mosaicked together in ICE and then manually georeferenced to an ESRI World Imagery base map in ArcGIS (ESRI, Redlands, USA) before being re-projected into the Irish Transverse Mercator (ITM) projection. Key identifying features, of fixed position, such as wall corners and distinctive rocks were used to improve accuracy. A single multispectral tile provided sufficient coverage of Béal an Daingin. After initially being cropped to remove noise, bands were aligned using the Auto-Georeference tool (ArcGIS Pro) and then stacked using the Composite Bands tool. The final composite image was then manually georeferenced to the RGB extent and projection.

4.2.3.2. UAV image processing

UAV RGB and multispectral data were processed using Pix4D Mapper (Pix4D, Lausanne, Switzerland), GCPs were imported in primarily to avoid layer co-registration errors (Bentoutou *et al*., 2005) and the calibration targets were imported to calculate reflectance through the empirical line approach (Smith and Milton, 1999). To focus solely on intertidal spectral signatures, the land and water were masked out. The land mask was manually created to remove any terrestrial features and the water mask using the Normalized Difference Water Index (NDWI), which enhances water features (Xu, 2006) and, using the appropriate threshold (> - 0.2), removed most of the water. These were then used to crop the aerial multispectral to the same extent. NDWI is expressed as follows (McFeeters, 1996):

$$NDWI = \frac{Green - NIR}{Green + NIR}$$

The satellite imagery was already georeferenced and owing to the coarse pixel size no additional processing steps were undertaken for the satellite imagery aside from cropping it to the extent of the aerial and UAV layers.

4.2.4. Multispectral classification

4.2.4.1. Image-derived training spectra

For the aerial and UAV data, image-derived endmember training spectra were identified using the RGB imagery, as a guiding dataset, with ENVI 5.4 (Harris Geospatial Solutions,

Boulder, USA). The usefulness of this approach has been noted by van Iersel *et al.* (2018) and involves the visual identification of target features (i.e. macroalgal species), using RGB imagery, and then the creation of training polygons around them prior to their spectral information being extracted from the aligned multispectral imagery. Training polygons were created, using the Region of Interest (ROI) tool, for areas where individual classes were easily observable, and this was easier in the UAV compared to the aerial imagery. The number of training areas per class was dependent on the observable area of that class and the area of each polygon depended on the extent of homogenous class cover. Larger, more homogenous cover classes required larger, more numerous training polygons. Species present at site and the class codes used to represent them are highlighted in **Tab. 4.1**. *Ascophyllum nodosum* was easily identifiable in the UAV imagery owing to its distinctive bright coloration and morphology (**Fig. 4.3**). Where *A. nodosum* was a distinct class for the UAV data, for the aerial data it was not possible to distinguish homogenous *A. nodosum* stands from those mixed with other fucoids so a combined class was created (**Fig. 4.4**). For both UAV-derived and aerial datasets, *F. vesiculosus*, *F. serratus* and *F. spiralis* were combined into a single category (*'Fucus* spp'). The shrubby nature of the three species leads to a mottled, darker appearance and it was difficult to confidently discern between them (**Fig 4.3 and 4.4**). *Pelvetia canaliculata* was also incorporated into this class as it occurred infrequently in small patches making it very difficult to observe in the RGB imagery and its inclusion as a separate class could have increased classification error owing to the spectral similarity between brown macroalgal species (Kotta *et al*., 2014). Macroalgae wrack (decaying seaweed) was observable in both sets of imagery, but the coarse resolution of the aerial imagery made it difficult to create accurate training area and, when its inclusion was tested, wrack was extensively over classified (**Fig. S4.1**). Small patches of unidentified green macroalgal ('Green') species were present in both datasets yet, again the coarse resolution of the aerial imagery made it difficult to accurately create training polygons. 'Green' was over-classified when included in the initial UAV imagery classification workflow (**Fig. S4.2**), and it was decided to exclude it from the final output. Red macroalgae, although present, were also not included as they were almost exclusively sub-canopy and remote sensing would not have been able to accurately determine their true extent. The spectral properties of rock, mixed sediment and sand are relatively similar to one another, and sufficiently distinct from macroalgae, that they are combined into their own class.

The spectral separability of endmember classes was determined prior to running a supervised classification algorithm. The mathematical separability of the classes is performed to assess whether sufficient and representative training data have been selected

(Richards and Jia., 2006). Training data were checked for class separability using the Jeffries-Matusita Distance (Jacobsen *et al*., 1999). The values of the resulting output between each pair of classes range from 0 to 2 with the latter indicating perfect separability between them (Richards and Jia, 2006). Good class separability would indicate that sufficient training areas had been selected, whereas lower values would indicate either the need for more training areas or that two classes were inherently similar in their spectral properties. This could then indicate that the two classes could potentially be combined (Petropoulos *et al*., 2010). Despite excluding 'Green' from the final classification, it was included in the spectral separability workflow (UAV imagery) to better understand its poor classification performance.

Tab. 4.1. Species and features present at site and the class codes used to represent each for the UAV and aerial imagery. *Ascophyllum nodosum* was identified as its own class in the UAV imagery (**Asco**) but only an *A. nodosum* dominated class (**Asco_*Fucus* spp.**) was identified in the aerial imagery along with a mixed fucoid class (***Fucus* spp**) in which *A. nodosum* was not present. *Himanthalia elongata* was present but not assigned a class owing to small coverage and *Ulva* spp (**Green**) were not classified in the aerial imagery.

Species	UAV Imagery Code	Aerial Imagery Code	Description
Ascophyllum nodosum	Asco	Asco_*Fucus* spp.	The **Asco** class is a pure *A. nodosum* class and **Asco_*Fucus* spp.** represents a mixed fucoid class dominated by *A. nodosum*.
Fucus vesiculosus	*Fucus* spp.	*Fucus* spp. / Asco_*Fucus* spp.	***Fucus* spp** is a mixed fucoid class and **Asco_*Fucus* spp.** represents a mixed fucoid class dominated by *A. nodosum.*
Fucus spiralis	*Fucus* spp.	*Fucus* spp. / Asco_*Fucus* spp.	***Fucus* spp** is a mixed fucoid class and **Asco_*Fucus* spp.** represents a mixed fucoid class dominated by *A. nodosum.*
Fucus serratus	*Fucus* spp.	*Fucus* spp. / Asco_*Fucus* spp.	***Fucus* spp** is a mixed fucoid class and **Asco_*Fucus* spp.** represents a mixed fucoid class dominated by *A. nodosum.*
Pelvetia canaliculata	*Fucus* spp.	*Fucus* spp. / Asco_*Fucus* spp.	***Fucus* spp** is a mixed fucoid class and **Asco_*Fucus* spp.** represents a mixed fucoid class dominated by *A. nodosum.*
***Ulva* spp.**	Green	-	**Green** is a class comprised of unidentified green macroalgal species
Himanthalia elongata	-	-	-
Decaying macroalgae	Wrack	Wrack	**Wrack** is a mixture of unidentified decaying macroalgal species in varying stages of decomposition
Substratum	Substratum	Substratum	**Substratum** represents a mixture of non-vegetated surfaces such as rock and sediment

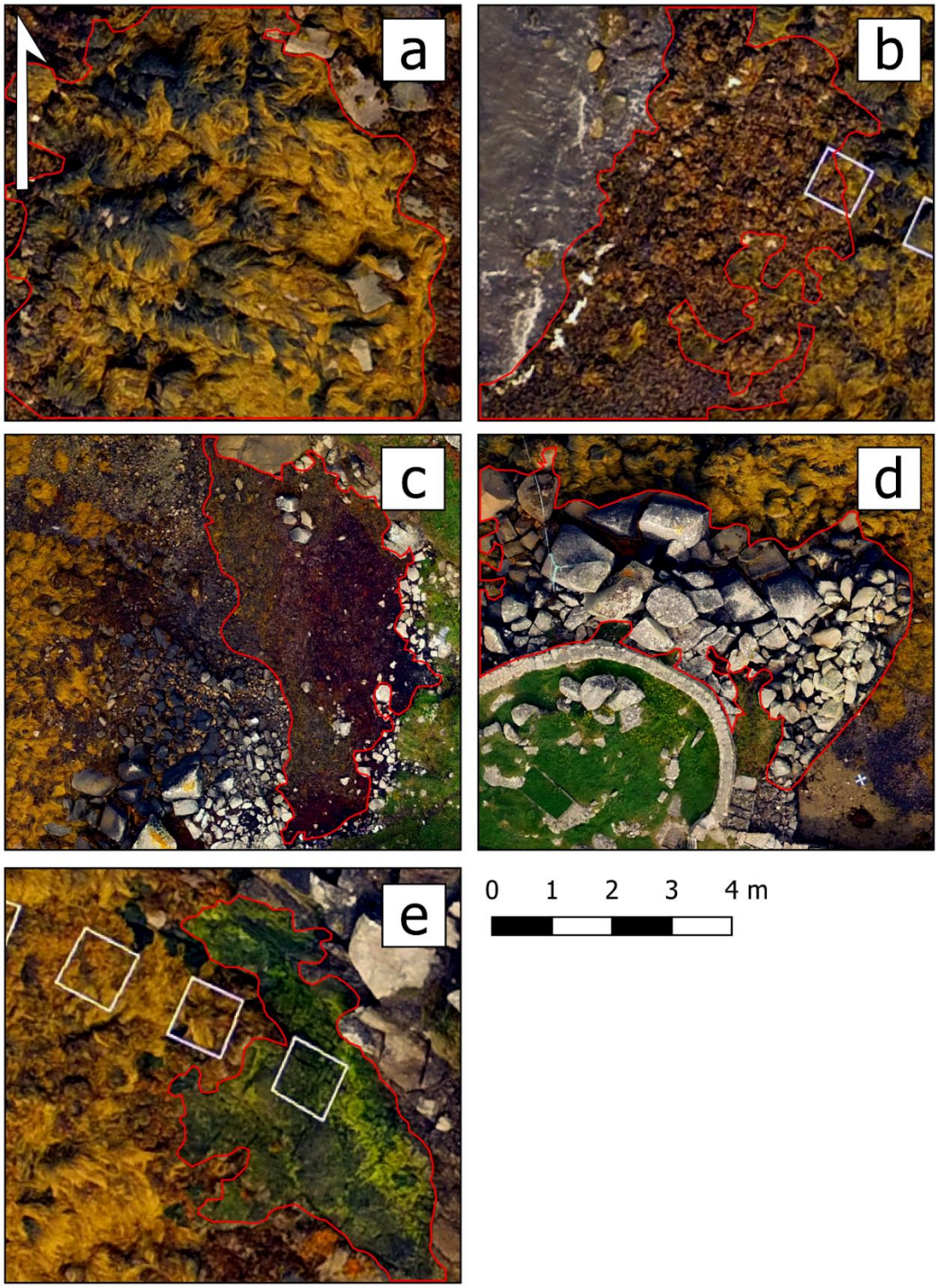

Fig. 4.3. Classification classes identifiable using high-resolution UAV RGB imagery (highlighted in red). *Ascophyllum nodosum* (**a**), *Fucus* spp. (**b**), decaying macroalgae (**c**), substratum (**d**) and unidentified green species (**e**). The distinctive morphological properties of each species were used to identify each of them.

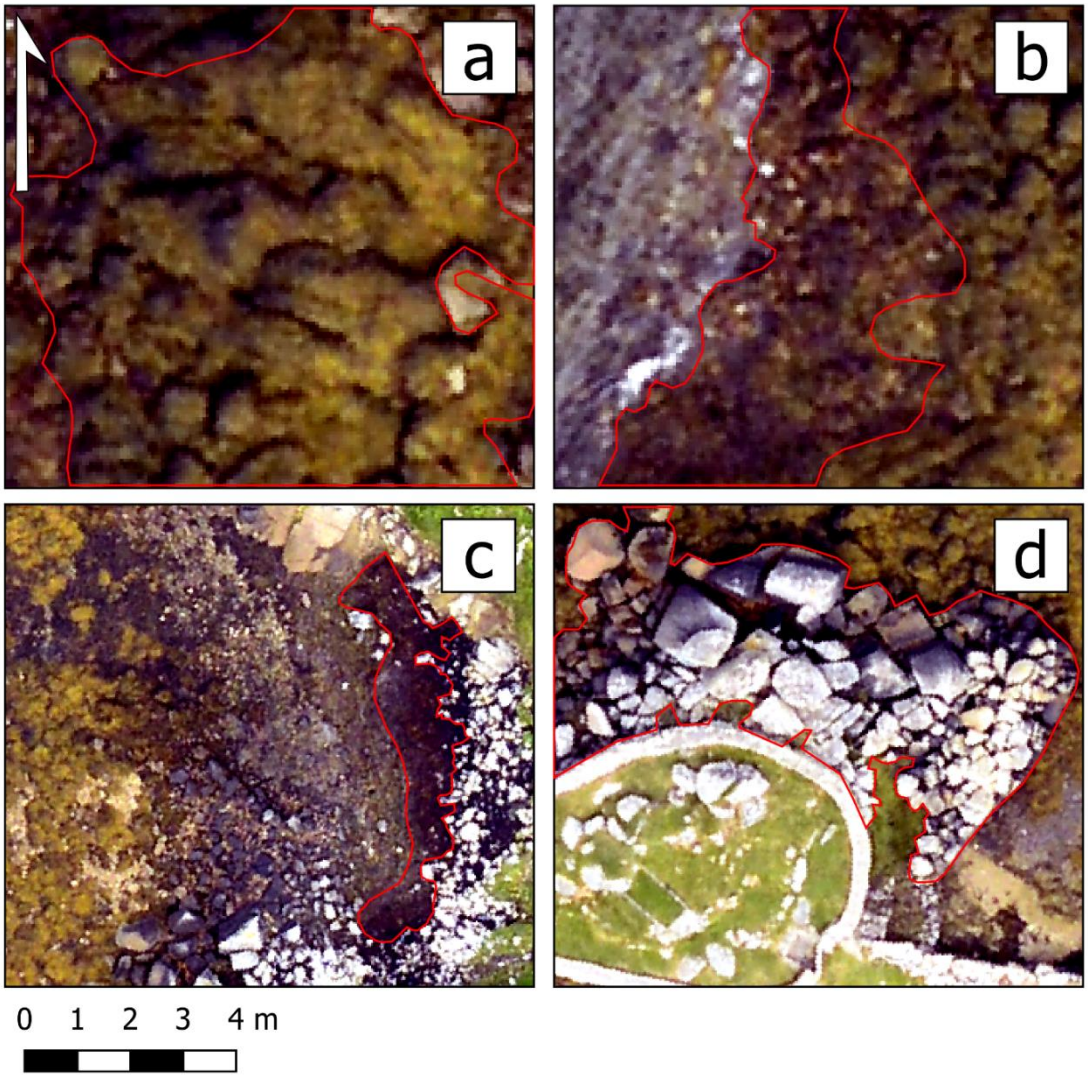

Fig. 4.4. Classification classes identifiable using aerial RGB imagery (highlighted in red). Mixed *Ascophyllum nodosum* and *Fucus* spp. (**a**), *Fucus* spp. (**b**), wrack (**c**) and substratum (**d**). Variations in canopy pattern and colour were used to identify each of them.

4.2.4.2. Supervised classification workflow

For both drone and aerial multispectral datasets, the supervised classification method Maximum Likelihood Classification (MLC) was used in ENVI 5.4. MLC is a popular classifier (Paola & Schowengerdt, 1995) calculating the probability that an individual pixel belongs to a specific class and is based on an estimated probability density function derived from the defined reference classes (Foody *et al.*, 1992). The MLC classifier assumes a Gaussian distribution for each of the inputted training classes (Jia & Richards, 1994) and can be expressed by the following equation:

$$g_i(\boldsymbol{x}) = \ln p(\omega_i) - \frac{1}{2}\ln|\Sigma_i| - \frac{1}{2}(\boldsymbol{x}-\boldsymbol{m}_i)t\sum_{i}^{-1}(\boldsymbol{x}-\boldsymbol{m}_i)$$

Where $\boldsymbol{i}$ is class, $\boldsymbol{x}$ equals *n*-dimensional data, $\boldsymbol{p(\omega_i)}$ is the probability that class $\boldsymbol{\omega_i}$ occurs in the image and is assumed the same for all classes, $|\sum_i|$ is the determinant of the covariance matrix of the data in class $\boldsymbol{\omega_i}$, $\sum_{\boldsymbol{i}}^{-\mathbf{1}}$ is the inverse matrix and $\boldsymbol{m_i}$ is the mean vector.

MLC was used to classify the training area spectra. No thresholds were selected so that all pixels would be classified, and we used the spectral separability results to determine whether sufficient training areas had been selected as to be representative of features present at the site (Richards & Jia, 2006).

4.2.4.3. Accuracy assessment

Ground-truth, or reference, data was derived from the high-resolution RGB imagery utilising the same rationale as for the training data collection. The accuracy of this approach was highlighted by Lechner *et al*. (2012) and it was also found to be more reliable and accurate than GPS-based validation methods (Laliberte & Rango, 2011). Reference data collected from *in-situ* field observations are considered the most accurate, however this can be time consuming meaning that data derived from imagery are more common (McDermid *et al*., 2005; McRoberts *et al*., 2018). Polygons were selected for each of the four (UAV) and three (aerial) classes and this was carried out independently of those used to create the training areas using ENVI 5.4 (Harris Geospatial Solutions, Boulder, USA). Polygons were created so that they covered as much of each class as possible and only in areas where homogeneous class coverage could be confidently identified. The accuracy assessment tool was used to create the confusion matrix and derive quantitative measures of accuracy (kappa, user/producer accuracy (UA/PA), errors of commission/omission).

4.3. Results

4.3.1. UAV classification results

Classification results for the UAV imagery showed the mid-intertidal zone to be dominated by dense beds of *A. nodosum* with narrow bands of mixed fucoid assemblages dominating in the upper (*F. vesiculosus, F. spiralis* and *P. canaliculata*) and lower (*F. vesiculosus* and *F. serratus*) zones. Decaying seaweed was present in patches in the extreme upper intertidal zone and this was most notable in the northeast corner of the site (**Fig. 4.5**).

Spectral separability results showed good separation between all classes with all pairs, apart from ‘Asco’ and ‘*Fucus* spp.’ (1.7) and ‘Green’ and *Fucus* spp.’ (1.86), having values greater than 1.9, indicating an almost perfect class separation (Richards & Jia, 2006). The slightly lower value for ‘Asco’ and ‘*Fucus* spp.’ separability highlighted their spectral

similarities. MLC resulted in an overall classification accuracy of 92 % and a Kappa Coefficient of 0.8733. All four classes showed high user/producer accuracies although, predictably, there is a small amount of misclassification between '*Fucus* spp.' and 'Asco', and also of 'Wrack' as '*Fucus* spp.' (**Tabs 4.2 & 4.3**). The misclassification of 'Asco' as '*Fucus* spp.' was spread throughout the site in small patches whilst the opposite occurs almost entirely in one area (**Fig. 4.6**). A small area of grass not removed by the land mask was classified as '*Fucus* spp.' in the northern section of the site. 'Asco' covered a total area of ~4,127 m^2, out of a total classified area of ~12,400 m^2.

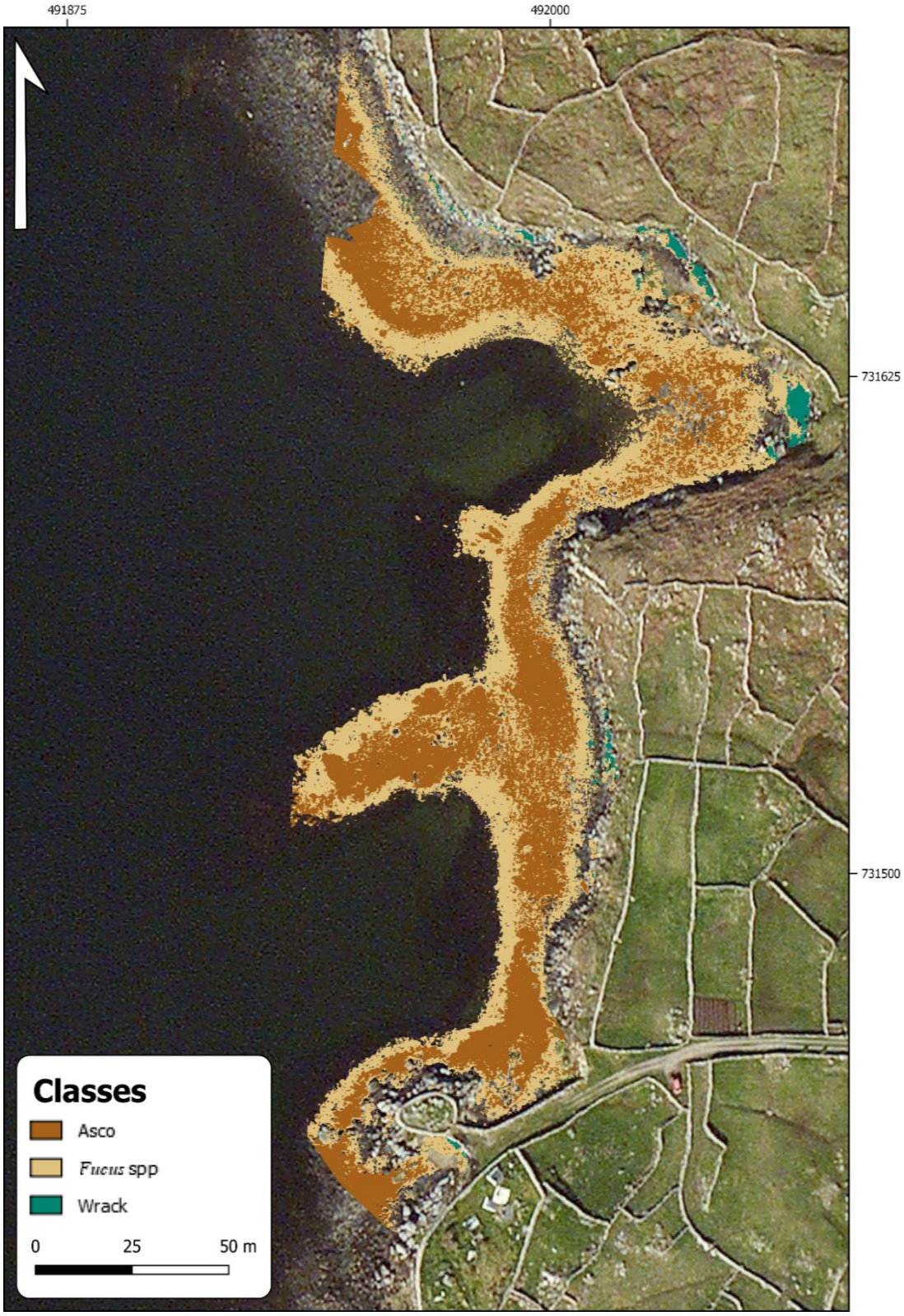

Fig. 4.5. Maximum Likelihood Classification (MLC) result from the multispectral UAV survey. Three macroalgal cover classes are displayed over Bing satellite imagery. 'Substratum' was not included. Class codes represent the following species: 'Asco', *Ascophyllum nodosum*; '*Fucus* spp.', mixed fucoids; 'Wrack', decaying macroalgae. Coordinates are in Irish Transverse Mercator (ITM).

Tab. 4.2. UAV multispectral Maximum Likelihood Classification (MLC) confusion matrix, calculated, using ENVI 5.4, by comparing pixels of known class locations to those predicted by the classification workflow, for each of the four cover classes, results are recorded as percentage of pixels assigned, correctly or incorrectly, to each class.

Class	**'Substratum'**	**'Wrack'**	***'Fucus* spp'**	**'Asco'**	**Total**
'Unclassified'	6.54	0.65	0.03	0.00	1.16
'Substratum'	**91.96**	2.25	0.82	0.01	16.22
'Wrack'	0.08	**91.48**	0.05	0.00	2.48
'Fucus spp.'	1.33	5.34	**93.63**	8.83	31.52
'Asco'	0.08	0.00	5.47	**91.16**	48.63
Total	100	100	100	100	**100**

Tab. 4.3. UAV multispectral Maximum Likelihood Classifier (MLC) User (probability of correct class assignment, calculated by dividing the number of correctly classified pixels by the total number of pixels in a class) and Producer (correctly classified reference pixels, calculated by dividing the number of correctly classified pixels by the total number of pixels that should be in a class) accuracies for each of the four cover classes computed using ENVI 5.4.

Class	**Prod Acc (Percent)**	**User Acc (Percent)**	**Prod Acc (Pixels)**	**User Acc (Pixels)**
'Substratum'	91.96	98.12	202760/220482	202760/206655
'Wrack'	91.48	98.86	31193/34100	31193/31552
'Fucus spp.'	93.63	84.35	338811/361862	338811/401660
'Asco'	91.16	96.78	599732/657877	599732/619692

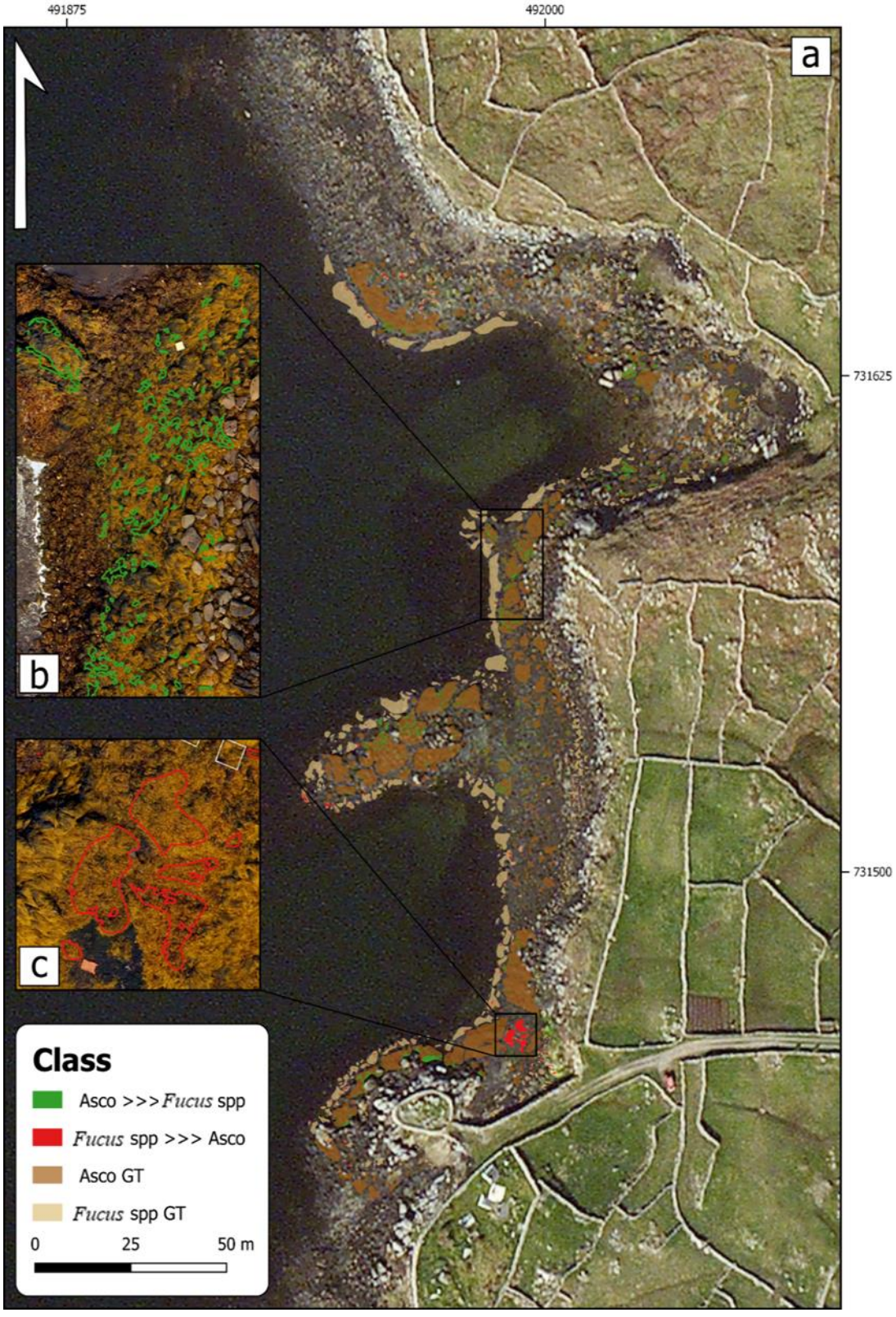

Fig. 4.6. Instances of misclassification between 'Asco' and '*Fucus* spp' displayed above each classes respective ground-truth (GT) polygons (**a**). Inset are notable misclassified areas, where, in green, **'Asco'** has been misclassified as **'*Fucus* spp.'** (**b**) and where, in red, the opposite occurs (**c**). Coordinates are in Irish Transverse Mercator (ITM).

4.3.2. Aerial classification results

Aerial multispectral classification results revealed a dense covering of an *A. nodosum* dominated mixed fucoid assemblage (*A. nodosum, F. vesiculosus* and *F. serratus*) in the mid-intertidal zone. Mixed fucoids dominate the upper (*F. vesiculosus, F. spiralis* and *P. canaliculata*) and mid-to-lower (*F. serratus* and *F. vesiculosus*, respectively) intertidal zones (**Fig. 4.7**).

There was poor spectral separability between 'Asco_*Fucus* spp.' and '*Fucus* spp.' (1.11) but both classes achieved good separation from 'Substratum' (>1.9). These two classes were retained and not combined as their poor spectral separability reflected their inherent spectral similarity. For the aerial imagery there was an overall classification accuracy of 78.9 % and a Kappa Coefficient of 0.6373. 'Substratum' had a high user/producer accuracy but there was significant misclassification of '*Fucus* spp.' as 'Asco_*Fucus* spp.' resulting in a low producer/user accuracy for the former and a low user accuracy for the latter (**Tabs 4.4 & 4.5**). This misclassification was spread throughout the entire '*Fucus* spp.' dominated zone (**Fig. 4.8**). 'Asco_*Fucus* spp.' covered a total area of ~5,342 m^2 out of a total classified area of ~12,000 m^2.

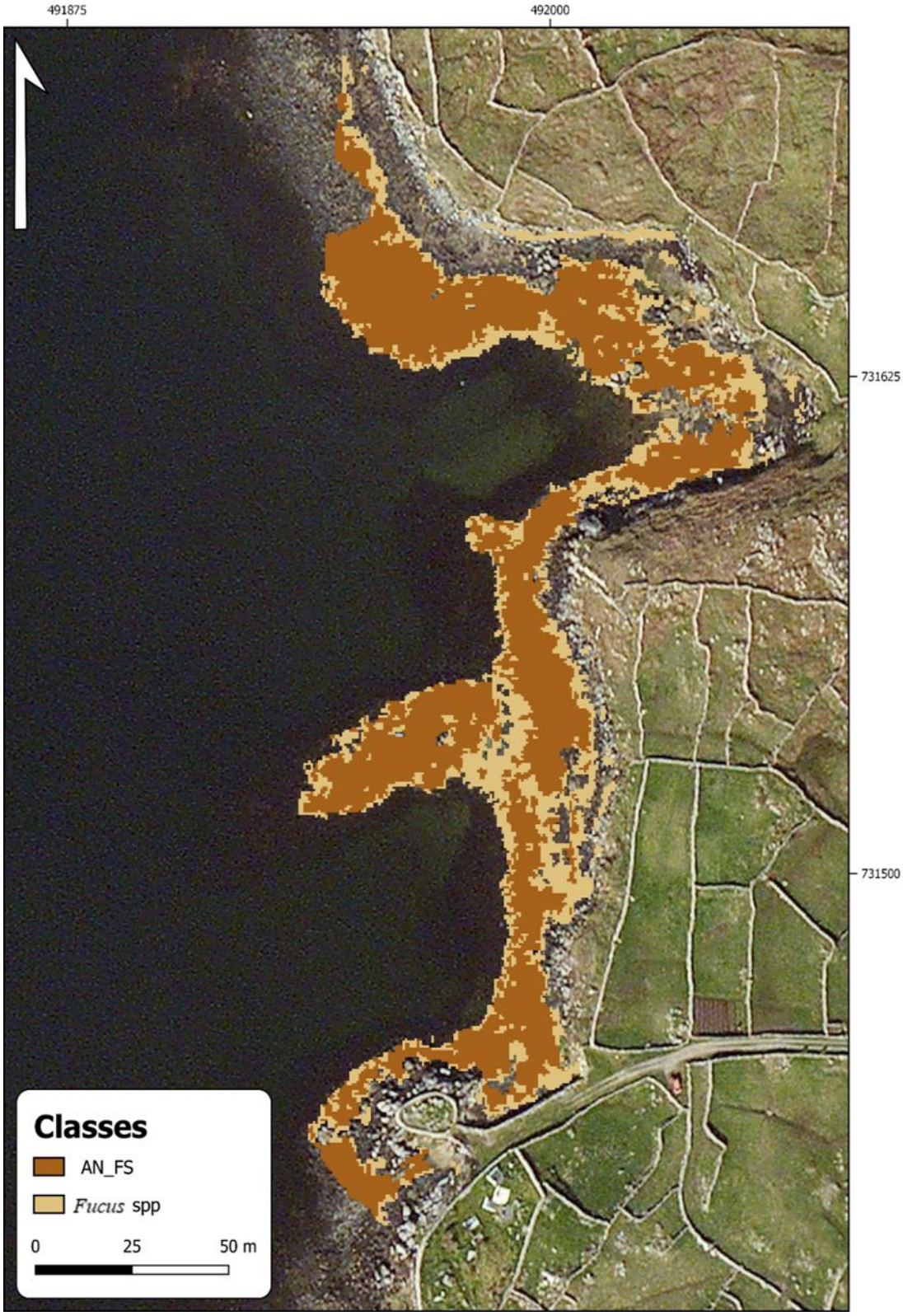

Fig. 4.7. Maximum-likelihood classification (MLC) result from the multispectral aerial survey. Two macroalgal cover classes are displayed over Bing satellite imagery. 'Substratum' was not included. Class codes represent the following species: fucoid mix dominated by *Ascophyllum nodosum* (abbreviated here to AN_FS and referred to in the text as 'Asco_*Fucus* spp.') and mixed fucoids ('*Fucus* spp.'). Coordinates are in Irish Transverse Mercator (ITM)

Tab. 4.4. Aerial multispectral Maximum Likelihood Classification (MLC) confusion matrix, calculated, using ENVI 5.4, by comparing pixels of known class locations to those predicted by the classification workflow, for each of the three cover classes, results are recorded as percentage of pixels assigned, correctly or incorrectly, to each class.

Class	**'Substratum'**	***'Fucus* spp'**	**'Asco_*Fucus* spp'**	**Total**
'Unclassified'	6.13	0.00	0.00	1.10
'Substratum'	**89.10**	5.79	0.97	18.20
'Fucus spp.'	4.02	**46.53**	5.82	17.31
'Asco_Fucus spp'	0.74	47.68	**93.22**	63.38
Total	100	100	100	**100**

Tab. 4.5. Aerial multispectral Maximum Likelihood Classifier (MLC) User (probability of correct class assignment, calculated by dividing the number of correctly classified pixels by the total number of pixels in a class) and Producer (correctly classified reference pixels, calculated by dividing the number of correctly classified pixels by the total number of pixels that should be in a class) accuracies for each of the three cover classes computed using ENVI 5.4.

Class	**Prod Acc (Percent)**	**User Acc (Percent)**	**Prod Acc (Pixels)**	**User Acc (Pixels)**
'Substratum'	89.10	87.96	1439/1615	1439/1636
'Fucus spp.'	46.53	78.02	1214/2609	1214/1556
'Asco_Fucus spp'	93.22	77.95	4440/4763	4440/5696

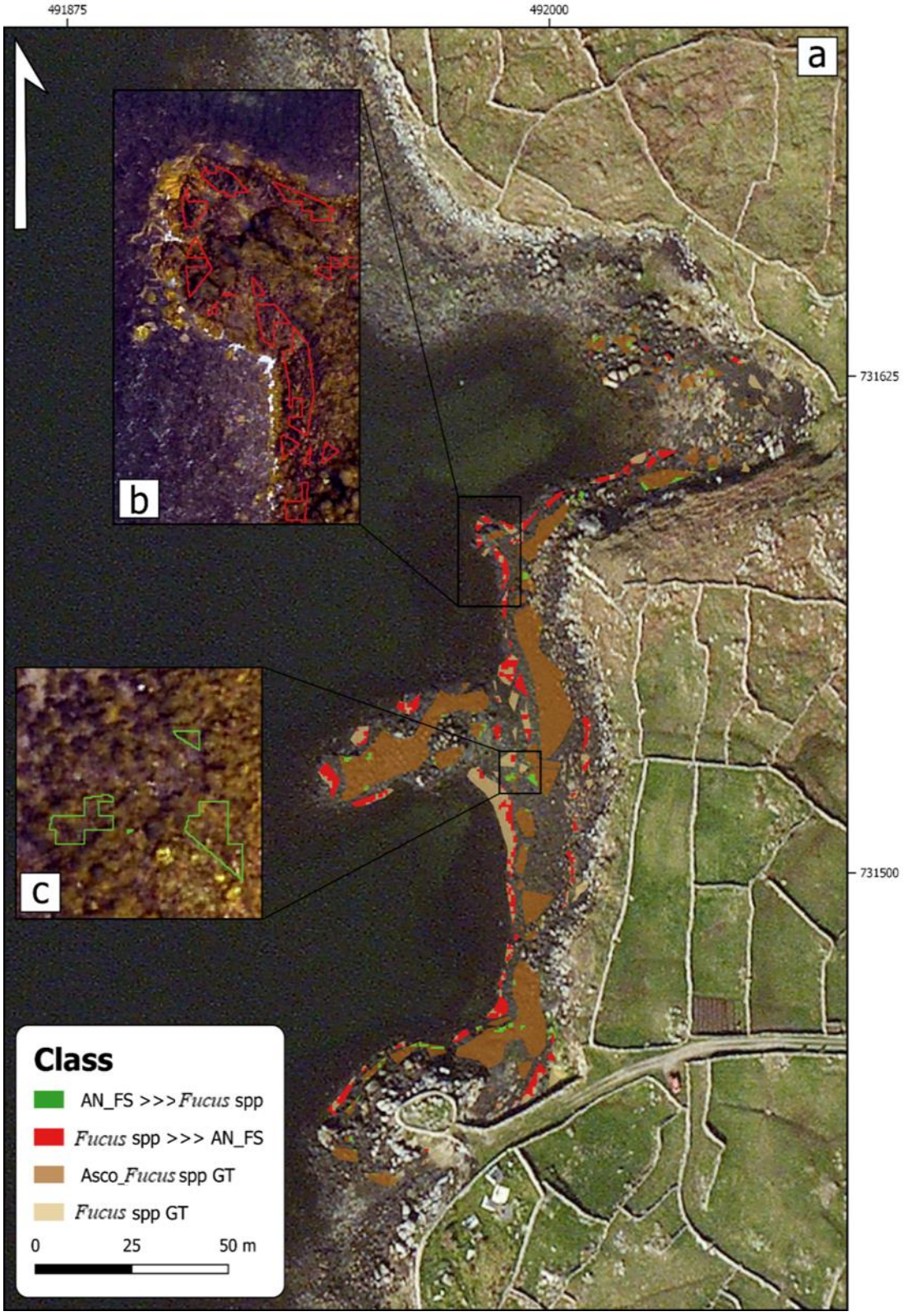

Fig. 4.8. Instances of misclassification between 'Asco_*Fucus* spp.' (labelled here as **AN_FS**) and '*Fucus* spp.' displayed above each classes respective ground-truth (GT) polygons (**a**). Inset are notable misclassified areas, where, in green, **'Asco_*Fucus* spp.'** has been misclassified as **'*Fucus* spp.'** (**c**) and where, in red, the opposite occurs (**b**). Coordinates are in Irish Transverse Mercator (ITM).

4.3.3. Satellite imagery

The coarse spatial resolution of the Sentinel-2 satellite imagery meant that it was not possible to identify any intertidal macroalgal species to use as training data for a supervised classification workflow. It was, however, possible to visually identify and separate the macroalgae-dominated intertidal zone, covering ~ 8000 m^2, from terrestrial vegetation and rock/manmade features.

4.4. Discussion

The increasing affordability of remote sensing technologies (Colefax *et al*., 2018) will support their application for a diverse range of ecological monitoring initiatives. The high spatial and spectral resolutions required for the accurate classification of intertidal macroalgal communities (Dekker *et al*., 2003) can often be expensive (i.e. hyperspectral), acting as a barrier to organizations and research groups. Here, the effectiveness of relatively low-cost multispectral sensors and their platform-dependent spatial resolutions for mapping the distribution of *A. nodosum* was explored. Of the three platforms used, UAV-mounted multispectral remote sensing provided the most accurate results.

UAV imagery accurately identified and classified a homogenous *A. nodosum* class ('Asco'), distinguishing it from surrounding mixed fucoid assemblages and from base substratum. The high spatial resolution of concurrently collected RGB data allowed for the visual identification of *A. nodosum* which was characterized by its distinctive morphology and colouration. Despite their inherent spectral similarities (Kotta *et al*., 2014) and the low spectral resolution of the sensor, clear separation between the macroalgal classes could be achieved. Coarser resolution aerial imagery was able to classify a lower taxonomic resolution mixed *A. nodosum* and *Fucus* spp. class ('Asco_*Fucus* spp.'). By contrast, freely available Sentinel-2 imagery was found to be too coarse for mapping intertidal macroalgal communities as it was not possible to observe the fine-scale assemblages, but it was possible to identify the macroalgal-dominated intertidal zone. Higher spatial resolutions (UAV RGB = 2.2 cm/pixel, Aerial RGB = 6 cm/pixel) enhanced not only our ability to visually identify species for training and reference data (Meddens *et al*., 2011), but also the ability of MLC to assign pixels to classes as, owing to their smaller size, there was less within-pixel spectral mixing (Doughty and Cavanaugh, 2019). In areas with a relatively low intertidal macroalgal species diversity but dense, homogenous stands, our results demonstrate that multispectral sensors provided an effective tool for species mapping and a lower cost alternative to hyperspectral sensors.

4.4.1. UAV multispectral imagery

Ascophyllum nodosum ('Asco') was accurately identified using the UAV platform (PA = 91 %, UA = 96.8 %) and we believe that the spectral differences between *A. nodosum* and the other classes became more apparent at the canopy (Meddens *et al*., 2011) over individual frond scales (Kotta *et al*., 2014). The spectral similarity between 'Asco' and '*Fucus* spp.' likely explains the small amount of misclassification between them. This was most evident towards the southern section of the site where a large area of '*Fucus* spp.' has been misclassified as 'Asco'. Visually this patch appeared significantly yellower and brighter than other '*Fucus* spp.' areas which may have led to confusion with the bright 'Asco' class. The remainder of the misclassification was spread throughout the site, highlighting some of the challenges when collecting training and reference data in spatially heterogeneous environments whereby polygons cannot necessarily account for small patches of different classes within their boundaries (Foody, 2002). Spatial complexity could not be fully accounted for in the collection of training and reference data and this includes intraspecific variation, for example many of the 'Asco' pixels misclassified as '*Fucus* spp.' appeared to be in shaded areas behind, or between, boulders which may have darkened their spectral response leading to misclassification (Wigmore *et al*., 2019). The creation of specific shaded classes may help to resolve this in the future (Ishida *et al*., 2018) but given the present low classification error, it was deemed not necessary here.

Owing to the bands used by the Parrot Sequoia, the spectral similarity observed between 'Green' and '*Fucus* spp.' was to be expected. Previous research has, using spectroradiometers, highlighted the strong spectral separability between macroalgal groups (Casal *et al*., 2013; Kotta *et al*., 2014). **Fig. S4.3** shows that the spectrum of 'Green' was similar to that of both brown macroalgal classes, and with this sensor not having any bands below 550 nm, or between 550–660 nm, key distinguishing features of green macroalgae (single peak at 550 nm) and brown macroalgae (three peaks and troughs between 550–660 nm) (Kutser *et al*., 2006b) were not recorded, potentially explaining the poor spectral separation. Ultimately, because of the small area covered by green macroalgal species, in comparison to other classes, its exclusion might not significantly alter the accuracy of the final classification.

4.4.2. Aerial multispectral imagery

Whilst the classification results from the aerial multispectral imagery broadly agreed with the UAV imagery, managing to identify an *A. nodosum* dominated ('Asco_*Fucus* spp.') belt, it was not able to identify a pure *A. nodosum* class. The resulting lower taxonomic resolution

class meant that it was not possible to determine an accurate area estimation for *A. nodosum* at the site. Coarser pixel sizes led to increased sub-pixel mixing of spectra, with one or more classes potentially being present within a single pixel (Su *et al*., 2006; Lyons *et al*., 2011). The coarser resolution meant that it was difficult to accurately select enough training data for classes that cover a small area, such as 'Wrack', leading to its exclusion from the final classification. Such exclusions highlight the need for finer levels of spatial resolution, but also show that the decision whether or not to include a class also depends on research objectives and it was determined to prioritise the classification accuracy of dominant cover classes over minor ones. Coarse pixel size was also responsible for the low spectral separability between 'Asco_*Fucus* spp.' and '*Fucus* spp.' where many pixels were spectrally heterogeneous (Belluco *et al*., 2006), containing mixtures of fucoid species that were not necessarily observable through visual analysis of the RGB imagery. The significant misclassification of '*Fucus* spp' pixels as 'Asco_*Fucus* spp.' appears most prevalent across the boundary between the mid-and-lower intertidal zone where there was a transition from an *A. nodosum* dominated assemblage to a *Fucus* spp. dominated one (**Fig. 4.8**). This highlights the difficulties in trying to distinguish between two spectrally similar classes.

4.4.3. Satellite multispectral imagery

The spatial resolution of Sentinel-2 data was too coarse to allow for macroalgal species identification as the highest band resolutions (10 m) were still larger than the footprint covered by species present within the intertidal. The relatively coarse spatial resolution of some satellite imagery does not preclude it's application for macroalgal monitoring, however. For species which form homogenous, monospecific stands, such as *Macrocystis pyrifera* off the coast of Santa Barbara, 10 m resolution satellite imagery was able to provide accurate canopy cover estimations (Cavanaugh *et al*., 2010). If well supported by *in-situ* sampling (i.e. abundance and percentage cover), the ability of the satellite to identify the intertidal zone could allow for the broad extrapolation of localized *in-situ* biological data to regional-scale estimates of macroalgal extent. Yet, the time involved in conducting such detailed *in-situ* surveys would negate the efficiency provided by satellite remote sensing and the resulting extent estimates will be significantly less accurate than those achieved through direct quantification of species extent using UAVs and aircraft.

4.4.4. Effectiveness of high-resolution RGB data for training and reference data collection

The collection of accurate reference and training data directly impacts upon classification accuracy. When considering the future potential for large-scale intertidal macroalgal surveys

it would be impractical (time and cost) to conduct extensive field campaigns. The potential for GPS (Laliberte and Rango, 2011) and image georeferencing errors (Jaud *et al*., 2018) would still create bias towards selecting training and reference data from large homogenous stands of macroalgae (Foody, 2002) which were observed when collecting data through visual assessment of the RGB imagery. UAVs can be used to efficiently collect training data over much larger areas than using field-based methods (Gray *et al*., 2018) and the accuracy of this method relies on achieving a high enough spatial resolution to enable complex patterns to be observed. The resolutions achieved by UAVs allow for the accurate and efficient collection of training and reference data through being able to accurately identify intertidal macroalgal species. Applicability, however, may depend on the target species, but the distinctive morphological and colour properties of *A. nodosum* at the study site enhanced the accuracy of its identification.

4.4.5. Operational considerations

From a spatial resolution perspective, this study has demonstrated how UAVs allow for the accurate classification and quantification of *A. nodosum* distribution. At present, such results are likely only achievable over small geographic areas owing to current national UAV regulatory policies (Baena *et al*., 2018), despite battery technology allowing many UAVs to fly between 60-180 min. Whilst aircraft can cover much larger areas, they tend to have coarser spatial resolutions (Anderson and Gaston, 2013) which, depending on research objectives, could reduce classification accuracy, limiting their usefulness for intertidal macroalgal resource assessment. The development and granting of beyond visual line of site (BVLOS) permission to companies and individuals who meet specified national aviation authority guidelines will allow the scaling up of UAV surveys to the point where they may offer a true mapping alternative to aircraft.

The cost-effectiveness of using remote sensing to map intertidal macroalgae will vary depending on project requirements, with factors such as geographic scale potentially informing on the most suitable platform to use. Both the UAV and aerial surveys required similar workhours for the data collection and processing, with the aerial survey able to collect data over a far larger geographic area. Hiring a company to conduct remote sensing surveys is the only feasible option for aerial surveys, yet, for UAV surveys it may end up more cost-effective, in the long-term, to bring data collection and processing capabilities ‘in-house’, especially if temporal studies are planned. The only caveat of this approach is the initial setup cost (i.e. UAV, GPS, sensor, software and pilot training), the requirement for specialised technical knowledge, computing capabilities and compliance with local regulations. Furthermore, the use of satellites may still prove a useful option depending on

the research question. Higher spatial resolution satellites, such as RapidEye (5 m/pixel) may be applicable for studies looking at identifying and mapping broader taxonomic classification classes, such as macroalgal groups, over large areas (Brodie *et al*., 2018).

4.4.6. Management implications of UAVs

At present, UAV technologies are well suited to the rapid, flexible and cost-effective mapping of relatively small geographical areas and is well-suited for the unique challenges of mapping in the intertidal zone. Their capability to conduct multiple, repeat measurements (Manfreda *et al*., 2018) will also enhance their application in monitoring dynamic ecosystems, short-term events (algal blooms etc.), mobile fauna and invasive species. Straightforward integration of multispectral sensors (e.g. DJI SkyPort) will further enhance applications for UAV technology and technological and regulatory developments will only improve the ability of UAVs to contribute towards the establishment of accurate environmental baseline monitoring and will, in turn, inform resource conservation and management decisions (Connell *et al*., 2008). The world is changing and developments in drone regulatory policy, such as common EU regulations (https://www.easa.europa.eu/easa-and-you/civil-drones-rpas), together with a global move towards BVLOS operations will present the possibility of long range coastal macroalgal surveys in the not too distant future. This will improve the ability of interested stakeholders to efficiently manage and conserve intertidal macroalgal communities over large geographic areas. In addition to this, decreasing costs of UAVs and sensors will make such technology accessible to a broader range of interested stakeholders, enabling a wide range of novel applications (Johnston, 2019).

Whilst the use of UAVs for monitoring macroalgal habitats is growing (Taddia *et al*., 2019; Tait *et al*., 2019), a range of different studies have incorporated UAVs into management and conservation research objectives. Monitoring of orangutans has been conducted using both RGB (Wich *et al*., 2016) and thermal sensors (Burke *et al*., 2019), the small size of UAVs making them ideal for operating in remote environments. UAVs have also proven capable of operating in challenging conditions, helping researchers to monitor the health (Pirotta *et al*., 2017) and physiology (Christiansen *et al*., 2016) of whales. Yet, there remains a need for standardization in UAV monitoring protocols to account for variations caused by solar conditions, survey accuracy and flight planning, to allow for direct comparisons of data between study sites and time (Assmann *et al*., 2019).

4.5. Conclusions

The likely increase of anthropogenic pressures upon intertidal macroalgal communities requires the development of accurate and efficient mapping methodologies to complement traditional field survey techniques and must also consider a range of different budgets. Different remote sensing platforms each offer unique advantages and disadvantage and their suitability for the mapping of intertidal macroalgal communities was compared. This study has demonstrated how UAV-mounted multispectral remote sensing was the most accurate of the three methods for assessing the distribution of *A. nodosum*, where having a high spatial resolution allowed complex spatial patterns to be observed. High-resolution RGB imagery facilitated the accurate collection of training and reference data and this method will likely complement the scaling up of UAV-based surveys in the future (Gray *et al*., 2018). The creation of sustainable resource management plans can now be underpinned by highly accurate, relatively low-cost, and spatially comprehensive remote sensing data collection methodologies. The development of machine learning techniques is likely to yield improved classification results and has already proven useful for automated identification of weeds within crop fields (de Castro *et al*., 2018; Gao *et al*., 2018).

Relatively inexpensive multispectral sensors, when mounted on a UAV, provide an effective macroalgal resource assessment tool when used in environments with low species diversity and homogenous cover of canopy forming species. For repeat surveys, the most cost-effective solution is to bring data collection, processing and analysis 'in-house' where decreasing technology costs, such as the 3dr Solo UAV (Johansen *et al*., 2018), are reducing financial barriers for those wishing to employ remote sensing technology to their research, for example, enabling those in remote but biodiverse regions of the globe to better monitor and conserve their ecological resources (Vargas-Ramírez and Paneque-Gálvez, 2019). Lower costs and an increase in turnkey multispectral sensors may also facilitate the use of UAVs and multispectral sensors by local conservation charities and citizen science groups which, with the development of standardized mapping methodologies, could facilitate the accurate, high-resolution, monitoring of macroalgal resources over much wider spatial and temporal scales than currently possible. Future work should explore potential seasonal and spatial trends in the accuracy of image capture and the implications for data processing. Likely variation in the intra and inter-specific spectral responses and relationships of intertidal macroalgae, often due to seasonal variation in localised light regimes (Stengel and Dring, 1998), may influence the ability of multispectral sensors to accurately discriminate between them.

Acknowledgements

The authors greatly appreciate the help provided by Fearghus Foyle, Aidan Magee, Daire Walsh and Sean Mannion with the collection of the UAV and aerial imagery. We are also grateful for the assistance of Cole and the company of his dog, Sailor. This Cullen Fellowship research (Grant-Aid Agreement No. CF/15/02) was supported by the Marine Institute and INFOMAR and funded under the Marine Research Sub-programme by the Irish Government.

Chapter 5: Multibeam mapping of subtidal kelp species

View off the stern of the RV Lir during the collection of subtidal acoustic data in Roaringwater Bay (Co. Cork).

Abstract

Large brown macroalgal kelp species (Laminariales, Ochrophyta) dominate subtidal rocky coastlines across temperate and sub-polar latitudes. Increasing awareness of their ecological importance is leading to the need for the implementation of sustainable management plans. To achieve this, accurate baseline ecological data collections methodologies must first be collected. Traditional field sampling is restricted in spatial scale and optical remote sensing techniques are often depth-limited by the attenuation of light in water. Acoustic remote sensing does not face the same constraints. A comparison of the ability of different Multibeam (MBES) sonar frequencies for the detection of kelp distribution and canopy height is presented here. For each of the three frequencies (200, 300, 400 kHz), water column data were logged to record the weak, scattered acoustic returns that would indicate the presence of a potential kelp bed. A ~5 ha site was surveyed, and acoustic data were validated by using a dropdown camera to identify the presence and absence of kelp species, along with identifying floral and faunal species. Baseline bathymetric maps were first created before analysing the water column by filtering out acoustic returns from the seabed and from the water column, through bottom and sidelobe suppression, to isolate a potential kelp signal. Once these soundings were identified they were then extracted and used to create canopy height and distribution maps. Results for each frequency show that similar kelp bed area values were mapped and that a similar range of kelp canopy height values were recorded (0–2 m). Kelp was confined to a rocky reef, occurring over depths of 4–15 m and video analysis confirmed the presence of a dense kelp, dominated by *Laminaria hyperborea*. In addition, trials of a mini-ROV showed that it was capable of identify different kelp and associated faunal species; this may be a useful tool for validating acoustic datasets.

5.1. Introduction

Kelps of the order Laminariales (Phaeophyceae) often dominate subtidal rocky coastlines across both temperate and subpolar latitudes (Smale *et al*., 2019). Through their status as a foundation species (Miller *et al*., 2011), kelps modify their surrounding environment by reducing water flow (Jackson, 1997, Gaylord *et al*., 2007), increasing sedimentation rates (Madsen *et al*., 2001) and the provision of habitat through the creation of complex three-dimensional structures (Dayton, 1985). The morphology of kelp individuals supports diverse floral and faunal communities as the holdfast, stipe and blade each provide distinct habitats (Teagle *et al*., 2017). In dampening waves, kelp forests provide coastal protection services (Steneck *et al*., 2008) and they can play an important role in carbon sequestration (Hill *et al*.,

2015) through carbon cycling, characterised by the rapid turnover of biomass (Reed & Brezinski, 2009).

Kelp habitats can often become denuded by a range of natural and anthropogenic pressures. Disease, grazing (most commonly by urchins, but not in Ireland) and physiological stress are common natural pressures (Steneck *et al*., 2008) and it is likely that changing climates could push some macroalgal species beyond the range of suitable habitats (Wernberg *et al*., 2011). Direct human impacts, such as harvesting, and indirect, such as increased turbidity through run-off (Desmond *et al*., 2015), and trophic cascades leading to urchin barrens, predicated by overfishing, also contribute to kelp deforestation, and variations in the frequency and intensity of these activities will affect recovery rates (Teagle *et al*., 2017).

Kelps are one of the most productive habitats found within the coastal zone (Steneck *et al*., 2002) and the importance, for food security (*i.e.* global fisheries), of effectively managing this zone cannot be overstated (Pauly *et al*., 2002). With a general lack of information on the impacts of anthropogenic pressures (Ierodiaconcou *et al*., 2007), detailed baseline ecological data must be collected to allow for informed, sustainable decision making on how to manage these resources and the anthropogenic activities associated with them (Jordan *et al*., 2005). Survey methods for kelp and other subtidal species, including seagrass and freshwater macrophytes, can be broadly assigned to three different categories. Field survey methodologies will typically involve the direct sampling and measurement of subtidal species (Abukawa *et al*., 2013) such as through SCUBA or video transects. Whilst allowing the collection of detailed biological data, such methods are costly, time-consuming (Hasan *et al*., 2011) depth limited (Spalding *et al*., 2003) and may not accurately capture the complexity of spatially heterogenous habitats (Brown & Collier, 2008). Regardless, detailed field surveys are the only way to collect important ecological information with which to characterise the habitat, such as predicting kelp bed biomass based on the relationship between stipe length and weight (Blight *et al*., 2011). Optical remote sensing technologies are typically considered as being unsuitable for assessing subtidal habitats as they can often be limited by depth owing to limited light penetration (Brown & Blondel, 2009; Bajjouk *et al*., 2015), particularly in turbid waters. Although several studies have successfully used satellites to accurately map the distribution of subtidal kelp beds, they have still been limited to relatively shallow depths of < 10 m (Casal *et al*., 2011; St-Pierre & Gagnon, 2020). This means that a full distribution map cannot be achieved for deeper occurring kelps, such as *Agarum cribrosum*, or kelps which occur over broad depth ranges, and occurrence depth and canopy height values cannot be determined (McGonigle *et al*., 2011).

Acoustic remote sensing technologies are not constrained by the optical properties of water (Kruss *et al*., 2017) as water is an effective medium for sound waves (Lurton, 2002). Acoustic remote sensing works by transmitting an acoustic signal from the transducer head and then recording the returning echoes. The time taken for the echo to return can be used to calculate depth (bathymetry) and the intensity of the return signal can be used to infer the physical nature of the seafloor (backscatter) (Masetti & Calder, 2012). Singlebeam Echosounders (SBES) were developed in the early 20th century to esonify an area directly beneath the survey vessel, primarily to calculate seabed depth (Colbo *et al*., 2014). The development of Multibeam Echosounders (MBES) in the 1970's (Renard & Allenou, 1979; Mayer, 2006) greatly improved mapping capabilities, allowing larger areas of the seafloor to be mapped because of the high number of beams and wide swath width of beams transmitting athwartship (Brown & Blondel, 2009), making them the preferred method for seabed mapping, albeit with reduced efficiency in shallow water (Costa *et al*., 2009). The ability to record acoustic returns, not just from the seabed, but also from the water column, enables the detection of fish (Cushing, 1952; Weber *et al*., 2009) and submerged aquatic vegetation (SAV). The use of MBES for water column applications has lagged behind SBES, primarily due to the immense data storage requirements (Colbo *et al*., 2014) which is why, despite the widespread application of MBES for seafloor mapping, many studies looking at mapping SAV still utilise SBES.

A typical rocky seabed would produce a strong acoustic return signal and analysis of the return ping would show a defined signal peak (Kruss *et al*., 2011). SAV will be visible as a weaker acoustic signal above the seabed, which is caused by the density contrast between SAV and the surrounding water (Warren & Peterson, 2007; Lefebvre *et al*., 2009) and also the diffuse reflection of acoustic energy (Lurton, 2002). This unique acoustic signature (weaker than the seabed, but stronger than the water column) can be isolated and theoretically used to determine the presence and height of SAV (Minami *et al*., 2010). Water column data was historically used for locating fish (McGonigle *et al*., 2011) and affords the opportunity to record and analyse acoustic signals in the water column (such as macroalgae) that may have been filtered out by sonar systems not recording water column. Height and distribution maps have been successfully created for *Laminaria* spp., in Japan (Minami *et al*., 2010) and Kongsfjorden (Kruss *et al*., 2017) using SBES, and in the USA, using MBES (McGonigle *et al*., 2011). Seagrass canopy height and abundance has also been successfully mapped in the UK with SBES (Lefebvre *et al*., 2009) as well as with MBES in Japan (Komatsu *et al*., 2003). In some cases, acoustic signatures have been used to discriminate between broad taxonomic groups, such as macroalgae and seagrass (Riegl *et al*., 2005) and laboratory tests have identified unique acoustic signatures of some kelp species (Kruss *et al*.,

2017; Shao *et al*., 2019). The choice of acoustic frequency will influence the sensors ability to detect SAV. For seabed detection lower frequencies are preferred as higher frequencies (> 100 kHz) suffer from greater attenuation in the water column, meaning less energy is transmitted to the seabed (Freitas *et al*., 2008). Previous studies mapping SAV used frequencies in the range of 200 kHz (Minami *et al*., 2010; Kruss *et al*., 2017) to 500 kHz (Komatsu *et al*., 2003; McGonigle *et al*., 2011) as they are better at detection features within the water column. Validation data are often collected using video transects (Ierodiaconou *et al*., 2007; Hasan *et al*., 2011; Mielck *et al*., 2014). Recent developments in ROV technology, including component miniaturisation, have created small and affordable mini-ROVs (Raoult *et al*., 2020) which may offer an alternative validation data collection solution.

Biological recording data indicates that kelps are present around the entire coastline of Ireland (Smale *et al*., 2013) where suitable substratum and conditions exist. Aside from preliminary studies conducted by Blight *et al*. (2011) and MacCraith & Hardy (2015) there has been no quantitative assessment of Irish kelp populations nor the development of a suitable methodology for achieving this. This study sought to investigate the ability of MBES, using water column and different acoustic frequencies, for mapping subtidal kelp. In Ireland, subtidal kelp beds are dominated by *Laminaria* spp., particularly *Laminaria hyperborea*, and these communities are of both economic, providing habitat for commercially important fish and invertebrate species, and ecological importance (Blight *et al*., 2011). A small experiment, using a mini-ROV, was also conducted to assess their potential application for the collection of validation data. To assess the potential of using MBES for the development of wider-scale kelp resource assessment methodologies, the following research questions were addressed:

i. Which acoustic sonar frequency is most suitable for identifying the presence of subtidal kelp beds?
ii. Is it possible to derive accurate distribution and canopy height values using MBES data?
iii. What recommendations can be made about the suitability of MBES and water column data in the development of a larger-scale resource assessment methodology?

5.2. Methods

5.2.1. Study Site

The survey site was located by Copper Point, off Long Island (51°30’06.8” N, 9°32’05.2” W), within Roaringwater Bay in Co. Cork (**Fig. 5.1**). The site was chosen owing to suitable

substratum and depths observed using existing INFOMAR bathymetric datasets. The bay is classified as a Special Area of Conservation (SAC) under the EU habitats directive and stretches from Long Island to Baltimore, encompassing the bay and most of the islands (NPWS, 2014). The bay is designated for submerged or partly submerged sea caves, reefs and large shallow inlets and bay and for the presence of *Halichoerus grypus* (grey seal) and *Phocoena phocoena* (harbour porpoise) (NPWS, 2011). The primary underlying bedrock is comprised of Devonian red sandstone reefs which run parallel to troughs of Devonian Carboniferous marine clastics (NPWS, 2014). Laminaria dominated subtidal reef communities occur on moderately exposed reefs and are dominated by *L. hyperborea*, with *L. digitata* and *S. latissima* present in shallower waters (< 15 m) (NPWS, 2011).

Fig. 5.1. Map showing the location of the acoustic survey site within Roaringwater Bay (Co. Cork) (**b**) in relation to Ireland (**a**). Footprint of the survey area is taken from the 200 kHz acoustic dataset (**c**). Coordinates are in UTM_29.

5.2.2. Multibeam survey

Acoustic surveys were carried out in July 2019 over a period of a couple of hours during high tide. The Geological Survey of Ireland's (GSI) survey vessel, the RV Lir (**Tab. 5.1**), mounted with a T20-P multibeam system (Teledyne Technologies International Corp, Thousand Oaks, USA), which was lowered into position through the hull, was used to

conduct the survey. The initial location of the kelp bed (herein referred to as kelp, indicating a subtidal assemblage of *Laminaria* spp., most likely dominated by *L. hyperborea*) was determined by consulting existing INFOMAR bathymetric data for the area, looking for suitable depths (<15 m) and rocky substrate. Once in place a drop-down GoPro Hero 4+ (GoPro, San Mateo, USA), mounted on a custom weighted frame, was used to confirm the presence of kelp. The survey began at 15:30 GMT and was conducted parallel, and as close as possible, to the shoreline. A rocky feature, of suitable depth(s) was identified on the vessels acoustic display and data were collected over this and in deeper water to the north and the south of the suspected kelp so that its distribution could be defined. Three passes were completed, each logging water column data at different frequencies (200, 300 and 400 khz), using the "Water column recording" (logs water column data — not enabled by default) and "Multidetect" (provides multiple detections in the water column and is useful when surveying complex underwater features such as wrecks, helping to detect otherwise overlooked features such as masts) features in the hydrographic survey planning, acquisition and data processing software QINSY (QPS, Zeist, Netherlands), all other settings remained constant (**Tab. 5.2**) and a single sound velocity profile (SVP) was taken to correct for localised variations in water column transmission properties. As water column data were being collected, the resulting files were large and each survey line was split into multiple lines, each capped at 1.5 GB.

Tab. 5.1. Technical specifications of the survey vessel, the RV Lir.

Model	Stormforce Jango (Rib)
Builder	Redbay
Length (m)	11
Beam (m)	3.31
Draft (m)	0.5 (equipment not deployed)
Top speed (knots)	30
Slow speed (knots)	4

Tab. 5.2. T20-P Multibeam shallow water survey settings.

Beam mode	Equi-Distant
Beams	512
Coverage	70°
Range (m)	90
Power (dB)	214
Pulse length (µs)	430
Gain (dB)	20
Max rate (p/s)	16

5.2.3. Ground-truth data collection

Once the acoustic surveys had been completed, the drop-down GoPro Hero 4+ was used to collect ground-truth data to validate the acoustic data. The GoPro was mounted on a PVC frame, weighted on each corner using 8 oz fishing weights (**Fig. S5.1**). 17 sampling locations were chosen to be representative of the different benthic habitats covered by the acoustic survey, chief of which being, the shallow rocky reef (where one or more kelp species were expected to be found), deeper benthic habitats and the transition zone between the two (**Fig. 5.5**). Owing to vessel drift, GPS coordinates were taken with a Garmin Montana 600 (Garmin, Olathe, USA) when the camera was deployed and again when it was recovered to help increase our confidence in location of the camera when it reached the seabed. The simple setup of the camera rig did not include any methods for the detection of scale (*i.e.* lasers) so it was not possible to determine kelp canopy density or height.

5.2.3.1. Video analysis

Videos were analysed to determine the dominant habitat and to identify the presence of kelp species. *Laminaria hyperborea* was expected to be the dominant kelp species present, as it has previously been recorded by NPWS (2011) throughout Roaringwater Bay and is easily identified by its rough stipe which is often colonised by epiphytic algae. This meant that it was important for the camera to pass through the kelp canopy to observe the stipe. The presence of other floral and faunal species was also recorded and, where possible, identified to species level. On occasion, the drop-down camera was unable to capture a clear video of the seafloor and these were recorded as potentially deep sites where kelp was unlikely to occur, based upon the depth limit observations by NPWS (2011).

5.2.3.2. Mini-ROV survey

A Trident ROV (**Fig. 5.2**) (Sofar, San Francisco, USA) was deployed from the shore in a different location to the acoustic survey, near Carraroe (53°14’37.9” N, 9°34’53.7” W), to tests its marine operational capabilities and its ability to identify different kelp species and associated fauna. The Trident ROV collects high-resolution video, has a battery life of ~3 h and a top speed of 2 ms^{-1} but was limited by the tether to a range of 25 m (a 100 m tether can be purchased separately). The ROV was deployed from the shore and controlled via a controller and mobile phone. Sea conditions were not ideal (moderate swell) and there was a significant amount of debris in the water column. Multiple test dives (n = 18) were conducted with the aim of locating and identify different kelp species. Dive length varied but

was usually between 1–5 min in duration. Sea conditions eventually became too rough and the ROV was safely recovered. Species were later analysed from the video recordings.

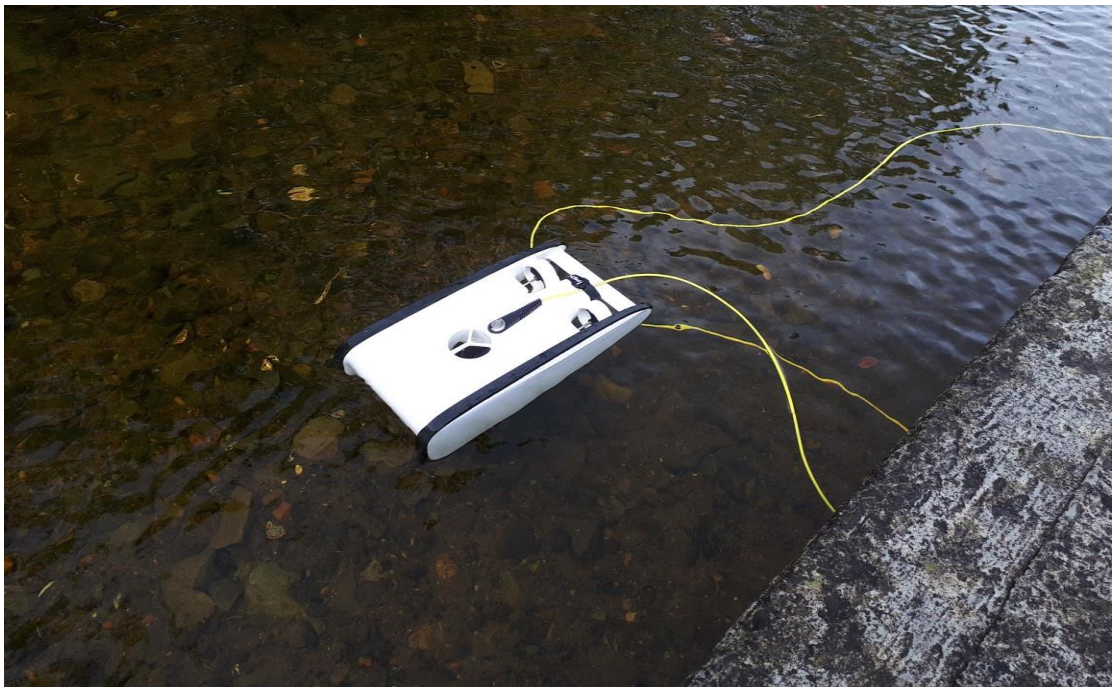

Fig. 5.2. Trident ROV undergoing freshwater trials using the 25 m tether.

5.2.4. Acoustic data processing

5.2.4.1. Bathymetric processing

The first processing step was to create accurate bathymetric maps for each of the three survey frequencies (200, 300, 400 kHz). Raw data files were imported into Qimera (QPS, Zeist, Netherlands) and were spatially correct and tidally referenced to concurrent Lowest Astronomical Tide (LAT) using the Malin Head Ordnance Datum. Navigation files were imported to correct vessel position and correct for variations in motion (pitch, roll and heave). The data were then manually cleaned to remove all non-seabed acoustic returns, including kelp. The software automatically detects the seabed, but incorrect detections can occur, for example with dense macrophyte canopies (Lefebvre *et al*., 2009), which can either be removed using additional filters or, in this case, manually as the study site was small. The final bathymetric maps were exported at a 0.5 m spatial resolution with a colour-blind friendly colour scheme created using ColorBrewer 2.0.

5.2.4.2. Kelp canopy extraction

For each of the three different acoustic frequency datasets, decibel (dB) thresholds, sidelobe suppression and bottom suppression were applied under the "water column settings" tab. The acoustic plot first had to be downsampled (from "none" to "8:1") as the high resolution of the acoustic data was slowing down the software. The sliding filter bar (**Fig. 5.3**) was used to set the minimum and maximum thresholds for the water column data which were then clipped to eliminate unnecessary data. Thresholds were constantly adjusted to enhance the signal of the potential kelp above the seabed. Removing the strong acoustic signal of the seabed is useful when analysing the weaker acoustic signal of the water column and this was achieved using bottom suppression, which was set to the default 95 %. Sidelobe suppression removes sidelobe artefacts in the water column data and this was again adjusted to better enhance the acoustic signal from the kelp. The kelp bed was most easily visible ~15 m either side of the vessel track line, similar to what was observed by McGonigle *et al*. (2011) and Kruss *et al*. (2017), and beyond that became difficult to identify (**Fig. 5.4**). Once the kelp signal had been isolated from the surrounding water column and seabed, soundings were manually selected and identified by Qimera as 'user additional soundings'. Using the 3D editor tool, all soundings not representing kelp were rejected and a new layer was created representing the potential distribution of the kelp and the depth of the top of the canopy.

Both the bathymetry and kelp layers were exported into ArcView Grid format so that they could be opened using QGIS 3.4. "Raster calculator" was used to create a kelp canopy height map by subtracting the bathymetry layer from the aligned kelp layer. Kelp canopy heights were provided in metres and the approximate area covered by different height classes was calculated by using the Polygonise tool, in QGIS, and then calculating the area (m^2) for each of the height classes. When vectorising, QGIS rounds values up or down into discrete classes whereas the original raster layer displayed height classes along a gradient.

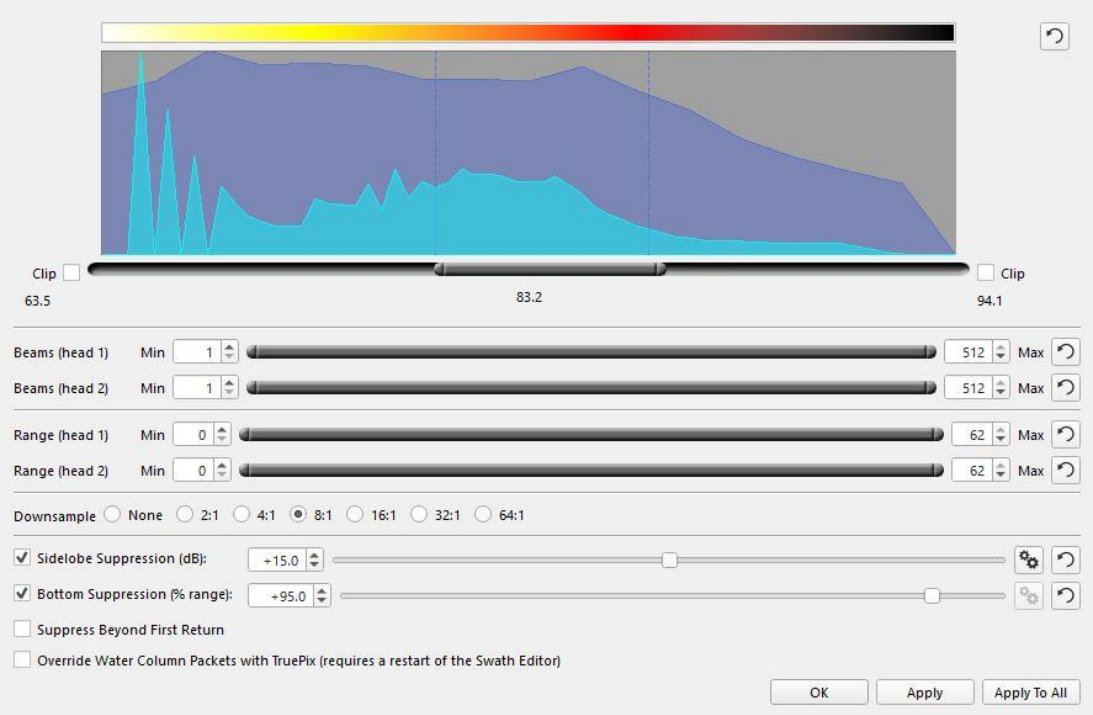

Fig. 5.3. Example of the water column processing dock showing the different water column thresholding settings that can be configured. The top graph shows a histogram of the water column data and different thresholds can be selected to filter out certain decibel (dB) ranges. Beam subsets and ranges can be modified along with sidelobe and bottom suppression. Downsample has been changed from "None" to "8:1" because of the large amount of data.

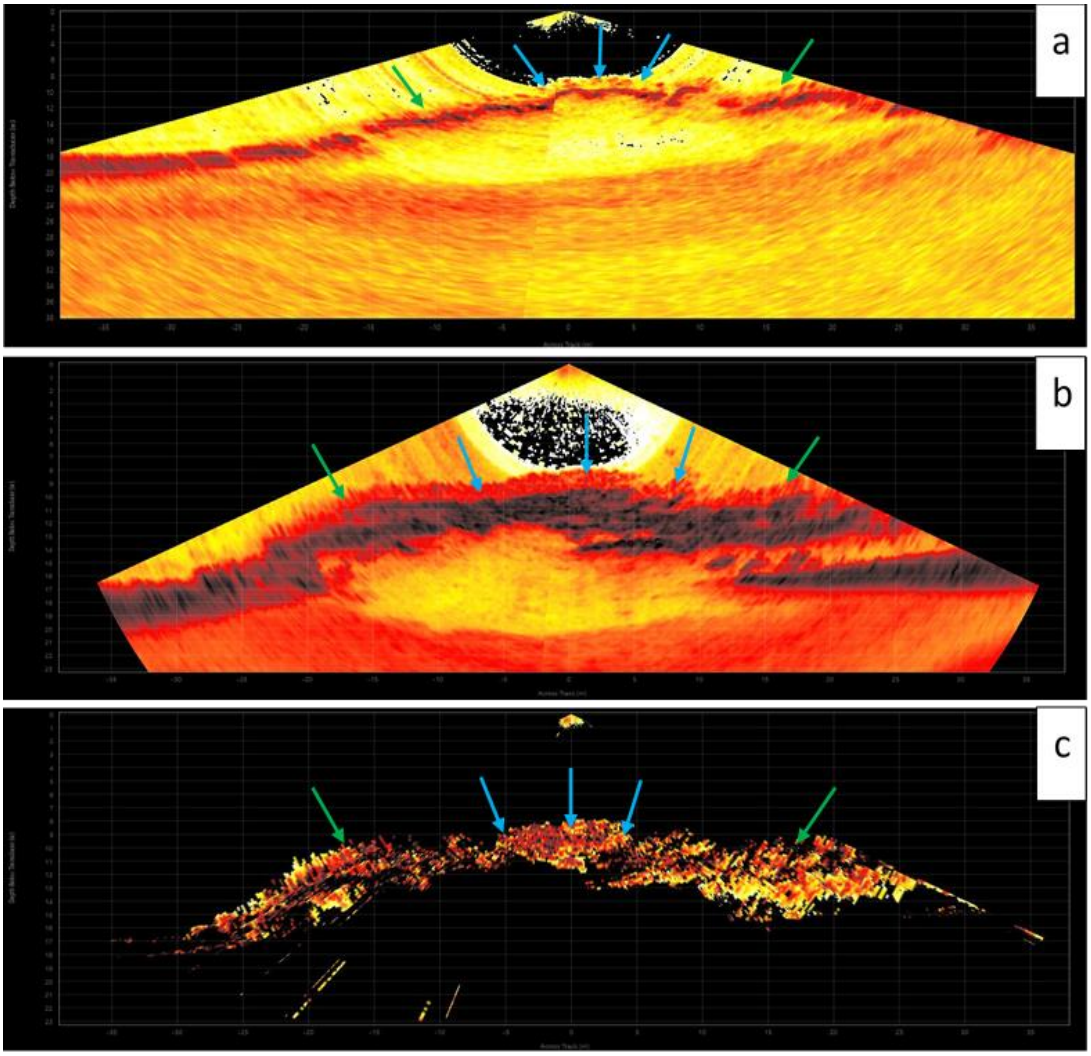

Fig. 5.4. Water column cross sections taken from the top off the rocky reef (300 kHz dataset). The three images show a single ping fan (**a**), a multi (stacked) ping fan (**b**) and the multi ping fan when thresholds to isolate the kelp signal have been applied (**c**). Blue arrows represent a potential, kelp signal which is contrasted against the filtered water column signal. Green arrows also indicate the presence of kelp which could be subject to sidelobe interference, reducing the quality of the acoustic signal.

5.3. Results

5.3.1. Site geology

Site depths ranged from -5 m for the rocky reef in the north of the site to -25 m in the south. Bathymetric data shows a series of ridges and troughs running, as expected, southwest to northeast and the backscatter indicated that that the ridges were rocky (Devonian red sandstone) and that the troughs were comprised of finer sediments (Devonian Carboniferous marine clastics). Slope data also supported this by showing the topographical complexity of the rocky ridges and the relative homogeneity of the sediment troughs (**Fig. S5.2**).

5.3.2. Biological sampling

A total of 17 drop-down video recordings were made throughout the study site (**Fig. 5.5)**. **Fig. 5.6** shows some video stills of some sampling points and **Tab. 5.3** shows the depths from each recording and the species observed. No kelp was observed at the southern region of the site, where depths approach -25 m (survey points 2560 & 2561). The area fringing the shallow rocky knoll was free of kelp and characterised by a mixture of small cobbles and mixed sediments. For some of the sampling points (2551, 2559 & 2558) the camera was not close enough to the bottom to capture detailed information on the flora and fauna present. Sea urchins were visible along with sponges and patchy, low-lying unidentified macroalgae. A single kelp individual was observed in 2558, at approximately 15 m deep.

The shallowest part of the rocky reef was dominated by a dense canopy of *L. hyperborea* and no other kelp species were observed. The stipes of *L. hyperborea* individuals were easily visible in the video footage and their identity was confirmed by the presence of epiphytic macroalgal species. In the canopy understory there were small kelp individuals, different species of red macroalgae and encrusting coralline algae. Common faunal species included *Echinus esculentus* Linnaeus and *Cliona celata* Grant. Fish were occasionally observed by species identification was not possible. Towards the tip of the rocky knoll (12306) the canopy of *L. hyperborea* began to thin out and *Alcyonium digitatum* Linnaeus was present. The lower limits of the kelp forest boundary (2556) were marked by a low density of *L. hyperborea* and an increase in the abundance of *A. digitatum*. This boundary was also captured by sampling point 12307 which identified sparse *L. hyperborea* and *S. latissima* on a mixed cobble substratum.

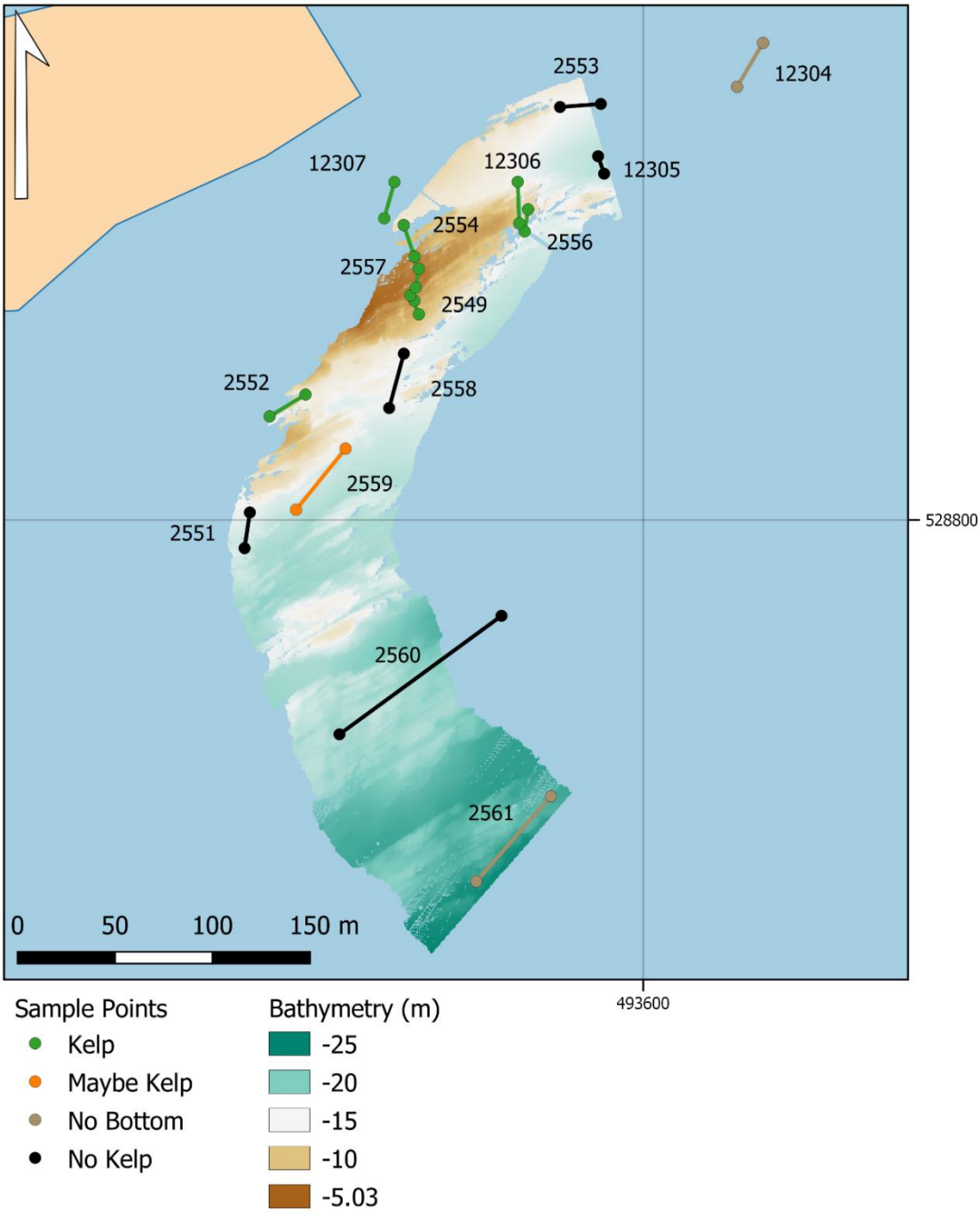

Fig. 5.5. Map showing the location, and number, of drop-down camera sampling stations overlain onto of the bathymetry layer created from the 200 kHz survey. Each sampling station consists of two GPS points, one for camera deployment and the other for retrieval (owing to currents and vessel drift). Sampling station numbers have unique identifying numbers. The location of the imagery taken for each video will fall somewhere between the two points, along the transect lines. Kelp = kelp observed, Maybe kelp = unable to clearly determine kelp presence, No bottom = seabed was too deep to be observed, No kelp = no kelp observable. Coordinates are in UTM_29.

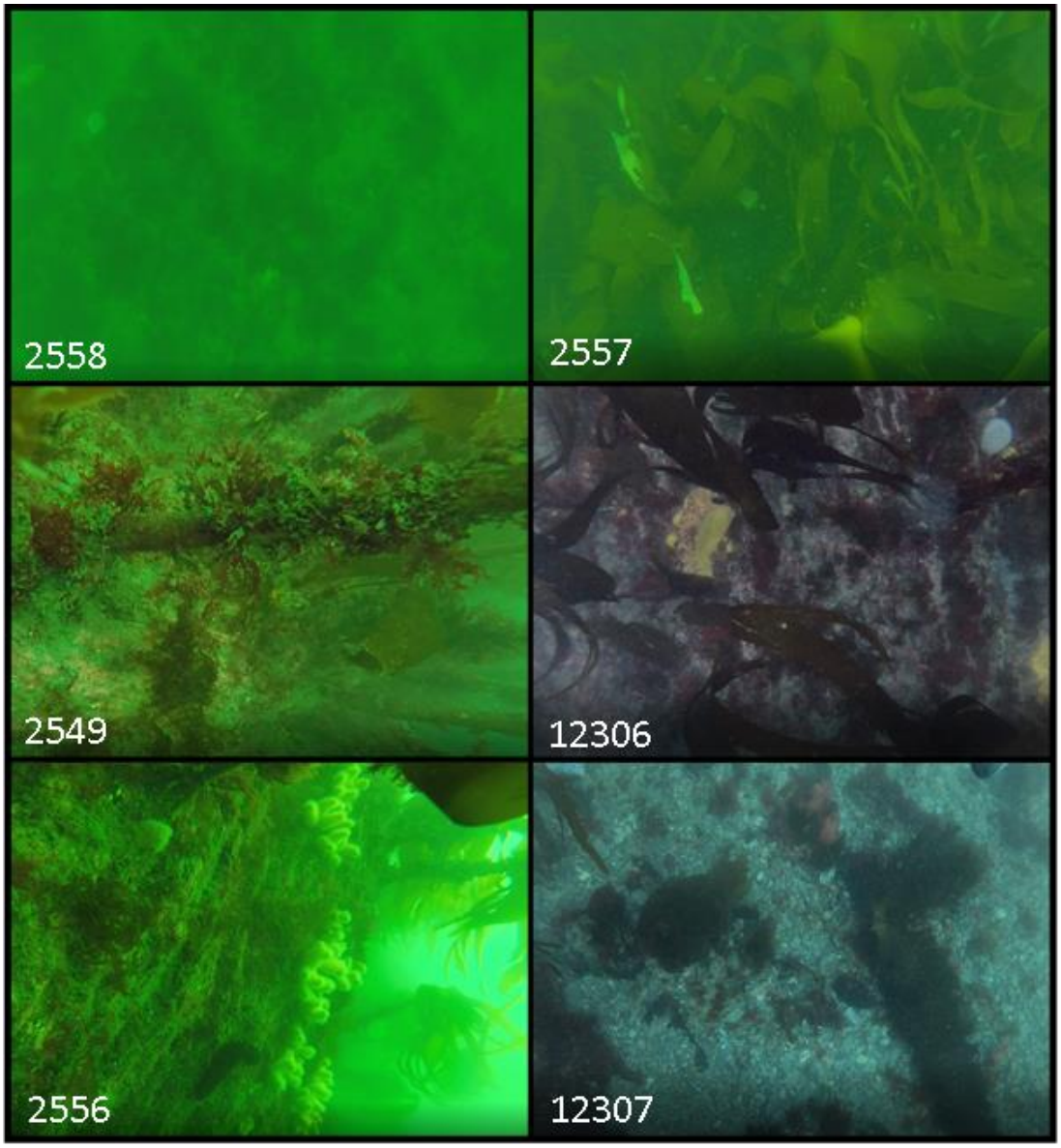

Fig. 5.6. Video stills from the drop-down GoPro sampling. **Fig. 5.2** shows the locations for each of these images.

Tab. 5.3. Table showing the depth (m), length (min), observation code and species observed in each of the video sampling points. Depths are recorded as the value midway between when the camera was deployed and when it was recovered.

Code	Depth (m)	Length (min)	Observation	Species present
2548	8	01:48	Kelp	*Laminaria hyperborea* *Echinus esculentus* Epiphitic red algae Coralline crusts *Cliona celata*
2549	8	02:09	Kelp	*Laminaria hyperborea* *Echinus esculentus* Epiphitic red algae Coralline crusts *Cliona celata* *Asterias rubens*
2551	15	01:57	No Kelp	*Echinus esculentus*
2552	14	02:00	Kelp	*Laminaria hyperborea* Epiphitic red algae Coralline crusts *Cliona celata*
2553	14	01:57	No Kelp	No identifiable species
2554	7	02:08	Kelp	*Laminaria hyperborea* *Echinus esculentus* Epiphitic red algae Coralline crusts *Delesseria sanguinea*
2556	12	01:39	Kelp	*Laminaria hyperborea* *Echinus esculentus* *Alcyonium digitatum* *Cliona celata* *Holothuria forskali*
2557	6.5	01:07	Kelp	*Laminaria hyperborea* *Marthasterias glacialis* *Echinus esculentus* Coralline crusts
2558	15.5	02:06	No Kelp	*Echinus esculentus* *Cliona celata*
2559	16.5	02:10	Maybe Kelp	No identifiable species
2560	18.5	05:16	No Bottom	No identifiable species
2561	23	03:34	No Bottom	No identifiable species
12304	18	01:55	No Bottom	No identifiable species
12305	17	01:35	No Kelp	No identifiable species
12306	12	01:37	Kelp	*Laminaria hyperborea* *Echinus esculentus* Epiphitic red algae Coralline crusts *Alcyonium digitatum* *Cliona celata*
12307	-	01:37	Kelp	*Laminaria hyperborea* *Saccharina latissima*

5.3.3. Kelp distribution and height maps

5.3.3.1. 200 kHz

Based on the 200 kHz data, the area identified as probably being kelp covered ~3,800 m^2 and kelp presence was recorded from a depth range of 4–15 m (**Fig. 5.7**). The kelp distribution was concentrated on the main rocky knoll of the site with a small patch present north of this, indicating the start of another rocky environment. Acoustic data indicated that the kelp was dominated by thalli between 0.4–1.6 m in height and there are anomalous values which likely do not represent the kelp (*i.e.* minus and extreme height values) (**Fig. 5.8 & Fig. 5.9**). The line of missing data observable within the distribution map marks the boundary point between two survey lines and it was not possible to extract data from this area.

5.3.3.2. 300 kHz

Using 300 kHz, kelp was shown to cover an area of ~2,740 m^2 and appeared to have a much patchier distribution than what was observed using the 200 kHz frequency. Kelp was recorded as present across similar depth ranges as observed in the 200 kHz data (**Fig. 5.7**). Kelp distribution was concentrated on the rocky knoll and also at the lower margins of a rocky reef to the north. Kelp distribution did not appear to stretch as far to the south-west (on the boundary of the acoustic dataset) as it did when derived from the 200 kHz dataset. The strongest and clearest signal was observed within ~10 m either side of the vessel track line, which ran rough along the ridgeline of the rocky reef. The dominant height range of the kelp canopy was between 0–2 m and there was less variation in the range of values compared to the 200 kHz dataset (**Fig. 5.8 & Fig. 5.9**). Along the ridgeline canopy heights of 1–2 m was more prevalent with 0–1 m occurring more frequently along the slopes of the reef.

5.3.3.3. 400 kHz

The 400 kHz frequency identified a potential kelp area of ~2,714 m^2, as with the other two frequencies the distribution was restricted to the main rocky reef and occurred over the same depth range (5–15 m) (**Fig. 5.7**). The small kelp patch to the north was not identified, which was likely due to the vessel taking a slightly different course. As with the 300 kHz dataset, the strongest kelp signal was observed ~10 m either side of the vessel track line and this was dominated by the kelp in the range of 1–2 m. Height values of 0–1 m were more commonly observed along the sides of the reef (8–15 m depth range) and there was less variation in the overall spread of canopy height values (**Fig. 5.8 & Fig. 5.9**).

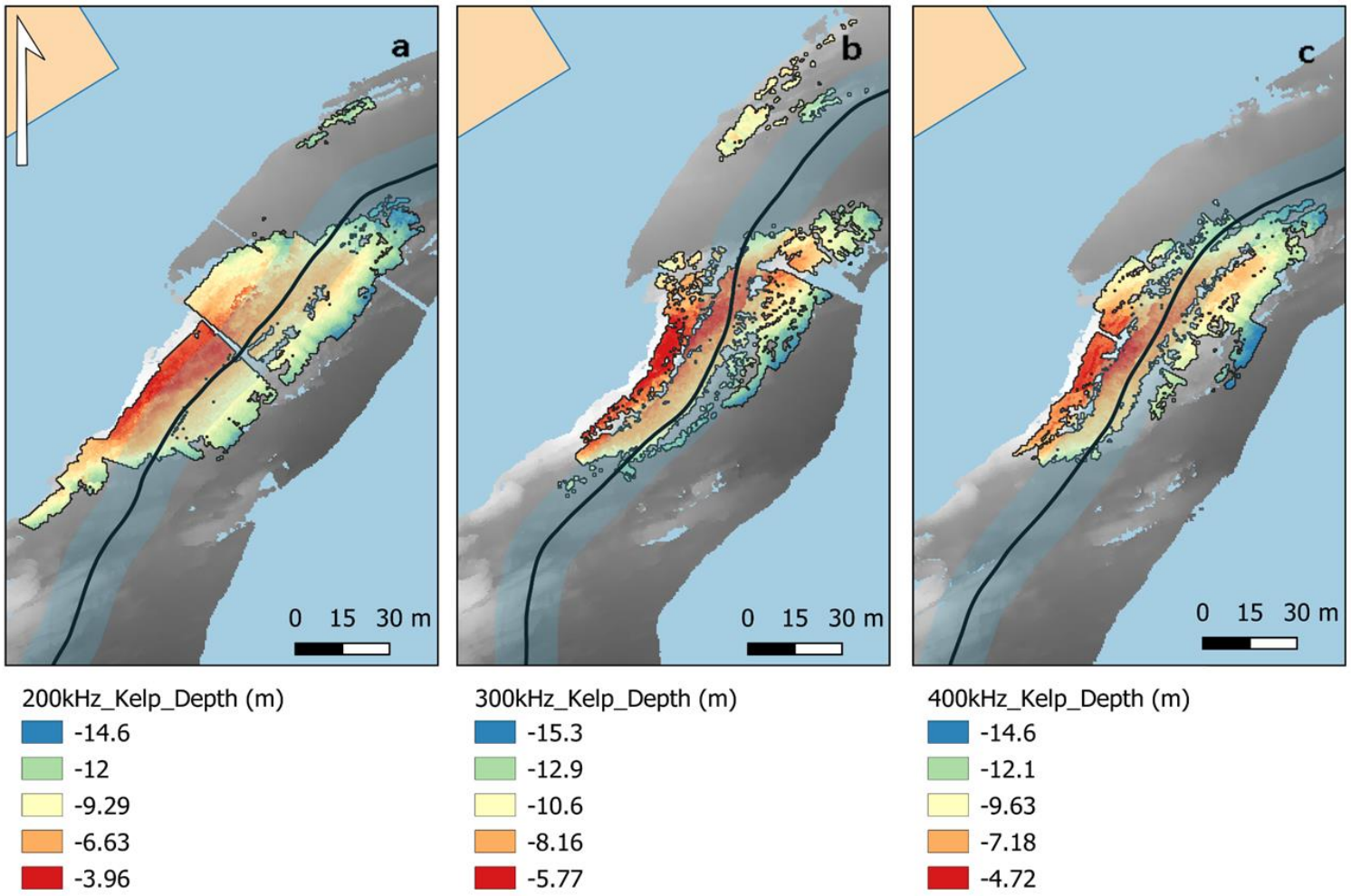

Fig. 5.7. Map showing the depths (m) that the observed kelp canopy occurred as detected by the three different survey frequencies (**a** = 200, **b** = 300, **c** = 400 kHz). The vessel track line is shown in black and 10 m either side is marked by the blue polygon buffer.

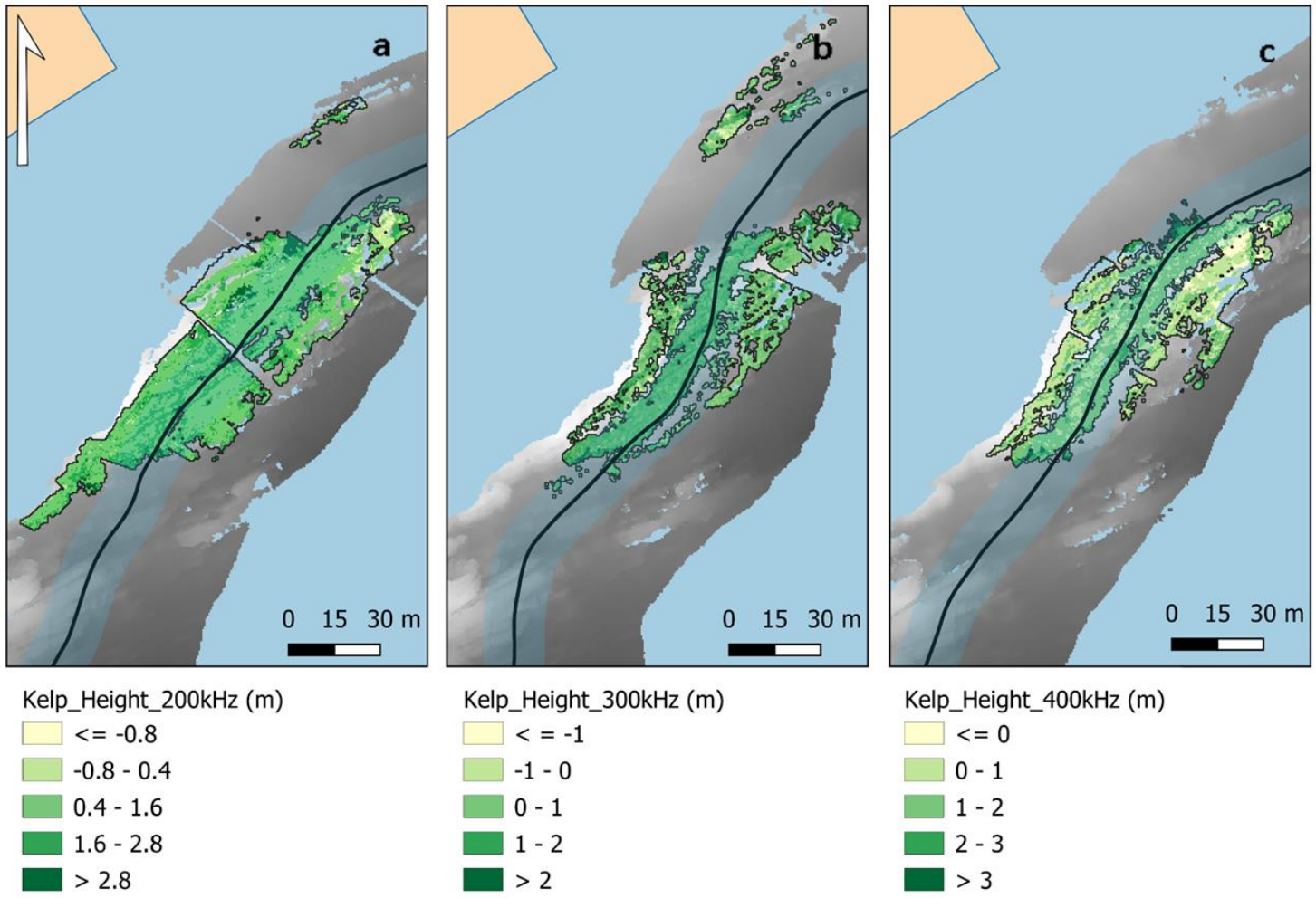

Fig. 5.8. Map showing the estimated range of height values recorded for the kelp bed as detected by each of the three frequencies (**a** = 200, **b** = 300, **c** = 400 kHz). The vessel track line is shown in black and 10 m either side is marked by the blue polygon buffer.

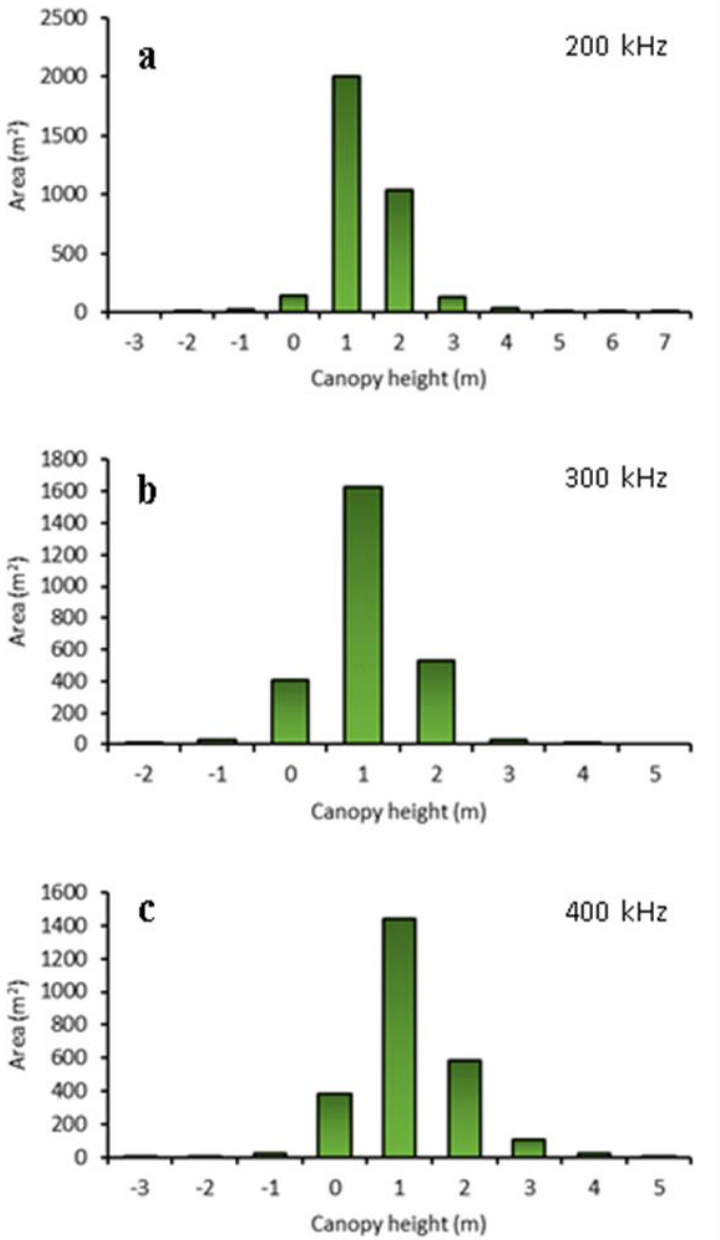

Fig. 5.9. Area (m^2) covered by each of the recorded height classes as detected by each of the three acoustic survey frequencies (**a** 200 kHz, **b** = 300 kHz, **c** = 400 kHz).

5.3.4. Mini-ROV species identification

The test ROV dives, at a different site, showed that it was possible to identify different kelp species using the Trident ROV video footage (**Fig. 5.10**). Distinctive morphology allowed for the identification of *S. latissima*, *L. hyperborea* (the rough stipe was easily recorded) and *Saccorhiza polyschides* with its characteristic bulbous holdfast. Faunal species were occasionally visible including *Crenilabrus melops* Linnaeus, *Gobiusculus flavescens* Fabricius and *Henricia oculata* Pennant. Drift algae were also present and included many fucoid species.

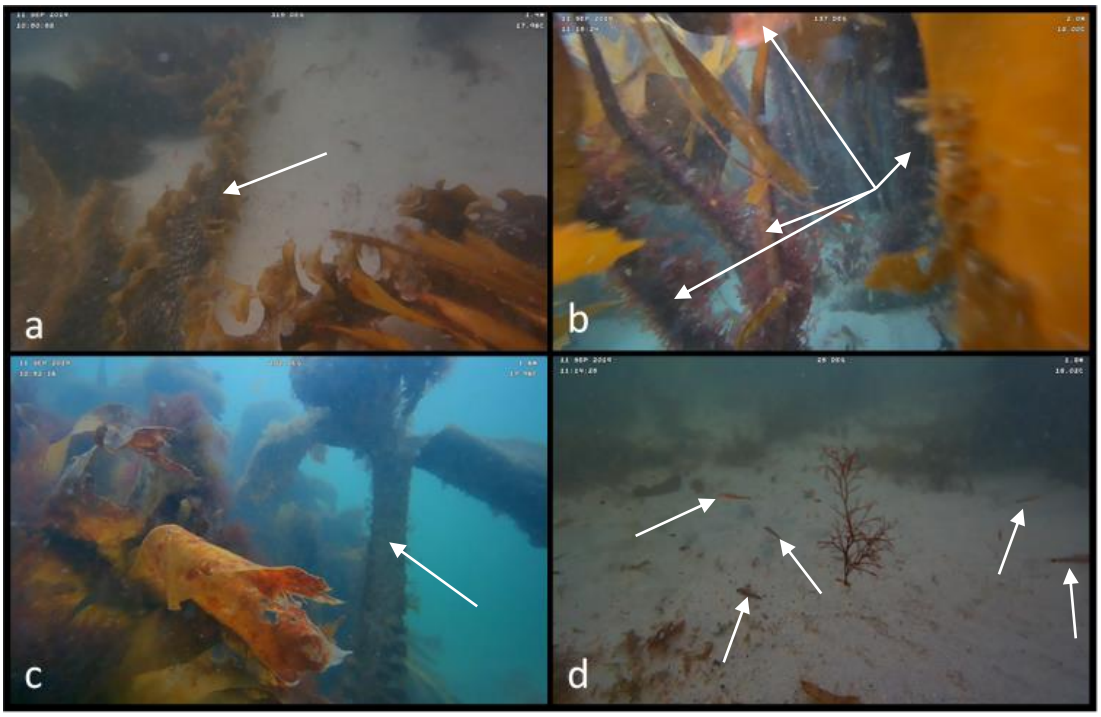

Fig. 5.10. Video stills taken from the Trident ROV showing (**a**) *Saccharina latissima*, (**b**) *Laminaria hyperborea* (with a curious male *Crenilabrus melops*), (**c**) *Saccorhiza polyschides* and (**d**) *Gobiusculus flavescens* with drift algae. Arrows indicate species described.

5.4. Discussion

Subtidal macroalgal communities are challenging to map, regardless of the methodology used. The use of acoustic remote sensing allows relatively large areas to be surveyed, whilst not facing the same constraints on depth as optical remote sensing (Abukawa *et al*., 2013). Here, the optimal acoustic survey frequency for quantifying the distribution and height of subtidal kelp was sought, with the aim of supporting the development of baseline ecological data collection methodologies with which to inform sustainable management decisions.

This study has demonstrated that the analysis of water column data, collected using MBES, can identify the presence of macroalgae, deriving both estimates of canopy height and bed distribution data. Each of the frequencies used identified subtle variations in the extent and height of the kelp bed, although it was difficult to know if this was due to differences in the ability of each frequency to identify water column features, or user error when processing the three independent datasets. Drop down camera surveys validated that the rocky reef was dominated by kelp forests (mostly *L. hyperborea*) and that the areas to the north and south of this reef, where either depth or substratum (or both) were unsuitable and therefore devoid of kelp. The lower reef margins, when observed, showed a thinning of the kelp canopy and an increase in faunal species such as *A. digitatum*. A small test conducted with a mini-ROV

demonstrated its ability to identify different floral and faunal species and offered an exciting glimpse into the future potential of mini-ROV technology for supplementing traditional field-survey methods for the collection of biological validation data.

5.4.1. Ability to identify kelp presence

Each of the three frequencies used was able to identify the presence of potential kelp and produce distribution and canopy height maps that were similar to one another. All three identified a dense kelp canopy on the ridgeline, which also happened to follow the vessel track line, and corresponded to the ground-truth information showing a dense canopy of *L. hyperborea.* In the 300 and 400 kHz datasets the effect of sidelobe interference was clearly visible in the presence of a dense ribbon of kelp occurring within ~10 m either side of the track line. The same effect was observed by McGonigle *et al.* (2011) and Kruss *et al.* (2017) who both described how sidelobe interference made it difficult to confidently identify kelp beyond the central beams of the MBES device as the interference was sometimes greater than the acoustic response of macroalgae. The same occurred here where it became more difficult to confidently identify kelp signals further away from the central beams, even when looking in areas of suitable depth and substratum, and with thresholding applied to minimise the signal from the seabed and water column.

Acoustic interference may have been further compounded by the topographical nature of the study site and the path of the vessel along the ridge of the rocky reef. Dense, shallow kelp could have reduced the energy of the acoustic signal reaching the kelp deeper down the sides of the reef, leading to gaps where no acoustic return signal was recorded. The lower frequency of the 200 kHz survey may explain why more continuous coverage was observed on the sides of the reef as lower frequencies would be less susceptible to water column interference (Freitas *et al.*, 2008) and more acoustic energy would reach the deeper kelps, where higher frequencies would be scattered, absorbed and reflected more by kelp.

Laminaria hyperborea, in the UK, typically reaches maximum lengths of 1-2 m (Kain & Jones, 1963; Christie *et al.*, 2003; Rinde & Sjøtun, 2005). Canopy height estimates from each of the three acoustic frequencies agree with the length values reported in the literature, having ranges between 0-2 m, with kelp ~1 m in height being the most common. Where extreme canopy height values have been observed most likely represents the incorrect selection of soundings, for example the selection of sidelobe interference (Kruss *et al.*, 2017). Fortunately, these height values represent only a small fraction of the total kelp bed. The north-eastern region of the identified kelp bed shows, across all frequencies, relatively high coverage of kelp averaging ~0 m in height in a region of about 12-14 m deep. Video footage from that region (2556) showed a relatively sparse kelp canopy which may indicate

that the low canopy height values observed actually represent bare patches of rock in between kelp individuals which could have been accidentally selected during the identification and processing of the kelp acoustic signal.

5.4.2. Validation of acoustic data

The video footage collected using the dropdown GoPro only confirmed three things, that *L. hyperborea* was the dominant kelp species present (*S. latissima* was recorded at video sampling station 12307), that there were clear differences in kelp canopy density (potentially linked with depth) and that no kelp was observed at depths greater than ~15 m (regardless of substratum). A key limitation was that insufficient video data existed to characterise the different canopy density gradients within the kelp bed which made it difficult to determine what was causing the differences in kelp distribution observed between the three frequencies. This meant that it was not possible to determine which acoustic frequency would yield to most accurate kelp mapping results.

As this was a pilot study, it was important to comprehensively validate the acoustic datasets using detailed biological data collection surveys to identify species presence or absence. The sampling methodology used was inefficient as, without a live video feed from the camera, it was difficult to know if the feature that was being observed (*i.e.* kelp boundary zone) was the intended one until the camera was recovered. Currents and vessel drift also made the accurate deployment of the camera difficult. Video analysis can be subjective and prone to user error (Lefebvre *et al*., 2009) and this was compounded by not being able to control where the camera was pointing. Mini-ROVs, such as the Trident ROV (Sofar, San Francisco, USA) and BlueROV2 (BlueRobotics, Torrance, USA), come with a range of different tether lengths, capture high-definition live video and are fully controllable from the surface. Raoult *et al*. (2020) found that a mini-ROV was equally as accurate as a snorkeler (with a camera) at identifying fish species richness and abundance, and this could offer a potential validation solution for kelp forest mapping. The small test conducted, at a separate site, in this study showed the potential of the Trident ROV for kelp validation surveys. Species were easily identified and the ROV was easy to deploy, retrieve and control meaning that different features of interest could be fully observed during a dive. However, turbidity and debris made accurate navigation difficult and poor visibility meant that species identification could only be confidently achieved from close. The ROV motors were also repeatedly clogged by algal debris, requiring it to be retrieved and the algae cleared. Navigation was also challenging as the sea conditions worsened, making it difficult to keep a heading. The ROV was only operating in shallow water (< 2m) and this may have affected buoyancy (despite extra weight) and made it more susceptible to swell. In deeper waters,

during calmer seas, and with more operator training, mini-ROVs could potentially to offer an alternative solution to both dropdown, and towed cameras, and SCUBA.

5.4.3. Biomass estimations

The use of SCUBA for the collection of detailed biological data cannot be wholly replaced by technological solutions. The accurate estimation of biomass (including density estimates) data is important for the effective management of kelp forests (Gorman *et al*., 2013) and sampling methods, such as SCUBA, allow for kelp length to weight relationships to be developed (Blight *et al*., 2011). This research has shown that it is possible to use acoustic remote sensing to define kelp canopy height and distribution and use video to identify the species present. The development of a site-specific stipe length to weight relationship would have, in theory, allowed the estimation of the total biomass of the kelp bed. However, Shao *et al*. (2019) recently showed that it is possible to derive a relationship between the echo intensity per unit of kelp, or target strength (TS) and weight meaning that it may be possible to remote sense biomass once these relationships have been established. Ground-truth kelp canopy density will be important for validation of the cover estimations made by each acoustic frequency and to derive more accurate biomass estimates (Pederson *et al*., 2012). At present, the use of SCUBA remains the only way to collect detailed biological information (Schroeder *et al*., 2019). Allometric relationships can also be developed for kelp carbon content, for example, basal tree area was found to be a good predictor of tree biomass carbon stock in Bangladesh (Alamgir & Al-Amin, 2008). Previous work has assumed a certain density of kelp individuals per m^2 (Hatcher *et al*., 1977) and to achieve carbon stock estimates for Irish kelp beds would require *in-situ* collection of stipe density data, which could not be resolved using the acoustic sonar used in this survey. A more spatially coherent dataset on Irish kelp distribution could facilitate better estimations of kelp standing stock and their contribution to the global carbon budget (Abdullah *et al*., 2017). Fluctuations in canopy biomass, for example increased nutrients leading to elongated fronds (Bell *et al*., 2018) can also affect carbon stock estimates. Such defined features as kelp fronds, as with stipe density, could also not be resolved using the resolution of the current acoustic sensor. Finer resolution sensors may yield better results but will also produce much larger volumes of data and will be required to be supported by extensive ground-truthing surveys.

5.4.4. Operational considerations

For all three acoustic surveys (each covering ~5 ha), approximately 20 GB of data were collected. The scaling up of this method would produce immense quantities of data and will require compression and storage solutions. There does not appear to be a lot of published research looking at the compression of MBES water column data. Portell *et al*. (2019)

compared their adapted compression algorithm to industry-standard ones, finding that it was able to compress data more efficiently whilst better preserving quality. Such advances, whilst they may be MBES sensor specific, may facilitate the wider application of water column data acquisition.

The presence of sidelobe interference, restricting the accurate identification of kelp to central beams (McGonigle *et al*., 2011; Kruss *et al*., 2017) reduced survey efficiency. Combined with the potential limitations imposed by data compression, storage and processing, large-scale surveys may be impractical. Instead, developing a multi-layer mapping approach, similar to that used by Bajjouk *et al*. (2015) is recommnded. The creation of regional models predicting kelp species distribution can be validated by using vessel-mounted acoustic remote sensing which will allow for a stratified sampling approach rather than the targeting mapping of known kelp beds. Additional datasets, such as optical remote sensing of shallow-water kelps (St-Pierre & Gagnon, 2020) can also be integrated which can allow for large areas to be covered (especially if suing satellite) but which may still face challenges associated with the limited penetration of light in turbid waters (Casal *et al*., 2011). This may be advantageous when conditions make it difficult and dangerous too survey so close to shore with a boat. SCUBA, or mini-ROVs, can be used to ground truth the acoustic datasets and this can also be conducted in a stratified way, with a predetermined set of sampling stations (Bajjouk *et al*., 2015) based on the acoustic data results.

5.5. Conclusions

The collection of baseline ecological data on habitats of ecological and economic importance is vital for their sustainable management in the face of a raft of increasing anthropogenic pressures. The potential application of acoustic remote sensing for mapping subtidal kelp populations has previously been highlighted (McGonigle *et al*., 2011; Kruss *et al*., 2017). This study sought to expand on this work in comparing different acoustic frequencies, showing that there is a difference in the ability of each to detect a macroalgal acoustic signal, but that sufficient validation data was not collected to identify the cause of this variation. A drop-down camera was a quick and low-cost method for the collection of validation data and was successful in identifying the presence or absence of kelp. A potential alternative, in the form of a mini-ROV, was trialled and shown to be easily capable of identifying different kelp and faunal species. Future work should include the collection of comprehensive ground-truth data to identify the optimum acoustic frequency for the identification of kelp. It should also consider the integration of MBES data into a regional, integrated, mapping survey.

Chapter 6: **A review on applying drones for monitoring intertidal macroalgal communities**

Collection ground control point (GCP) data using a RTK-GPS prior to the December 2017 drone survey at An Cheathrú Rua (Co. Galway).

Abstract

Remote sensing allows large areas to be mapped, revealing ecological processes not previously observable. The limited spatial scale of using field survey methods for mapping intertidal macroalgal communities can be overcome with the use of remote sensing. The spatial and temporal resolution of satellites and aircraft are often considered too coarse for species-level mapping within spatially heterogeneous intertidal environments. The use of drones is increasingly widespread in terrestrial and marine research, yet their application for intertidal habitat mapping is still in its infancy. The high spatial, spectral and temporal resolution of drones makes them an ideal remote sensing platform choice for mapping such spatially complex communities. This review sets out to provide the prospective researcher, interested in utilising drones for intertidal macroalgal research, with a detailed baseline of theoretical, methodological and technical knowledge to support the application of drones for their particular research question. With a focus on optical remote sensing solutions, up-to-date information is provided on the latest drone, sensor and software technology. In identifying the unique challenges associated with using drones for intertidal mapping we identified three key characteristics of intertidal macroalgae that will influence survey design, 1) the size of individuals within a species 2) homogeneity of coverage and 3) spectral similarity to surrounding species and substratum. Based on these considerations, we explore the methodologies developed by other studies, and highlight how they can be applied to address the three characteristics of intertidal macroalgal assemblages identified here.

6.1. Introduction

Geographic scale is an increasingly important consideration in the planning for intertidal macroalgal resource assessments and has arisen out of the need to better understand the anthropogenic impacts of increasing levels of human activity and development throughout the coastal zone (Gillanders *et al*., 2008). This is driving the push to supplement traditional field survey techniques with those that allow large areas to be surveyed efficiently, cost-effectively and accurately (Anderson & Gaston, 2013). Whilst traditional field-based survey methods are still the 'gold-standard' of habitat assessment, allowing for species level identification (Konar & Iken, 2018), they are often time consuming, costly and restricted in scale (Bajjouk *et al*., 1996; Vis *et al*., 2003; Oppelt *et al*., 2012).

Remote sensing approaches allow for the monitoring of large-scale areas at a range of spatial, spectral and temporal resolutions (Govender *et al*., 2007), offering new insights into intertidal ecological processes. Many earlier studies applying remote sensing to intertidal habitat mapping used airborne (Bajjouk *et al*., 1996; Thomson *et al*., 1998), satellite (Guillaumont *et al.*, 1993; Donoghue *et al*., 1994; Casal *et al*., 2011) and even a blimp

(Guichard *et al*., 2000). The relatively coarse spatial resolution of these platforms (Vis *et al*., 2003; Brodie *et al*., 2018) appears to have limited the further application of remote sensing within the intertidal zone. Often, these platforms will suffer from restricted operational flexibility (Colefax *et al*., 2018) and atmospheric interference, such as cloud cover (Dekker *et al*., 2003), which, with the tidal constraints of the intertidal zone, can reduce the amount of good survey days. Since 2000, relatively few remote sensing studies using airplanes and satellites have been published (Dekker *et al*., 2003; Garono *et al*., 2004; Theimann *et al*., 2005; Hennig *et al*., 2007; Oppelt *et al*., 2012). Recently however, there is a renewed interest in the remote sensing of intertidal macrophyte communities using drones (Murfitt *et al*., 2017; Duffy *et al*., 2018b; Kellaris *et al*., 2019; Taddia *et al*., 2019; Tait *et al*., 2019).

Drones, very much the mainstay of agricultural monitoring (Horton *et al*., 2017), are, owing to rapid technological development and component miniaturisation, being integrated into a wide range of ecological monitoring studies, from faunal monitoring (Christiansen *et al*., 2016; Wich *et al*., 2016) and forestry (Adão *et al*., 2017; Sankey *et al*., 2017) to coastal environments (Ventura *et al*., 2016; Casella *et al*., 2017). The operational flexibility (Baena *et al*., 2018) and high spatial resolution (Weil *et al*., 2017) of drones makes them well suited to the unique challenges of mapping intertidal macroalgal species and responding to short-term events such as algal blooms (Kislik *et al*., 2018). Many intertidal communities can be characterised as being spatially and spectrally complex (Oppelt *et al*., 2012) and this complexity can be difficult to identify using aircraft and satellites (Doughty & Cavanaugh, 2019). Many modern drones allow for multiple types of sensors to be mounted (e.g. RGB, thermal, multispectral, hyperspectral) and these can provide unique insights into intertidal patterns and relationships potentially not observable using on-foot survey methods.

Initially having been developed for military applications (Lechner *et al*., 2012), advances in drone technology, such as component miniaturisation and improved battery life (Colefax *et al*., 2018) lead to an increase in the choice of drones available across a wide price range (**Tab. 6.1**). This is concurrent with the rapid development of new lightweight sensors (Colomina & Molina, 2014) which, along with drone technology, provides any prospective researcher with a multitude of technological options to suit their research objectives. This review aims to provide an overview of available drone platform and sensor technology to use, along with specific operational factors that must be considered when surveying intertidal macroalgal communities.

6.2. Terminology

There exists a range of different terms that can be applied to drones, including unoccupied aerial vehicles (UAVs), unoccupied aerial systems (UAS) and remotely piloted aircraft systems (RPAS). The use of the term unoccupied, rather than unmanned, was highlighted by Johnston (2018) as a more inclusive term. There appears to be no clear consensus on the most appropriate term, with aviation agencies appearing to differ, for example, the International Civil Aviation Organisation (ICAO), US Federal Aviation Administration (FAA) and UK Civil Aviation Authority (CAA) use UAS, whereas the European Union Aviation Safety Agency (EASA) uses drones. For the sake of brevity and simplicity we shall only use the term drones.

Two key terms, spatial and spectral, must be defined as they are important considerations when choosing a suitable drone and sensor. Spatial resolution refers to the pixel size of the data collected by the sensor (Kerr & Ostrovsky, 2003) and is a function of the sensor design and flight height of the survey platform. The optimal spatial resolution should be determined by considering the spatial properties of the target feature to ensure that key information is observable (Treitz & Howarth, 2000; Smith, 2012). Spectral resolution is defined by the number and width of bands present within a sensor. A sensor can still cover a large portion of the EM yet have a low spectral resolution if only a small number of wide bands are used (Govender *et al*., 2007; Barillé *et al*., 2010). Conversely, many higher spectral resolution sensors (i.e. hyperspectral) can have dozens, or hundreds, of narrow bands covering the same potion of the EM spectrum. Higher spectral resolutions allow for spectral features to be observed (such as subtle variations in reflectance spectra between macroalgal species) which may be missed by coarser spectral resolution sensors (Adão *et al*., 2017), and are thus, theoretically more useful when trying to map spectrally similar features.

6.3. Drone technology

Drones can be broadly separated into two categories based, primarily, on their flight capabilities, and these are multirotor and fixed wing. Both types (and their sub-categories) have similar characteristics such as the capability to fly pre-planned flights, the presence of inertial measurement units (IMU) and internal GPS/GNSS, of varying levels of accuracy, whilst typically weighing less than 20 kg (Anderson & Gaston, 2013). All survey-grade drones come equipped with internal GPS/GNSS which allow for relatively precise positional accuracies of approximately 2–5 m (Johnston, 2018). IMUs are an essential part of the drone flight controller system, using accelerometers and gyroscopes to measure the pitch, roll and yaw of the drone. Integrated gyroscopes act to improve the flight stability of the

drone allowing it, for example, to hover in the wind. Combined with stabilised gimbals and high-resolution cameras this allows for the collection of high-quality images and video (Cruzan *et al*., 2016). Across the two broad categories, the battery life of drones has been constantly improving (**Fig. 6.1**), increasing their usefulness for mapping larger areas.

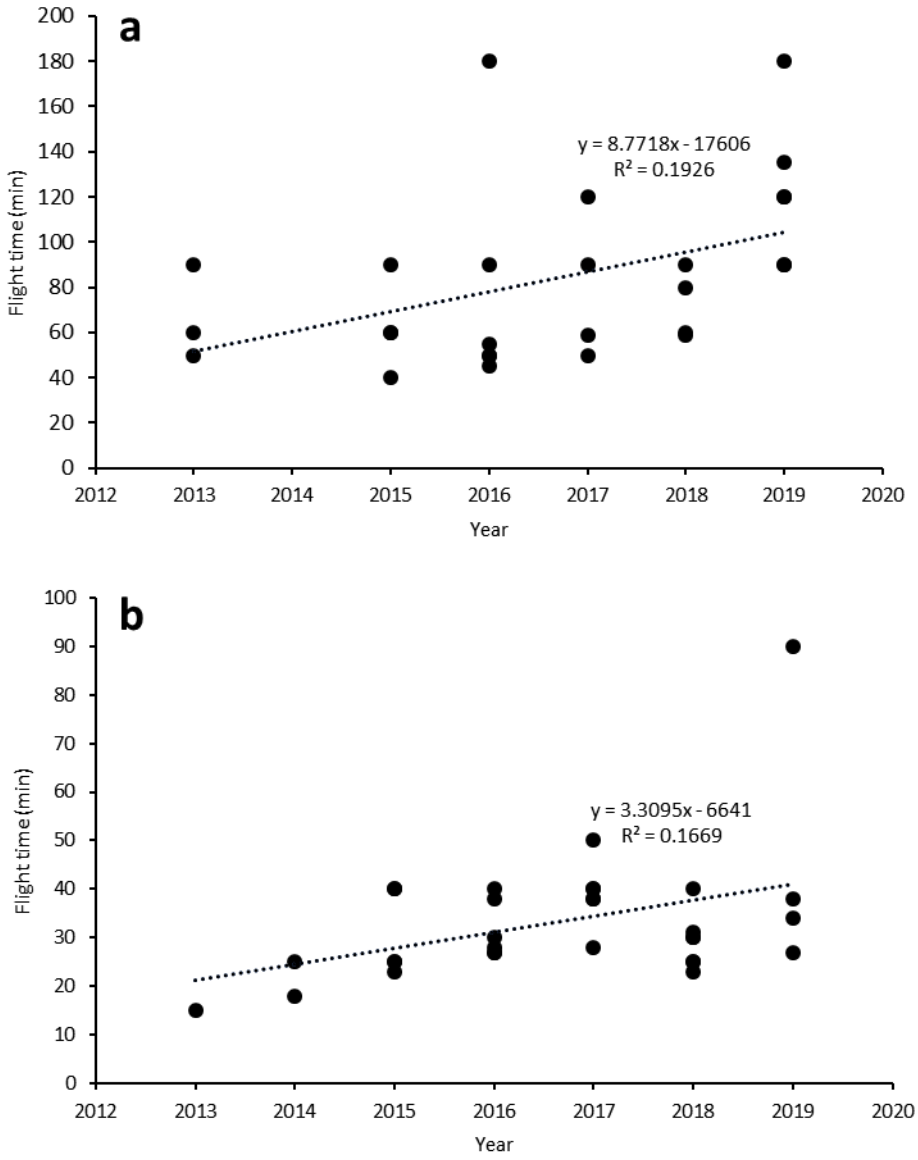

Fig. 6.1. Improvement in battery life for (**a**) fixed wing and (**b**) multirotor drones. Dates refer to the drone release date and, where possible, maximum payload flight times were used. Information was obtained through an internet search for all the drone models listed in this review.

6.3.1. Drone Types

6.3.1.1 Multirotor drones

Multirotor drones use multiple propellers to provide lift and propulsion whilst also controlling pitch, roll and yaw. They are available in a wide range of designs (**Tab. 6.1**) and are usually either quadcopters, hexacopters or octocopters (Cruzan *et al*., 2016). The advantage of having more propellers being that if one was to fail then the drone would continue to operate (Johnston, 2018). Multirotor drones have no minimum speed allowing them to conduct complex flight plans (Aasen *et al*. 2014) and to operate within spatially constrained areas. Combined with their ability to hover (Anderson & Gaston, 2013), this makes them well suited to detailed surveys and for monitoring features that occur over fine spatial scales (Lucieer *et al*., 2014). Their vertical take-off and landing (VTOL) capability means they require very little space for deployment, making them well suited for topographically complex environments such as can be found in the intertidal zone. Battery life for many multirotor drones' ranges from 20–30 min (on average) and this can limit their range, potentially rendering them unsuitable for largescale surveys, although this will also depend on the flight height, payload and local regulations.

6.3.1.2. Fixed wing drones

Once the preserve of the military, fixed-wing drones have evolved into commercially viable, user-friendly remote sensing platforms (Anderson & Gaston, 2013). This has coincided with a reduction in size and weight, to the point where they are often lighter than some of the 'heavy-lift' multirotor drones. Propulsion is provided by multiple engines and propellers (Johnston, 2018) and, whilst most are battery powered, some are powered by internal combustion engines (greatly increasing their range) and some by hydrogen fuel cells (**Tab. 6.1**). Fixed-wing drones often require more space (i.e. soft, flat terrain) for take-off and landing than multirotor drones. Some can be launched by hand or via a bungee propulsion systems and most perform glider landings although some, such as the Bramor range (C-Astral, Ajdovscina, Slovenia) deploy parachutes instead. Flight times range from 40–180 min for battery powered models and up to 18 hr for fuel powered, making them ideal for surveying large areas. Whilst not limited by battery life to the same extent as multirotor drones, fixed-wing drones are still subject to local regulations which may restrict the area that can be surveyed unless permissions are granted to fly further.

6.3.1.3. VTOL fixed-wing drones

The space required by fixed-wing drones for take-off and landing can be limiting in some circumstances and can put high value payloads at risk. VTOL-enabled fixed wing drones combine the efficiency and range of a fixed-wing drone with the vertical take-off and landing capability of a multirotor. This can allow for operations in topographically complex environments where safe take-off and landing areas are not present (Ventura *et al*., 2018). The number of commercially available VTOL fixed-wing drones is increasing across a broad price spectrum (**Tab. 6.1**).

Tab. 6.1. Commercially available drone models including information on drone type (M = multirotor, F = fixed-wing, V = VTOL fixed-wing, F/L = fixed-wing with launcher), flight time (in minutes), compatibility with real-time/post-processing kinematic (RTK/PPK) correctional GPS technology, weight and maximum take-off weight (in grams), price (in euros) and sensor integration options (Integrated RGB/multispectral = drone supplied with RGB/multispectral sensor, Quickmount = allows seamless integration with DJI drones, Custom = custom mounts can be developed for a wide range of sensors, Various = A range of sensors are available for integration, contact manufacturer for details, Skyport = integration of industry standard sensors with certain DJI drones). All information is correct as of time of submission (02/2020).

Company	Model	Type	Flight (min)	RTK/ PPK	Weight (g)	Max. Weight (g)	Price (€)	Sensor
3DR	Solo[q]	M	20[e]	No	1,500	1,920	-	Various[c], Custom[c]
Aerialtronics	Altura Zenith	M	40	-	6,650	9,650	POA	Various[c], Custom[c]
Aeromao	Aeromapper Talon[r]	F	120	Yes[c]	3,500	-	~11,000[l]	Various[c], Custom[c]
	Aeromapper 300	F	90	Yes[c]	4,650	5,350	12,756	Various[c], RGB[o]
Altavian	F7200 NOVA	F	90	-	5,300	6,500	POA	Various[c], Custom[c]
Atmos UAV	Marlyn	V	50	Yes[c]	5,700	6,700	POA	Various[c]
Autel	Evo	M	30	-	863	-	915	Integrated RGB
Baam.Tech	Futura	F	90	Yes	4,000	5,400	12,500[m]	Various[c], RGB[o]
	Elipse	V	80	Yes	-	-	4,000[m]	Various[c], RGB[o]
BFD Systems	SE-8	M	50	-	8,000	20,250	POA	Various[c], Custom[c]
	H2-6	M	90[t]	-	12,000	14,000	POA	Various[c], Custom[c]
C-Astral	Atlas C4EYE	F	60	-	2,000	2,300	POA	Various[c], Custom[c]
	Atlas ppX	F	60	Yes	2,000	2,300	POA	Various[c], Custom[c]
	Bramor C4EYE	F	90	Yes[i]	-	4,500	POA	Various[c], Integrated[c]
	Bramor mSX	F	~180	-	4,300	4,900	POA	Various[c], Custom[c]
	Bramor ppX	F	~180	Yes	4,200	4,700	POA	Various[c], Custom[c]
Delair	UX11	F	59	Yes	-	1,500[e]	POA	Integrated RGB

	DT26 Open Payload	F/L	135	-	15,500	18,500	POA	Various[c], Custom[c]
DJI	Phantom 4 Pro V2	M	30	No	1,375	-	~1,600	Integrated RGB[d]
	Phantom 4 Pro V2 RTK	M	30	Yes	1,391	-	~7,800[k]	Integrated RGB[d]
	P4 Multispectral	M	27	Yes	1,487	-	-	Integrated Multispectral/RGB
	Inspire 2	M	23-27[a]	No	3,440[b]	-	3,399-14,250[l]	Quickmount, Various[c]
	Mavic 2 Pro/Zoom	M	31	No	907/905	-	1,499-1,249	Integrated RGB
	Matrice 600 Pro	M	16-18[e]	Yes[c]	9,500-10,000[f]	15,000	5,699	Quickmount, Custom, Various[c]
	Matrice 100	M	Varies	No	2,355-2,431[f]	3,600	3,599	Quickmount, Custom, Various[c]
	Matrice 200 V2	M	24-38	No	4,690	6,140	POA	Quickmount, Skyport, Custom, Various[c]
	Matrice 210 V2	M	24-34	No	4,800	6,140	POA	Quickmount, Skyport, Custom, Various[c]
	Matrice 210 RTK V2	M	24-33	Yes	4,910	6,140	POA	Quickmount, Skyport, Custom, Various[c]
	Wind-4	M	Varies[a]	-	11,000	21,000	POA	Custom[c]
	Wind-8	M	Varies[a]	-	15,700	26,000	POA	Custom[c]
Draganfly	Tango2	F/L	120	-	5,900	6,900	POA	Various[c]
Foxtech	Nimbus VTOL V2	V	~80	Yes[c]	2,850[n]	4,800	1,850-4,310[l]	Various[c], Custom[c]
Freefly	Alta8	M	15[e]	-	6,200	18,000	16,000	Various[c]
	AltaX	M	10-50[a]	-	10,400	34,860	14,600[m]	Various[c,p]
Hitec	Xeno-FX	F	60	-	~1,100[e]	-	6,200-7,100[a]	Various[c]
Insitu	ScanEagle	F/L	1,440[s]	-	16,000	-	POA	Various[c], Custom[c]
	ScanEagle2	F/L	1,080[s]	-	21,500	26,500	POA	Various[c], Custom[c]
	ScanEagle3	F	1,080[s]	-	27,200	36,300	POA	Various[c], Custom[c]
Parrot	Anafi	M	25	No	320	-	699	Integrated RGB
	Bluegrass Fields	M	25	No	1,800	-	POA	Integrated RGB

Quantum Systems	Trinity F90+	V	90+	Yes	4,300[b]	5,000	14,900[m]	Various[c], Custom[c]
	Tron F90+	V	90+	Yes	11,500	13,500	44,900[m]	Various[c,p], Custom[c]
QuestUAV	Q-200 Surveyor	F	60	Yes[i]	4,000	4,600	POA	Various[c], Custom[c]
	DATAhawk PPK	F	45	Yes	-	2,150	POA	Integrated RGB[d]
senseFly	eBee X	F	90	Yes	1,100-1,400[a,e]	-	POA	Various[c]
	eBee Classic	F	50	No	690	-	POA	Various[c]
	eBee SQ	F	55	No	1,100	-	POA	Various[c]
Sentera	PHX RTK	F	59	Yes	1,800	-	7,510-10,400[a]	Sentera only
SUI	Endurance	F	~40[a]	-	3,200	-	12,000-16,325[a]	Various[c], Custom[c]
SwellPro	SplashDrone 3+	M[u]	23	-	1,447[n]	3,000	1,234[m]	Integrated RGB
Trimble	UX5	F	50	-	2,500	-	POA	Integrated RGB[d], Various[c]
	UX5 Multispectral	F	45	-	2,500	-	POA	MicaSense RedEdge[d], Various[c]
Tuffwing	UAV Mapper	F	~40	-	1,600	2,000	2,200-6,985[l]	Various[c], Custom[c]
Wingtra	WingtraOne	V	55	Yes[c]	3,700	4,500	POA	Various[c]
Yuneec	H520	M	28[a,f]	Yes	1,633	2,500	POA	Various[c]

A = depends on payload, B = without sensor or gimbal, C = purchase separately , D = can be removed, E = with full payload, F = depends on battery used, G = Zenmuse XT adaptor required, H = supplied with Parrot Sequoia, I = RTK/PPK optional, J = depends on version , K = includes D-RTK 2 Mobile Station, L = depends on selected package, M = starting price, N = without battery, O = supplied with, P = LIDAR suitable, Q = not supplied by company, use reseller, R = water landing option available, S = powered using internal combustion engine, T = hydrogen fuel cell powered, U = waterproof.

6.3.1.4. Drone flight basics

Flight, or mission, planning is an important first step in ensuring the collection of accurate data (Colomina & Molina, 2014). All the drones highlighted in this review can be controlled, via a controller and smartphone/tablet or laptop, either manually, or automatically, and all come supplied with proprietary flight planning software. There are also stand-alone flight planning software options available, such as DroneDeploy and Pix4D Capture which are compatible with a range of different drones (**Tab. 6.2**). Automated surveys require the creation of a flight plan, the design of which is influenced by the survey area, drone speed, height, sensor FOV and image overlap. The larger the overlap between the images, the more tie-points there are available to mosaic them together (Cruzan *et al*., 2016), increasing detail and accuracy, as each tie-point must be visible in at least three separate images (Westoby *et al*., 2012). Software, such as DroneDeploy, recommend an overlap of at least 75 % and it is important to note that higher overlap equals more images, increasing the amount of data produced. Drone speed will influence frontal overlap, and this must also consider the rate at which the chosen sensor is able to take images to avoid poor image overlap or potential gaps between images. Image overlap and coverage is lower at the margins of the study area (**Fig. 6.2**) (Cruzan *et al*., 2016) and flight plans should always be created to cover more area than needed to avoid distortion over areas of interest (D'Oleire-Oltmanns *et al*., 2012).

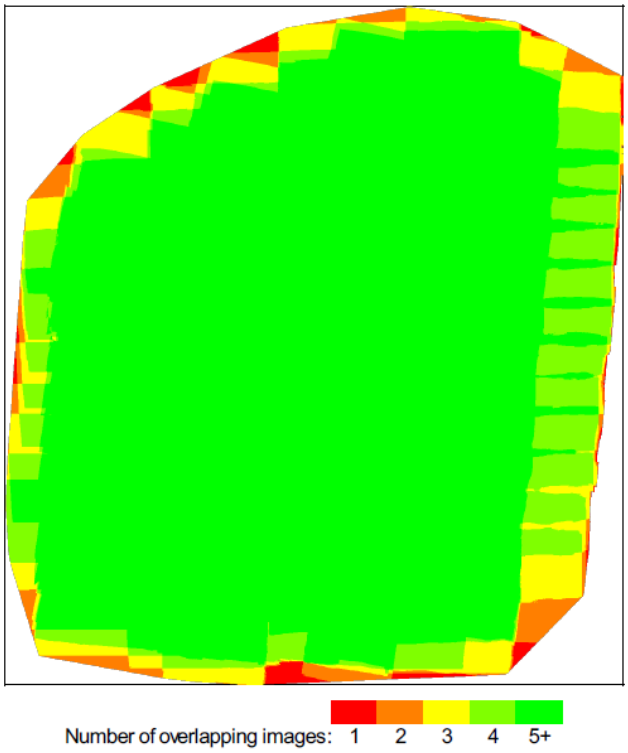

Fig. 6.2. RGB mosaic overlapping images map taken from a 2017 survey in Carraroe, Ireland. Lower numbers of overlapping images can be observed at the mosaic margins in red. Created using Pix4D.

6.3.2. Sensor types

There are a range of different sensors that are small and light-enough to be mounted on a drone. Each has certain attributes that may or may not make it suitable for a particular research objective. Differences in spatial and spectral resolution along with the range of wavelengths that can be detected are important considerations when choosing the correct sensor.

6.3.2.1. RGB sensors

RGB (red, green blue) sensors collect data from three broad bands within the visible spectrum. These sensors often have the lowest spectral resolution and the highest spatial resolution (Aasen *et al*., 2018). Many lower cost survey grade drones come with integrated, high-resolution (~20 MP) complementary metal-oxide semiconductor (CMOS) RGB sensors, this includes the DJI Phantom and Inspire series (DJI, Shenzhen, China) and the Parrot Anafi (Parrot SA, Paris, France). The relatively low cost of these devices makes them accessible to a wide range of researchers and non-researchers (Tait *et al*., 2019), significantly advancing their application within environmental monitoring. Integrated RGB sensors allow the user to view video feed in real-time on a mobile tablet device connected to the operating controller. Images and video can be captured, and the screen interface can be used to alter camera parameters such as ISO, aperture, shutter speed and exposure settings.

6.3.2.2. Multispectral sensors

Multispectral sensors typically contain between 4–12 bands (Adão *et al*., 2017) and can record data in the visible and non-visible regions of the EM spectrum. Increased technological development has led to a large range of multispectral sensors that can be drone mounted (**Tab. 6.3**). Some, such as the Parrot Sequoia+ (Parrot SA, Paris, France) and the MicaSense (MicaSense, Seattle, USA) range are easily mounted on different drones whereas others, such as the Tetracam range (Tetracam inc., Chatsworth, Canada), require a more specialised, custom approach to mounting. Certain models can be integrated with a drone, allowing them to be operated from the flight planner, for example, the DJI SkyPort (DJI, Shenzhen, China) allows integration of the SlantRange 4p (Slantrange, San Diego, USA), MicaSense RedEdge-MX and Altum (MicaSense, Seattle, USA) with the DJI Matrice 200/210/RTK (DJI, Shenzhen, China). Many commercially available multispectral sensors have been designed with agricultural monitoring in mind (Lum *et al*., 2016) and often focus on bands which pertain most to plant health, such as the red and near infrared (NIR), allowing for the calculation of a range of vegetation indices (Dash *et al*., 2018), but can often lack the blue band as a result of this focus. Blue light can be useful in shallow subtidal

environments too as it strongly penetrates the water column (Peichl *et al*., 2001) and its inclusion can improve submerged feature detection. Some sensors, such as the MicaSense Altum, do record a blue band.

6.3.2.3. Hyperspectral sensors

Hyperspectral sensors can contain hundreds of narrow contiguous bands across the EM spectrum (Govender *et al*., 2007), providing much greater spectral resolutions than available with RGB or multispectral sensors. This gives them greater spectral discriminatory capabilities and makes them well suited for use in spectrally complex environments like the intertidal zone where there may be several species that are spectrally similar to one another. There are two main types of hyperspectral sensor that are suitable for drone operations and they are defined, primarily, by how the collect data (**Tab. 6.4**). Pushbroom devices scan a single line at a time across the horizontal field of view (HFOV) of the sensor. A narrow optical slit limits the amount of light entering the sensor to that of a narrow strip which focuses light through a prism and onto a detector, usually a charged couple device (CDD) (Gómez-Chova *et al*., 2008). These scan lines should theoretically be parallel and equidistant (Ringaby *et al*., 2010) but platform instability can lead to scan-line to scan-line errors (Hruska *et al*., 2012) and issues with exposure (Adão *et al*., 2017). Their relatively simple design means that pushbroom sensors do not require trade-offs between spatial and spectral resolutions (Jaud *et al*., 2018).

These trade-offs have been responsible for the limited development of the second sensor type, full-frame, or snapshot devices which have high spectral but coarser spatial resolutions. Instead of capturing a single spatial and spectral dimension, full-frame sensors capture two spatial (x, y) and one spectral dimension (Aasen *et al*., 2014), meaning they capture the entire scene visible within the sensor field-of-view (FOV) simultaneously. This makes image mosaicking and georeferencing simpler than for pushbroom devices (Aasen *et al*., 2014) as standard photogrammetry practices can be applied (Aasen *et al*., 2018). Coarser spatial resolutions can, in some cases, be mitigated by sharpening to a finer resolution panchromatic band (Behmann *et al*., 2018). Whilst full-frame sensors can also experience noise, manifesting as image blur, this is much simpler to account for during processing than scan-line errors (Hagen & Kudenov, 2013). Despite their potential advantages there are relatively few commercially available full-frame sensors (**Tab. 6.4**). Bareth *et al.* (2015) demonstrate the technical capabilities of two early models from Cubert (Cubert GmbH, Ulm, Germany) and Senop (formely Rikola) (Senop, Finland) for drone mapping operations and a more recent paper by Jackisch *et al.* (2018) successfully applied a Senop sensor for acid mine drainage monitoring.

A detailed review of drone sensor technology can be found in Adão *et al*. (2017) and Aasen *et al*. (2018).

Tab. 6.2. Different mission planning and flight control software, compatible drones and operating systems (OS). Proprietary software is marked with an *.

Software	Compatible drones	OS
DJI GS Pro*	DJI Phantom 4 Pro V2 DJI Inspire 2 DJI Mavic 2 Zoom/Pro DJI Matrice 600/600 Pro DJI Matrice 100 DJI Matrice 200/210 V2 DJI Wind	iOS[a]
DJI GS RTK*	RTK-enabled DJI Models	iOS[a]
Pix4D Capture	DJI Phantom 4 Pro V2 DJI Inspire 2 DJI Mavic 2 Zoom/Pro DJI Matrice 600/600 Pro DJI Matrice 100 DJI Matrice 200/210 V2 Parrot Anafi Parrot Bluegrass Yuneec H520	iOS, Android[a]
DroneDeploy	DJI Phantom 4 Pro V2 DJI Inspire 2 DJI Mavic 2 Zoom/Pro DJI Matrice 600/600 Pro DJI Matrice 100 DJI Matrice 200/210 V2 DJI Wind	iOS, Android[a]
Freeflight 6*	Parrot Anafi	iOS, Android[a]
ParrotFields*	Parrot Bluegrass	iOS[a]
senseFly eMotion3*	senseFly eBee X senseFly eBee Classic	Windows[a]
senseFly eMotion Ag*	senseFly eBee SQ	Windows[a]
Sentera FieldAgent™*	Sentera PHX/RTK	
QBase3D*	Tron F90+ Trinity F90+	Windows[a]
Mission Control*	Xeno-FX	Android[b]
Mission Planner	Tuffwing UAV Mapper Hitec Xeno-FX SUI Endurance 3dr Solo	Windows[a]
QuestUAV*	Q-200 Surveyor DATAhawk PPK	Windows[a]
Yuneec DataPilot™*	Yuneec H520	Android, Windows, iOS[a]
Map Pilot	DJI Phantom 4 Pro V2 DJI Inspire 2	iOS[a,c]

	DJI Mavic 2 Zoom/Pro DJI Matrice 600/600 Pro DJI Matrice 100 DJI Matrice 200/210 V2 DJI Wind	
C-Astral C^{3}P*	C-Astral Atlas C4EYE C-Astral Atlas ppX C-Astral Bramor C4EYE C-Astral Bramor mSX C-Astral Bramor ppX	Windows[b]
Delair Flight Deck*	Delair UX11	Android[a]
Atmos UAV MarLynk*	Atmos UAV Marlyn	Windows[b]
WingtraPilot*	WingtraOne	Android[b]
Freefly Alta*	Alta8 AltaX	iOS[a], Android[a]
Insitu ICOMC2* **Insitu INEXA Control***	ScanEagle ScanEagle2 ScanEagle3	Windows

A = software version and device vary, **B** = hardware supplied by manufacturer, **C** = supports older models as well

Tab. 6.3. Commercially available multispectral sensors. Information is included on sensor weight (grams), integrated RGB sensors, bands and wavelength range, spatial resolution (pixels) (MP = megapixel), key lens information (HFOV = horizontal field of view), presence of an integrated light sensor (ILS) and method of integration with drones (Gimbal Mount = can integrate with drone gimbal and enable live feed, Various = various mounting options for drones available, Quickmount/Skyport = Integration with DJI drones, Custom = may require designing of custom mount). Information is accurate at time of submission (02/2020).

Company	Model	Weight (g)	RGB	Bands / WL Range (nm)	Spatial Resolution (px)	Lens	ILS	Integration
FluxData	FD-1665-MS3	1250[a]	No	3 (400-1000)	659x494 – 1628x1236[b]	Nikon F/T-Mount	No	-[c]
	FD-1665-MS5	1250[a]	No	5 (400-1000)	659x494 – 1628x1236[b]	Nikon F/T-Mount	No	-[c]
	FD-1665-MS7	1250[a]	No	7 (400-1000)	659x494 – 1628x1236[b]	Nikon F/T-Mount	No	-[c]
Hiphen	Airphen	200	No	6 (450-800)	1280x960	8 / 4.2 mm	No	Various[h]
MAIA	MAIA WV[e]	420	Yes	9 (395-950)	1280x960	7.5 mm (35° HFOV)	Yes	Gimbal Mount[c,d]
	MAIA S2[f]	420	Yes	9 (433-899.5)	1280x960	7.5 mm (35° HFOV)	Yes	Gimbal Mount[c,d]
	MAIA M2[g]	-	Optional	2 (395-950)	-	-	Yes	-[c]
MAPIR	Kernal	45+[i]	Optional	1-6 (350-1100)	-[b]	3.5 (87° HFOV) – 35 mm (9° HFOV)	No	Various[h,m]
MicaSense	Altum	406.5[j]	Yes	5 (450-900) / (8000-14,000[k])	2064x1544 / 160x120[k]	8 mm (48°x37°) / 1.77 mm (57°x44°)[k]	Yes	Quickmount/SkyPort[h]
	RedEdge-MX	231.9[j]	Yes	5 (400-900)	1280x960	5.4 mm(47.2° HFOV)	Yes	Quickmount/SkyPort[h]
Parrot	Sequoia +	107[j]	Yes	4 (550-800)	1280x960 4608x3456[l]	4 mm (61.9° HFOV) / 4.9 mm (63.9° HFOV)[l]	Yes	Various[h]
Sentera	Quad Sensor	170	Yes	3 (600-900)	1248x950	(50° HFOV)	Yes	Various[h]
	Double 4K	80	Yes	5 (440-840)	12.3 MP	(60° HFOV)	Yes	Various[h]
SILIOS	CMS-C	75[a]	No	8 (430-700)	1280x1024	16 mm (30.7 °) / 12-36 mm	No	Custom[o]

						(41°-13.6°)		
	CMS-S	75[a]	No	8 (650-930)	1280x1024	16 mm (30.7 °) / 12-36 mm (41°-13.6°)	No	Custom[o]
	CMS-V	75[a]	No	8 (550-830)	1280x1024	16 mm (30.7 °) / 12-36 mm (41°-13.6°)	No	Custom[o]
SlantRange	3PX	400	No[n]	4 (410-950)	1280x1024	-	Yes	SkyPort[h]
	3p	350	No[n]	4 (410-950)	1280x1024	-	Yes	Various[h]
	4p	350	Yes	6 (410-950)	1280x1024	-	Yes	Various[h], Skyport[h]
Tetracam	ADC Micro	90	No	3 (520-920)	2048x1536	8.43 mm (42.48° HFOV)	Yes	Custom[c]
	ADC Snap	90	No	3 (520-920)	1280x1024	8.43 mm (37.67° HFOV)	Yes	Custom[c]
	Micro-MCA[p,g]	497-1000	Optional	6-12 (450-1000)	1280x1024	9.6mm (38.26° HFOV)	Yes	Custom[c]
	Micro-MCA Snap[p,g]	497-1000	Optional	6-12 (450-1000)	1280x1024	9.6 mm (38.26° HFOV)	Yes	Custom[c]
	MCAW	600	Optional	6 (450-1000)	1280x1024	9.6 mm (38.26° HFOV)	Yes	Custom[c]

A = without lens, B = varies with lens, C = Contact manufacturer, D = Capable of reading internal IMU, E = Same wavelength intervals of WorldView-2, F = Same wavelength intervals of Sentinel-2, G = Modular (multiple filter options), H = Mounts available for multiple drone models – contact manufacturer , I = Depends on sensor/lens chosen, J = With ILS, K = Thermal camera, L = RGB Sensor, M = May not be compatible with all DJI drones – contact manufacturer , N = Band positions selectable at order, RGB can be attained, O = Company does not provide, needs to be custom designed, P = Available with 4, 6 or 12 cameras.

Tab. 6.4. Commercially available hyperspectral sensors. Information is included on the weight (grams), wavelength range (nm), number of spectral bands, spectral resolution (nm), spatial resolution (pixels), key lens properties (e.g. focal length and field of view) and acquisition method (Full-frame or push-broom). All information was correct at time of initial submission (02/2020).

Company	Model	Weight (g)	WL Range (nm)	Bands	Spectral Res (nm)	Spatial Res (px)	Lens	Acquisition
BaySpec	OCI-F	570	400-1000	120	5-7	800	16 mm (21°)	Push-broom
	OCI-U-1000	180	600-1000	100[b]	~5	2048	35 mm (18°)	Push-broom
	OCI-U-2000	190	600-1000	25[b]	12-15	200 x 400	35 mm (18°)	Full-frame
	GoldenEye™	-	400-1000	40-52	7-12[c]	648x488	50 mm (13°)	Full-frame
	GoldenEye™	-	900-1700	40-52	7-12[c]	648x488	50 mm (13°)	Full-frame
Corning	microHSI™ 410 VIS-NIR	450	400-800[a]	120	3.3	680	16 mm (30°) – 33 mm (15°)	Push-broom
			400-1000[a]	180	3.3	680	16 mm (30°) – 33 mm (15°)	Push-broom
			380-880[a]	150	3.3	680	16 mm (30°) – 33 mm (15°)	Push-broom
	microHSI™ alpha-VIS	2100	400-800[a]	40	10	1280	195 mm (4.9°)	Push-broom
			350-1000[a]	60	10	1280	195 mm (4.9°)	Push-broom
Cubert	Firefleye S185 SE	470	450-950	125	8	2x1[d]	10 mm (33°) – 50 mm (7°)	Full-frame
	ULTRIS 20	350	450-850	100	4	400x400	(40°)	Full-frame
Headwall	Nano-Hyperspec®	500	400-1000	270	6[c]	640	4.8 mm – 70 mm	Push-broom
	Micro-Hyperspec®	700 (A-Series) /	400-1000	324	2.9[c]	1004	4.8 mm – 70 mm	Push-broom
		1100 (E-Series)	400-1000	369	-	1600	4.8 mm – 70 mm	Push-broom
HySpex	VNIR-1024	4200	400-1000	108	5.4	1024	16°	Push-broom
	VNIR-1800	5000	400-1000	182	3.26	1800	17°	Push-broom
	Mjolnir V-1240	4000	400-1000	200	3	1240	20°	Push-broom
	Mjolnir VS-620	6000	400-2500	490	3-5.1	620	20°	Push-broom

Itres	MicroCASI 1920	2500	400-1000	288	2.1	1920	36.6°	Push-broom
Resonon	Pika L	600	400-1000	281	2.1	900	6 mm (47.5°) – 70 mm (4.3°)	Push-broom
	Pika XC2	2220	400-1000	447	1.3	1600	6 mm (76°) – 70 mm (7.7°)	Push-broom
	Pika NUV	2100	350-800	196	2.3	1600	17 mm (30.8°)	Push-broom
Senop	HSC-2	986	400-1000	1000[b]	5-10	1024x1024	~10 mm (36.8°)	Full-frame
Specim	FX10	1260	400-1000	224	5.5[c]	1024	(38°)	Push-broom
Ximea	MQ022HG-IM-LS150-VISNIR	32	470-900	150	3	2048x5	-	Push-broom

A = multiple wavelength range options, B = bands are selectable, C = full width half maximum (FWHM), D = Megapixel

6.3.2.4. Sensor calibration

Multispectral and hyperspectral sensors require calibration to local insolation conditions to produce accurate reflectance values (Markelin *et al*., 2013). To obtain absolute reflectance for local insolation conditions, white reference calibration targets should be measured. Ideally, a Lambertian surface (Jablonski *et al*., 2016), being a diffuse reflector, should be used as the white reference, and many sensors are supplied with their own targets and instructions on calibration routines. If insolation levels change significantly during a flight (i.e. from sunny to cloudy) then the drone should be safely landed and recalibrated before continuing (or restarting) the survey. Many multispectral sensors (**Tab. 6.3**) are supplied with incident light sensors (ILS) which can compensate for changes in light conditions during a survey (i.e. passing cloud cover) ensuring the accuracy of the empirical line linear relationship (established during pre-flight calibration) for the resulting multispectral imagery (Assmann *et al*., 2019). Obtaining absolute reflectance values (reflectance being an inherent property), through calibration, allows data from several flights, different locations and different times to be directly compared.

6.4. Operational parameters

6.4.1. Survey accuracy

A primary consideration when planning any form of drone-based remote sensing survey is the required level of accuracy which will determine whether time and money needs to be invested in correctional GPS technology. If centimetre level accuracy is not required, then spatial positioning based on the drone's internal GPS will suffice (Joyce *et al*., 2018) provided GPS data from field surveys is not being integrated into analysis workflows. Correctional GPS technology is typically either real-time kinematic (RTK) or post-processing kinematic (PPK) and can be applied through GCPs or through compatible drone models. RTK and PPK work by triangulating, not only with satellites, but also with base stations to achieve highly accurate horizontal and vertical positional data. These base stations, of known coordinates, calculate the positional error of satellites and this correctional information is used to enhance the geolocation of survey images, allowing for centimetre level accuracy (Yoo *et al*., 2018). The difference between the two technologies is how they apply this correction, as their names imply; RTK applies them during the survey, using a dedicated base station, whilst PPK applies them afterwards.

Deploying GCPs is a well-established method for georeferencing drone imagery (Chen *et al*., 2016). GCPs are usually a distinctive pattern where the centre point is clearly visible to a drone, the size of which should depend on the drone sensor spatial resolution (Dash *et al*.,

2018). The location of the centre point of these markers is then recorded using an RTK/PPK enabled GPS device, such as a Trimble GPS (Trimble, Sunnyvale, USA). Whilst accurate, this is a very time-consuming method (d'Oleire-Oltmanns *et al*., 2012; Forlani *et al*., 2018) as GCPs are required to be spread out across the entire survey area. The number of GCPs required for a site will depend on the survey area. Assmann *et al*. (2019) recommend, for a topographically simple site of < 1 ha, that five GCPs should be enough and that any more does not provide a substantial improvement in geolocation accuracy. The required number of GCPs may also depend on the desired precision of the survey. James *et al*. (2017) found that in order to reach a survey precision of 50 mm, only 15 out of the 30 GCPs deployed were required to achieve the desired precision. A study by the Nevada Department of Transport found that placing more than 5–10 GCPs did not yield increased levels of survey accuracy (Pix4D, 2020). The lack of clarity from the literature reinforces the need for thorough pre-flight planning and this should include evaluating the required number of GCPs for a chosen study site. The development of RTK/PPK enabled drones (**Tab. 6.1**) eliminates the need for GCPs, vastly improving the efficiency of drone surveys (Hill, 2019). Some drones can also be outfitted with a separate RTK/PPK system, such as the DJI D-RTK GNSS, which is compatible with all DJI drones using the A3 controller system. PPK may be the more useful option for drone surveys as, unlike RTK, it does not require a dedicated base station, reducing costs, and can use national GPS stations such as the OSI's GNSS network in Ireland, OS Net in the UK or the CORS network in the USA. PPK does not require a direct connection between the base station and the drone, as it post-processes the time stamped images and is much less susceptible to signal loss. Not requiring a dedicated base station means that PPK provides much greater range and operational flexibility than RTK, potentially allowing much larger areas to be surveyed, taking full advantage of the increased range of fixed-wing drones (Hill, 2019).

6.4.2. Regulations

Prior to any drone survey it is necessary to check local drone licensing requirements and regulations which should, if necessary, be factored into the flight plan. This is important as restrictions can limit where, how high and how far a drone can fly, and these can vary by country (Duffy *et al*., 2018a). Regulations can also vary within countries, for example around restricted airspace, such as near airports and special permissions and effective communication with local air traffic controllers are most likely required (Duffy *et al*., 2018a). Baena *et al.* (2017) highlights some of the variation in international drone regulations that they experienced, from those which have no regulations to those that do and also highlight the need to consider local communities by, for example, gaining landowner permission before surveying. Typically, national drone regulations are managed by

respected national aviation authorities (such as the IAA in Ireland) and these should be consulted when planning drone surveys.

It is also important to consider the social implications of drone flying. In rural coastal areas there can be a degree of sensitivity over activities occurring within the intertidal zone. With drones hardly being inconspicuous, we have found that engaging with local people and explaining the purpose of the research, has elicited a positive response and has facilitated the parking of extra vehicles on private property near one of our study sites. Awareness of local and regional societal issues that may affect people's perceptions of a drone survey should be considered. When necessary, efforts should be made to provide information to relevant communities and individuals to facilitate positive, rather than negative responses, thus improving the perception of drones as effective and safe conservation tools (Sandbrook, 2015).

6.4.3. Weather

Weather is one of the most important factors influencing the success of any drone survey, especially in often exposed coastal environments. Moderate wind speeds will reduce flight time, whilst higher winds will pose a significant risk to the drone, particularly during take-off and landing. Most drones are not waterproof (Johnston, 2018), although the SwellPro SplashDrone 3+ (SwellPro, Shenzhen, China) is entirely waterproof and can land in and take off again from water. For most commercially available drones however, the general advice would be to avoid rain and if it starts to rain during a survey, land as quickly and safely as possible. Bright sunlight can create problems in the intertidal zone from sun glint off wet macroalgae and shallow submerged areas. This can be mitigated in two ways, planning flight lines as close to perpendicular to the sun as possible (O'Neill *et al*., 2011) and flying when the sun is at a lower angle, in relation to solar noon, to reduce glint (Flynn & Chapra, 2014). Flying earlier or later in the day may increase shadows, which, depending on site topography and vegetation height (Gray *et al*., 2018), can negatively impact the data quality (Ishida *et al*., 2018). Flying closer to solar noon will help to reduce the presence of shadows (Dash *et al*., 2018; Duffy *et al*., 2018a; Otsu *et al*., 2019). A two-hour window either side of solar noon has been recommended as suitable for shadow reduction (MicaSense, 2019) which may help mitigate tidal constraint limitations on flying time. Surveying under constant light conditions is the optimal scenario as variation in illumination can cause shading, bright spots and over/under-exposure which can negatively affect reflectance values (Doughty & Cavanaugh, 2019).

6.4.4. Local/regional knowledge

Local and regional knowledge are vital for an efficient drone survey (Garono *et al*., 2004) and sites of interest should be visited at least once prior to surveying. This is important for intertidal macroalgal mapping for two reasons, first, to verify the presence of target species or communities and second, to define site limits. This may vary depending on research objectives, for example if one is looking to survey a large area (pursuant to appropriate permissions) then a different approach may need to be taken, such as visits to multiple sites within the study area. With regulations often limiting how far a drone can be flown, for the operator it is important to determine whether the feature of interest is sufficiently covered by the proposed flight plan (this may not be necessary if conducting a holistic mapping survey). Other factors may also determine the size of the study area including research objectives, such as mapping long term monitoring sites (Díaz-Delgado *et al*., 2018) and restricted airspace. Regional knowledge is important for helping to identify potential study sites and can be used in combination with satellite imagery to help identify points of entry to a site, such as the presence of a pier or entry road. Depending on the equipment used in the survey, identifying a point of entry close to the study site is useful to avoid carrying heavy, and often expensive, equipment across the hazardous intertidal zone. Owing to the nature of the intertidal zone, at least one member of the survey team should be familiar with working there and be responsible for site risk assessments (Burrows *et al*., 2010).

6.4.5. Processing and analysis

Data outputs will depend on the sensor used, with RGB data being less complex to process and analyse compared to multispectral and hyperspectral but limited in terms of the types of quantitative analysis that can be performed.

There are a range of available open source and subscription-based image processing and analysis software. Software including Maps Made Easy (San Diego, USA) and DroneMapper (Cedaredge, USA) offer free image processing (with resolution limitations) for small papers with the option of paying for larger maps and extra features. Agisoft (Agisoft LLC, St. Petersburg, Russia), Pix4D (Lausanne, Switzerland) and ENVI One Button (Harris Geospatial, Boulder, USA) are established subscription-based software for image processing that provide a simple set of tools allowing for the easy processing and mosaicking of drone imagery through the process of structure-from-motion (SfM) which produces detailed orthomosaics and digital surface models (DSM) (Windle *et al*., 2019). A key advantage of these software packages is their radiometric calibration toolset which allow for the easy calculation of absolute reflectance values. Whilst fill-frame hyperspectral datasets can theoretically be processing using the aforementioned software, many sensors

(including pushbroom) come with proprietary software allowing for accurate image processing.

The open source software, QGIS, has a range of image analysis and classification tools which can be supplemented by plugins and toolboxes such as Orfeo Toolbox (OTB), SAGA and GRASS, each adding extra functionality. R packages have also been used in by several studies (Brodie *et al*., 2018; Duffy *et al*., 2018b) to analyse RGB and multispectral datasets. ENVI (subscription-based) is an established, powerful image analysis software with a raft of different options and processing algorithms (Wu & Sun, 2013), making it a suitable choice for the processing of all types of remote sensing data. Functionality can be increased through the purchase of different modules. Other software packages such as eCognition (Trimble, Sunnyvale, USA) and ArcGIS (ESRI, Redlands, USA) also provide different image analysis packages based on traditional classification techniques and object-based image analysis (OBIA).

6.4.5.1. Object-based image analysis (OBIA)

Object-based image analysis (OBIA), also known as image segmentation in software such as ArcGIS, differs from traditional pixel-based classification approaches. Instead of assigning each pixel to a class based on its spectral properties, OBIA groups neighbouring pixels of similar spectral properties together (Ventura *et al*., 2018) forming 'super-pixels' and, as such, is less susceptible to increased spectral variability caused by higher resolution imagery (Lechner *et al*., 2012). OBIA also allows for the inclusion of additional information such as object shape and texture in addition to spectral information (Dronova, 2015). After grouping pixels together, the next step is to classify each segment into recognisable classes (*e.g.* seaweed species, groups, assemblages etc.) (Blaschke, 2010) with training areas being selected from the polygons created during the initial segmentation step and this data is then used to train a classifier to create a final classification map. OBIA functionality is available in both open source and subscription-based software and can be a useful tool for relatively low-cost mapping studies where target features are relatively distinct from one another, such as classifying shallow aquatic vegetation using multispectral imagery (Chabot *et al*., 2018), mapping coastal marine habitats using RGB data (Ventura *et al*., 2018) and mapping of swamp vegetation extent, again using high resolution RGB imagery (Lechner *et al*., 2012).

6.4.5.2. Pixel-based classification methods

Pixel-based classifiers seek to assign each individual pixel in an image to a pre-determined class (supervised) or a class based on groupings of pixels with common characteristics (unsupervised). Supervised classification methods, such as Maximum Likelihood Classifier

(MLC) (Paola & Schowengerdt, 1995) and Spectral Angle Mapper (SAM) (Kruse *et al*., 1993) require the input of spectral training data to create classes (*e.g.* seaweed species) into which individual pixels are classified based on the similarity of the spectral signatures (Vahtmäe & Kutser, 2013). Unsupervised classification, such as K-means and ISODATA (Tou & Gonzalez, 1974), classifies pixels using statistics alone, without the need for inputted training classes. The need to collect training data can make using the supervised classification more time-consuming, but it allows for the creation of more detailed classes (Thomson *et al*., 1999), providing better representation of the habitat of interest. In environments of relatively optically distinct cover classes, the simplicity of unsupervised classification methods may be a useful first step in image classification (Duffy *et al*., 2018b) and may also be an effective method for creating water masks (Pe'eri *et al*., 2008).

6.4.5.3. Structure from motion (SfM)

Structure from motion (SfM) techniques allow the creation of three-dimensional structures from a series of two-dimensional images (Johnston, 2019). Algorithms use the relative positions of pixels from overlapping imagery, obtained at different angles to create both orthorectified imagery and three-dimensional scenes, also known as digital surface models (DSM) (Assmann *et al*., 2019). Software, such as Agisoft (Agisoft LLC, St. Petersburg, Russia) and Pix4D (Lausanne, Switzerland) can create digital surface models (Yoo *et al*., 2018) which, in the intertidal zone, could provide information on site topography and elevation. SfM techniques have been use in monitoring terrestrial vegetation, such as grassland sward height, where, unlike intertidal macroalgae, the structure can be measured providing data on height and area (Forsmoo *et al*., 2018) and relationships between volume and biomass can be derived (Cunliffe *et al*., 2016). This particular approach is difficult to apply in the intertidal zone as emersed macroalgal species loose their structure and submerged species are difficult to map owing to the limited penetration of light through the water column. Conversely, the unique zonation patterns present within the intertidal zone, particularly the defined vertical zonation of some species (Lubchenco, 1980), may improve classification workflows through the addition of elevation data. Regarding the target species for this research, *Ascophyllum nodosum*, information gained through the additional of DSM data may not enhance classification accuracy as it is often found in mixtures with *Fucus vesiculosus* along similar vertical elevations.

6.5. Application for intertidal macroalgal mapping

The intertidal macroalgal species, group, or community of interest will determine the sensor and drone choice along with key operational parameters such as flying height and speed.

This study defines three key characteristic of intertidal macroalgae that will influence these decisions, **1)** the size of individuals within a species, **2)** homogeneity of coverage and **3)** spectral similarity to surrounding species and substratum. If conducting a community-level mapping survey one should apply these criteria for each species present and determine which species can or cannot be mapped using a certain method (Nagendra, 2001). The choice of drone is also influenced by the area that needs to be surveyed, for large areas, where regulations permit, fixed-wing (or VTOL) models are the most appropriate, covering larger areas than multirotor drones and offering flexible mounting solutions for a range of sensors (heavy-lift models can carry multiple sensors).

6.5.1. Unique operational challenges of intertidal macroalgal mapping

Site access is an important consideration when selecting a study site as, particularly in remote areas, it will influence survey planning logistics. Depending on the type of drone and associated survey equipment, vehicles and people, it may not be possible to traverse difficult terrain, such as the rocky intertidal or muddy flats. It is important to consider the size of the study site(s) and if multiple locations are to be surveyed within a region, how best to travel between them (e.g. on-foot, by boat, car etc.). Easy access points such as roads and piers are suitable options allowing vehicles to be brought close to the study site and allowing sensitive equipment to be protected in case of rain.

The intertidal zone can often pose challenges for the deployment and recovery of drones. Some fixed-wing drones perform glider landings, requiring a large, open space free of obstacles. Some also require launching systems (Hodgson *et al*., 2013) which can be of varying size and portability depending on the drone model. The choice of study site must consider the availability of take-off and landing spaces (Diaz-Delgado *et al*., 2018), the availability of which will vary depending local topography and cover type. Multirotor and VTOL-enabled fixed-wing drones do not have to contend with this and can be safely deployed and recovered in much smaller spaces (Ventura *et al*., 2018), such as from open patches of substratum interspersing macroalgal beds. Depending on the size of drone one should consider bringing a landing pad to avoid contact between the drone and sand and sediment which can cause damage.

Tidal constraints are, in higher latitudes, the most unique and restrictive challenge associated with conducting drone research in the intertidal zone. The low tide window limits all aspects of survey operations, from flight time, GCP measurements and concurrent field work surveys. Flying within 30 min either side of maximum low tide (Tait *et al*., 2019) should provide a sufficient window in which to collect representative data on intertidal macroalgal communities, with many current drone models having flight times of between 20-90 min

(**Tab. 6.1**). This time window may vary when mapping species and communities occurring in the upper intertidal, such as *P. canaliculata*, which experiences greater periods of emersion. Depending on the geographic region and season, bad weather and unsuitable atmospheric conditions can combine with tidal constraints to reduce the time available to survey. This requires the need for redundancy to be included in survey planning whereby extra time (i.e. a week) should be allocated to surveys, especially in areas where the weather is more unpredictable (this includes issues discussed in section **4.3**). Satellite imagery can be a useful tool for planning flights over study areas (Tay *et al*., 2018) but the state of the tide during image acquisition may make it difficult to determine the true extent of the intertidal, necessitating a pre-survey site visit to accurately determine the flight area.

If using GCPs, it is important that the amount of time needed to deploy, measure and then collect them is considered in the survey plan. The intertidal zone can be a difficult environment to traverse but this process must be completed quickly and safely so as not to delay the drone survey or to be a risk from the incoming tide. The amount of GCPs used by other mapping studies using drones varies greatly depending on the size of the study area. On topographically flat sites of < 1 ha, Assmann *et al*. (2019) recommend that 5 GCPs are suitable, but also noting that for more topographically complex sites, more GCPs may be required. Dash *et al*. (2018) used nine GCPs in their drone survey of a 2.7 ha forested site, Tait *et al*. (2019) used 12 GCPs for their ~2 ha rocky intertidal mapping work, and six GCPs were used by Flynn & Chapra (2013) for each 1 km stretch of river surveyed. Larger sites will require more GCPs which will increase the amount of time required to deploy them, for example d'Oleire-Oltmanns *et al*. (2012) noted that it took 2–4 h to deploy and measure 20–25 GCPs and for eighty GCPs, it took 7–8 h.

Any water present within a scene can usually be masked out during processing, either through thresholding using the NIR band, or through vegetation indices (VI) such as the normalised difference water index (NDWI) (McFeeters, 1996). Along with masking out terrestrial features this is a useful first step in analysis intertidal imagery as it reduces external noise and improves classification accuracy (Casal *et al*., 2011). The presence of water can affect the reflectance spectra of submerged macroalgae, particularly towards the non-visible region of the EM spectrum (Fyfe, 2003), and turbid conditions can reduce light penetration (Kutser *et al*., 2006b), potentially altering the final classification accuracy. Land masks can either be done manually (Roelfsema & Phinn, 2010) or using VI's (Noiraksar *et al*., 2014).

Understanding variations in the spectral response of different macroalgal species and how this affects their spectral separability from one another is an important consideration.

Seasonal variations in pigment composition and concentrations (Stengel & Dring, 1998) may influence the choice of survey season, for example reproductive *A. nodosum* forms receptacles which appear yellow and may elicit a different spectral response to the thallus sections. Survey planning should consider this, particularly if collecting *in-situ* spectral library data, which, depending on the species or community of interest should be collected concurrently with the drone survey.

Duffy *et al*. (2018a) reviewed their experiences of operating drones in challenging environments, including deserts and the arctic, and highlight some of the issues raised here along with additional ones.

6.5.2. Challenging macroalgae to map

The exact same survey planning rationale can be applied to mapping both individual species and mixed communities (*i.e.* multiple species occurring within one study site). The only difference is that when mapping a single species (even if it occurs within a mixed community of macroalgal species) it is only necessary to determine whether the species of interest is spectrally distinct from all other species and substratum. The successful spectral separation of non-target species is not necessary. For mixed communities, however, it is important to determine that the species of interest are all distinct from one another and also from any other species and substratum present within the site.

The following examples represent intertidal species/communities that may not be well suited for quantification using drone-mounted remote sensing methodologies. The primary focus here is on the size of species' individuals and how easily they can be observed from a drone. Species that are relatively small in size and that do not form homogenous stands, such as *Codium* spp., would, even if spectrally distinct from surrounding species, be very difficult to map, regardless of the method used. Mapping over extremely fine spatial scales is possible but would require flying at extremely low altitudes to attain the necessary spatial resolution (Lucieer *et al*., 2014). Flying so low would reduce the area that can be covered and thus the survey efficiency and would only be feasible if using a multirotor drone, which can fly at very slow speeds. Such high spatial resolutions will also increase spectral complexity, potentially making spectral discrimination more difficult (Ventura *et al*., 2018). Some small species, such as *Pelvetia canaliculata*, are often found in relatively homogenous assemblages (also found mixed with *Fucus spiralis*) in the upper intertidal zone making them easier to observe from higher flying drones. Relatively large macroalgal species, such as *Halidrys siliquosa*, often confined to rockpools (Bunker *et al*., 2017), and *S. muticum*, tend to have more fragmented distributions which would likely present a challenge for mapping if they are mixed with other brown macroalgal communities. Sub-canopy species,

such as many red macroalgal species, cannot be mapped using current remote sensing technology. Whilst some, for example *Chondrus crispus* and *Palmaria palmata* are not exclusively sub-canopy (Kübler & Davison, 1995; Lubchenco, 1980), it would still not be possible to get an accurate assessment of their true extent.

6.5.3. Mapping homogeneous cover species

Species, including macroalgae and seagrass, which form large monospecific assemblages can potentially be mapped using relatively low-cost approaches. Intertidal and subtidal seagrass can grow in dense monospecific beds and have recently been mapped using a low-cost drones and RGB sensors (Duffy *et al*., 2018b; Nahirnick *et al*., 2018; Ventura *et al*., 2018). The monospecific nature of these beds means that their spectral complexity is low as, for example, seagrass and substratum are visually distinct from one another. OBIA techniques are a useful classification method for RGB imagery and have been successfully used to map optically distinct terrestrial habitats (Laliberte & Rango, 2011; Lechner *et al*., 2012) and can be applied for the accurate classification of intertidal ecosystems. Concurrently, pixel-based classification methods have also successfully been applied to dominant, monospecific intertidal macroalgal communities (Murfitt *et al*., 2017). The desired level of taxonomic resolution will also influence the choice of remote sensing hardware (Dekker *et al*., 2003). Taddia *et al*. (2019) sought only to identify the presence of submerged green seaweed using a multispectral sensor and were able to accurately monitor seasonal variation in coverage.

The relative homogeneity of these environments may mean that fine spatial resolution is not always required, and surveys can be conducted at higher heights, covering larger areas. The optimum survey ground sampling distance (GSD) should consider the spatial scales at which spectral variation occurs (Assmann *et al*., 2019). This should also consider whether additional data needs to be collected, for example, Duffy *et al*. (2018b) were able, flying at 15 m altitude, to observe faunal species, such as cockles, within a seagrass bed. Depending on the scale of distribution, where regulations and distance may limit drone applications, satellites can also be a suitable mapping choice (Barillé *et al*., 2010). Where homogenous, monospecific coverage is present, VI's can be used to explore intraspecific variations in the physiology of the target species. One popular VI is normalised difference vegetation index (NDVI), which is correlated with plant condition, physiological stress and photosynthetic activity (Dash *et al*., 2018). For intertidal seagrass meadows, relationships have been developed between NDVI and biomass (Barillé *et al*., 2010) and NDVI and percentage cover (Valle *et al*., 2015). Similar relationships do not appear to exist for intertidal macroalgal species, and this may prove an interesting future research topic.

6.5.4. Mapping mixed macroalgal communities

Mapping constituent species within mixed communities of intertidal macroalgae can offer additional mapping challenges than more homogenous ones. The spatial scale over which the mixture of species occurs will determine the optimal GSD and thus, factoring in sensor choice, the survey height. For mixtures that occur over fine spatial scales, flying low will improve the ability of the sensor to observe individual species and/or key biological processes (Lucieer *et al*., 2014). Very low flying heights will also necessitate the use of a multirotor drone which is also able to fly at extremely low speeds (Aasen *et al*., 2014), which cannot be achieved using fixed-wing drones (Anderson & Gaston, 2013). Mixed assemblages comprised of large macroalgal species, forming relatively homogenous stands, can likely be observed from higher survey heights so long as spectral homogeneity remains larger than the survey GSD.

Mixtures of spectrally distinct species can likely be discriminated between using either RGB or multispectral sensors, which have been used successfully for distinguishing between macroalgal groups (Brodie *et al*., 2018) and between different macroalgal species (Tait *et al*., 2019). Mixtures of spectrally similar species (i.e. intertidal fucoid assemblages) will require both a high spatial and spectral resolution to achieve species-level discrimination (Fyfe, 2003). The difficulties of distinguishing between one or more spectrally similar macroalgal species has previously been highlighted (Kutser *et al*., 2006b; Kotta *et al*., 2014; Uhl *et al*., 2013), demonstrating the challenges of surveying in these complex environments. However, Fyfe (2003) did demonstrate that it was possible to discriminate between three spectrally similar seagrass species. In these situations, the high spectral and, when drone-mounted, spatial resolution of hyperspectral sensors are necessary to identify subtle spectral differences between species (Adam *et al*., 2010; Casal *et al*., 2013). High spatial resolutions will also help to reduce within-pixel spectral mixing, improving classification accuracy (Costa *et al*., 2007). Oppelt *et al*. (2012) utilised a pushbroom hyperspectral sensor, flown at 693 m using a motorised glider, to survey the intertidal zone at Heligoland. Using existing habitat maps and several supervised, pixel-based, classification techniques they were able to successfully identify multiple seaweed classes across a range of different taxonomic resolutions. This remains the only study to apply both high spatial and high spectral resolution technology to map intertidal macroalgal communities. Several studies, including Oppelt *et al*. (2012), Brodie *et al*. (2018) and Tait *et al*. (2019), identified classes of mixed taxonomic resolution, some to species level and others only to the group level, and the achievable taxonomic resolution will ultimately depend on research objectives as to whether a targeted or holistic mapping approach is desired.

In spectrally complex environments it is important to first understand the spectral properties of dominant canopy-forming species. The creation of a spectral library for dominant canopy-forming species can be used to train supervised classification methods, saving time by avoiding the need to collect training data through extensive GPS-based field surveys (Kotta *et al*., 2014). An alternative method for the collection of training and reference data is to manually extract the data from high resolution RGB imagery (Husson *et al*., 2016; Otsu *et al*., 2019). The success, or failure, of this method will, again, depend on the spatial and spectral properties of the macroalgal assemblages within a scene. Homogenous stands of spectrally distinct species will be easy to identify in the imagery whereas more spectrally similar, mixed stands may prove a challenge. The collection of *in-situ* spectral library data must account for spatial and temporal variations in the spectral properties of macroalgal species and how this may, or may not, influence the ability to spectrally distinguish between them.

6.6. Concluding remarks

The potential applications of drone-based remote sensing technology for intertidal macroalgal mapping are broad and diverse and it is difficult to provide clear technological recommendations for all potential research scenarios. However, regardless of what is to be mapped, the decision-making process regarding the choice of hardware, software and methodologies remains the same. Mapping intertidal macroalgal communities provides a set of unique challenges not found in other environments. The advice provided herein aims to ensure that a prospective researcher has sufficient tools and knowledge required to make informed decisions when planning drone surveys. This is not meant to be a one stop shop encyclopaedia of knowledge on drone technology and, with the pace of development and applications of drone-based technology, the prospective researcher should use the information here as a broad introduction to further relevant and insightful research.

Chapter 7: Conclusions

Somewhere beyond the sea…

7.1. Overview

This thesis sought to develop an integrated resource assessment methodology, utilising remote sensing technologies, to address the significant current biological knowledge data gap for key Irish macroalgal species. In doing so, the current research aimed to develop a methodology that was standardised, repeatable, reliable and cost-effective. The mapping capabilities of both optical and acoustic remote sensing technologies along with the ancillary validation work that accompanies them were investigated. The growing interest in the commercial and ecological value of many macroalgal species, both in Ireland (Anon, 2019) and globally (FAO, 2014) demands the development of accurate ecological data with which to support informed, sustainable decision-making practices. The two target organisms investigated, *Ascophyllum nodosum* and *Laminaria hyperborea*, represent species that, in Ireland, are of commercial interest and also of significant ecological importance, and for which little data exists. To support decision making, there is a need to develop survey methodologies that can cover large areas.

In-situ biological observations set the 'gold standard' for the collection of detailed biological information and their importance cannot be overstated. However, as a methodology to conduct large-scale habitat mapping surveys for the quantification of species distribution, they are incredibly time-consuming and limited in the spatial extent that can be covered (Kerr & Ostrovsky, 2003). The use of remote sensing technology allows much larger areas to be covered, yet, key challenges remain in linking biological processes to observable and identifiable features in both the optical and acoustic datasets. This study represents a comprehensive investigation into the remote sensing of both intertidal and subtidal macroalgal distributions. This thesis has been able to draw conclusions of the suitability of different remote sensing methodologies for the assessment of different macroalgal communities and these can now be used to inform future research, within Ireland, on the scaling up of remote sensing surveys to support the development of regional and national resource management plans.

7.2. Spectral properties of intertidal macroalgal species

Previous studies investigating the spectral properties of macroalgae have identified strong spectral separability between macroalgal groups (Bajjouk *et al*., 1996), yet there appeared to be little evidence for spectral separability within these groups (Kutser *et al*., 2006; Casal *et al*., 2013). Developing a mapping approach that targets a single species (*i.e. A. nodosum*) required an understanding of its spectral properties and spectral separability from other common intertidal canopy-forming species. Determining spectral separability between

spectrally similar species (*e.g.* brown macroalgae) was, thus, a priority for this research. Alongside this, temporal changes in pigment concentrations (Schmid *et al*., 2017) likely cause variations in spectral response and this research aimed to understand how inter and intra-specific spectral relationships varied across four seasons intra-annually. Visually, *A. nodosum* often has a distinct colour gradient from the tips (lighter) to the base (darker) owing to different light regimes (Stengel & Dring, 1998) and the relationship between the two was also something we sought to understand.

To address the above research questions, a TriOS RAMSES Hyperspectral Radiance and Irradiance sensor, measuring over a 320-950 nm WL range, was deployed across four seasons in 2018, at a single site near Carraroe (Co. Galway). The results showed that, as expected, there was clear separation between the macroalgal groups, across the four sampling seasons, which provided confidence that the applied methodology, initially developed by Kotta *et al*. (2014), would also yield accurate results for species-level spectral separation. It could be demonstrated that it was possible to accurately separate between spectrally similar brown macroalgal species, including the light and dark variants of *A. nodosum*, across all seasons, apart from winter. The addition of seasonal variability into the ability to accurately separate between species strongly suggests that future surveys should incorporate this variation into their methodology development. However, having only sampled a single site, there was a lack of spatial variation required to draw a comprehensive conclusion on whether similar variations in spectral relationships were observed over different spatial scales, rather than being specific to the chosen study site. Further to this, it was demonstrated that the removal of macroalgae for spectral sampling (*i.e.* not *in-situ*) sampling did not cause any significant variation in the spectral response, agreeing with Kotta *et al*. (2014) who observed that canopy geometry and thallus orientation are not coupled with reflectance spectra.

The methodology used has shown that, apart from winter, the light and dark variants of *A. nodosum* were spectrally separable from all other species and one-another and will undoubtedly facilitate the development of a larger-scale resource assessment methodology for this economically and ecologically important macroalgae. Results also highlight the need for spectral library sampling to be concurrent with drone surveys and that a single spectral library from a single season should not be relied on for different seasons.

7.3. Drone-mounted hyperspectral mapping of intertidal macroalgae

Until recently, few studies have used drones to monitor intertidal macroalgal communities (Murfitt *et al*., 2017., Kellaris *et al*., 2019; Taddia *et al*., 2019; Tait *et al*., 2019) and, to our knowledge, this research remains the first and only study to combine drones and

hyperspectral sensors for intertidal macroalgal habitat mapping. The high spatial and spectral resolutions obtainable from the fusion of these two technologies were necessary for accurate mapping and species identification in the spatially and spectrally complex intertidal zone. The recent and rapid development in drone technology (Colefax *et al*., 2017) has made them a viable alternative to aircraft and satellites for habitat surveys. Continued improvements in battery life, payload capacity, along with efforts to develop BVLOS operations, could soon see drones being used to collect data over much larger areas than currently possible. To this end, the capabilities of higher resolution drone imagery were investigated to see if they could facilitate the accurate identification and mapping of *A. nodosum*, in turn, supporting the future scaling up of these surveys.

Whilst the core aim of **Chapter 3** remained the accurate remote identification and mapping of *A. nodosum,* an objective was to determine which other species could be identified as, based on the results of **Chapter 2**, most of the common intertidal brown seaweed species would be spectrally distinguishable from each other. The collection of training and validation data often appeared overlooked in the literature, with regards to using it to support larger-scale surveys. If the efficiency of these methods is not scaled up in parallel to the drone survey, then mapping larger areas would still remain a costly and time-consuming process. The collection of two different types of training and validation datasets address this concern. Spectral libraries are an established source of training data (Casal *et al*., 2013; Dierssen *et al*., 2015) and can be relatively straightforward to develop. The work was aided by the high spatial resolution of the drone mounted RGB sensor, which allowed individual species to be identified and were able to collect training data rapidly and accurately (Lechner *et al*., 2012). Of the two classifiers used, MLC was the more accurate of the two (MLC: OA 94.7 %, SAM: OA 76.3 %) which was likely due to the noise present in the hyperspectral data meaning that the spectral library training data could not be directly compared with. Crucially, both classifiers were able to identify *A. nodosum,* with MLC producing the highest classification accuracies (UA = 96 %, PA = 94 %) and SAM achieving reasonable levels of accuracy (UA = 98 %, PA = 73.9%). The accurate delineation of a homogenous *A. nodosum* bed can then be used for the accurate prediction of biomass once a relationship between biomass and a quantifiable metric, observable using remote sensing, can be established. This was something that was not tested in this study and should be investigated in future work.

This research demonstrated that it was possible to accurately identify, using remote sensing, different macroalgal species occurring in spatially and spectrally complex environments. The visual identification of species from high-resolution RGB imagery could facilitate the scaling up of drone surveys as it offers an efficient way in which to collect data. However,

caution must be exercised as the visual interpretation of imagery can be subjective (Olofsson *et al*., 2014), requiring trained observers. Further validation of the accuracy of this method is required for other locations or times of year where the macroalgae may appear different. It was almost impossible to visually distinguish between *F. spiralis*, *F. vesiculosus* and *F. serratus* as they all appeared to have similar colouration and morphology when viewed in the imagery. There were clear limitations within the current study, particularly the technical challenges posed by mounting a pushbroom hyperspectral sensor on a drone which were most apparent in the data strip gaps and image noise levels. Without significant dampening, the vibrations from the drone increased the noise levels in the hyperspectral imagery, reducing the quality of the data output. Thus, future research should consider using full-frame hyperspectral imagers instead (such as the Senop HSC-2) which are less susceptible to noise and are easier to process as standard photogrammetry methods can be applied (Honkavaara *et al*., 2016).

7.4. Multispectral mapping of intertidal macroalgae

The cost of hyperspectral sensors is likely a prohibitive for many organisations and is likely to not be utilised as a widespread mapping solution. **Chapter 4** sought to investigate whether multispectral remote sensors, which are significantly cheaper, can be as effective at mapping *A. nodosum* as hyperspectral sensors. Multispectral sensors, having a coarser spectral resolution, were unlikely to achieve accurate classification results in sites with a high diversity of spectrally similar species. Instead, a site with a lower macroalgal species diversity where *A. nodosum* was also present was surveyed. Three different multispectral remote sensing platforms (drone, plane and satellite) were compared to see which could most accurately map the distribution of *A. nodosum* as each of these three mapping platforms provides different benefits and disadvantages depending on the feature of interest to be mapped. The drone and plane data were collected during summer over separate years (plane = 2016, drone = 2017) and a cloud-free Sentinel-2 satellite image was taken from summer 2018.

Visual analysis confirmed that Sentinel-2 imagery, with a GSD of 10 m/pixel, was too coarse to allow for the identification of macroalgal species. Its relatively coarse spatial resolution would be better applied to the mapping of homogenous macroalgal and macrophyte species (Cavanaugh *et al*., 2010; Casal *et al*., 2011). Training and reference data were again collected through visual analysis of high-resolution drone and aerial RGB imagery. There was broad agreement in the classification results for the drone and aerial multispectral datasets, but the drone imagery was able to identify mono-specific *A. nodosum* stands whereas the aerial imagery could only identify a mixed *A. nodosum* and *Fucus* spp.,

class. Drone imagery was more accurate (PA = 91 %, UA = 96.9 %) than aerial imagery (PA = 93 %, UA = 77.9 %).

Multispectral sensors proved an accurate mapping tool in relatively low species diversity site and these results encapsulated the trade-off between the high spatial resolution but limited spatial coverage of drones and the high spatial coverage but low resolution of aircraft. At present, it would be difficult to recommend one survey platform over the other as each has a quality necessary for the scaling up of macroalgal remote sensing surveys. However, in terms of cost and operational flexibility drones are a more attractive solution for intertidal mapping as they can respond quickly to short-term events (Jensen *et al*., 2011). The battery life of many fixed-wing and VTOL drones is increasing (**Fig. 5.1**) to the point where they can survey ~ 1 h each side of maximum low tide, making them more competitive with the area that can be covered by aircraft. Achieving the high spatial resolutions required for accurate discrimination of macroalgal species will still require low survey flight heights, potentially restricting the area that can be covered during a single tide cycle. Ultimately, the specific research objectives, particularly desired taxonomic resolution, will determine the choice of remote sensing platform.

7.5. Acoustic remote sensing of subtidal kelp species

Whilst the focus of this thesis was on the intertidal application of remote sensing technology, **Chapter 6** was devoted to a pilot study looking at using MBES for mapping kelp species. Kelps, a foundation species (Miller *et al*., 2011), and thus vital ecological components of coastal ecosystems are increasingly being looked to for their commercial applications (Bennion *et al*., 2017). Under the broad remit of developing an integrated approach to seaweed resource assessment in Ireland, it was important to assess the suitability of MBES for the identification of subtidal kelp beds. Whilst optical remote sensing has been successfully used to map subtidal kelp, although not to species level (Casal *et al*., 2011; St-Pierre & Gagnon, 2020), it is often depth limited by the attenuation of light in the water column and this is exacerbated in turbid coastal waters (Brown & Blondel, 2009; Bajjouk *et al*., 2015). Because water is an effective medium for sound waves, there are no depth limitations to the use of acoustic sonar (Lurton, 2002).

Previous studies have successfully applied acoustic remote sensing to map seagrass (Komatsu *et al*., 2003) and kelp (McGonigle *et al*., 2011; Kruss *et al*., 2017) and this study aimed to compare the kelp identification abilities of three different MBES survey frequencies (200, 300, 400 kHz) in Roaringwater Bay (Co. Cork). Lower acoustic frequencies would be less attenuated in the water column than higher ones but would also record less information in the water column (Freitas *et al*., 2008). An objective was to define

an optimum frequency that would balance between too much noise recorded in the water column, thus obscuring kelp, and too little noise recorded, also obscuring kelp. A drop-down camera was used to collect validation data.

Results indicated that each of the three acoustic frequencies used were able to identify the kelp bed, each recording similar area and canopy height values. The difference between the three was the lower density of kelp recorded by the 300 and 400 kHz frequencies on the slopes of the reef compared to the continuous dense canopy recorded in the 200 kHz dataset. Whilst the drop-down camera (GoPro Hero 4+) confirmed the presence of a kelp bed, without conducting a more comprehensive ground truth survey it was not possible to determine whether the difference between frequencies was due to user error, owing to the subjective nature of kelp sounding extraction, or the different abilities of each frequency to identify kelp. Canopy heights recorded by each frequency demonstrated the majority of kelps to be ~1 m in height and there were only a few extreme values that likely represented the incorrect selection of soundings. Kelp distribution did align closely with the margins of the rocky reef (~14 m in depth) and no kelp signals were observed in deeper areas or in areas of unsuitable substratum, which was also validated using the drop-down camera.

Owing to the limited scope of this study it was difficult to conclude on the suitability of MBES for the mapping of subtidal kelp populations. Each acoustic frequency was able to identify the kelp bed correctly, but without further testing it was not possible to recommend a suitable mapping frequency. Further work should focus on mapping more areas, involving a 'blind' processing workflow where the processor has no knowledge of the distribution of kelp within the study area. This will remove some of the potential bias present here due to knowledge of the location of the kelp prior to the study which may have influenced processing and analysis workflows. The more comprehensive use of ground-truth data collection is recommended and previous studies have used video transects (Ierodiaconou *et al*., 2007) and SCUBA (Blight *et al*., 2011) to validate their datasets. The exciting possibility of using a new generation of mini-ROVs for data collection was tested at a separate site and provided a low-cost, safe and flexible solution with high enough resolution to easily identify different kelp species. This could serve as an alternative to existing validation methodologies (SCUBA, drop-down cameras etc.) for ground-truthing acoustic remote sensing data.

7.6. Recommendations on the use of drones for intertidal macroalgal mapping

From the results presented in **Chapters 3 & 4** it was difficult to draw broad conclusions regarding the application of drones for intertidal habitat mapping as each chapter occupied its own niche within the topic. As the application of drones for intertidal macroalgal habitat mapping is still in its infancy, it is important to identify the key challenges of using drones

for intertidal habitat mapping. **Chapter 5** aimed to make recommendations on the technology and methodologies that can be used to address these challenges in macroalgal mapping according to specific future research questions.

Three key characteristics of macroalgal species and assemblages influence survey design and operation, **1)** the size of individuals within a species, **2)** homogeneity of coverage and **3)** spectral similarity to surrounding species and substratum. **Chapter 5** draws on examples from other studies on macroalgae, seagrass communities and terrestrial environments (using different platforms) to highlight important survey planning considerations.

55 different drone models currently available to date, across 27 companies, were compared and whilst excluding those drones that are generally not suitable for survey-grade mapping, this list is not exhaustive. The variation in drone design, operational capabilities, flight time and payload capacity is astonishing, from drones that are able to land on water (SplashDrone 3+), to heavy-lift VTOL-capable fixed-wings (Quantum series), drones are being developed to fill a multitude of operational roles. Advancements in sensor technology were also impressive. The application of drones for precision agriculture (Barrero *et al*., 2018) has led to a wide range of lightweight multispectral sensors, designed with band-sets for vegetation health monitoring (Candiago *et al*., 2015). Twenty-four lightweight multispectral sensor models were identified in this study. Many of these sensors are easily integrated with drones and processing software packages (*i.e.* Pix4D), offering a turnkey mapping solution. A similar number (22) of hyperspectral sensors were also identified, many of which operated as pushbroom devices but there are recently released models now operating as full-frame sensors (*e.g.* Senop HSC-2 & Cubert ULTRIS 20) which tend to offer a simpler, more user-friendly, mapping solution to traditional, pushbroom sensors.

There was a general trend towards greater integration between drones, sensors and software, creating a more accessible and affordable mapping solution, leading to their increased use for macroalgal mapping studies which will only continue as more turnkey mapping solutions are developed. It is hoped that this review will be well placed to support the growth of drone applications for macroalgal habitat monitoring.

7.7. Concluding remarks

This thesis has demonstrated that remote sensing technologies are capable of mapping the key macroalgal species occurring in Ireland that are of economic and ecological importance. Being able to spectrally distinguish between canopy-forming intertidal macroalgal species has shown the suitability of optical remote sensing for use in the targeted assessment of individual species, rather than the broad scale mapping approaches previously used.

Previous research had indicated that it was potentially not possible to spectrally distinguish between different species within the three macroalgal groups (Kutser *et al*., 2006b; Casal *et al*., 2013), whilst other studies, specifically focused on the spectral separability of macroalgal species (Kotta *et al*., 2014; Chao Rodríguez *et al*., 2017), chose only to explore separability between groups. The accurate mapping of subtidal kelp species will require further research, yet this research has demonstrated the potential of acoustic remote sensing technology and builds upon a fairly strong Irish research interest in acoustic mapping of kelp (Blight *et al*., 2011; McGonigle *et al*., 2011; MacCraith & Hardy, 2015). Ireland is also home to world leading experts in acoustic remote sensing (INFOMAR) who have the knowledge and equipment to potentially support the development of acoustic remote sensing of kelp in Ireland.

The results of this work will support the development of large-scale macroalgal monitoring assessments both in Ireland and the rest of the world. The rapid advancement of remote sensing technology will, over time, make some of the technology used here redundant and some of this emerging technology has been highlighted in this thesis (e.g. full-frame hyperspectral sensors). With decreasing costs and an increase in turnkey remote sensing solutions it is likely that the use of optical remote sensing systems (*i.e.* drones) will increase rapidly amongst users as cost will no longer be a barrier. The increase in choice for both sensors and drones will require users to think carefully about what combination of technology is needed to accurately map their study species or habitat. Selecting the appropriate spectral and spatial resolution will, in some circumstances, be equally weighted against equipment cost and accessibility (Ventura *et al*., 2018). Yet, the scaling up of drone surveys will require the development and granting of special flight permissions which will, in turn, require significant investment in training and methodology development to ensure safe operation. Under current Irish drone regulations, specific operating permissions can be granted for those individuals and companies who wish to operate outside current operational limits and who have received appropriate training. Soon, standardised EU drone regulations will come into force, creating a clear set of drone operations classes, allowing for recreational and professional flights, whilst also meaning that drone users can operate seamlessly throughout Europe (https://www.easa.europa.eu/easa-and-you/civil-drones-rpas/drones-regulatory-framework-background). While regulation and technology (e.g. battery life) will strongly influence the scale of macroalgal resource assessment, future national licensing and regulatory frameworks may also be important factors. Surveys could potentially take place in areas with pending foreshore licensing applications to develop a baseline assessment of available macroalgal resources with which to support their sustainable management.

This research has also shown that different optical remote sensing technologies (*e.g.* hyperspectral and multispectral) can be successfully applied for intertidal habitat mapping, further supporting their utilisation by potential users with different budgets. It is imperative to stress that further validation of the optical remote sensing technologies used in this thesis is required owing to the limited spatial area covered. Spatial variation (regional scale) in intertidal macroalgal assemblages and variation in the concentration and composition of pigments within species (Schmid *et al*., 2017), may necessitate regional or localised modifications to the survey method. Such modifications could include the addition or exclusion of particular macroalgae classes or the collections of new *in-situ* spectral reflectance profiles. The social implications of flying large-scale drone surveys (Sandbrook, 2015) were not explored in this research and these will need to be included in the planning of future work, especially when considering the social sensitives surrounding the management and conservation of seaweed resources in Ireland (Mac Monagail & Morrison, 2020).

Acoustic remote sensing of kelp faces significantly more challenges than optical remote sensing methodologies. The relatively shallow depths at which Irish kelp forests occur limits the efficiency of MBES systems and logging water column data produces vast quantities of data. Research from France (Bajjouk *et al*., 2015) and the UK (Bennion *et al*., 2017) highlight the power of predictive modelling, using MBES-derived environmental layers (*i.e.* slope, roughness etc.) for identifying kelp forest distribution. Whilst the accuracy of this invariably depends on existing high-resolution nearshore bathymetric and backscatter datasets, MBES and SCUBA surveys could then be used in a ground-truthing capacity, addressing some of the logistical issues surrounding larger-scale operations, similar to what was done by Bajjouk *et al*. (2015).

The use of SCUBA, whilst providing the detailed biological information required to properly characterise Irish kelp forests, is expensive, spatially limited and logistically complicated (especially in remote regions). Recent Health and Safety Authority (HSA) guidelines (https://www.hsa.ie/eng/your_industry/diving/diving_at_work/diving_training/) also mandate additional training and operational requirements, needing further investment in safe SCUBA practices. Exciting advances in mini-ROV technology will improve the collection of accurate reference data for subtidal surveys, offering not a replacement, but an accompaniment to SCUBA, and the potential applications of these devices for species identification were demonstrated in this thesis. Expanding on the acoustic research conducted in this study will help to identify optimum survey frequencies and inform on the use of acoustic sonar in supporting the sustainable management of kelp forests.

Ultimately, the collection of accurate baseline species distribution data will support informed sustainable management decision making. This thesis sought to develop a methodology with which to achieve this and we believe, that whilst future research is still required, that we have achieved this objective. Judgement is not passed on how future methodologies will be applied, nor by whom, yet it is hoped that the goal of advancing human betterment whilst protecting coastal ecosystems will be central to future work. The 'Age of Drones', both above and below the waves, may well be nigh, and we look forward to seeing the growth of responsible drone use in promoting the sustainable management of global macroalgal resources.

References

* References cited in the appendix only

Aasen, H., Bendig, J., Bolten, A., Bennertz, S., Willkomm, M., & Bareth, G. (2014). Introduction and preliminary results of a calibration for full-frame hyperspectral cameras to monitor agricultural crops with UAVs. *International Archives of the Photogrammetry, Remote Sensing and Spatial Information Sciences - ISPRS Archives*, *40*(7), 1–8. https://doi.org/10.5194/isprsarchives-XL-7-1-2014

Aasen, Helge, Honkavaara, E., Lucieer, A., & Zarco-Tejada, P. J. (2018). Quantitative remote sensing at ultra-high resolution with UAV spectroscopy: A review of sensor technology, measurement procedures, and data correctionworkflows. *Remote Sensing*, *10*(7), 1–42. https://doi.org/10.3390/rs10071091

Abbott, I. A. (1978). The uses of seaweed as food in Hawaii. *Economic Botany*, 32(4), 409–412. https://doi.org/10.1007/BF02907938

Abdullah, M. I., Fredriksen, S., & Christie, H. (2017). The impact of the kelp (*Laminaria hyperborea*) forest on the organic matter content in sediment of the west coast of Norway. *Marine Biology Research*, *13*(2), 151–160. https://doi.org/10.1080/17451000.2016.1240369

Åberg, P. (1992). A demographic study of two populations of the seaweed *Ascophyllum nodosum*. *Ecology*, *73*(4), 1473–1487. https://doi.org/10.2307/1940691

Åberg, P. (1996). Patterns of reproductive effort in the brown alga *Ascophyllum nodosum*. *Marine Ecology Progress Series*, *138*(1–3), 199–207. https://doi.org/10.3354/meps138199

Abukawa, K., Yamamuro, M., Kikvidze, Z., Asada, A., Xu, C., & Sugimoto, K. (2013). Assessing the biomass and distribution of submerged aquatic vegetation using multibeam echo sounding in Lake Towada, Japan. *Limnology*, *14*(1), 39–42. https://doi.org/10.1007/s10201-012-0383-7

Adam, E., Mutanga, O., & Rugege, D. (2010). Multispectral and hyperspectral remote sensing for identification and mapping of wetland vegetation: A review. *Wetlands Ecology and Management*, *18*(3), 281–296. https://doi.org/10.1007/s11273-009-9169-z

Adão, T., Hruška, J., Pádua, L., Bessa, J., Peres, E., Morais, R., & Sousa, J. J. (2017). Hyperspectral imaging: A review on UAV-based sensors, data processing and applications for agriculture and forestry. *Remote Sensing*, *9*(11). https://doi.org/10.3390/rs9111110

Alamgir, M., & Al-Amin, M. (2008). Allometric models to estimate biomass organic carbon stock in forest vegetation. *Journal of Forestry Research*, *19*(2), 101–106. https://doi.org/10.1007/s11676-008-0017-4

Allen, J., Gosden, C., Jones, R., & White, P. (1988). Pleistocene dates for the human occupation of New Ireland, northern Melanesia. *Nature*, 331, 450.

Allouche, O., Tsoar, A., & Kadmon, R. (2006). Assessing the accuracy of species distribution models: Prevalence, kappa and the true skill statistic (TSS). *Journal of Applied Ecology*, *43*(6), 1223–1232. https://doi.org/10.1111/j.1365-2664.2006.01214.x

Amad, P. (2012). From God's-eye to camera-eye: aerial photography's post-humanist and neo-humanist visions of the world. *History of Photography*, *36*(1), 66–86. https://doi.org/10.1080/03087298.2012.632567

Anderson, K., Milton, E. J., & Rollin, E. M. (2006). Calibration of dual-beam spectroradiometric data. *International Journal of Remote Sensing*, *27*(5), 975–986. https://doi.org/10.1080/01431160500213375

Anderson, K., & Gaston, K. J. (2013). Lightweight unmanned aerial vehicles will revolutionize spatial ecology. *Frontiers in Ecology and the Environment*, *11*(3), 138–146. https://doi.org/10.1890/120150

Andrefouet, S., Zubia, M., & Payri, C. (2004). Mapping and biomass estimation of the invasive brown algae *Turbinaria ornata* (Turner) J. Agardh and *Sargassum mangarevense* (Grunow) Setchell on heterogeneous Tahitian coral reefs using 4-meter resolution IKONOS satellite data. *Coral Reefs*, 23(1), 26–38. https://doi.org/10.1007/s00338-003-0367-5

Anon. (2015a). Joint committee on environment, culture and the Gaeltacht report of the committee on developing the seaweed industry in Ireland. https://www.oireachtas.ie/en/press-centre/press-releases/20150529-environment-committee-report-calls-for-national-strategy-for-the-seaweed-harvesting-sector/ (Accessed: 31/10/19)

Anon. (2015b). Report supporting appropriate assessment of aquaculture and risk assessment of fisheries in Kilkieran Bay and Islands SAC (Site code: 2111). *Marine Institute*. Retrieved from: https://www.agriculture.gov.ie/media/migration/seafood/aquacultureforeshoremanagement/aquaculturelicensing/appropriateassessments/KilkieranBayIslAppAss040316.pdf (Accessed: 23/1/20)

Anon. (2018). Relief of distress on the west coast of Ireland. https://archive.org/details/op1250955-1001 (Accessed: 31/10/19)

Anon. (2019). Harnessing our ocean wealth. An integrated marine plan for Ireland. Review of progress 2018. *Our Ocean Wealth*. Retrieved from: https://www.ouroceanwealth.ie/sites/default/files/Publications/harnessing_our_ocean_wealth_-_review_of_progress_2018-web.pdf (Accessed: 23/01/2020)

Arroyo-Mora, J., Kalacska, M., Inamdar, D., Soffer, R., Lucanus, O., Gorman, J., Naprstek, T., Schaaf, E., Ifimov, G., Elmer, K., Leblanc, G. (2019). Implementation of a UAV–hyperspectral pushbroom imager for ecological monitoring. *Drones*, *3*(1), 12. https://doi.org/10.3390/drones3010012

Askari, M. S., McCarthy, T., Magee, A., & Murphy, D. J. (2019). Evaluation of grass quality under different soil management scenarios using remote sensing techniques. *Remote Sensing*, *11*(15), 1-23. https://doi.org/10.3390/rs11151835

Assmann, J. J., Kerby, J. T., Cunliffe, A. M., & Myers-Smith, I. H. (2019). Vegetation monitoring using multispectral sensors — best practices and lessons learned from high latitudes. *Journal of Unmanned Vehicle Systems*, *7*(1), 54–75. https://doi.org/10.1139/juvs-2018-0018

Baena, S., Boyd, D. S., & Moat, J. (2018). UAVs in pursuit of plant conservation - real world experiences. *Ecological Informatics*, *47*, 2–9. https://doi.org/10.1016/j.ecoinf.2017.11.001

Baer, J., & Stengel, D. B. (2010). Variability in growth, development and reproduction of the non-native seaweed *Sargassum muticum* (Phaeophyceae) on the Irish west coast. *Estuarine, Coastal and Shelf Science*, *90*(4), 185–194. https://doi.org/10.1016/j.ecss.2010.08.011

Bajjouk, T., Guillaumont, B., & Populus, J. (1996). Application of airborne imaging spectrometry system data to intertidal seaweed classification and mapping. *Hydrobiologia*, *326–327*(1), 463–471. https://doi.org/10.1007/BF00047847

Bajjouk, T., Rochette, S., Laurans, M., Ehrhold, A., Hamdi, A., & Le Niliot, P. (2015). Multi-approach mapping to help spatial planning and management of the kelp species *L. digitata and L. hyperborea*: Case study of the Molène Archipelago, Brittany. *Journal of Sea Research*, *100*, 2–21. https://doi.org/10.1016/j.seares.2015.04.004

Baker, N. (2019) Court dismisses appeal over kelp harvesting in Bantry Bay. Retrieved from: https://www.irishexaminer.com/breakingnews/ireland/court-dismisses-appeal-over-kelp-harvesting-in-bantry-bay-930088.html (Accessed: 04/05/2020)

Ballantine, W. (1961). A biologically-defined exposure scale for the comparative description of rocky shores. *Field Studies*, *1*, 1–19.

Balasse, M., Mainland, I., & Richards, M. P. (2009). Stable isotope evidence for seasonal consumption of marine seaweed by modern and archaeological sheep in the Orkney archipelago (Scotland). *Environmental Archaeology*, 14(1), 1–14. https://doi.org/10.1179/174963109X400637

Bareth, G., Aasen, H., Michels, R., Soukkamäki, J., Bendig, J., Gnyp, M. L., Bolten, A., Jung, A., Michels, R., Soukkamaki, J. (2015). Low-weight and UAV-based hyperspectral full-frame cameras for monitoring crops: spectral comparison with portable spectroradiometer measurements. *Photogrammetrie - Fernerkundung - Geoinformation*, *2015*(1), 69–79. https://doi.org/10.1127/pfg/2015/0256

Barillé, L., Robin, M., Harin, N., Bargain, A., & Launeau, P. (2010). Increase in seagrass distribution at Bourgneuf Bay (France) detected by spatial remote sensing. *Aquatic Botany*, *92*(3), 185–194. https://doi.org/10.1016/j.aquabot.2009.11.006

Barrero, O., & Perdomo, S. A. (2018). RGB and multispectral UAV image fusion for *Gramineae* weed detection in rice fields. *Precision Agriculture*, *19*(5), 809–822. https://doi.org/10.1007/s11119-017-9558-x

Barreto, M., Johansen, K., Angel, Y., & McCabe, M. (2019). Radiometric Assessment of a UAV-based push-broom hyperspectral camera. *Sensors*, *19*(21), 4699. https://doi.org/10.3390/s19214699

Bartholomé, E., & Belward, A. S. (2005). GLC2000: A new approach to global land cover mapping from earth observation data. *International Journal of Remote Sensing*, *26*(9), 1959–1977. https://doi.org/10.1080/01431160412331291297

Behmann, J., Acebron, K., Emin, D., Bennertz, S., Matsubara, S., Thomas, S., Bohnenkamp, D., Kuska, M., Jussila, J., Salo, H., Mahlein, A., Rascher, U. (2018). Specim IQ: Evaluation of a new, miniaturized handheld hyperspectral camera and its application for plant phenotyping and disease detection. *Sensors* (Switzerland), 18(2). https://doi.org/10.3390/s18020441

Bekkby, T., Smit, C., Gundersen, H., Rinde, E., Steen, H., Tveiten, L., Gitmark, J., Fredriksen, S., Albretsen. J., & Christie, H. (2019). The abundance of kelp is modified

by the combined impact of depth, waves and currents. *Frontiers in Marine Science*, *6*(JUL), 1–10. https://doi.org/10.3389/fmars.2019.00475

Bell, T. W., Cavanaugh, K. C., & Siegel, D. A. (2015). Remote monitoring of giant kelp biomass and physiological condition: an evaluation of the potential for the Hyperspectral Infrared Imager (HyspIRI) mission. *Remote Sensing of Environment*, *16*, 218–228. https://doi.org/10.1016/j.rse.2015.05.003

Bell, T. W., Allen, J. G., Cavanaugh, K. C., & Siegel, D. A. (2020). Three decades of variability in California's giant kelp forests from the Landsat satellites. *Remote Sensing of Environment*, *238*(March 2018), 110811. https://doi.org/10.1016/j.rse.2018.06.039

Belluco, E., Camuffo, M., Ferrari, S., Modenese, L., Silvestri, S., Marani, A., & Marani, M. (2006). Mapping salt-marsh vegetation by multispectral and hyperspectral remote sensing. *Remote Sensing of Environment*, *105*(1), 54–67. https://doi.org/10.1016/j.rse.2006.06.006

Bennion, M., Yesson, C., Brodie, J. (2017) Remote sensing of kelp: novel methods for mapping and monitoring wild kelp resources. *Report for The Crown Estate*. London, United Kingdom

Bentoutou, Y., Taleb, N., Kpalma, K., & Ronsin, J. (2005). An automatic image registration for applications in remote sensing. *IEEE Transactions on Geoscience and Remote Sensing*, *43*(9), 2127–2137. https://doi.org/10.1109/TGRS.2005.853187

Bird, J. B., & Morrison, A. (1964). American Geographical Society Awards. *Geographical Review*, *54*(4), 436–486. Retrieved from https://www.jstor.org/stable/212977

Blaschke, T. (2010). Object based image analysis for remote sensing. *ISPRS Journal of Photogrammetry and Remote Sensing*, *65*(1), 2–16. https://doi.org/10.1016/j.isprsjprs.2009.06.004

Blight, A, Foster-Smith, R., Sotheran, I., Egerton, J., McAllen, R., & Savidge, G. (2011). Development of a methodology for the quantitative assessment of Ireland's inshore kelp resource. *Marine Institute Ireland*.

Briggs, L. (1935). The stratosphere balloon flight. *The Scientific Monthly*, 40(6), 578–580. Retrieved from https://www.jstor.org/stable/15879%0D (Accessed: 23/01/2020)

Brodie, J., Ash, L. V., Tittley, I., & Yesson, C. (2018). A comparison of multispectral aerial and satellite imagery for mapping intertidal seaweed communities. *Aquatic Conservation: Marine and Freshwater Ecosystems*, 1-10. https://doi.org/10.1002/aqc.2905

Brodie, J., Williamson, C. J., Smale, D. A., Kamenos, N. A., Mieszkowska, N., Santos, R., Cunliffe, M., Steinke, M., Yesson, C., Anderson, K., Asnaghi, V., Brownlee, C., Burdett, H., Burrows, M., Collins, S., Donohue, P., Harvey, B., Foggo, A., Noisette, F., Nunes, J., Ragazzola, F., Raven, J., Schmidt, D., Suggett, D., Teichberg, M., Hall-Spencer, J. M. (2014). The future of the northeast Atlantic benthic flora in a high CO_2 world. *Ecology and Evolution*, *4*(13), 2787–2798. https://doi.org/10.1002/ece3.1105

Brown, C. J., & Blondel, P. (2009). Developments in the application of multibeam sonar backscatter for seafloor habitat mapping. *Applied Acoustics*, *70*(10), 1242–1247. https://doi.org/10.1016/j.apacoust.2008.08.004

Brown, C. J., & Collier, J. S. (2008). Mapping benthic habitat in regions of gradational

substrata: An automated approach utilising geophysical, geological, and biological relationships. *Estuarine, Coastal and Shelf Science*, *78*(1), 203–214. https://doi.org/10.1016/j.ecss.2007.11.026

Brown, C., Beaudoin, J., Brissette, M., & Gazzola, V. (2019). Multispectral Multibeam Echo Sounder backscatter as a tool for improved seafloor characterization. *Geosciences*, *9*(3), 126. https://doi.org/10.3390/geosciences9030126

Bruno, J. F., & Bertness, M. D. (2000). Habitat modification and facilitation in benthic marine communities. *Marine Community Ecology*. Retrieved from http://johnfbruno.web.unc.edu/files/2011/11/Bruno-Bertness-2001.pdf (Accessed: 31/10/2019)

Bunker, F., Brodie, J., Maggs, C., Bunker, A. (2017) *Seaweeds of Britain and Ireland*. Plymouth: Wild Nature Press

Burns, P. D., Berns, R. S., & York, N. (1996). Analysis multispectral image capture. *The fourth color imaging conference: Color Science, Systems and Applications*, (November), 19–22. Retrieved from https://www.researchgate.net/publication/239666107_Analysis_Multispectral_Image_Capture

Burrows, M. T., Macleod, M., & Orr, K. (2010). Mapping the intertidal seaweed resources of the Outer Hebrides. *Scottish Association for Marine Science Internal Report No. 269.* October 2010, (269), 1–45.

Bushing, W. (2000). Monitoring the Persistence of Giant Kelp around Santa Catalina Island using a Geographic Information System. *Journal of Phycology*, 36(3), 448–460. https://doi.org/10.1046/j.1529-8817.1999.00001-27.x

Butera, K. (1978). A determination of the optimum time of year for remotely classifying marsh vegetation from Landsat multispectral scanner data. *NASA*. 1-24. https://doi.org/10.1017/CBO9781107415324.004

Buters, T. M., Bateman, P. W., Robinson, T., Belton, D., Dixon, K. W., & Cross, A. T. (2019). Methodological ambiguity and inconsistency constrain unmanned aerial vehicles as a silver bullet for monitoring ecological restoration. *Remote Sensing*, *11*(10), 1–16. https://doi.org/10.3390/rs11101180

Butler D. Many eyes on Earth. *Nature*. 2014;505(7482),143-144. https://doi.org/10.1038/505143a

Cahalane, C., Walsh, D., Magee, A., Mannion, S., Lewis, P., & McCarthy, T. (2017). Sensor pods: multi-resolution surveys from a light aircraft. *Inventions*, 2(1), 2. https://doi.org/10.3390/inventions2010002

Campbell, J. (2002) *Introduction to remote sensing third edition*. New York: The Guildford Press

Candiago, S., Remondino, F., De Giglio, M., Dubbini, M., & Gattelli, M. (2015). Evaluating multispectral images and vegetation indices for precision farming applications from UAV images. *Remote Sensing*, *7*(4), 4026–4047. https://doi.org/10.3390/rs70404026

Carrasco-Escobar, G., Manrique, E., Ruiz-Cabrejos, J., Saavedra, M., Alava, F., Bickersmith, S., Prussing, C., Vinetz, M., Conn, J., Moreno, M., Gamboa, D. (2019). High-accuracy detection of malaria vector larval habitats using drone-based

multispectral imagery. *PLOS Neglected Tropical Diseases*, *13*(1), e0007105. https://doi.org/10.1371/journal.pntd.0007105

Casal, G., Kutser, T., Domínguez-Gómez, J. A., Sánchez-Carnero, N., & Freire, J. (2013). Assessment of the hyperspectral sensor CASI-2 for macroalgal discrimination on the Ría de Vigo coast (NW Spain) using field spectroscopy and modelled spectral libraries. *Continental Shelf Research*, *55*, 129–140. https://doi.org/10.1016/j.csr.2013.01.010

Casal, G., Sánchez-Carnero, N., Domínguez-Gómez, J. A., Kutser, T., & Freire, J. (2012). Assessment of AHS (Airborne Hyperspectral Scanner) sensor to map macroalgal communities on the Ría de vigo and Ría de Aldán coast (NW Spain). *Marine Biology*, *159*(9), 1997–2013. https://doi.org/10.1007/s00227-012-1987-5

Casal, G., Sánchez-Carnero, N., Sánchez-Rodríguez, E., & Freire, J. (2011). Remote sensing with SPOT-4 for mapping kelp forests in turbid waters on the south European Atlantic shelf. Estuarine, *Coastal and Shelf Science*, *91*(3), 371–378. https://doi.org/10.1016/j.ecss.2010.10.024

Casella, E., Collin, A., Harris, D., Ferse, S., Bejarano, S., Parravicini, V., Hench, J., Rovere, A. (2017). Mapping coral reefs using consumer-grade drones and structure from motion photogrammetry techniques. *Coral Reefs*, *36*(1), 269–275. https://doi.org/10.1007/s00338-016-1522-0

Cavanaugh, K. C., Siegel, D. A., Kinlan, B. P., & Reed, D. C. (2010). Scaling giant kelp field measurements to regional scales using satellite observations. *Marine Ecology Progress Series*, *403*, 13–27. https://doi.org/10.3354/meps08467

Chabot, D., Dillon, C., Shemrock, A., Weissflog, N., & Sager, E. (2018). An object-based image analysis workflow for monitoring shallow-water aquatic vegetation in multispectral drone imagery. *ISPRS International Journal of Geo-Information*, *7*(8), 294. https://doi.org/10.3390/ijgi7080294

Chao Rodríguez, Y., Domínguez Gómez, J. A., Sánchez-Carnero, N., & Rodríguez-Pérez, D. (2017). A comparison of spectral macroalgae taxa separability methods using an extensive spectral library. *Algal Research*, *26*, 463–473. https://doi.org/10.1016/j.algal.2017.04.021

Chen, D., Twitty, C., Schanfeldt, B., Johnson, J., & Federico, J. (2016). United States Patent US10189567B2. United States of America. Retrieved from https://patents.google.com/patent/US10189567B2/en (Accessed: 31/10/19)

Choi, H. G., & Norton, T. A. (2005). Competition and facilitation between germlings of *Ascophyllum nodosum* and *Fucus vesiculosus*. *Marine Biology*, 147(2), 525–532. https://doi.org/10.1007/s00227-005-1593-x

Christiansen, F., Dujon, A. M., Sprogis, K. R., Arnould, J. P. Y., & Bejder, L. (2016). Noninvasive unmanned aerial vehicle provides estimates of the energetic cost of reproduction in humpback whales. *Ecosphere*, *7*(10), e01468. https://doi.org/10.1002/ecs2.1468

Christie, H., Jørgensen, N. M., Norderhaug, K. M., & Waage-Nielsen, E. (2003). Species distribution and habitat exploitation of fauna associated with kelp (*Laminaria hyperborea*) along the Norwegian Coast. *Journal of the Marine Biological Association of the United Kingdom*, *83*(4), 687–699. https://doi.org/10.1017/S0025315403007653h

Chust, G., Grande, M., Galparsoro, I., Uriarte, A., & Borja, Á. (2010). Capabilities of the bathymetric Hawk Eye LiDAR for coastal habitat mapping: a case study within a Basque estuary. *Estuarine, Coastal and Shelf Science, 89*(3), 200–213. https://doi.org/10.1016/j.ecss.2010.07.002

Clark, M. L., Roberts, D. A., & Clark, D. B. (2005). Hyperspectral discrimination of tropical rain forest tree species at leaf to crown scales. *Remote Sensing of Environment, 96*(3–4), 375–398. https://doi.org/10.1016/j.rse.2005.03.009

Clevers, J., & Gitelson, A. (2013). Remote estimation of crop and grass chlorophyll and nitrogen content using red-edge bands on sentinel-2 and -3. *International Journal of Applied Earth Observation and Geoinformation, 23*(1), 344–351. https://doi.org/10.1016/j.jag.2012.10.008

Coelho S.M., Rijstenbil J.W., & Brown M.T. (2000). Impacts of anthropogenic stresses on the early development stages of seaweeds. *Journal of Aquatic Ecosystem Stress and Recovery*, 7, 317–333.

Cohen, W. B., & Goward, S. N. (2004). Landsat's role in ecological applications of remote sensing. *BioScience*, 54(6), 535–545. https://doi.org/10.1641/0006-568(2004)054[0535:LRIEAO]2.0.CO;2

Colbo, K., Ross, T., Brown, C., & Weber, T. (2014). A review of oceanographic applications of water column data from multibeam echosounders. *Estuarine, Coastal and Shelf Science, 145*, 41–56. https://doi.org/10.1016/j.ecss.2014.04.002

Colefax, A. P., Butcher, P. A., & Kelaher, B. P. (2018). The potential for unmanned aerial vehicles (UAVs) to conduct marine fauna surveys in place of manned aircraft. *ICES Journal of Marine Science*, 75(1), 1–8. https://doi.org/10.1093/icesjms/fsx100

Colman, J. (1940). On the faunas inhabiting intertidal seaweeds. *Journal of the Marine Biological Association of the United Kingdom*, 24(1), 129–183. https://doi.org/10.1017/S0025315400054503

Colomina, I., & Molina, P. (2014). Unmanned aerial systems for photogrammetry and remote sensing: A review. *ISPRS Journal of Photogrammetry and Remote Sensing*. https://doi.org/10.1016/j.isprsjprs.2014.02.013

*Comaniciu, D., & Meer, P. (2002). Mean shift: a robust approach toward feature space analysis. *IEEE Transactions on Pattern Analysis and Machine Intelligence*, *24*(5), 603–619. https://doi.org/10.1109/34.1000236

Connell, S., Turner, D., Shepherd, S., Miller, D., Russell, B., Kildea, T., Miller, D., Airoldi, L., Cheshire, A. (2008). Recovering a lost baseline: missing kelp forests from a metropolitan coast. *Marine Ecology Progress Series, 360*, 63–72. https://doi.org/10.3354/meps07526

Connor, D., Allen, J., Golding, N., Howell. K., Lieberknecht, L., Northen, K., Reker, J. (2004) The marine habitat classification for Britain and Ireland version 04.05, *JNCC*. https://mhc.jncc.gov.uk/ (Accessed: 02/12/2019)

Costa, B. M., Battista, T. A., & Pittman, S. J. (2009). Comparative evaluation of airborne LiDAR and ship-based multibeam SoNAR bathymetry and intensity for mapping coral reef ecosystems. *Remote Sensing of Environment, 113*(5), 1082–1100. https://doi.org/10.1016/j.rse.2009.01.015

Costa, M., Loos, E. A., Shaw, A., Steckler, C., & Hill, P. (2007). Hyperspectral imagery for mapping intertidal vegetation at Roberts Bank tidal flats, British Columbia, Canada. *Canadian Journal of Remote Sensing*, *33*(1–4), 130–141. https://doi.org/10.5589/m07-017

Cote, D., Ollerhead, L. M. N., Scruton, D. A., McKinley, R. S. (2003). Microhabitat use of juvenile Atlantic cod in a coastal area of Newfoundland determined by 2D telemetry. *Marine Ecology Progress Series*, 265, 227–234. https://doi.org/10.3354/meps265227

Crain, C. M., Halpern, B. S., Beck, M. W., & Kappel, C. V. (2009). Understanding and managing human threats to the coastal marine environment. *Annals of the New York Academy of Sciences*, 1162, 39–62. https://doi.org/10.1111/j.1749-6632.2009.04496.x

Cruzan, M. B., Weinstein, B. G., Grasty, M. R., Kohrn, B. F., Hendrickson, E. C., Arredondo, T. M., & Thompson, P. G. (2016). Small Unmanned Aerial Vehicles (Micro-Uavs, Drones) in plant ecology. *Applications in Plant Sciences*, *4*(9). https://doi.org/10.3732/apps.1600041

Cunliffe, A. M., Brazier, R. E., & Anderson, K. (2016). Ultra-fine grain landscape-scale quantification of dryland vegetation structure with drone-acquired structure-from-motion photogrammetry. *Remote Sensing of Environment*, *183*, 129–143. https://doi.org/10.1016/j.rse.2016.05.019

Cushing, D. H. (1952). Echo-Surveys of Fish. *ICES Journal of Marine Science*, *18*(1), 45–60. https://doi.org/10.1093/icesjms/18.1.45

d'Oleire-Oltmanns, S., Marzolff, I., Peter, K., & Ries, J. (2012). Unmanned Aerial Vehicle (UAV) for monitoring soil erosion in Morocco. *Remote Sensing*, *4*(11), 3390–3416. https://doi.org/10.3390/rs4113390

Dash, J. P., Pearse, G. D., & Watt, M. S. (2018). UAV multispectral imagery can complement satellite data for monitoring forest health. *Remote Sensing*, *10*(8), 1–22. https://doi.org/10.3390/rs10081216

David, H. M. (1943). Studies in the autecology of *Ascophyllum nodosum* Le Jol. *The Journal of Ecology*, 31(2), 178. https://doi.org/10.2307/2256547

Davies, A. J., Johnson, M. P., & Maggs, C. A. (2007). Limpet grazing and loss of *Ascophyllum nodosum* canopies on decadal time scales. *Marine Ecology Progress Series*, *339*, 131–141. https://doi.org/10.3354/meps339131

Davison, I. R., & Pearson, G. A. (1996). Stress tolerance in intertidal seaweeds. *Journal of Phycology*, *32*(2), 197–211. https://doi.org/10.1111/j.0022-3646.1996.00197.x

Dawes, C. (1998) *Marine Botany*. New York: John Wiley & Sons Inc.

Dayton, P. (1985). Ecology of kelp communities. *Annual Review of Ecology and Systematics*, (63). Retrieved from http://www.jstor.org/stable/2097048 (Accessed: 31/10/2019)

de Castro, A., Torres-Sánchez, J., Peña, J., Jiménez-Brenes, F., Csillik, O., & López-Granados, F. (2018). An automatic Random Forest-OBIA algorithm for early weed mapping between and within crop rows using UAV imagery. *Remote Sensing*, *10*(3), 285. https://doi.org/10.3390/rs10020285

de Moustier, C. (1985). Beyond bathymetry: Mapping acoustic backscattering from the deep seafloor with Sea Beam. *The Journal of the Acoustical Society of America*, 79(2), 316–331. https://doi.org/10.1121/1.393570

de Oliveira, E., Populus, J., Guillaumont, B. (2006) Predictive modelling of coastal habitats using remote sensing data and fuzzy logic: a case for seaweed in Brittany (France). *EARSeL eProceedings, 5*(2), 208-223. Retrieved from: https://archimer.ifremer.fr/doc/00000/2279/ (Accessed: 22/01/2020)

Dekker, A. G., Byrne, G. T., Brando, V. E., & Anstee, J. M. (2003). Hyperspectral mapping of intertidal rock platform vegetation as a tool for adaptive management, *CSIRO*. Retrieved from http://www.clw.csiro.au/publications/technical2003/tr9-03.pdf (Accessed: 31/10/2019)

Delaney, A., Frangoudes, K., & Ii, S. A. (2016). Society and seaweed: understanding the past and present. *Seaweed in Health and Disease Prevention* (Vol. 2). https://doi.org/10.1016/B978-0-12-802772-1.00002-6

Desmond, M. J., Pritchard, D. W., & Hepburn, C. D. (2015). Light limitation within southern New Zealand kelp forest communities, 1–18. https://doi.org/10.5061/dryad.6mc8k.Funding

Díaz-Delgado, R., Cazacu, C., & Adamescu, M. (2018). Rapid assessment of ecological integrity for LTER wetland sites by using UAV multispectral mapping. *Drones, 3*(1), 3. https://doi.org/10.3390/drones3010003

Dierssen, H. M., Chlus, A., & Russell, B. (2015). Hyperspectral discrimination of floating mats of seagrass wrack and the macroalgae *Sargassum* in coastal waters of Greater Florida Bay using airborne remote sensing. *Remote Sensing of Environment, 167*(March 2016), 247–258. https://doi.org/10.1016/j.rse.2015.01.027

Dillehay, T. D., Ramírez, C., Pino, M., Collins, M. B., Rossen, J., & Pino-Navarro, J. D. (2008). Monte Verde: seaweed, food, medicine, and the peopling of South America. *Science*, *320*(5877), 784–786. https://doi.org/10.1126/science.1156533

Dockrill, S. J., & Bond, J. M. (2009). Sustainability and resilience in prehistoric North Atlantic Britain: the importance of a mixed paleoeconomic system. *Journal of the North Atlantic, 2*(1), 33–50. https://doi.org/10.3721/037.002.0105

Doughty, C., & Cavanaugh, K. (2019). Mapping coastal wetland biomass from high resolution Unmanned Aerial Vehicle (UAV) imagery. *Remote Sensing, 11*(5), 540. https://doi.org/10.3390/rs11050540

Dronova, I. (2015). Object-based image analysis in wetland research: a review. *Remote Sensing, 7*(5), 6380-6413. https://doi.org/10.3390/rs70506380

Duffy, J. P., Cunliffe, A. M., DeBell, L., Sandbrook, C., Wich, S. A., Shutler, J. D., Myers-Smith, I., Varela, M., Anderson, K. (2018a). Location, location, location: considerations when using lightweight drones in challenging environments. *Remote Sensing in Ecology and Conservation, 4*(1), 7–19. https://doi.org/10.1002/rse2.58

Duffy, J. P., Pratt, L., Anderson, K., Land, P. E., & Shutler, J. D. (2018b). Spatial assessment of intertidal seagrass meadows using optical imaging systems and a lightweight drone. *Estuarine, Coastal and Shelf Science*, 200, 169–180. https://doi.org/10.1016/j.ecss.2017.11.001

Dymond, J., Shepard, J., & Qi, J. (2001) A simple physical model of vegetation reflectance for standardising optical satellite imagery, *Remote Sensing of Environment*, *75*(2), 350-359. https://doi.org/10.1016/s0034-4257(01)00287-5

Easterday, K., Kislik, C., Dawson, T., Hogan, S., & Kelly, M. (2019). Remotely sensed water limitation in vegetation: Insights from an experiment with Unmanned Aerial Vehicles (UAVs). *Remote Sensing*, *11*(16), 1853. https://doi.org/10.3390/rs11161853

Eismann, M., & Hardie, R. (2005). Hyperspectral resolution enhancement using high-resolution multispectral imagery with arbitrary response functions. *IEEE Geoscience and Remote Sensing Letters*, *43*(3), 455–465.https://doi.org/10.1109/TGRS.2004.837324

Erlandson, J. M. (2002). Anatomically modern humans, maritime voyaging, and the Pleistocene colonization of the Americas. In. Jablonski, N. (2002) *The First Americans: The Pleistocene Colonization of the New World*, San Francisco: California Academy of Sciences

Erlandson, J. M., Graham, M. H., Bourque, B. J., Corbett, D., Estes, J. A., & Steneck, R. S. (2007). The kelp highway hypothesis: marine ecology, the coastal migration theory, and the peopling of the Americas. *Journal of Island and Coastal Archaeology*, *2*(2), 161–174. https://doi.org/10.1080/15564890701628612

Falace, A., Kaleb, S., Annunziatellis, A., Salvati, E., Tunesi, L. (2014). Macroalgal composition of rhodolith beds in a pilot area of the Tuscan Aarchipelago (Tyrrhenian Sea): primary elements to evaluate the degree of conservation of this habitat. *In 2nd Mediterranean Symposium on the conservation of Coralligenous & other Calcareous Bio-Concretions* (pp. 213–214).

Fischer, H. (1937). Chlorophyll. *Chemical Reviews*, *20*(1), 41–68. https://doi.org/10.1021/cr60065a002

Flynn, K. F., & Chapra, S. C. (2014). Remote sensing of submerged aquatic vegetation in a shallow non-turbid river using an unmanned aerial vehicle. *Remote Sensing*, *6*(12), 12815–12836. https://doi.org/10.3390/rs61212815

Foody, G. M. (2002). Status of land cover classification accuracy assessment. *Remote Sensing of Environment*, *80*(1), 185–201. https://doi.org/10.1016/S0034-257(01)00295-4

Foody, G. M., Campbell, N. A., Trodd, N. M., & Wood, T. F. (1992). Derivation and applications of probabilistic measures of class membership from the maximum-likelihood classification. *Photogrammetric Engineering and Remote Sensing*, *58*(9), 1335–1341. Retrieved from: https://www.asprs.org/wp-ontent/uploads/pers/1992journal/sep/1992_sep_1335-1341.pdf

Forlani, G., Dall'Asta, E., Diotri, F., di Cella, U. M., Roncella, R., & Santise, M. (2018). Quality assessment of DSMs produced from UAV flights georeferenced with on-board RTK positioning. *Remote Sensing*, 10(2). https://doi.org/10.3390/rs10020311

Forsmoo, J., Anderson, K., Macleod, C. J. A., Wilkinson, M. E., & Brazier, R. (2018). Drone-based structure-from-motion photogrammetry captures grassland sward height variability. *Journal of Applied Ecology*, *55*(6), 2587–2599. https://doi.org/10.1111/1365-2664.13148

Forsythe, W. (2006). The archaeology of the kelp industry in the northern islands of Ireland. *International Journal of Nautical Archaeology*, 35(2), 218–229. https://doi.org/10.1111/j.1095-9270.2006.00104.x

Freitas, R., Rodrigues, A. M., Morris, E., Perez-Llorens, J. L., & Quintino, V. (2008). Single-beam acoustic ground discrimination of shallow water habitats: 50 kHz or 200 kHz frequency survey? *Estuarine, Coastal and Shelf Science*, *78*(4), 613–622. https://doi.org/10.1016/j.ecss.2008.02.007

Fyfe, J., Israel, S., Chong, A., Ismail, N., Hurd, C. L., & Probert, K. (1999). Mapping marine habitats in Otago, southern New Zealand. *Geocarto International*, 14(3), 17–28. https://doi.org/10.1080/10106049908542113

Fyfe, S. K. (2003). Spatial and temporal variation in spectral reflectance: are seagrass species spectrally distinct? *Limnology and Oceanography*, *48*(1/2), 464–479. https://doi.org/10.4319/lo.2003.48.1_part_2.0464

Gagné, J. A., Mann, K. H., & Chapman, A. R. O. (1982). Seasonal patterns of growth and storage in *Laminaria longicruris* in relation to different patterns of availability of nitrogen in the water. *Marine Biology*, 69, 91–101.

Gao, J., Nuyttens, D., Lootens, P., He, Y., & Pieters, J. G. (2018). Recognising weeds in a maize crop using a random forest machine-learning algorithm and near-infrared snapshot mosaic hyperspectral imagery. *Biosystems Engineering*, *170*, 39–50. https://doi.org/10.1016/j.biosystemseng.2018.03.006

Garono, R. J., Simenstad, C. A., Robinson, R., & Ripley, H. (2004). Using high spatial resolution hyperspectral imagery to map intertidal habitat structure in Hood Canal, Washington, U.S.A. *Canadian Journal of Remote Sensing*, *30*(1), 54–63. https://doi.org/10.5589/m03-052

Garrod, D. A. E., Buxton, L. H. D., Smith, G. E., Bate, D. M. A., Spiller, C., Hinton, M. A. C., & Fischer, P. (1928). Excavation of a Mousterian rock-shelter at Devil's Tower Gibraltar. *The Journal of the Royal Anthropological Institute of Great Britain and Ireland*, 58. 33–113. https://www.jstor.org/stable/4619528

Gaylord, B., Rosman, J. H., Reed, D. C., Koseff, J. R., Fram, J., MacIntyre, S., & Mardian, B. (2007). Spatial patterns of flow and their modification within and around a giant kelp forest. *Limnology and Oceanography*, *52*(5), 1838–1852. https://doi.org/10.4319/lo.2007.52.5.1838

Gevaert, F., Janquin, M. A., Davoult, D. (2008). Biometrics in *Laminaria digitata*: A useful tool to assess biomass, carbon and nitrogen contents. *Journal of Sea Research*, 60(3), 215–219. https://doi.org/10.1016/j.seares.2008.06.006

Gheyle, W., Saey, T., Van Hollebeeke, Y., Verplaetse, S., Note, N., Bourgeois, J., Van Meirvenne, M., van Eetvelde, V., & Stichelbaut, B. (2016). Historical aerial photography and multi-receiver EMI soil sensing, complementing techniques for the study of a Great War conflict landscape. *Archaeological Prospection*, *23*(3), 149–164. https://doi.org/10.1002/arp.1534

Gillanders, S. N., Coops, N. C., Wulder, M. A., Gergel, S. E., & Nelson, T. (2008). Multitemporal remote sensing of landscape dynamics and pattern change: describing

natural and anthropogenic trends. *Progress in Physical Geography*, *32*(5), 503–528. https://doi.org/10.1177/0309133308098363

Godet, L., Fournier, J., Toupoint, N., & Olivier, F. (2009). Mapping and monitoring intertidal benthic habitats: a review of techniques and a proposal for a new visual methodology for the European coasts. *Progress in Physical Geography*, *33*(3), 378–402. https://doi.org/10.1177/0309133309342650

Goetz, A. F. H. (2009). Three decades of hyperspectral remote sensing of the Earth: a personal view. *Remote Sensing of Environment*, *113*(SUPPL. 1), S5–S16. https://doi.org/10.1016/j.rse.2007.12.014

Gómez-Chova, L., Alonso, L., Guanter, L., Camps-Valls, G., Calpe, J., & Moreno, J. (2008). Correction of systematic spatial noise in push-broom hyperspectral sensors: application to CHRIS/PROBA images. *Applied Optics*, *47*(28), F46. https://doi.org/10.1364/AO.47.000F46

*Gonor, J. J. & Kemp, P. F. (1978). Procedures for quantitative ecological assessments in intertidal environments. *U.S. Environmental Protection Agency, Washington, D.C., EPA/600/3-78/087 (NTIS PB289816)*. Retrieved from: https://cfpub.epa.gov/si/si_public_record_Report.cfm?Lab=ORD&dirEntryID=42803 Accessed: 23/01/2020.

Gorman, D., Bajjouk, T., Populus, J., Vasquez, M., & Ehrhold, A. (2013). Modeling kelp forest distribution and biomass along temperate rocky coastlines. *Marine Biology*, *160*(2), 309–325. https://doi.org/10.1007/s00227-012-2089-0

Govender, M., Chetty, K., & Bulcock, H. (2007). A review of hyperspectral remote sensing and its application in vegetation and water resource studies. *Water SA*, *33*(2), 145–151. https://doi.org/10.4314/wsa.v33i2.49049

Gray, P. C., Ridge, J. T., Poulin, S. K., Seymour, A. C., Schwantes, A. M., Swenson, J. J., & Johnston, D. W. (2018). Integrating drone imagery into high resolution satellite remote sensing assessments of estuarine environments. *Remote Sensing*, *10*(8). https://doi.org/10.3390/rs10081257

Grohmann, C. H. (2015). Effects of spatial resolution on slope and aspect derivation for regional-scale analysis. *Computers and Geosciences*, *77*, 111–117. https://doi.org/10.1016z/j.cageo.2015.02.003

Grosholz, E. (2002). Ecological and evolutionary consequences of coastal invasions. *Trends in Ecology & Evolution*, *17*(1), 22–27. https://doi.org/10.1016/S0169-5347(01)02358-8

Guichard, F., Bourget, E., & Agnard, J.-P. (2000). High-resolution remote sensing of intertidal ecosystems: a low-cost technique to link scale-dependent patterns and processes. *Limnology and Oceanography*, *45*(2), 328–338. https://doi.org/10.4319/lo.2000.45.2.0328

Guillaumont, B., Callens, L., & Dion, P. (1993). Spatial distribution and quantification of *Fucus* species and *Ascophyllum nodosum* beds in intertidal zones using spot imagery. *Hydrobiologia*, *260–261*(1), 297–305. https://doi.org/10.1007/BF00049032

Guihéneuf, F., Gietl, A., Stengel, D. B. (2018). Temporal and spatial variability of mycosporine-like amino acids and pigments in three edible red seaweeds from western Ireland. *Journal of Applied Phycology*, 3-(4), 2573-2586. https://doi.org/10.1007/s10811-018-1436-z

Guiry. M. (2010). History of Seaweed in Ireland. In., Steele, S., Lyons, H., Guiry, M., Kraan, S. (2010). The seaweed of Ireland's coastline, *The Heritage Council.* https://www.heritagecouncil.ie/content/files/irelands_coastline_seaweed_2008_4mb.pdf (Accessed: 31/10/2019)

Hagen, N. T. (1995). Recurrent destructive grazing of successionally immature kelp forests by green sea urchins in Vestsfjorden, northern Norway. *Marine Ecology Progress Series*, 123(1-3), 95–106. https://doi.org/10.3354/meps123095

Hagen, N., & Kudenov, M. W. (2013). Review of snapshot spectral imaging technologies. *Optical Engineering*, *52*(9), 090901. https://doi.org/10.1117/1.OE.52.9.090901

Hamylton, S. (2017). *Spatial analysis of coastal environments*. Cambridge: Cambridge University Press

Han, J., Mamber, M., & Pei, J. (2012). *Data mining concepts and techniques*. Waltham: Morgan Kaufmann

Harley, C. D. G., Anderson, K. M., Demes, K. W., Jorve, J. P., Kordas, R. L., Coyle, T. A., & Graham, M. H. (2012). Effects of climate change on global seaweed communities. *Journal of Phycology*, *48*(5), 1064–1078. https://doi.org/10.1111/j.1529-8817.2012.01224.x

Harper, D. (1974) Kelp burning in the glens of Antrim https://antrimhistory.net/kelp-burning-in-the-glens-of-antrim-by-douglasharper/##targetText=The%20prosperity%20of%20this%20industry,of%20iodine%20which%20kelp%20contains.&targetText=In%20the%20Glens%20the%20weed,of%20the%20sea%20was%20deposited. (Accessed: 31/10/19)

Hasan, R. C., Ierodiaconou, D., Rattray, A., Monk, J., & Laurenson, L. (2011). Applications of multibeam echosounder data and video observations for biological monitoring on the south east Australian continental shelf, *SG 2011: Proceedings of the 10th International Symposium and Exhibition on Geoinformation: Seamless Innovative Geospatial Solutions.* Retrieved from: http://dro.deakin.edu.au/view/DU:30042301

Hatcher, B. G., Chapman, A. R. O., & Mann, K. H. (1977). An annual carbon budget for the kelp *Laminaria longicruris. Marine Biology*, *44*(1), 85–96. https://doi.org/10.1007/BF00386909

Hawkins, S. J., & Harkin, E. (1985). Preliminary canopy removal experiments in algal dominated communities low on the shore and in the shallow subtidal on the Isle of Man. *Botanica Marina*, 28(6), 223–230. https://doi.org/10.1515/botm.1985.28.6.223

Hawkins, S., Moore, P., Burrows, M., Poloczanska, E., Mieszkowska, N., Herbert, R., Jenkins, S., Thompson, R., Genner, M., Southward, A. (2008). Complex interactions in a rapidly changing world: Responses of rocky shore communities to recent climate change. *Climate Research*, 37(2-3), 123–133. https://doi.org/10.3354/cr00768

Headwall. (2020). Hyperspectral drone camera field of view. Retrived from: https://www.headwallphotonics.com/field-of-view (Accessed: 04/05/2020)

Hedley, J. D., & Mumby, P. J. (2002). Biological and remote sensing perspectives of pigmentation in coral reef organisms. *Advances in Marine Biology*, *43*, 277–317. https://doi.org/10.1016/S0065-2881(02)43006-4

Helmuth, B. S. T., & Hofmann, G. E. (2001). Microhabitats, thermal heterogeneity, and patterns of physiological stress in the rocky intertidal zone. *The Biological Bulletin*, 201(3), 374–384. https://doi.org/10.2307/1543615

Hennequart, F., Dalias, N., Barraqué Garat, de Labories, L., Scourzic, T. (2006) Review of kelp biomass assessment techniques – application to the inshore and coastal waters of Ireland. *OCEANIDE*, 1-145.

Hennig, B. D., Cogan, C. B., & Bartsch, I. (2007). Hyperspectral remote sensing and analysis of intertidal zones: a contribution to monitor coastal biodiversity. *Proceedings of the First Geoinformatics Forum Salzburg 2007*, 62–73. Retrieved from http://epic.awi.de/Publications/Hen2007c.pdf (Accessed: 24/01/2020)

Herrero, R., Cadirola, M., & Ingle, V. K. (2015). Preprocessing and compression of hyperspectral images captured onboard UAVs. *Proceedings of SPIE - The International Society for Optical Engineering*, *9647*(October 2015). https://doi.org/10.1117/12.2186169

*Heumann, B. W. (2011). An object-based classification of mangroves using a hybrid decision tree —support vector machine approach. *Remote Sensing*, *3*(11), 2440–2460. https://doi.org/10.3390/rs3112440

Hill, A. C. (2019). Economical drone mapping for archaeology: comparisons of efficiency and accuracy. *Journal of Archaeological Science: Reports*, *24*(January), 80–91. https://doi.org/10.1016/j.jasrep.2018.12.011

Hodgson, A., Kelly, N., & Peel, D. (2013). Unmanned aerial vehicles (UAVs) for surveying marine fauna: a dugong case study. *PLoS ONE*, *8*(11), 1–15. https://doi.org/10.1371/journal.pone.0079556

Honkavaara, E., Eskelinen, M. A., Polonen, I., Saari, H., Ojanen, H., Mannila, R., Holmlund, C., Hakala, T., Litkey, P., Rosnell, T., Viljanen, N., & Pulkkanen, M. (2016). Remote sensing of 3-D geometry and surface moisture of a peat production area using hyperspectral frame cameras in visible to short-wave infrared spectral ranges onboard a small Unmanned Airborne Vehicle (UAV). *IEEE Transactions on Geoscience and Remote Sensing*, *54*(9), 5440–5454. https://doi.org/10.1109/TGRS.2016.2565471

Horton, R., Cano, E., Bulanon, D., & Fallahi, E. (2017). Peach flower monitoring using aerial multispectral imaging. *Journal of Imaging*, *3*(1), 2. https://doi.org/10.3390/jimaging3010002

Hruska, R., Mitchell, J., Anderson, M., & Glenn, N. F. (2012). Radiometric and geometric analysis of hyperspectral imagery acquired from an unmanned aerial vehicle. *Remote Sensing*, *4*(9), 2736–2752. https://doi.org/10.3390/rs4092736

*Huang, C., Davis, L. S., & Townshend, J. R. G. (2002). An assessment of support vector machines for land cover classification. *International Journal of Remote Sensing*, *23*(4), 725–749. https://doi.org/10.1080/01431160110040323

Hurd, C., Harrison, P., Bischof, K., Lobban, C. (2014). *Seaweed ecology and physiology*. Cambridge: Cambridge University Press

Husson, E., Ecke, F., & Reese, H. (2016). Comparison of manual mapping and automated object-based image analysis of non-submerged aquatic vegetation from very-high-resolution UAS images. *Remote Sensing*, *8*, 1-18. https://doi.org/10.3390/rs8090724

Ierodiaconou, D., Laurenson, L., Burq, S., & Reston, M. (2007). Marine benthic habitat mapping using Multibeam data, georeferenced video and image classification techniques in Victoria, Australia. *Journal of Spatial Science, 52*(1), 93–104. https://doi.org/10.1080/14498596.2007.9635105

Ishida, T., Kurihara, J., Viray, F. A., Namuco, S. B., Paringit, E. C., Perez, G. J., Takahashi, Y., & Marciano, J. J. (2018). A novel approach for vegetation classification using UAV-based hyperspectral imaging. *Computers and Electronics in Agriculture, 144*(November 2017), 80–85. https://doi.org/10.1016/j.compag.2017.11.027

Jablonski, J., Durell, C., Slonecker, T., Wong, K., Blair, S., Eichelberger, A., & Osterberg, J. (2016). Best practices in passive remote sensing VNIR hyperspectral system hardware calibrations. *Proc. SPIE 9860, Hyperspectral Imaging Sensors: Innovative applications and sensor standards*. https://doi.org/10.1117/12.2224022

Jackisch, R., Lorenz, S., Zimmermann, R., Möckel, R., & Gloaguen, R. (2018). Drone-borne hyperspectral monitoring of acid mine drainage: an example from the Sokolov lignite district. *Remote Sensing*, *10*(3). https://doi.org/10.3390/rs10030385

Jackson, G. A. (1997). Currents in the high drag environment of a coastal kelp stand off California. *Continental Shelf Research*, *17*(15), 1913–1928. https://doi.org/10.1016/S0278-4343(97)00054-X

Jacobsen, A., Nielsen, A. A., Ejrnaes, R., & Groom, G. B. (1999). Spectral identification of Danish grassland classes related to management and plant species composition. *Proceedings of 4th International Airborne Remote Sensing Conference and Exhibition/21st Canadian Symposium on Remote Sensing*, (June), 74–81. Retrieved from: http://www.neri.dk/1_Viden/2_Publikationer/3_Ovrige/rapporter/Artikel3_anne_LAND.pdf (Accessed: 24/01/2020)

Jakob, S., Zimmermann, R., & Gloaguen, R. (2017). Processing of drone-borne hyperspectral data for geological applications. *Workshop on Hyperspectral Image and Signal Processing, Evolution in Remote Sensing*, (October 2017). https://doi.org/10.1109/WHISPERS.2016.8071689

James, M. R., Robson, S., D'Oleire-Oltmanns, S., & Niethammer, U. (2017). Optimising UAV topographic surveys processed with structure-from-motion: Ground control quality, quantity and bundle adjustment. *Geomorphology*, *280*, 51–66. https://doi.org/10.1016/j.geomorph.2016.11.021

Jaud, M., Le Dantec, N., Ammann, J., Grandjean, P., Constantin, D., Akhtman, Y., Barbieux, K., Allemand, P., Delacourt, C., & Merminod, B. (2018). Direct georeferencing of a pushbroom, lightweight hyperspectral system for mini-UAV applications. Remote Sensing, 10(2), 1–15. https://doi.org/10.3390/rs10020204

Jenkins, S. R., Norton, T. A., & Hawkins, S. J. (2004). Long term effects of *Ascophyllum nodosum* canopy removal on mid shore community structure. *Journal of the Marine Biological Association of the United Kingdom*, *84*(2), 327–329. https://doi.org/10.1017/S0025315404009221h

Jensen, A. M., Hardy, T., McKee, M., & Chen, Y. Q. (2011). Using a multispectral autonomous unmanned aerial remote sensing platform (AggieAir) for riparian and wetlands applications. *International Geoscience and Remote Sensing Symposium (IGARSS)*, 3413–3416. https://doi.org/10.1109/IGARSS.2011.6049953

Jia, X., & Richards, J. A. (1994). Efficient maximum likelihood classification for imaging spectrometer data sets. *IEEE Transactions on Geoscience and Remote Sensing, 32*(2), 274–281. https://doi.org/10.1109/36.295042

Jiang, L., Liao, M., Lin, H., & Yang, L. (2009). Synergistic use of optical and InSAR data for urban impervious surface mapping: a case study in Hong Kong. *International Journal of Remote Sensing, 30*(11), 2781–2796. https://doi.org/10.1080/01431160802555838

Jiménez, M., & Díaz-Delgado, R. (2015). Towards a standard plant species spectral library protocol for vegetation mapping: A case study in the shrubland of Doñana National Park. *ISPRS International Journal of Geo-Information, 4*(4), 2472–2495. https://doi.org/10.3390/ijgi4042472

Johansen, K., Raharjo, T., & McCabe, M. F. (2018). Using multi-spectral UAV imagery to extract tree crop structural properties and assess pruning effects. *Remote Sensing, 10*(6). https://doi.org/10.3390/rs10060854

Johnston, D. W. (2019). Unoccupied aircraft systems in marine science and conservation. *Annual Review of Marine Science, 11*(1), 439–463. https://doi.org/10.1146/annurev-marine-010318-095323

Jonsson, P. R., Granhag, L., Moschella, P. S., Åberg, P., Hawkins, S. J., Thompson, R. C. (2006). Interactions between wave action and grazing control the distribution of intertidal macroalgae. *Ecology, 87*(5), 1169–1178. https://doi.org/https://doi.org/10.1890/0012-9658(2006)87[1169:IBWAAG]2.0.CO;2

Jordan, A., Lawler, M., Halley, V., & Barrett, N. (2005). Seabed habitat mapping in the Kent group of islands and its role in marine protected area planning. *Aquatic Conservation: Marine and Freshwater Ecosystems*, *15*(1), 51–70. https://doi.org/10.1002/aqc.657

Joyce, K. E., Duce, S., Leahy, S. M., Leon, J., & Maier, S. W. (2018). Principles and practice of acquiring drone-based image data in marine environments. *Marine and Freshwater Research*, *70*(7), 952. https://doi.org/10.1071/MF17380

Jueterbock, A., Tyberghein, L., Verbruggen, H., Coyer, J. A., Olsen, J. L., & Hoarau, G. (2013). Climate change impact on seaweed meadow distribution in the North Atlantic rocky intertidal. *Ecology and Evolution*, 3(5), 1356–1373. https://doi.org/10.1002/ece3.541

Kain, J. M. (1962). Aspects Of the biology of *Laminaria hyperborea* I. vertical distribution. *Journal of the Marine Biological Association of the United Kingdom*, 42(2), 377–385. https://doi.org/10.1017/S0025315400001363

Kain, J. M., & Jones, N. S. (1963). Aspects of the biology of *Laminaria hyperborea* : II. Age, Weight and Length. *Journal of the Marine Biological Association of the United Kingdom*, *43*(1), 129–151. https://doi.org/10.1017/S0025315400005312

Kain, J. M. (1971). Synopsis of biological data on *Laminaria hyperborea*. *FAO Fish, Synopsis*(87), 68 pp. Retrieved from http://www.fao.org/3/c3845e/c3845e.pdf

Kain, J. M., & Jones, N. S. (1975). The biology of *Laminaria hyperborea* VII. Reproduction of the sporophyte. *Journal of the Marine Biological Association of the United Kingdom*, 55(3), 567–582. https://doi.org/10.1017/S0025315400017264

Kalvas, A., & Kautsky, L. (1993). Geographical variation in *Fucus vesiculosus* morphology in the Baltic and North Seas. *European Journal of Phycology*, 28(2), 85–91. https://doi.org/10.1080/09670269300650141

Kazantsev, T., Samberg, A., Ametov, F., Shevchenko, V., Bondarenko, O., Furier, M., & Iakovenko, V. (2018). COTS UAV-borne multispectral system for vegetation monitoring. *Remote Sensing for Agriculture, Ecosystems, and Hydrology*, 1-10. https://doi.org/10.1117/12.2501859

Keane, J. F., & Carr, S. S. (2013). A brief history of early unmanned aircraft. Johns Hopkins APL Technical Digest (Applied Physics Laboratory), 32(3), 558–571. http://citeseerx.ist.psu.edu/viewdoc/summary?doi=10.1.1.686.7958 (Accessed: 31/10/2019)

Keeling, P. J. (2010). The endosymbiotic origin, diversification and fate of plastids. *Philosophical Transactions of the Royal Society B: Biological Sciences*, 365(1541), 729–748. https://doi.org/10.1098/rstb.2009.0103

Kellaris, A., Gil, A., Faria, J., Amaral, R., Moreu-Badia, I., Neto, A., & Yesson, C. (2019). Using low-cost drones to monitor heterogeneous submerged seaweed habitats: A case study in the Azores. *Aquatic Conservation: Marine and Freshwater Ecosystems*, (May 2019). https://doi.org/10.1002/aqc.3189

Kenny, A. (2003). An overview of seabed-mapping technologies in the context of marine habitat classification. *ICES Journal of Marine Science*. 60, 1352–1360. https://doi.org/10.1016/S1054-3139(03)00141-3

Kerr, J. T., & Ostrovsky, M. (2003). From space to species: ecological applications for remote sensing. *Trends in Ecology and Evolution*, *18*(6), 299–305. https://doi.org/10.1016/S0169-5347(03)00071-5

Kislik, C., Dronova, I., & Kelly, M. (2018). UAVs in support of algal bloom research: a review of current applications and future opportunities. *Drones*, *2*(35), 1-35. https://doi.org/10.3390/drones2040035

Kitching, J. A. (1941). Studies in sublittoral ecology. *The Biological Bulletin*, 80(3), 324–337. https://doi.org/10.2307/1537719

Knight, M., & Parke, M. (1950). A biological study of *Fucus vesiculosus* L. and *F. serratus* L. *Journal of the Biological Association of the United Kingdom, 29*(2), 439–515. https://doi.org/10.1017/S0025315400055454

Knudby, A., & Nordlund, L. (2011). Remote sensing of seagrasses in a patchy multi-species environment. *International Journal of Remote Sensing*, *32*(8), 2227–2244. https://doi.org/10.1080/01431161003692057

Komatsu, T., Igarashi, C., Tatsukawa, K., Sultana, S., Matsuoka, Y., & Harada, S. (2003). Use of multi-beam sonar to map seagrass beds in Otsuchi Bay on the Sanriku Coast of Japan. *Aquatic Living Resources*, *16*(3), 223–230. https://doi.org/10.1016/S0990-7440(03)00045-7

Konar, B., & Iken, K. (2018). The use of unmanned aerial vehicle imagery in intertidal monitoring. *Deep-Sea Research Part II: Topical Studies in Oceanography*, *147*, 79–86. https://doi.org/10.1016/j.dsr2.2017.04.010

Könnecker, G., & Keegan, B. (1983). Littoral and benthic investigations on the west coast of Ireland: XVII. The epibenthic animal associations of Kilkieran Bay. *Proceedings of the Royal Irish Academy, Section B: Biological, Geological, and Chemical Science*, 83B, 309–324. https://www.jstor.org/stable/20494425

Kostylev, V. E., Courtney, R. C., Robert, G., Todd, B. J. (2003). Stock evaluation of giant scallop (*Placopecten magellanicus*) using high-resolution acoustics for seabed mapping. *Fisheries Research*, 60(2-3), 479–492. https://doi.org/10.1016/S0165-7836(02)00100-5

Kotta, J., Remm, K., Vahtmäe, E., Kutser, T., & Orav-Kotta, H. (2014). In-air spectral signatures of the Baltic Sea macrophytes and their statistical separability. *Journal of Applied Remote Sensing*, *8*(1), 083634. https://doi.org/10.1117/1.JRS.8.083634

Krumhansl, K. A., Scheibling, R. E. (2012). Production and fate of kelp detritus. *Marine Ecology Progress Series*, 467, 281–302. https://doi.org/10.3354/meps09940

Kruse, F., Lefkoff, A., Boardman, J., Heidebrecht, K., Shapiro, A., Barloon, P., & Goetz, A. (1993). The Spectral Image Processing System (SIPS) - Interactive Visualization and Analysis of Imaging Spectrometer Data. *Remote Sensing of Environment*. https://doi.org/10.1016/0034-4257(93)90013-N

Kruss, A., Tegowski, W., Tatarek, A., Olenin, S., Daunys, D., Gorska, N., Klusek, Z. (2006). Acoustic characterisation of benthic habitats in Hornsund Fjord (The Svalbard Archipelago). *Proceedings of the Eighth European Conference on Underwater Acoustics, 8th ECUA*, 1-6. https://www.researchgate.net/profile/Sergej_Olenin/publication/228528322_Acoustic_characterisation_of_benthic_habitats_in_Hornsund_Fjord_the_Svalbard_Archipelago/links/09e415106e97bcab33000000.pdf (Accessed: 31/10/2019)

Kruss, A., Blondel, P., Tegowski, J., Wiktor, J., & Tatarek, A. (2008). Estimation of macrophytes using single-beam and multibeam echosounding for environmental monitoring of Arctic fjords (Kongsfjord, West Svalbard Island). *The Journal of the Acoustical Society of America*, *123*(5), 3213–3213. https://doi.org/10.1121/1.2933397

Kruss, A, Blondel, P., & Tegowski, J. (2011). Mapping macrophytes and habitats: single-beam and multibeam imaging in the Arctic. *4th International Conference and Exhibition on "Underwater Acoustic Measurements: Technologies and Results,"* 1687–1694. Retrieved from: https://people.bath.ac.uk/pyspb/AIM_HI/2011_UAM_Kruss_etal.pdf (Accessed: 22/01/2020)

Kruss, A., Tęgowski, J., Tatarek, A., Wiktor, J., & Blondel, P. (2017). Spatial distribution of macroalgae along the shores of Kongsfjorden (West Spitsbergen) using acoustic imaging. *Polish Polar Research*, *38*(2), 205–229. https://doi.org/10.1515/popore-2017-0009

Krzywinski, M., & Altman, N. (2017). Classification and regression trees. *Nature Methods*, *14*(8), 757–758. https://doi.org/10.1038/nmeth.4370

Kübler, J. E., & Davison, I. R. (1995). Thermal acclimation of light-use characteristics of *Chondrus crispus* (Rhodophyta). *European Journal of Phycology*, *30*(3), 189–195. https://doi.org/10.1080/09670269500650971

Kutser, T., Dekker, A. G., & Skirving, W. (2003). Modelling spectral discrimination of Great Barrier Reef benthic communities by remote sensing instruments. *Limnology and*

Oceanography, *48*(1, part 2), 497–510. https://doi.org/10.4319/lo.2003.48.1_part_2.0497

Kutser, T., Miller, I., & Jupp, D. L. B. (2006a). Mapping coral reef benthic substrates using hyperspectral space-borne images and spectral libraries. *Estuarine, Coastal and Shelf Science*, *70*(3), 449–460. https://doi.org/10.1016/j.ecss.2006.06.026

Kutser, T., Vahtmäe, E., & Metsamaa, L. (2006b). Spectral library of macroalgae and benthic substrates in Estonian coastal waters. *Proceedings of the Estonian Academy of Science, Biology and Ecology*, *55*(4), 329–340. Retrieved from http://www.kirj.ee/public/va_bo/bio-2006-4-5.pdf (Accessed: 31/10/2019)

Laliberte, A. S., & Rango, A. (2011). Image processing and classification procedures for analysis of aub-decimeter imagery acquired with an unmanned aircraft over arid rangelands. *GIScience & Remote Sensing*, *48*(1), 4–23. https://doi.org/10.2747/1548-1603.48.1.4

Le Bas, T. P., Huvenne, V. A. I. (2009). Acquisition and processing of backscatter data for habitat mapping - comparison of multibeam and sidescan systems. *Applied Acoustics*, 70(10), 1248–1257. https://doi.org/10.1016/j.apacoust.2008.07.010

Le Corguillé, G., Pearson, G., Valente, M., Viegas, C., Gschloessl, B., Corre, E., Bailly, X., Peters, A., Jubin, C., Vacherie, B., Cock, M., & Leblanc, C. (2009). Plastid genomes of two brown algae, *Ectocarpus siliculosus* and *Fucus vesiculosus*: further insights on the evolution of red-algal derived plastids. *BMC Evolutionary Biology*, 9(1), 253. https://doi.org/10.1186/1471-2148-9-253

Lechner, A. M., Fletcher, A., Johansen, K., & Erskine, P. (2012). Characterising upland swamps using object-based classification methods and hyper-spatial resolution imagery derived from an unmanned aerial vehicle. *ISPRS Annals of the Photogrammetry, Remote Sensing and Spatial Information Sciences*, *1*(September), 101–106. https://doi.org/10.5194/isprsannals-I-4-101-2012

Leclerc, J.-C., Riera, P., Laurans, M., Leroux, C., Lévêque, L., & Davoult, D. (2015). Community, trophic structure and functioning in two contrasting *Laminaria hyperborea* forests. *Estuarine, Coastal and Shelf Science*, 152, 11–22. https://doi.org/10.1016/j.ecss.2014.11.005

Lefebvre, A., Thompson, C. E. L., Collins, K. J., & Amos, C. L. (2009). Use of a high-resolution profiling sonar and a towed video camera to map a *Zostera marina* bed, Solent, UK. *Estuarine, Coastal and Shelf Science*, *82*(2), 323–334. https://doi.org/10.1016/j.ecss.2009.01.027

Leliaert, F., Smith, D. R., Moreau, H., Herron, M. D., Verbruggen, H., Delwiche, C. F., & De Clerck, O. (2012). Phylogeny and molecular evolution of the green algae. *Critical Reviews in Plant Sciences*, 31(1), 1–46. https://doi.org/10.1080/07352689.2011.615705

Leon, J. X., Phinn, S. R., Hamylton, S., & Saunders, M. I. (2013). Filling the "white ribbon" - a multisource seamless digital elevation model for Lizard Island, northern Great Barrier Reef. *International Journal of Remote Sensing*, *34*(18), 6337–6354. https://doi.org/10.1080/01431161.2013.800659

Li, L., Li, N., Lu, D., & Chen, Y. (2019). Mapping Moso bamboo forest and its on-year and off-year distribution in a subtropical region using time-series Sentinel-2 and Landsat 8

data. *Remote Sensing of Environment*, *231*(June), 111265. https://doi.org/10.1016/j.rse.2019.111265

Lillesand, T., Kiefer, R., Chipman, J. (2004) *Remote sensing and image interpretation*. 5th Edn. New York: John Wiley & Sons

Littler, M. M. (1980). Morphological form and photosynthetic performances of marine macroalgae: tests of a functional / form hypothesis. *Botanica Marina*, 23(3), 161–166. https://doi.org/10.1515/botm.1980.23.3.161

Løvås, S. M., & Tørum, A. (2001). Effect of the kelp *Laminaria hyperborea* upon sand dune erosion and water particle velocities. *Coastal Engineering*, *44*(1), 37–63. https://doi.org/10.1016/S0378-3839(01)00021-7

Lubchenco, J. (1980). Algal zonation in the New England rocky intertidal community: an experimental analysis. *Ecology*, *61*(2), 333–344. https://doi.org/10.2307/1935192

Lucieer, A., Malenovský, Z., Veness, T., & Wallace, L. (2014). HyperUAS-Imaging Spectroscopy from a multirotor unmanned aircraft system. *Journal of Field Robotics*, *31*(4), 571–590. https://doi.org/10.1002/rob.21508

Lum, C., Mackenzie, M., Shaw-Feather, C., Luker, E. & Dunbabin, M. (2016). Multispectral imaging and elevation mapping from an unmanned aerial system for precision agriculture applications. *A Paper from the Proceedings of the 13th International Conference on Precision Agriculture*, 1–17. Retrieved from: https://www.aa.washington.edu/sites/aa/files/student/kchen248/publications/FinalPaper101.pdf (Accessed: 31/10/2019)

Lüning, K., & Dring, M. J. (1979). Continuous underwater light measurement near Helgoland (North Sea) and its significance for characteristic light limits in the sublittoral region. *Helgoländer Wissenschaftliche Meeresuntersuchungen*, *32*(4), 403–424. https://doi.org/10.1007/BF02277985

Lurton X. (2002). *An introduction to underwater acoustics: principles and applications*. Berlin: Springer/Praxis

Lyons, M., Phinn, S., & Roelfsema, C. (2011). Integrating Quickbird multi-spectral satellite and field data: mapping bathymetry, seagrass cover, seagrass species and change in Moreton Bay, Australia in 2004 and 2007. *Remote Sensing*, *3*(1), 42–64. https://doi.org/10.3390/rs3010042

Madsen, J. D., Chambers, P. A., James, W. F., Koch, E. W., & Westlake, D. F. (2001). The interaction between water movement, sediment dynamics and submersed macrophytes. *Hydrobiologia*, *444*, 71–84. https://doi.org/10.1023/A:1017520800568

Mac Arthur, A., MacLellan, C. J., & Malthus, T. (2012). The fields of view and directional response functions of two field spectroradiometers. *IEEE Transactions on Geoscience and Remote Sensing*, *50*(10), 3892–3907. https://doi.org/10.1109/TGRS.2012.2185055

Mac Craith, E., & Hardy, D. (2015) Inishbofin kelp mapping study – preliminary report. Assessment of suitability of EA400 single-beam sonar in mapping kelp distribution. *INFOMAR*.

MacAlister, C., & Mahaxay, M. (2009). Mapping wetlands in the Lower Mekong Basin for wetland resource and conservation management using Landsat ETM images and field

survey data. *Journal of Environmental Management*, *90*(7), 2130–2137. https://doi.org/10.1016/j.jenvman.2007.06.031

Manfreda, S., McCabe, M., Miller, P., Lucas, R., Pajuelo Madrigal, V., Mallinis, G., Ben Dor, E., Helman, D., Estes, L., Ciraolo, G., Mullerova, J., Tauro, F., de Lima, I., de Lima, J., Maltese, A., Frances, F., Caylor, K., Kohv, M., Perks, M., Ruiz-Perez, G., Su, Z., Vico, G., & Toth, B. (2018). On the use of unmanned aerial systems for environmental monitoring. *Remote Sensing*, *10*(4), 641. https://doi.org/10.3390/rs10040641

*Mantero, P., Moser, G., & Serpico, S. B. (2005). Partially Supervised classification of remote sensing images through SVM-based probability density estimation. *IEEE Transactions on Geoscience and Remote Sensing*, *43*(3), 559–570. https://doi.org/10.1109/TGRS.2004.842022

Marçal, A. R. S., Borges, J. S., Gomes, J. A., & Pinto Da Costa, J. F. (2005). Land cover update by supervised classification of segmented ASTER images. *International Journal of Remote Sensing*, *26*(7), 1347–1362. https://doi.org/10.1080/01431160412331291233

Marean, C. W., Bar-Matthews, M., Bernatchez, J., Fisher, E., Goldberg, P., Herries, A. I. R., Jacobs, Z., Jerardino, A., Karkanas, P., Minichillo, T., Nilssen, P., Thompson, E., Watts, I., & Williams, H. M. (2007). Early human use of marine resources and pigment in South Africa during the Middle Pleistocene. *Nature*, *449*(7164), 905–908. https://doi.org/10.1038/nature06204

Markelin, L., Honkavaara, E., Takala, T., & Pellikka, P. (2013). Calibration and validation of hyperspectral imagery using a permanent test field. *Workshop on Hyperspectral Image and Signal Processing, Evolution in Remote Sensing*, 1–4. https://doi.org/10.1109/WHISPERS.2013.8080708

Markham, B. L., Storey, J. C., Williams, D. L., & Irons, J. R. (2004). Landsat sensor performance: history and current status. *IEEE Transactions on Geoscience and Remote Sensing*, *42*(12), 2691–2694. https://doi.org/10.1109/TGRS.2004.840720

Marshall, M., & Thenkabail, P. (2015). Advantage of hyperspectral EO-1 Hyperion over multispectral IKONOS, GeoEye-1, WorldView-2, Landsat ETM+, and MODIS vegetation indices in crop biomass estimation. *ISPRS Journal of Photogrammetry and Remote Sensing*, *108*, 205–218. https://doi.org/10.1016/j.isprsjprs.2015.08.001

Masetti, G., & Calder, B. (2012). Remote identification of a shipwreck site from MBES backscatter. *Journal of Environmental Management*, *111*, 44–52. https://doi.org/10.1016/j.jenvman.2012.06.037

Matese, A., Toscano, P., Filippo de Gennaro, S., Genesio, L., Vaccari, F., Primicerio, J., Belli, C., Zaldei, A., Bianconi, R., Gioli, B. (2015). Intercomparison of UAV, aircraft and satellite remote sensing platforms for precision viticulture. *Remote Sensing*, *7*(3), 2971–2990. https://doi.org/10.3390/rs70302971

Mayer, L. A. (2006). Frontiers in sea floor mapping and visualization. *Marine Geophysical Researches*, *27*, 7–17. https://doi.org/10.1007/s11001-005-0267-x

McDermid, G., Franklin, S., & LeDrew, E. (2005). Remote Sensing for large area multi-jurisdictional habitat mapping. *Progress in Physical Geography*, *4*, 449–474. https://doi.org/10.1191/0309133305pp455ra

McFeeters, S. K. (1996). The use of the Normalized Difference Water Index (NDWI) in the delineation of open water features. *International Journal of Remote Sensing, 17*(7), 1425–1432. https://doi.org/10.1080/01431169608948714

McGonigle, C., Grabowski, J. H., Brown, C. J., Weber, T. C., & Quinn, R. (2011). Detection of deep water benthic macroalgae using image-based classification techniques on multibeam backscatter at Cashes Ledge, Gulf of Maine, USA. *Estuarine, Coastal and Shelf Science, 91*(1), 87–101. https://doi.org/10.1016/j.ecss.2010.10.016

McPherson, J. M., Jetz, W., & Rogers, D. J. (2004). The effects of species' range sizes on the accuracy of distribution models: ecological phenomenon or statistical artefact? *Journal of Applied Ecology, 41*(5), 811–823. https://doi.org/10.1111/j.0021-8901.2004.00943.x

McRoberts, R. E., Stehman, S. V., Liknes, G. C., Næsset, E., Sannier, C., & Walters, B. F. (2018). The effects of imperfect reference data on remote sensing-assisted estimators of land cover class proportions. *ISPRS Journal of Photogrammetry and Remote Sensing, 142*(May), 292–300. https://doi.org/10.1016/j.isprsjprs.2018.06.002

Meddens, A., Hicke, J., & Vierling, L. (2011). Evaluating the potential of multispectral imagery to map multiple stages of tree mortality. *Remote Sensing of Environment, 115*, 1632-1642. https://doi.org/10.1016/j.rse.2011.02.018

MicaSense. (2019) Best practices: collecting data with MicaSense sensors. https://support.micasense.com/hc/en-us/articles/224893167-Best-practices-Collecting-Data-with-MicaSense-RedEdge-and-Parrot-Sequoia (Accessed: 01/11/2019)

Mielck, F., Bartsch, I., Hass, H., Wolfl, A., Burk, D., & Betzler, C. (2014) Predicting spatial kelp abundance in shallow coastal waters using the acoustic ground discrimination system RoxAnn. *Estuarine, Coastal and Shelf Science, 143*, 1-11. https://doi.org/10.1016/j.ecss.2014.03.016

Miller, R. J., Reed, D. C., & Brzezinski, M. A. (2011). Partitioning of primary production among giant kelp (*Macrocystis pyrifera*), understory macroalgae, and phytoplankton on a temperate reef. *Limnology and Oceanography*, *56*(1), 119–132. https://doi.org/10.4319/lo.2011.56.1.0119

Milton, E. J. (2004). Field Spectroscopy. UNESCO-Encyclopedia of life support systems (EOLSS), 30.

Minami, K., Yasuma, H., Tojo, N., Fukui, S., Ito, Y., Nobetsu, T., & Miyashita, K. (2010). Estimation of kelp forest, *Laminaria* spp., distributions in coastal waters of the Shiretoko Peninsula, Hokkaido, Japan, using echosounder and geostatistical analysis. *Fisheries Science*, *76*(5), 729–736. https://doi.org/10.1007/s12562-010-0270-2

Monagail, M. Mac, & Morrison, L. (2020). The seaweed resources of Ireland: a twenty-first century perspective. *Journal of Applied Phycology*, (January). https://doi.org/10.1007/s10811-020-02067-7

Mineur, F., Arenas, F., Assis, J., Davies, A. J., Engelen, A. H., Fernandes, F., Malta, E., Thibaut, T., Nguyen, T., Vaz-Pinto, F., Vranken, S., Serrao, E., & De Clerck, O. (2015). European seaweeds under pressure: consequences for communities and ecosystem functioning. *Journal of Sea Research*, *98*, 91–108. https://doi.org/10.1016/j.seares.2014.11.004

*Mountrakis, G., Im, J., & Ogole, C. (2011). Support vector machines in remote sensing: a review. *ISPRS Journal of Photogrammetry and Remote Sensing*, *66*(3), 247–259. https://doi.org/10.1016/j.isprsjprs.2010.11.001

Morrissey, K., C., Donoghue, & Hynes, S. (2011). Quantifying the value of multi-sectoral marine commercial activity in Ireland. *Marine Policy*, *35*(5), 721–727. https://doi.org/10.1016/j.marpol.2011.02.013

Mumby, P. J., Green, E. P., Edwards, A. J., & Clark, C. D. (1999). The cost-effectiveness of remote sensing for tropical coastal resources assessment and management. *Journal of Environmental Management*, *55*(3), 157–166. https://doi.org/10.1006/jema.1998.0255

Murfitt, S. L., Allan, B. M., Bellgrove, A., Rattray, A., Young, M. A., & Ierodiaconou, D. (2017). Applications of unmanned aerial vehicles in intertidal reef monitoring. *Scientific Reports*, *7*(1), 1–11. https://doi.org/10.1038/s41598-017-10818-9

Murray, E. V. (2007). Molluscs and Middens: The Archaeology of 'Ireland's Early Savage Race'? In Murphy, E., & Whitehouse, N. (2007), *Environmental Archaeology in Ireland*, Oxford: Oxbow Books.

Nagendra, H. (2001). Using remote sensing to assess biodiversity. *International Journal of Remote Sensing*, *22*(12), 2377–2400. https://doi.org/10.1080/01431160117096

Nahirnick, N. K., Reshitnyk, L., Campbell, M., Hessing-Lewis, M., Costa, M., Yakimishyn, J., & Lee, L. (2019). Mapping with confidence; delineating seagrass habitats using Unoccupied Aerial Systems (UAS). *Remote Sensing in Ecology and Conservation*, *5*(2), 121–135. https://doi.org/10.1002/rse2.98

Nicodemus, F., Richmond, J., Hsia, J., Ginsberg, I., & Limperis, T. (1977). Geometrical considerations and nomenclature for reflectance. *National Bureau of Standards*, 1–51. https://doi.org/10.1109/LPT.2009.2020494

NASA. (2016). TIROS. Retrieved from: https://science.nasa.gov/missions/tiros/ (Accessed: 31/10/2019)

Nisizawa, K., Noda, H., Kikuchi, R., & Watanabe, T. (1987). The main seaweed foods in Japan, 151, 24. https://doi.org/10.1117/12.2224081

NPWS. (2011). Roaringwater Bay and Islands SAC (site code: 101) Conservation objectives supporting document- marine habitats, (April), 31. Retrieved from: https://www.npws.ie/sites/default/files/publications/pdf/000101_Roaringwater Bay and Islands SAC Marine Supporting Doc_V1.pdf (Accessed: 30/11/2019)

NPWS. (2014). Site Synopsis: Roaringwater Bay and Islands SAC, 1–4. Retrieved from https://www.npws.ie/sites/default/files/protected-sites/synopsis/SY000101.pdf

Noel, C., Viala, C., Coquet, M., Zerr, B., & Perrot, T. (2008). Acoustic data fusion devoted to underwater vegetation mapping. *The Journal of the Acoustical Society of America*, *123*(5), 3951–3951. https://doi.org/10.1121/1.2936060

Noiraksar, T., Sawayama, S., Phauk, S., & Komatsu, T. (2014). Mapping *Sargassum* beds off the coast of Chon Buri Province, Thailand, using ALOS AVNIR-2 satellite imagery. *Botanica Marina*, *57*(5), 367–377. https://doi.org/10.1515/bot-2014-0015

Nomura, M., Kamogawa, H., Susanto, E., Kawagoe, C., Yasui, H., Saga, N., Hosohawa, M., & Miyashita, K. (2013). Seasonal variations of total lipids, fatty acid composition, and

fucoxanthin contents of *Sargassum horneri* (Turner) and *Cystoseira hakodatensis* (Yendo) from the northern seashore of Japan. *Journal of Applied Phycology, 25*(4), 1159–1169. https://doi.org/10.1007/s10811-012-9934-x

Norderhaug, K. M., Christie, H., Fosså, J. H., & Fredriksen, S. (2005). fish–macrofauna interactions in a kelp (*Laminaria hyperborea*) forest. *Journal of the Marine Biological Association of the United Kingdom*, 85(5), 1279–1286. https://doi.org/10.1017/S0025315405012439

Norton, T. A. (1969). Growth form and environment in *Saccorhiza polyschides*. *Journal of the Marine Biological Association of the United Kingdom*, 49(4), 1025–1045. https://doi.org/10.1017/S0025315400038078

Note, N., Gheyle, W., den Berghe, H. Van, Saey, T., Bourgeois, J., Van Eetvelde, V., Van Meirvenne, M., & Stichelbaut, B. (2018). A new evaluation approach of World War One's devastated front zone: A shell hole density map based on historical aerial photographs and validated by electromagnetic induction field measurements to link the metal shrapnel phenomenon. *Geoderma, 310*(October 2017), 257–269. https://doi.org/10.1016/j.geoderma.2017.09.029

O'Donohoe, G., Hensey, M., & O'Connor, B. (2000). Assessment of water quality data from Kilkieran Bay, Co. Galway. *Marine Environment and Health Series, 1*(November), 1–57. Retrieved from: https://oar.marine.ie/handle/10793/219 (Accessed: 31/10/2019)

O'Neill, J. D., Costa, M., & Sharma, T. (2011). Remote sensing of shallow coastal benthic substrates: In situ spectra and mapping of eelgrass (*Zostera marina*) in the Gulf Islands National Park Reserve of Canada. *Remote Sensing, 3*(5), 975–1005. https://doi.org/10.3390/rs3050975

Olofsson, P., Foody, G. M., Herold, M., Stehman, S. V., Woodcock, C. E., & Wulder, M. A. (2014). Good practices for estimating area and assessing accuracy of land change. *Remote Sensing of Environment, 148*(January 2013), 42–57. https://doi.org/10.1016/j.rse.2014.02.015

Olsen, J., Zechman, F., Hoarau, G., Coyer, J., Stam, W., Valero, M., Åberg, P. (2010). The phylogeographic architecture of the fucoid seaweed *Ascophyllum nodosum*: An intertidal "marine tree" and survivor of more than one glacial-interglacial cycle. *Journal of Biogeography*, 37(5), 842–856. https://doi.org/10.1111/j.1365-2699.2009.02262.x

Oppelt, N., Schulze, F., Bartsch, I., Doernhoefer, K., & Eisenhard, I. (2012). Hyperspectral classification approaches for intertidal macroalgae habitat mapping: a case study in Heligoland. *Optical Engineering, 51*(11), 111703. https://doi.org/10.1117/1.OE.51.11.111703

Otsu, K., Pla, M., Duane, A., Cardil, A., & Bronton, L. (2019). Estimating the threshold of detection on tree crown defoliation using vegetation indices from UAS multispectral imagery. *Drones*, *3*(4), 23. https://doi.org/10.3390/drones3040080

Palmer, J. D., Soltis, D. E., & Chase, M. W. (2004). The plant tree of life: an overview and some points of view. *American Journal of Botany*, 91(10), 1437–1445. https://doi.org/10.3732/ajb.91.10.1437

Paola, J. D., & Schowengerdt, R. A. (1995). A detailed comparison of backpropagation neural network and maximum-likelihood classifiers for urban land use classification.

Geoscience and Remote Sensing, IEEE Transactions, *33*(4), 981–996. https://doi.org/10.1109/36.406684

Parnum, I., Gavrilov, A. (2012). High-frequency seafloor acoustic backscatter from coastal marine habitats of Australia. *Proceedings of Acoustics 2012*, 1–5. http://www.acoustics.asn.au/conference_proceedings/AAS2012/papers/p93.pdf (Accessed: 02/12/2019)

Passaquet, C., Thomas, J. C., Caron, L., Hauswirth, N., Puel, F., & Berkuloff, C. (1991). Light-harvesting complexes of brown algae biochemical characterization and immunological relationships. *FEBS Letters*, *280*(1), 21–26. https://doi.org/10.1016/0014-5793(91)80195-9

Pauly, D. (1995). Anecdotes and the shifting baseline syndrome of fisheries. *Trends in Ecology & Evolution*, *10*(10), 430. https://doi.org/10.1016/S0169-5347(00)89171-5

Pauly, D., Christensen, V., Guénette, S., Pitcher, T. J., Sumaila, U. R., Walters, C. J., Zeller, D. (2002). Towards sustainability in world fisheries. *Nature*, *418*(6898), 689–695. https://doi.org/10.1038/nature01017

Pehlke, C., & Bartsch, I. (2008). Changes in depth distribution and biomass of sublittoral seaweeds at Helgoland (North Sea) between 1970 and 2005. *Climate Research*, 37(2-3), 135–147. https://doi.org/10.3354/cr00767

Pe'eri, S., Morrison, J. R., Short, F., Mathieson, A., Brook, A., & Trowbridge, P. (2008). Macroalgae and eelgrass mapping in Great Bay Estuary using AISA hyperspectral imagery. *A Final Report to The New Hampshire Estuaries Project*, *1*, 148pp. Retrieved from http://www.prep.unh.edu/resources/pdf/macroalgae_and_eelgrass-unh-09.pdf (Accessed: 31/10/2019)

Peddle, D. R., Peter White, H., Soffer, R. J., Miller, J. R., & LeDrew, E. F. (2001). Reflectance processing of remote sensing spectroradiometer data. *Computers and Geosciences*, *27*(2), 203–213. https://doi.org/10.1016/S0098-3004(00)00096-0

Pedersen, M., Nejrup, L., Fredriksen, S., Christie, H., & Norderhaug, K. (2012). Effects of wave exposure on population structure, demography, biomass and productivity of the kelp *Laminaria hyperborea*. *Marine Ecology Progress Series*, *451*, 45–60. https://doi.org/10.3354/meps09594

Peichl, L., Behrmann, G., & Kröger, R. H. H. (2001). For whales and seals the ocean is not blue: a visual pigment loss in marine mammals. *European Journal of Neuroscience*, *13*(8), 1520–1528. https://doi.org/10.1046/j.0953-816x.2001.01533.x

Petropoulos, G. P., Vadrevu, K. P., Xanthopoulos, G., Karantounias, G., & Scholze, M. (2010). A comparison of spectral angle mapper and artificial neural network classifiers combined with Landsat TM imagery analysis for obtaining burnt area mapping. *Sensors*, *10*(3), 1967–1985. https://doi.org/10.3390/s100301967

Pix4D. (2020). Do more GCPs equal more accurate drone maps? Retrieved from: https://www.pix4d.com/blog/GCP-accuracy-drone-maps (Accessed: 04/05/2020)

Pontius, R. G., & Millones, M. (2011). Death to Kappa: birth of quantity disagreement and allocation disagreement for accuracy assessment. *International Journal of Remote Sensing*, *32*(15), 4407–4429. https://doi.org/10.1080/01431161.2011.552923

Poore, A., Campbell, A., Coleman, R., Edgar, G., Jormalainen, V., Reynolds, P., Sotka, E., Stachoqicz, J., Taylor, E., Vanderklift, M., Duffy, E. (2012). Global patterns in the impact of marine herbivores on benthic primary producers. *Ecology Letters*, 15(8), 912–922. https://doi.org/10.1111/j.1461-0248.2012.01804.x

Popper, Z. A., Michel, G., Hervé, C., Domozych, D. S., Willats, W. G. T., Tuohy, M. G., Loareg, B., & Stengel, D. B. (2011). Evolution and diversity of plant cell walls: from algae to flowering plants. *Annual Review of Plant Biology*, 62(1), 567–590. https://doi.org/10.1146/annurev-arplant-042110-103809

Portell, J., Amblas, D., Mitchell, G., Morales, M., Villafranca, A. G., Iudica, R., & Lastras, G. (2019). High-performance compression of multibeam echosounders water column data. *IEEE Journal of Selected Topics in Applied Earth Observations and Remote Sensing*, *12*(6), 1771–1783. https://doi.org/10.1109/JSTARS.2019.2915844

Preston, J. (2009). Automated acoustic seabed classification of multibeam images of Stanton Banks. *Applied Acoustics*, 70(10), 1277–1287. http://dx.doi.org/10.1016/j.apacoust.2008.07.011

Quintino, V., Freitas, R., Mamede, R., Ricardo, F., Rodrigues, A. M., Mota, J., Pérez-Ruzafa, A., & Marcos, C. (2010). Remote sensing of underwater vegetation using single-beam acoustics. *ICES Journal of Marine Science*, 67, 594–605. https://doi.org/10.1093/icesjms/fsp251

Radoux, J., & Bogaert, P. (2017). Good practices for object-based accuracy assessment. *Remote Sensing*, *9*(7), 1-23. https://doi.org/10.3390/rs9070646

Ramus, J., Beale, S. I., Mauzerall, D., & Howard, K. L. (1976). Changes in photosynthetic pigment concentration in seaweeds as a function of water depth. *Marine Biology*, *37*(3), 223–229. https://doi.org/10.1007/BF00387607

Rasti, B., Scheunders, P., Ghamisi, P., Licciardi, G., & Chanussot, J. (2018). Noise reduction in hyperspectral imagery: Overview and application. *Remote Sensing*, *10*(3), 1–28. https://doi.org/10.3390/rs10030482

Raoult, V., Tosetto, L., Harvey, C., Nelson, T. M., Reed, J., Parikh, A., Chan, A., Smith, T., & Williamson, J. E. (2020). Remotely operated vehicles as alternatives to snorkellers for video-based marine research. *Journal of Experimental Marine Biology and Ecology*, *522*(May 2019), 151253. https://doi.org/10.1016/j.jembe.2019.151253

Reed, D., & Brezinski, M. (2009). Kelp forests. In. Laffoley, D., & Grimsditch, G. (2009). *The management of natural coastal carbon sinks (IUCN)*, Gland: SwissPrinters IRL

Remm, K., & Kelviste, T. (2014). An online calculator for spatial data and its applications. *Computational Ecology and Software*, *4*, 22–34. https://doi.org/10.0000/issn-2220-721x-compuecol-2014-v4-0003

Renard, V., & Allenou, J.-P. (1979). Sea Beam, Multibeam echosounding. *International Hydrographic Review*, *1*.

Reyes-Prieto, A., Weber, A. P. M., & Bhattacharya, D. (2007). The Origin and establishment of the plastid in algae and plants. *Annual Review of Genetics*, 41(1), 147–168. https://doi.org/10.1146/annurev.genet.41.110306.130134

Richards, J., & Jia, X. (2006) *Remote sensing digital image analysis: An introduction*.

Berlin: Spinger-Verlag

Riegl, B. M., Moyer, R. P., Morris, L. J., Virnstein, R. W., & Purkis, S. J. (2005). Distribution and seasonal biomass of drift macroalgae in the Indian River Lagoon (Florida, USA) estimated with acoustic seafloor classification (QTCView, Echoplus). *Journal of Experimental Marine Biology and Ecology*, *326*(1), 89–104. https://doi.org/10.1016/j.jembe.2005.05.009

Rinde, E., & Sjøtun, K. (2005). Demographic variation in the kelp *Laminaria hyperborea* along a latitudinal gradient. *Marine Biology*, *146*(6), 1051–1062. https://doi.org/10.1007/s00227-004-1513-5

Ringaby, E., Ahlberg, J., Wadströmer, N., & Forssén, P.-E. (2010). Co-aligning aerial hyperspectral push-broom strips for change detection. *Electro-Optical Remote Sensing, Photonic Technologies, and Applications IV*, *7835*(October), 78350Y. https://doi.org/10.1117/12.865034

Roberts, T., & Upham, P. (2012). Prospects for the use of macro-algae for fuel in Ireland and the UK: An overview of marine management issues. *Marine Policy*, *36*(5), 1047–1053. https://doi.org/10.1016/j.marpol.2012.03.001

Roelfsema, C., & Phinn, S. (2010). Integrating field data with high spatial resolution multispectral satellite imagery for calibration and validation of coral reef benthic community maps. *Journal of Applied Remote Sensing*, *4*(1), 043527. https://doi.org/10.1117/1.3430107

Saari, H., Pellikka, I., Pesonen, L., Tuominen, S., Heikkilä, J., Holmlund, C., Makynen, J., Ojala, K., & Antila, T. (2011). Unmanned Aerial Vehicle (UAV) operated spectral camera system for forest and agriculture applications. *Remote Sensing for Agriculture, Ecosystems, and Hydrology XIII* (Vol. 8174, p. 81740H). https://doi.org/10.1117/12.897585

Sabol, B. M., Melton, R., Chamberlain, R., Doering, P., & Haunert, K. (2002). Evaluation of a digital echo sounder system for detection of submersed aquatic vegetation. *Estuaries*, 25(1), 133–141. https://doi.org/10.1007/BF02696057

Sampath-Wiley, P., Neefus, C. D., & Jahnke, L. S. (2008). Seasonal effects of sun exposure and emersion on intertidal seaweed physiology: fluctuations in antioxidant contents, photosynthetic pigments and photosynthetic efficiency in the red alga *Porphyra umbilicalis* Kützing (Rhodophyta, Bangiales). *Journal of Experimental Marine Biology and Ecology*, *361*(2), 83–91. https://doi.org/10.1016/j.jembe.2008.05.001

Sánchez, Í., & Fernández, C. (2005). Impact of the invasive seaweed *Sargassum muticum* (Phaeophyta) on an intertidal macroalgal assemblage. *Journal of Phycology*, *41*(5), 923–930. https://doi.org/10.1111/j.1529-8817.2005.00120.x

Sandbrook, C. (2015). The social implications of using drones for biodiversity conservation. *Ambio*, *44*(S4), 636–647. https://doi.org/10.1007/s13280-015-0714-0

Sankey, T., Donager, J., McVay, J., & Sankey, J. B. (2017). UAV lidar and hyperspectral fusion for forest monitoring in the southwestern USA. *Remote Sensing of Environment*, *195*, 30–43. https://doi.org/10.1016/j.rse.2017.04.007

Schaepman-Strub, G., Schaepman, M. E., Painter, T. H., Dangel, S., & Martonchik, J. V. (2006). Reflectance quantities in optical remote sensing—definitions and case studies.

Remote Sensing of Environment, 103(1), 27–42. https://doi.org/10.1016/j.rse.2006.03.002

Scherner, F., Ventura, R., Barufi, J. B., & Horta, P. A. (2013). Salinity critical threshold values for photosynthesis of two cosmopolitan seaweed species: Providing baselines for potential shifts on seaweed assemblages. *Marine Environmental Research, 91*, 14–25. https://doi.org/10.1016/j.marenvres.2012.05.007

Schmid, M., Guihéneuf, F., & Stengel, D. B. (2017). Ecological and commercial implications of temporal and spatial variability in the composition of pigments and fatty acids in five Irish macroalgae. *Marine Biology*, *164*(8). https://doi.org/10.1007/s00227-017-3188-8

Schmidt, A. L., Coll, M., Romanuk, T. N., & Lotze, H. K. (2011). Ecosystem structure and services in eelgrass Zostera marina and rockweed *Ascophyllum nodosum* habitats. *Marine Ecology Progress Series*, 437, 51–68. https://doi.org/10.3354/meps09276

Schoenrock, K. M., O'Callaghan, T., O'Callaghan, R., & Krueger-Hadfield, S. A. (2019). First record of *Laminaria ochroleuca* Bachelot de la Pylaie in Ireland in Béal an Mhuirthead, County Mayo. *Marine Biodiversity Records, 12*(1), 9. https://doi.org/10.1186/s41200-019-0168-3

Schonbeck, M. W., & Norton, T. A. (1979). Drought-hardening in the upper-shore seaweeds *Fucus spiralis* and *Pelvetia canaliculata*. *The Journal of Ecology*, 67(2), 687. https://doi.org/10.2307/2259120

Schroeder, S. B., Dupont, C., Boyer, L., Juanes, F., & Costa, M. (2019). Passive remote sensing technology for mapping bull kelp (*Nereocystis luetkeana*): A review of techniques and regional case study. *Global Ecology and Conservation*, *19*, e00683. https://doi.org/10.1016/j.gecco.2019.e00683

Seeley, R. H., & Schlesinger, W. H. (2012). Sustainable seaweed cutting? The rockweed (*Ascophyllum nodosum*) industry of Maine and the Maritime Provinces. *Annals of the New York Academy of Sciences*, 1249(1), 84–103. https://doi.org/10.1111/j.1749-6632.2012.06443.x

Shao, H., Minami, K., Shirakawa, H., Kawauchi, Y., Matsukura, R., Tomiyasu, M., & Miyashita, K. (2019). Target strength of a common kelp species, *Saccharina japonica*, measured using a quantitative echosounder in an indoor seawater tank. *Fisheries Research*, *214*(May 2018), 110–116. https://doi.org/10.1016/j.fishres.2019.01.009

Sides, E. M., Picton, B. E., Emblow, C. S., Morrow, C. C., & Costello, M. J. (1994). Marine communities of Kilkieran Bay, the Aran Islands and the Skerd Rocks and an assessment of their conservation importance. Trinity College, Dublin. Retrieved from: https://www.npws.ie/content/publications/marine-communities-kilkieran-bay-aran-islands-and-skerd-rocks-and-assessment (Accessed: 31/10/2019)

Silva, T. S. F., Costa, M. P. F., Melack, J. M., & Novo, E. M. L. M. (2008). Remote sensing of aquatic vegetation: theory and applications. *Environmental Monitoring and Assessment*, *140*(1–3), 131–145. https://doi.org/10.1007/s10661-007-9855-3

Simms, É. L. (2005). Submerged kelp biomass assessment using CASI. *Coastal and Marine Geo-Information Systems*, 501–509. https://doi.org/10.1007/0-306-48002-6_36

Skoog, A. I. (2008). The Alfred Nobel rocket camera. An early aerial photography attempt. *International Astronautical Federation - 59th International Astronautical Congress 2008, IAC 2008*, 14(3–4), 9229–9243. https://doi.org/10.1016/j.actaastro.2009.06.011

Slaton, M. R., Raymond Hunt, E., & Smith, W. K. (2001). Estimating near-infrared leaf reflectance from leaf structural characteristics. *American Journal of Botany*, *88*(2), 278–284. https://doi.org/10.2307/2657019

Smale, D. A., Burrows, M., Moore, P., O'Connor, N., & Hawkins, S. (2013). Threats and knowledge gaps for ecosystem services provided by kelp forests: a northeast Atlantic perspective, *Ecology and Evolution*, *3*(11). https://doi.org/10.1002/ece3.774

Smale, D. A. (2019). Impacts of ocean warming on kelp forest ecosystems. *New Phytologist*, nph.16107. https://doi.org/10.1111/nph.16107

Smith. G., & Milton, E. (1999). The use of the empirical line method to calibrate remotely sensed data to reflectance. *International Journal of Remote Sensing*, *20*(13), 2653-2662. https://doi.org/10.1080/014311699211994

Smith, R. (2012). Introduction to remote sensing of environment (RSE), MicroImages Inc. https://www.microimages.com/documentation/Tutorials/introrse.pdf (Accessed: 02/12/2019)

Spalding, H., Foster, M. S., & Heine, J. N. (2003). Composition, distribution and abundance of deep-water (>30 m) macroalgae in central California. *Journal of Phycology*, *39*(2), 273–284. https://doi.org/10.1046/j.1529-8817.2003.02010.x

South, S., Qi, J., & Lusch, D. P. (2004). Optimal classification methods for mapping agricultural tillage practices. *Remote Sensing of Environment*, *91*(1), 90–97. https://doi.org/10.1016/j.rse.2004.03.001

Stanton, T. K. (2012). 30 years of advances in active bioacoustics: A personal perspective. *Methods in Oceanography*, 1-2, 49–77. https://doi.org/10.1016/j.mio.2012.07.002

St-Pierre, A. P., & Gagnon, P. (2020). Kelp-bed dynamics across scales: enhancing mapping capability with remote sensing and GIS. *Journal of Experimental Marine Biology and Ecology*, *522*(May 2019), 151246. https://doi.org/10.1016/j.jembe.2019.151246

Stekoll, M. S., Deysher, L. E., & Hess, M. (2006). A remote sensing approach to estimating harvestable kelp biomass. *Journal of Applied Phycology*, *18*(3–5), 323–334. https://doi.org/10.1007/s10811-006-9029-7

Steneck, R., Graham, M., Bourque, B., Corbett, D., Erlandson, J. M., Estes, J., Tegner, M. (2002). Kelp forest ecosystems: Biodiversity, stability, resilience and future. *Environmental Conservation*, *29*(4), 439–459. https://doi.org/10.1017/S0376892902000322

Steneck, R. S., Bustamante, R. H., Dayton, P. K., Jones, G. P., & Hobday, A. J. (2008). Current status and future trends in kelp forest ecosystems. In N. V. C. Polunin (Ed.), *Aquatic Ecosystems* (pp. 226–241). Cambridge: Cambridge University Press. https://doi.org/10.1017/CBO9780511751790.021

Stengel, D. B., & Dring, M. J. (1997). Morphology and *in-situ* growth rates of plants of *Ascophyllum nodosum* (Phaeophyta) from different shore levels and responses of plants

to vertical transplantation. *European Journal of Phycology*, *32*(2), 193–202. https://doi.org/10.1017/S0967026297001200

Stengel, D. B., & Dring, M. J. (1998). Seasonal variation in the pigment content and photosynthesis of different thallus regions of *Ascophyllum nodosum* (Fucales, Phaeophyta) in relation to position in the canopy. *Phycologia*, *37*(4), 259–268. https://doi.org/10.2216/i0031-8884-37-4-259.1

Stengel, D., Wilkes, R., & Guiry, M. (1999). Seasonal growth and recruitment of *Himanthalia elongata* (Fucales, Phaeophycota) in different habitats on the Irish west coast. *European Journal of Phycology*, 34(3), 213–221. https://doi.org/10.1080/09670269910001736272

Stephenson, T. A., & Stephenson, A. (1949). The universal features of zonation between tide-marks on rocky coasts, *Journal of Ecology*, *37*(2), 289–305. http://www.jstor.org/stable/2256610

Stevens, J. P., Blackstock, T. H., Howe, E. A., & Stevens, D. P. (2004). Repeatability of Phase 1 habitat survey. *Journal of Environmental Management*, *73*(1), 53–59. https://doi.org/10.1016/j.jenvman.2004.05.009

Su, H., Karna, D., Fraim, E., Fitzgerald, M., Dominguez, R., Myers, J. S., Coffland, B., Handley, L., & Mace, T. (2006). Evaluation of eelgrass beds mapping using a high-resolution airborne multispectral scanner. *Photogrammetric Engineering & Remote Sensing*, *72*(7), 789–797. https://doi.org/10.14358/PERS.72.7.789

Taddia, Y., Russo, P., Lovo, S., & Pellegrinelli, A. (2019). Multispectral UAV monitoring of submerged seaweed in shallow water. *Applied Geomatics*. 1-16. https://doi.org/10.1007/s12518-019-00270-x

Tait, L., Bind, J., Charan-Dixon, H., Hawes, I., Pirker, J., & Schiel, D. (2019). Unmanned Aerial Vehicles (UAVs) for monitoring macroalgal biodiversity: Comparison of RGB and multispectral imaging sensors for diodiversity assessments. *Remote Sensing*, *11*(19), 2332. https://doi.org/10.3390/rs11192332

Tatem, A. J., Goetz, S. J., & Hay, S. I. (2009). UKPMC Funders Group Fifty Years of Earth Observation Satellites. *American Scientist*, *96*(5), 1–7. https://doi.org/10.1511/2008.74.390

Tay, J. Y. L., Erfmeier, A., & Kalwij, J. M. (2018). Reaching new heights: can drones replace current methods to study plant population dynamics? *Plant Ecology*, *219*(10), 1139–1150. https://doi.org/10.1007/s11258-018-0865-8

Teagle, H., Hawkins, S. J., Moore, P. J., & Smale, D. A. (2017). The role of kelp species as biogenic habitat formers in coastal marine ecosystems. *Journal of Experimental Marine Biology and Ecology*, *492*, 81–98. https://doi.org/10.1016/j.jembe.2017.01.017

Theimann, S., & Inka, B. (2005). Biotope mapping of the intertidal zone of Heligoland (North Sea) using hyperspectral remote sensing images, 802(20), 20. Retrieved from http://epic.awi.de/Publications/Thi2005j.pdf (Accessed: 31/10/2019)

Thenkabail, P. (2015) *Remotely sensed data characterisation, classification and accuracies*. Miami: CRC Press. https://doi.org/10.1201/b19294

Thomas, V., Treitz, P., Jelinski, D., Miller, J., Lafleur, P., & McCaughey, J. H. (2003). Image classification of a northern peatland complex using spectral and plant community

data. *Remote Sensing of Environment, 84*(1), 83–99. https://doi.org/10.1016/S0034-4257(02)00099-8

Thomson, A. G., Fuller, R. M., Sparks, T. H., Yates, M. G., & Eastwood, J. A. (1998). Ground and airborne radiometry over intertidal surfaces: waveband selection for cover classification. *International Journal of Remote Sensing, 19*(6), 1189–1205. https://doi.org/10.1080/014311698215685

Thomson, A. G., Eastwood, J. A., Yates, M. G., Fuller, R. M., Wadsworth, R. A., & Cox, R. (1999). Airborne remote sensing of intertidal biotopes: BIOTA I. *Marine Pollution Bulletin, 37*(3–7), 164–172. https://doi.org/10.1016/S0025-326X(98)00119-2

Tirichine, L., & Bowler, C. (2011). Decoding algal genomes: tracing back the history of photosynthetic life on Earth. *Plant Journal, 66*(1), 45–57. https://doi.org/10.1111/j.1365-313X.2011.04540.x

Tou, J., & Gonzalez, R. (1974). *Pattern recognition principles.* Reading: Addison-Wesley Publishing Co.

Transon, J., d'Andrimont, R., Maugnard, A., & Defourny, P. (2018). Survey of hyperspectral Earth Observation applications from space in the Sentinel-2 context. *Remote Sensing, 10*(2), 1–32. https://doi.org/10.3390/rs10020157

Treitz, P., & Howarth, P. (2000). High spatial resolution remote sensing data for forest ecosystem classification: an examination of spatial scale. *Remote Sensing of Environment, 72*(3), 268–289. https://doi.org/10.1016/S0034-4257(99)00098-X

Tully, O., & O'Ceidigh, P. (1989). The ichthyoneuston of Galway Bay (Ireland). *Marine Biology, 101*, 27–41. Retrieved from: https://link.springer.com/article/10.1007/BF00393475 (Accessed: 31/10/2019)

Uhl, F., Oppelt, N., & Bartsch, I. (2013). Spectral mixture of intertidal marine macroalgae around the island of Helgoland (Germany, North Sea). *Aquatic Botany, 111*, 112–124. https://doi.org/10.1016/j.aquabot.2013.06.001

Uhl, F., Bartsch, I., & Oppelt, N. (2016). Submerged kelp detection with hyperspectral data. *Remote Sensing, 8*(6), 487. https://doi.org/10.3390/rs8060487

Ullah, A., Rundquist, D., & Derry, D. (2000). Characterising spectral signatures for three selected emergent aquatic macrophytes: A controlled experiment. *Geocarto International, 15*(4), 29–39. Retrieved from http://calmit.unl.edu/people/drundquist1/pdf/2000/Ullah 2000 15-4-29-39.pdf (Accessed: 31/10/2019)

USGS. (2019) https://www.usgs.gov/land-resources/nli/landsat/landsat-satellite-issions?qt-science_support_page_related_con=2#qt-science_support_page_related_con (Accessed: 31/10/19)

Vabson, V., Kuusk, J., Ansko, I., Vendt, R., Alikas, K., Ruddick, K., Ansper, A., Bresciani, M., Burmester, H., Costa, M., D'Alimonte, D., Dall'Olmo, G., Damiri, B., Dinter, T., Giardino, C., Kangro, K., Ligi, M., Paavel, B., Tilstone, G., Van Dommelen, D., Wiegmann, S., Bracher, A., Donlon, C., & Casal, T. (2019). Field intercomparison of radiometers used for satellite validation in the 400–900 nm range. *Remote Sensing, 11*(9), 1129. https://doi.org/10.3390/rs11091129

Vadas, Sr., R. L., Wright, W. a., & Beal, B. F. (2004). Biomass and productivity of intertidal rockweeds (*Ascophyllum nodosum* LeJolis) in Cobscook Bay. *Northeastern Naturalist, 11*(2). https://www.jstor.org/stable/60225652

Vahtmäe, E., & Kutser, T. (2013). Classifying the Baltic sea shallow water habitats using image-based and spectral library methods. *Remote Sensing*, *5*(5), 2451–2474. https://doi.org/10.3390/rs5052451

Valle, M., Palà, V., Lafon, V., Dehouck, A., Garmendia, J. M., Borja, Á., & Chust, G. (2015). Mapping estuarine habitats using airborne hyperspectral imagery, with special focus on seagrass meadows. *Estuarine, Coastal and Shelf Science*, *164*, 433–442. https://doi.org/10.1016/j.ecss.2015.07.034

van Deventer, H., Cho, M. A., & Mutanga, O. (2019). Multi-season RapidEye imagery improves the classification of wetland and dryland communities in a subtropical coastal region. *ISPRS Journal of Photogrammetry and Remote Sensing*, *157*(February), 171–187. https://doi.org/10.1016/j.isprsjprs.2019.09.007

van Iersel, W., Straatsma, M., Middelkoop, H., & Addink, E. (2018). Multitemporal classification of river floodplain vegetation using time series of UAV images. *Remote Sensing*, *10*(7), 1144. https://doi.org/10.3390/rs10071144

Ventura, D., Bonifazi, A., Gravina, M. F., Belluscio, A., & Ardizzone, G. (2018). Mapping and classification of ecologically sensitive marine habitats using Unmanned Aerial Vehicle (UAV) imagery and object-based image analysis (OBIA). *Remote Sensing*, *10*(9), 1–23. https://~doi.org/10.3390/rs10091331

Vis, C., Hudon, C., & Carignan, R. (2003). An evaluation of approaches used to determine the distribution and biomass of emergent and submerged aquatic macrophytes over large spatial scales. *Aquatic Botany*, *77*(3), 187–201. https://doi.org/10.1016/S0304-3770(03)00105-0

Walker, D. I., & Kendrick, G. A. (1998). Threats to macroalgal diversity: marine habitat destruction and fragmentation, pollution and introduced species. *Botanica Marina*, *41*(1), 105–112. https://doi.org/10.1515/botm.1998.41.1-6.105

Walsh, M., & Watson, L. (2011). A market analysis towards the further development of seaweed aquaculture in Ireland. *Irish Sea Fisheries Board, Dublin*, *Part 1*, 1–48. Retrieved from: http://scholar.google.com/scholar?hl=en&btnG=Search&q=intitle:A+Market+Analysis+towards+the+Further+Development+of+Seaweed+Aquaculture+in+Ireland#6 (Accessed: 01/11/2019)

Warren, J. D., & Peterson, B. J. (2007). Use of a 600-kHz Acoustic Doppler Current Profiler to measure estuarine bottom type, relative abundance of submerged aquatic vegetation, and eelgrass canopy height. *Estuarine, Coastal and Shelf Science*, *72*(1–2), 53–62. https://doi.org/10.1016/j.ecss.2006.10.026

Warren, G. (2015). "Mere food gatherers they, parasites upon nature...": Food and drink in the Mesolithic of Ireland. *Proceedings of the Royal Irish Academy, Section C: Archaeology, Celtic Studies, History, Linguistics and Literature*, *115*(1), 1–26. https://doi.org/10.3318/PRIAC.2015.115.09

Watts, A. C., Ambrosia, V. G., & Hinkley, E. A. (2012). Unmanned aircraft systems in remote sensing and scientific research: classification and considerations of use. *Remote Sensing*, *4*(6), 1671–1692. https://doi.org/10.3390/rs4061671

Webb, D. (1966). William Henry Harvey 1811-1866 and the tradition of systematic botany. *Hermathena*, *103*, 32–45. https://www.jstor.org/stable/23039826

Weber, T. C., Peña, H., & Jech, J. M. (2009). Consecutive acoustic observations of an Atlantic herring school in the Northwest Atlantic. *ICES Journal of Marine Science*, *66*(6), 1270–1277. https://doi.org/10.1093/icesjms/fsp090

Webster, T., MacDonald, C., McGuigan, K., Crowell, N., Lauzon-Guay, J.-S., and Collins, K. (2020). Calculating macroalgal height and biomass using bathymetric LiDAR and a comparison with surface area derived from satellite data in Nova Scotia, Canada. *Botanica Marina*, *63*(1), 43–59. https://doi.org/10.1515/bot-2018-0080

Weil, G., Lensky, I. M., Resheff, Y. S., & Levin, N. (2017). Optimizing the timing of unmanned aerial vehicle image acquisition for applied mapping of woody vegetation species using feature selection. *Remote Sensing*, *9*(11). https://doi.org/10.3390/rs9111130

Wernberg, T. (2005). Holdfast aggregation in relation to morphology, age, attachment and drag for the kelp *Ecklonia radiata*. *Aquatic Botany*, *82*(3), 168–180. https://doi.org/10.1016/j.aquabot.2005.04.003

Wernberg, T., Thomsen, M. S., Tuya, F., Kendrick, G. A., Staehr, P. A., & Toohey, B. D. (2010). Decreasing resilience of kelp beds along a latitudinal temperature gradient: potential implications for a warmer future. *Ecology Letters*, *13*(6), 685–694. https://doi.org/10.1111/j.1461-0248.2010.01466.x

Wernberg, T., Russell, B. D., Thomsen, M. S., Gurgel, C. F. D., Bradshaw, C. J. A., Poloczanska, E. S., & Connell, S. D. (2011). Seaweed communities in retreat from ocean warming. *Current Biology*, *21*(21), 1828–1832. https://doi.org/10.1016/j.cub.2011.09.028

Wernberg, T., Krumhansl, K., Filbee-Dexter, K., & Pedersen, M. F. (2019). Status and trends for the world's kelp forests. In Shappard, C. (2019) *World seas: An environmental evaluation* (pp. 57–78). Cambridge: Elsevier https://doi.org/10.1016/B978-0-12-805052-1.00003-6

Westoby, M. J., Brasington, J., Glasser, N. F., Hambrey, M. J., & Reynolds, J. M. (2012). "Structure-from-Motion" photogrammetry: a low-cost, effective tool for geoscience applications. *Geomorphology*, *179*, 300–314. https://doi.org/10.1016/j.geomorph.2012.08.021

Westropp, M. (1920) *Irish glass: an account of glassmaking in Ireland from the XVIth century to the present day*. London: Herbert Jenkins Limited

Wheeler, W. N. (1990). Kelp forests of British Columbia: A unique resource. *Fisheries Development Report 37*.

Wich, S., Dellatore, D., Houghton, M., Ardi, R., & Koh, L. P. (2016). A preliminary assessment of using conservation drones for Sumatran orang-utan (*Pongo abelii*) distribution and density. *Journal of Unmanned Vehicle Systems*, *4*(1), 45–52. https://doi.org/10.1139/juvs-2015-0015

Wigmore, O., Mark, B., McKenzie, J., Baraer, M., & Lautz, L. (2019). Sub-metre mapping of surface soil moisture in proglacial valleys of the tropical Andes using a multispectral

unmanned aerial vehicle. *Remote Sensing of Environment*, *222*(January 2018), 104–118. https://doi.org/10.1016/j.rse.2018.12.024

Wilkinson, M., Wood, P., Wells, E., & Scanlan, C. (2007). Using attached macroalgae to assess ecological status of British estuaries for the European Water Framework Directive. *Marine Pollution Bulletin*, 55(1–6), 136–150. https://doi.org/10.1016/j.marpolbul.2006.09.004

Wilson, C. J., Wilson, P. S., & Dunton, K. H. (2013). Assessing the low frequency acoustic characteristics of *Macrocystis pyrifera*, *Egregia menziessi*, and *Laminaria solidungula*. *The Journal of the Acoustical Society of America*, *133*(6), 3819–3826. https://doi.org/10.1121/1.4802637

Windle, A. E., Poulin, S. K., Johnston, D. W., & Ridge, J. T. (2019). Rapid and accurate monitoring of intertidal oyster reef habitat using unoccupied aircraft systems and structure from motion. *Remote Sensing*, *11*(20), 2394. https://doi.org/10.3390/rs11202394

Worm, B., & Chapman, A. R. O. (1996). Interference competition among two intertidal seaweeds: *Chondrus crispus* strongly affects survival of *Fucus evanescens* recruits. *Marine Ecology Progress Series*, *145*(1–3), 297–301. https://doi.org/10.3354/meps145297

Wu, D., & Sun, D. W. (2013). Advanced applications of hyperspectral imaging technology for food quality and safety analysis and assessment: A review - Part I: Fundamentals. *Innovative Food Science and Emerging Technologies*, *19*, 1–14. https://doi.org/10.1016/j.ifset.2013.04.014

Xu, H. (2006). Modification of normalised difference water index (NDWI) to enhance open water features in remotely sensed imagery. *International Journal of Remote Sensing*, *27*(14), 3025–3033. https://doi.org/10.1080/01431160600589179

Yang, L., Huang, C., Homer, C. G., Wylie, B. K., & Coan, M. J. (2003). An approach for mapping large-area impervious surfaces: synergistic use of Landsat-7 ETM+ and high spatial resolution imagery. *Canadian Journal of Remote Sensing*, *29*(2), 230–240. https://doi.org/10.5589/m02-098

Yang, C., Everitt, J., & Bradford, J. (2008). Yield estimation from hyperspectral imagery using Spectral Angle Mapper (SAM). *Transactions of the ASABE*, *51*(2), 729–737. https://doi.org/10.13031/2013.24370

Yesson, C., Bush, L. E., Davies, A. J., Maggs, C. A., & Brodie, J. (2015). Large brown seaweeds of the British Isles: evidence of changes in abundance over four decades. *Estuarine, Coastal and Shelf Science*, 155, 167–175. https://doi.org/10.1016/j.ecss.2015.01.008

Yoo, C. I., Oh, Y. S., & Choi, Y. J. (2018). Coastal mapping of jinu-Do with UAV for Busan smart city, Korea. *International Archives of the Photogrammetry, Remote Sensing and Spatial Information Sciences - ISPRS Archives*, *42*(4), 101–106. https://doi.org/10.5194/isprs-archives-XLII-4-725-2018

Yuhas, R., Goetz, A., & Boardman, J. (1992). Discrimination among semi-arid landscape endmembers using the spectral angle mapper (SAM) algorithm, 147–149. Retrieved from https://ntrs.nasa.gov/archive/nasa/casi.ntrs.nasa.gov/19940012238.pdf (Accessed: 31/10/2019)

Zoffoli, M. L., Frouin, R., & Kampel, M. (2014). Water column correction for coral reef studies by remote sensing. *Sensors* (Switzerland) (Vol. 14). https://doi.org/10.3390/s140916881

Appendix

Sailor the dog assisting with spectral reflectance sampling.

Chapter 2

```
=INDEX($X$10:$X$201:Y$10:Y$201,MATCH($BD10,$X$10:$X$201,1),2)+($BD10-
INDEX($X$10:$X$201:Y$10:Y$201,MATCH($BD10,$X$10:$X$201,1),1))*(INDEX($X$10:$X$201:Y$1
0:Y$201,MATCH($BD10,$X$10:$X$201,1)+1,2)-
INDEX($X$10:$X$201:Y$10:Y$201,MATCH($BD10,$X$10:$X$201,1),2))/(INDEX($X$10:$X$201:Y$1
0:Y$201,MATCH($BD10,$X$10:$X$201,1)+1,1)-
INDEX($X$10:$X$201:Y$10:Y$201,MATCH($BD10,$X$10:$X$201,1),1))
```

Fig. S2.1. Linear interpolation formula used in Microsoft Excel.

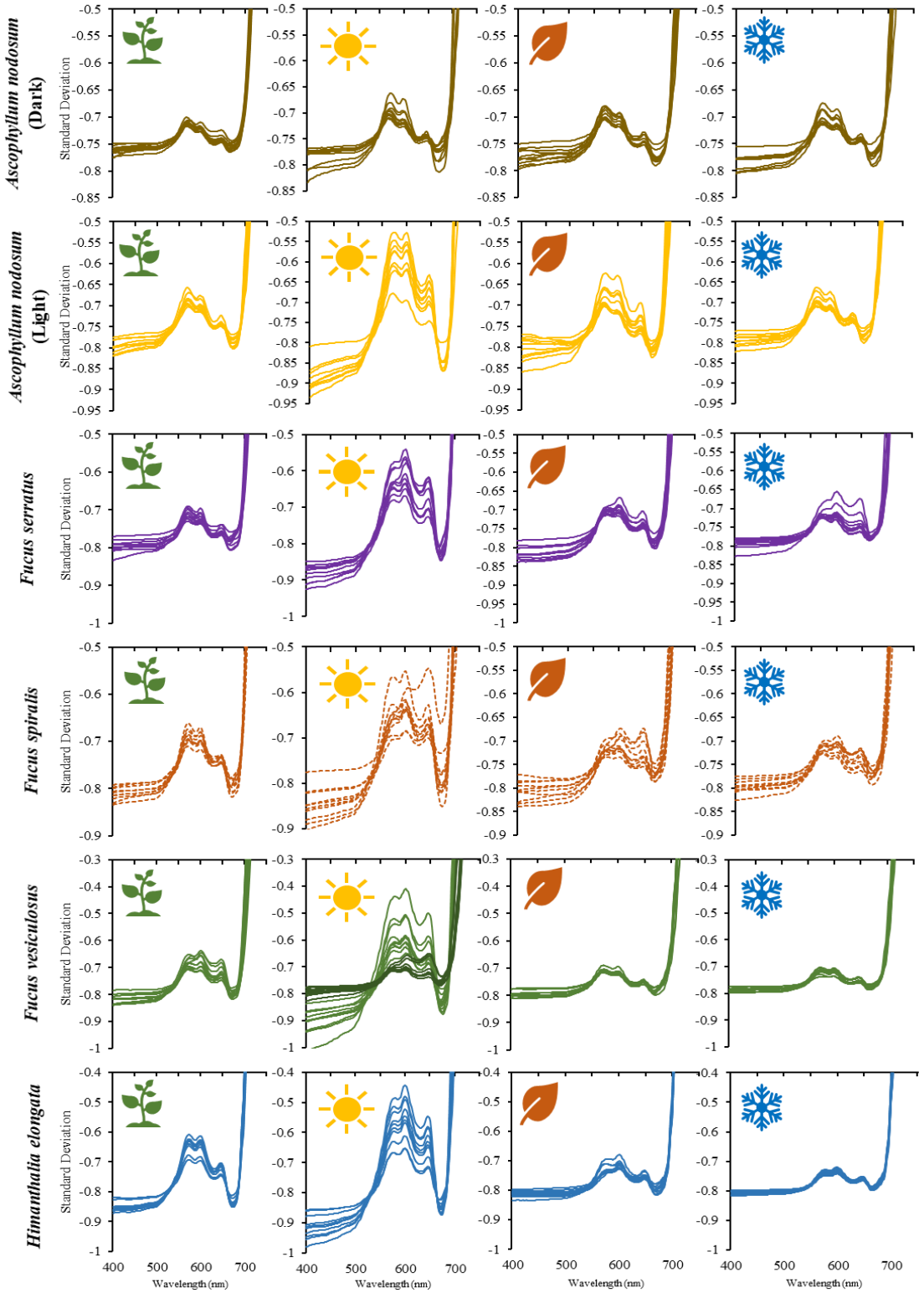
Ascophyllum nodosum (Dark)
Ascophyllum nodosum (Light)
Fucus serratus
Fucus spiralis
Fucus vesiculosus
Himanthalia elongata
Standard Deviation
Wavelength (nm)

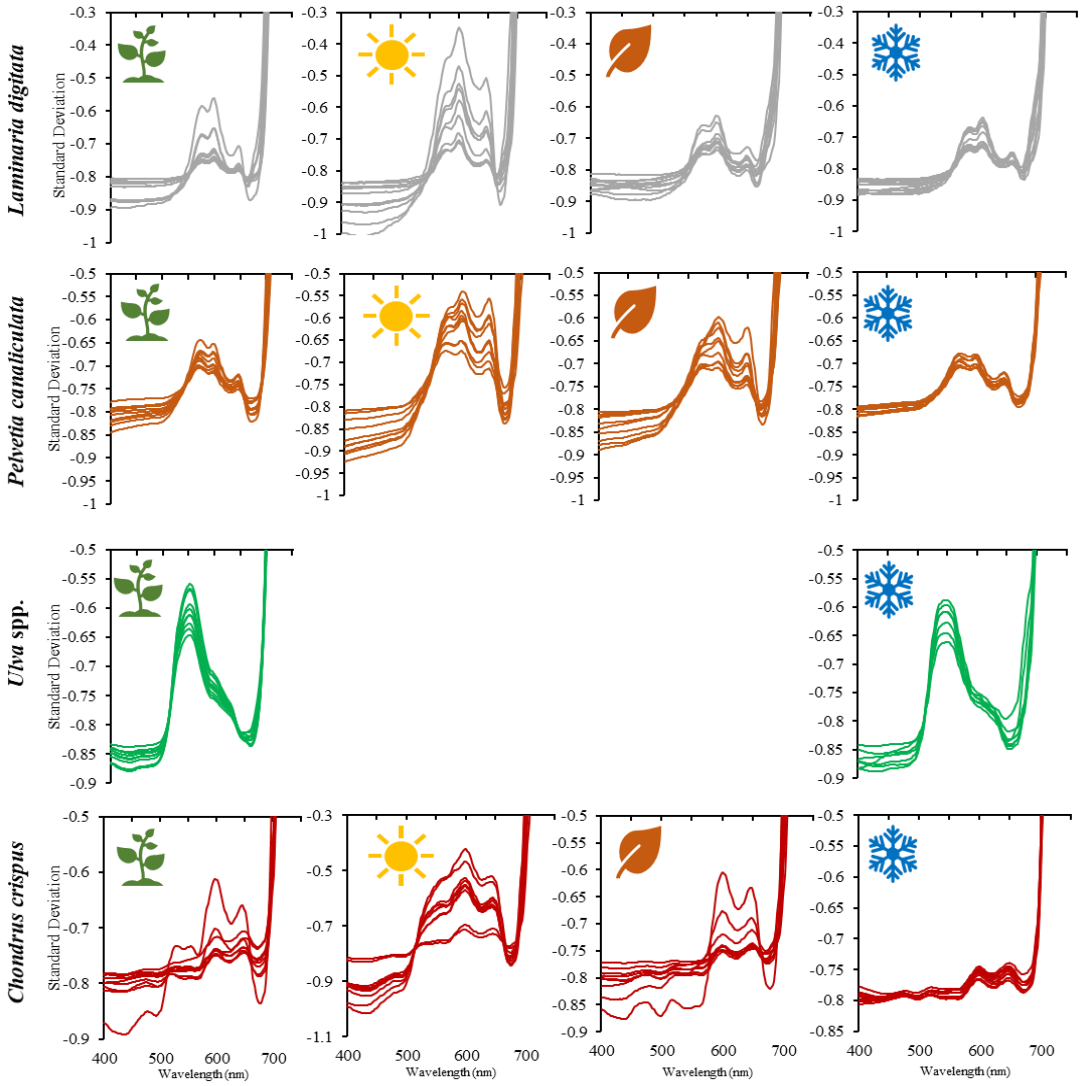

Fig. S2.2. Seasonal variation in sampled species reflectance spectra (10 replicates for each species) sampled using a spectroradiometer during spring, summer, autumn and winter 2018 in Carraroe (Co. Galway). Gaps for *Ulva* spp. represent seasons where no measurements were carried out.

Chapter 3

Tab. S3.1. Previous data for intertidal hyperspectral survey spatial resolutions, or ground sampling distance (GSD) (m/pixel) achieved using airborne remote sensing platforms and the average survey flight height.

Study	**Flight Height**	**Pixel Resolution (GSD**
Theimann & Bartsch (2007)	1600m	1 m
Costa *et al.* (2007)	1520 m	2 m
Dekker *et al*. (2003)	2500 m / 550 m	4 m / 0.8 m
Hennig *et al.* (2007)	1600 m	1 m
Oppelt *et al.* (2012)	690 m	1 m
Garono *et al*. (2004)	1140 m	1.5 m

Tab. S3.2. Spectral separability results of the Jeffries-Matusita Distance for image-derived spectra, calculated using ENVI 5.4. Class pairings are ranked in order of separability, from low to high.

Class Pairs	
Kelp - Submerged	1.780114
Him- Kelp	1.94819
Asco - *Fucus* spp	1.967773
Fucus spp - Him	1.969406
Submerged - Substratum	1.987847
Fucus spp - Him	1.990936
Asco - PelC	1.994388
Fucus spp - Kelp	1.996708
Asco - Him	1.996934
PelC- Substratum	1.997263
Kelp - Substratum	1.997935
Him - Submerged	1.998164
Fucus spp - Substratum	1.999288
Him - PelC	1.999396
Fucus spp - Submerged	1.999423
Kelp - PelC	1.999598
PelC - Submerged	1.999599
Asco - Kelp	1.999743
Him - Substratum	1.999817
Asco - Submerged	1.999967
Asco - Substratum	1.999972
Fucus spp - Green	1.999998
Him - Green	1.999999
Kelp - Green	1.999999
Submerged - Green	2
Asco - Green	2
PelC - Green	2
Substratum - Green	2

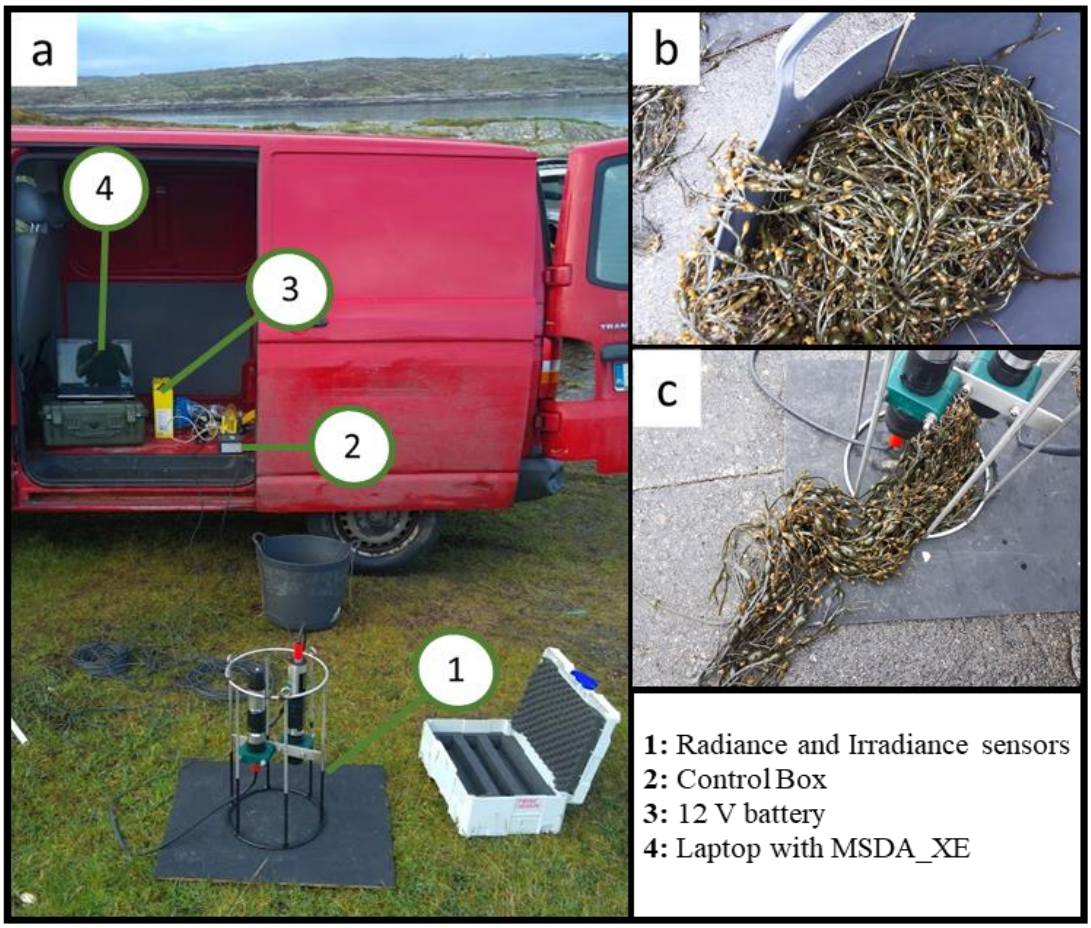

Fig. S3.1. The setup of the spectroradiometer is (**a**). Samples are collected from the intertidal zone and quickly brought to the measurement area in a bucket containing seawater (**b**) and are then arranged to cover the entire ground field of view (GFOV) of the downward facing radiance sensor (**c**).

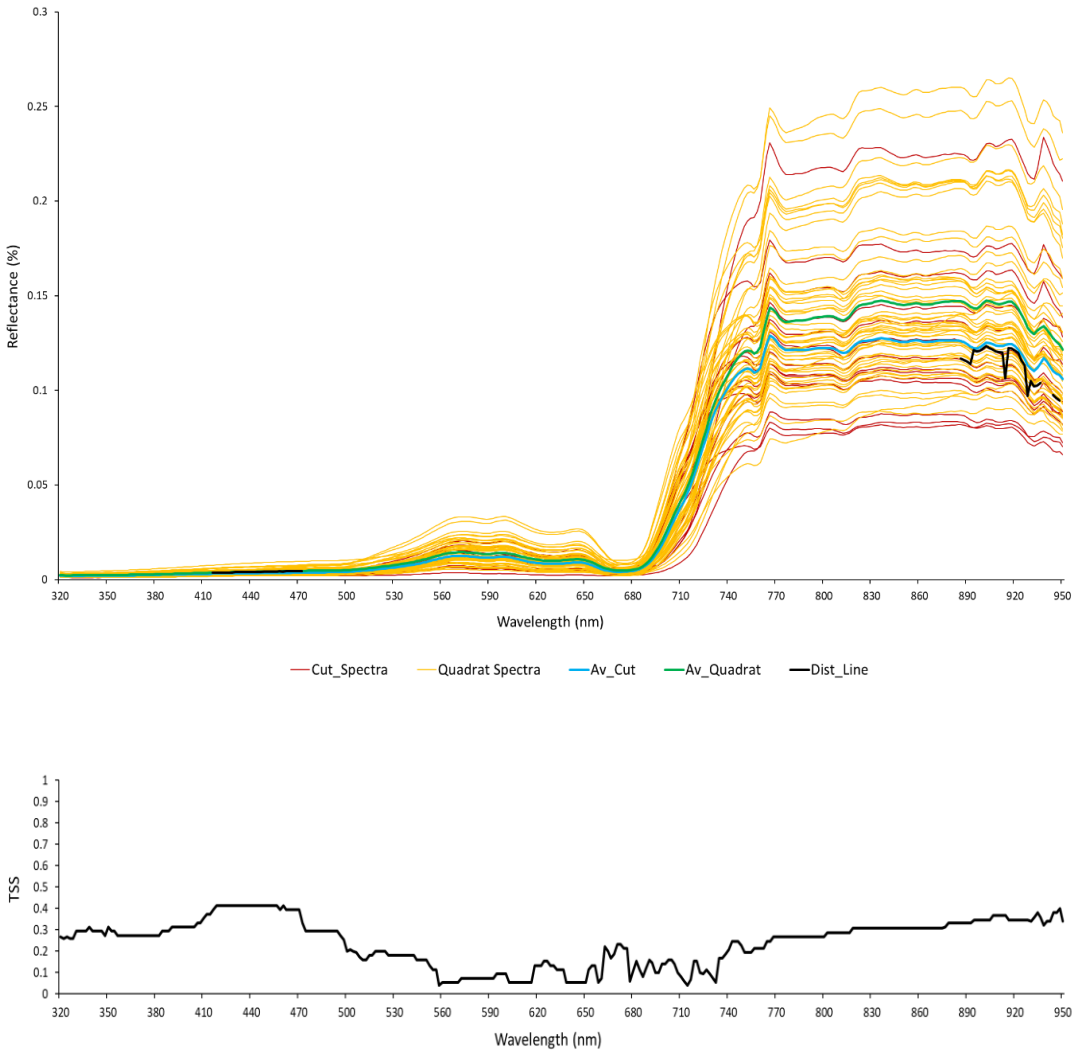

Fig. S3.2. Spectral separability results comparing canopy spectra ('Quadrat Spectra') to spectra of individual seaweed samples removed from the canopy for measurement ('Cut Spectra'). The black line ('Dist_Line') represents the optimum separation boundary between both classes for wavelengths that were statistically separable based upon the results of a Mann-Whitney U test. True Skill Statistic (TSS) is shown below where a value of 1 indicates perfect separation between two samples and 0 indicates a random decision. The averaged spectra for 'Cut_Spectra' and 'Quadrat-Spectra' are shown respectively in the blue and green lines. Further details of the applied methodology can be found in Kotta *et al*. (2014).

Fig. S3.3. Training polygons for all classes. The same class polygons were used for assessing the accuracy of both classifiers (MLC & SAM). The black lines mark the boundary of the hyperspectral data strips, and the background image is from the high resolution RGB UAV survey. Coordinates are in Irish Transverse Mercator (ITM). Class codes represent the following species. *Ascophyllum nodosum* (Asco), mixed fucoids (*Fucus* spp), unidentified green species (Green), *Himanthalia elongata* (Him), *Laminaria digitata* (Kelp), *Pelvetia canaliculata* (PelC), unidentified submerged macroalgae (Submerged), combined substratum (Substratum).

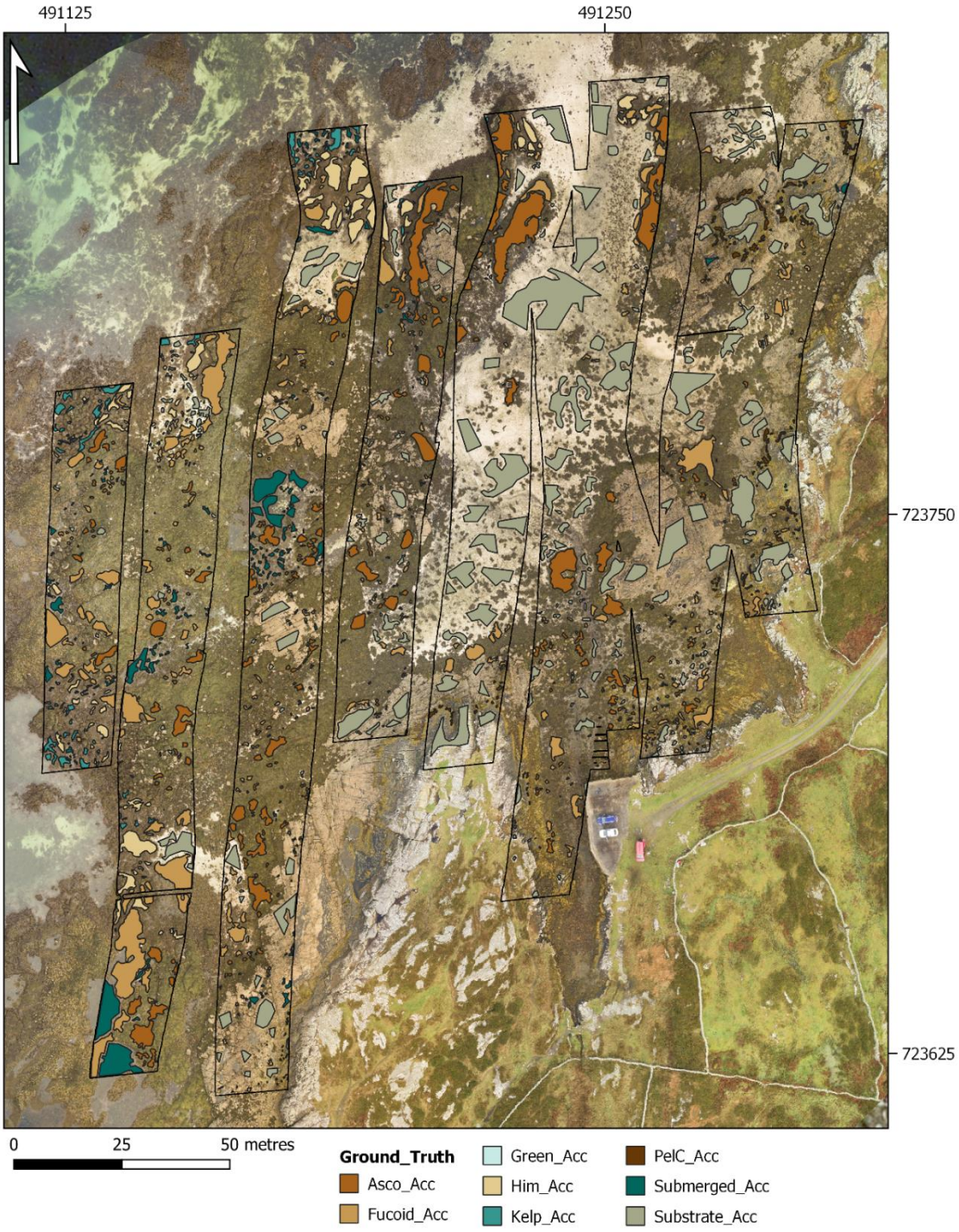

Fig. S3.4. Ground truth polygons for all classes. The same class polygons were used for assessing the accuracy of both classifiers (MLC & SAM). The black lines mark the boundary of the hyperspectral data strips, and the background image is from the high resolution RGB UAV survey. Coordinates are in Irish Transverse Mercator (ITM). Class codes represent the following species. *Ascophyllum nodosum* (Asco_Acc), mixed fucoids (Fucoid_Acc), unidentified green species (Green_Acc), *Himanthalia elongata* (Him_Acc), *Laminaria digitata* (Kelp_Acc_, *Pelvetia canaliculata* (PelC_Acc), unidentified submerged macroalgae (Submerged_Acc), combined substratum (Substrate_Acc).

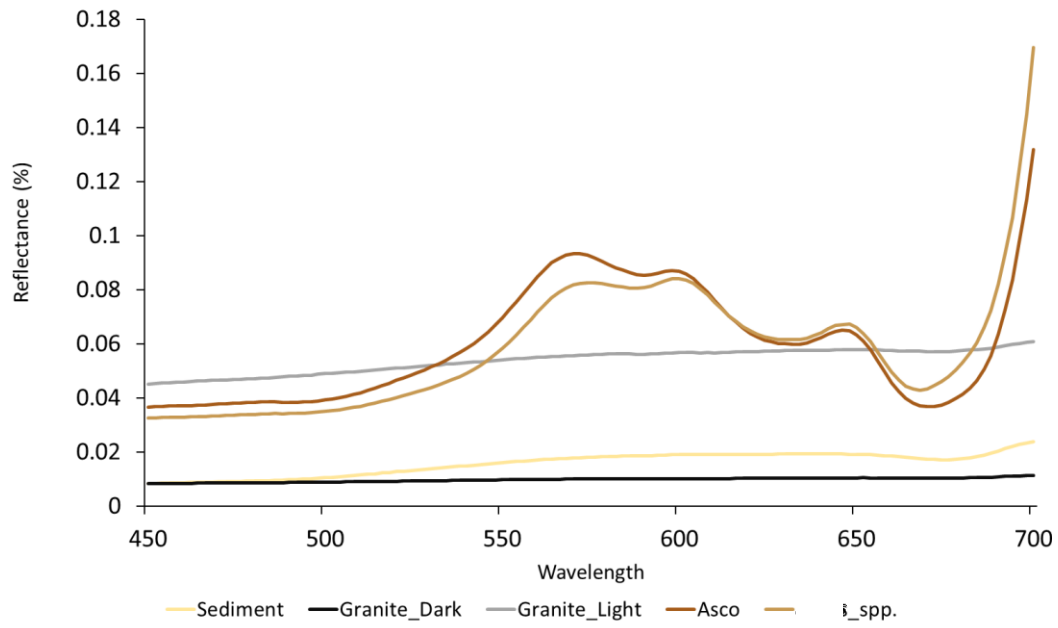

Fig. S3.5. Averaged image-derived spectral profiles of three different substratum cover classes, sandy sediment (Sediment), dark granite (Granite_Dark) and light granite (Granite_Light) compared against one another and two common intertidal macroalgal cover classes, *Ascophyllum nodosum* (Asco) and mixed fucoids (*Fucus* spp.)

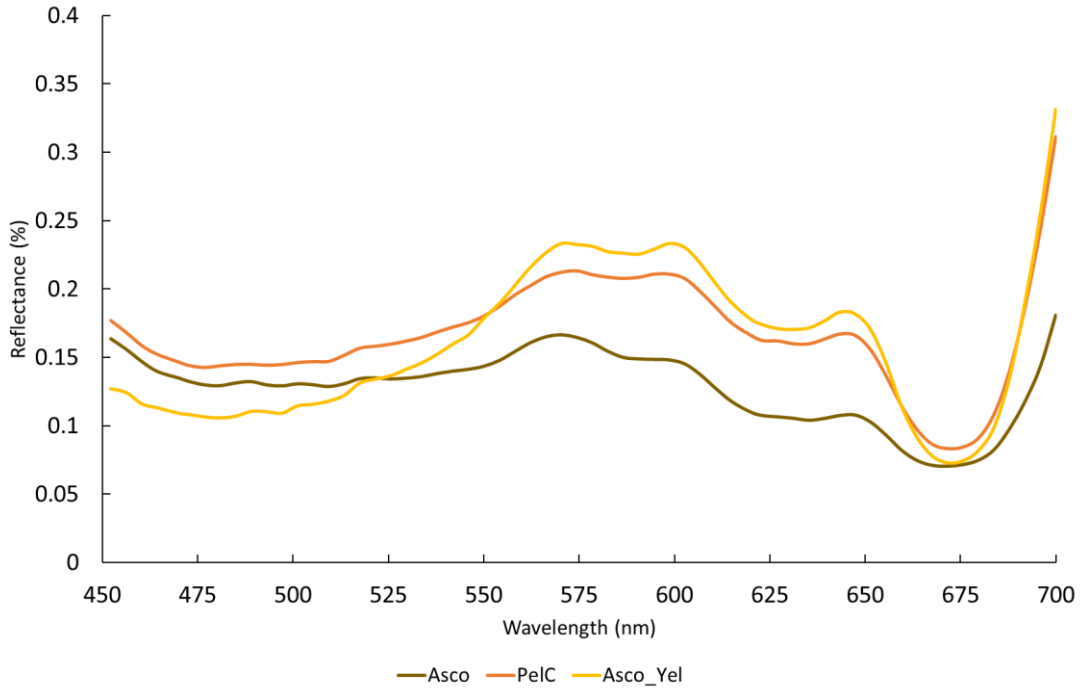

Fig. S3.6. Averaged image-derived spectral profiles of two *Ascophyllum nodosum* colour variants (n = 10/colour variant), from near the pier (Asco_Yel) and from the lower shore (Asco), and of *Pelvetia canaliculata* (PelC). Spectra were collected through, first identifying classes using visual analysis of the RGB drone dataset and subsequently extracting their spectral information from the aligned hyperspectral drone image.

Chapter 4

Tab. S4.1 Band information for the Sentinel-2 Multispectral Imager (MSI). Source: Clevers and Gitelson. (2013).

Band	Centre wavelength (nm)	Band width (nm)	Spatial resolution (m)
1	443	20	60
2	490	65	10
3	560	35	10
4	665	30	10
5	705	15	20
6	740	15	20
7	783	20	20
8	842	115	10
8a	865	20	20
9	945	20	60
10	1380	30	60
11	1610	90	20
12	2190	180	20

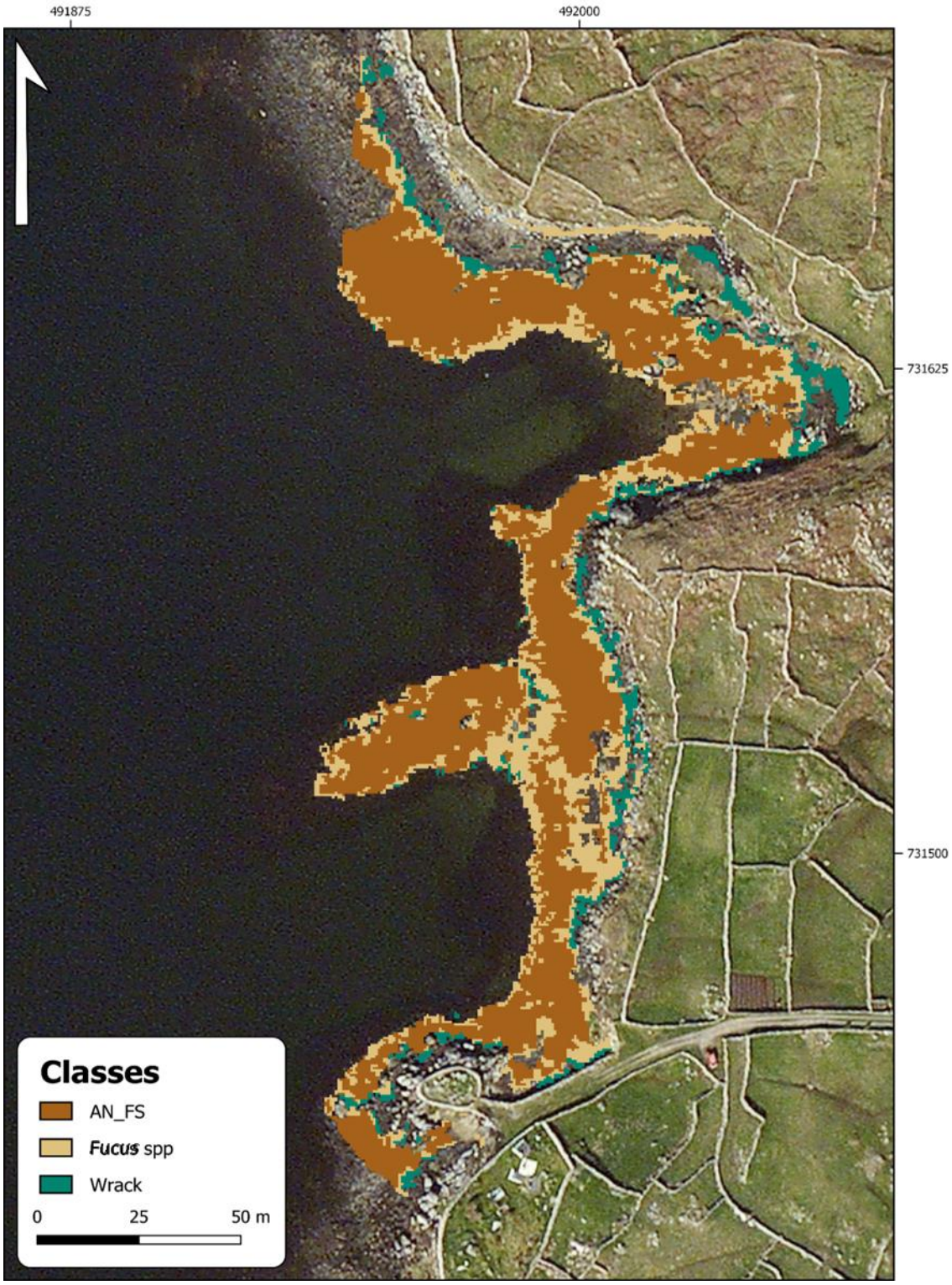

Fig. S4.1. Maximum Likelihood Classification (MLC) result from the multispectral aerial survey. Three macroalgal cover classes are displayed over Bing satellite imagery. 'Substratum' was not included. Class codes represent the following species. *Ascophyllum nodosum* dominated fucoid mix (abbreviated here to AN_FS, referred to in text as 'Asco_*Fucus* spp'), mixed fucoids (*Fucus* spp) and macroalgal wrack ('Wrack') which was overclassified. Coordinates are in Irish Transverse Mercator

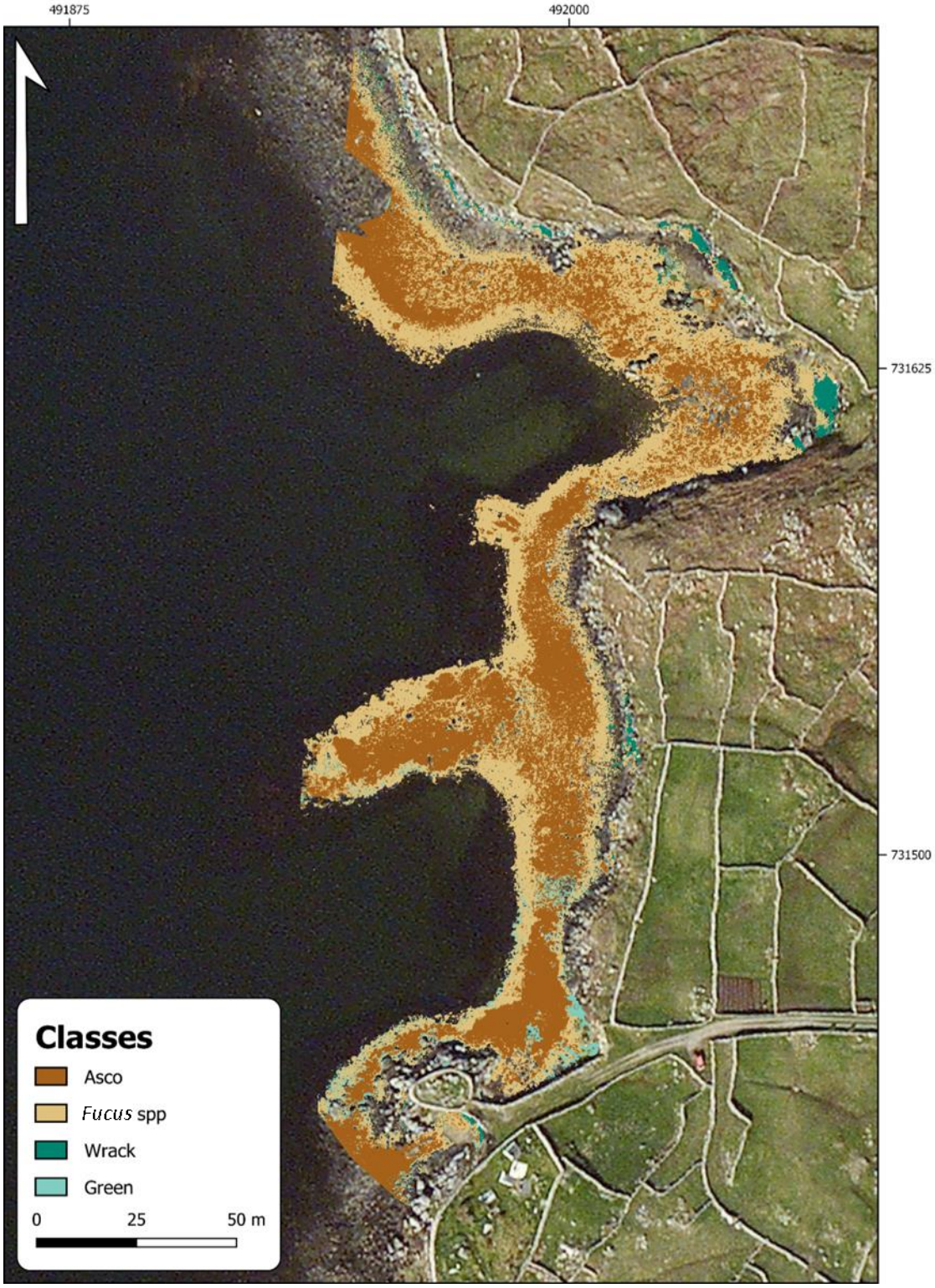

Fig. S4.2. Maximum Likelihood Classification (MLC) result from the multispectral UAV survey. Four macroalgal cover classes are displayed over Bing satellite imagery. 'Substratum' was not included. Class codes represent the following species. *Ascophyllum nodosum* ('Asco'), mixed fucoids (*Fucus* spp), macroalgal wrack ('Wrack') and Ulva spp ('Green') which was overclassified. Coordinates are in Irish Transverse Mercator (ITM).

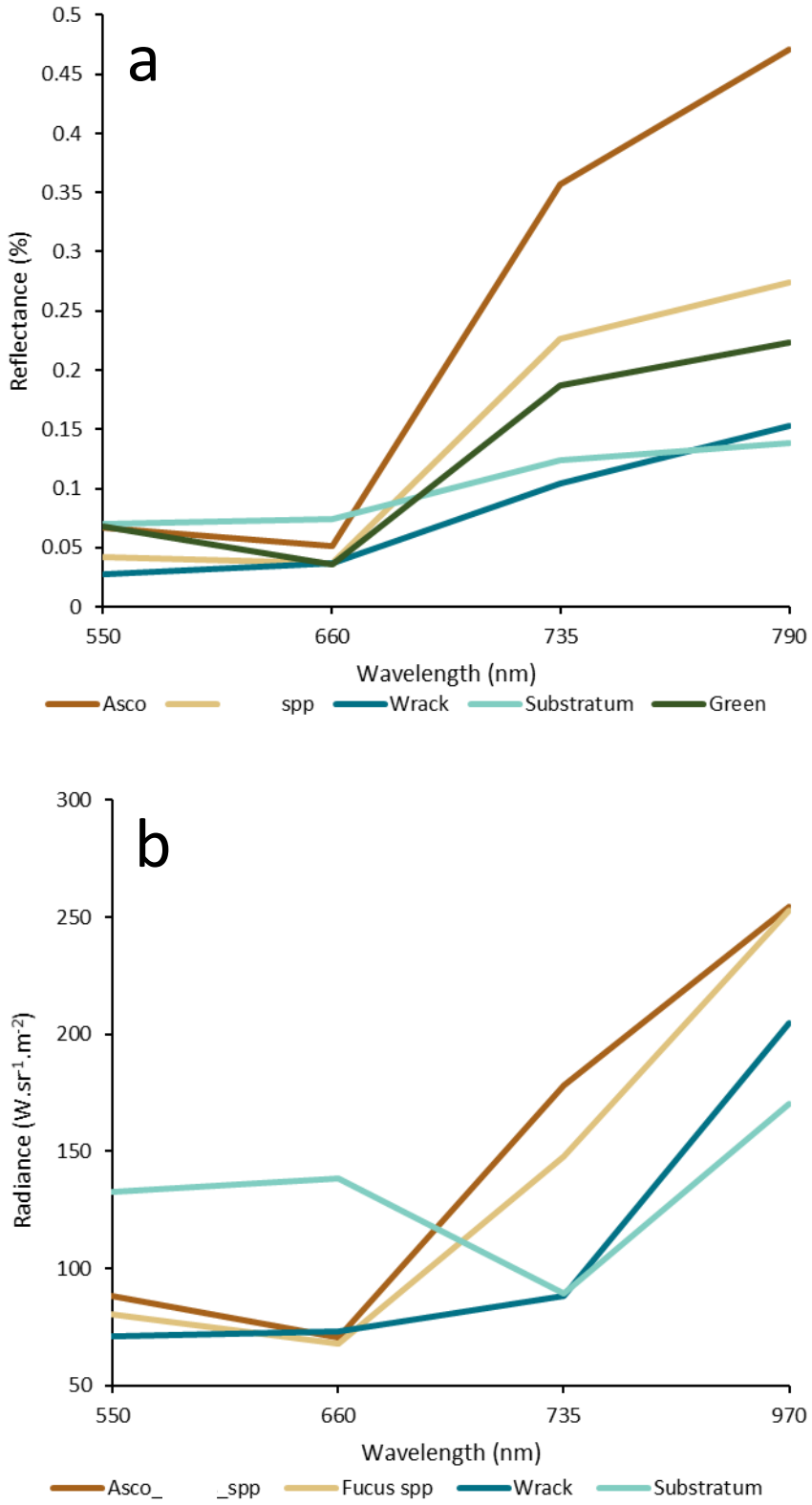

Fig. S4.3. Spectral profiles of species derived from image endmember data for the UAV (**a**) and aerial (**b**) data. Class codes represent the following species and features. *Ascophyllum nodosum* (Asco), *Ascophyllum nodosum* dominated fucoid mix (Asco_*Fucus* spp), mixed fucoids (*Fucus* spp), macroalgal wrack (Wrack), substratum (Substratum) and unidentified *Ulva* spp (Green).

Chapter 5

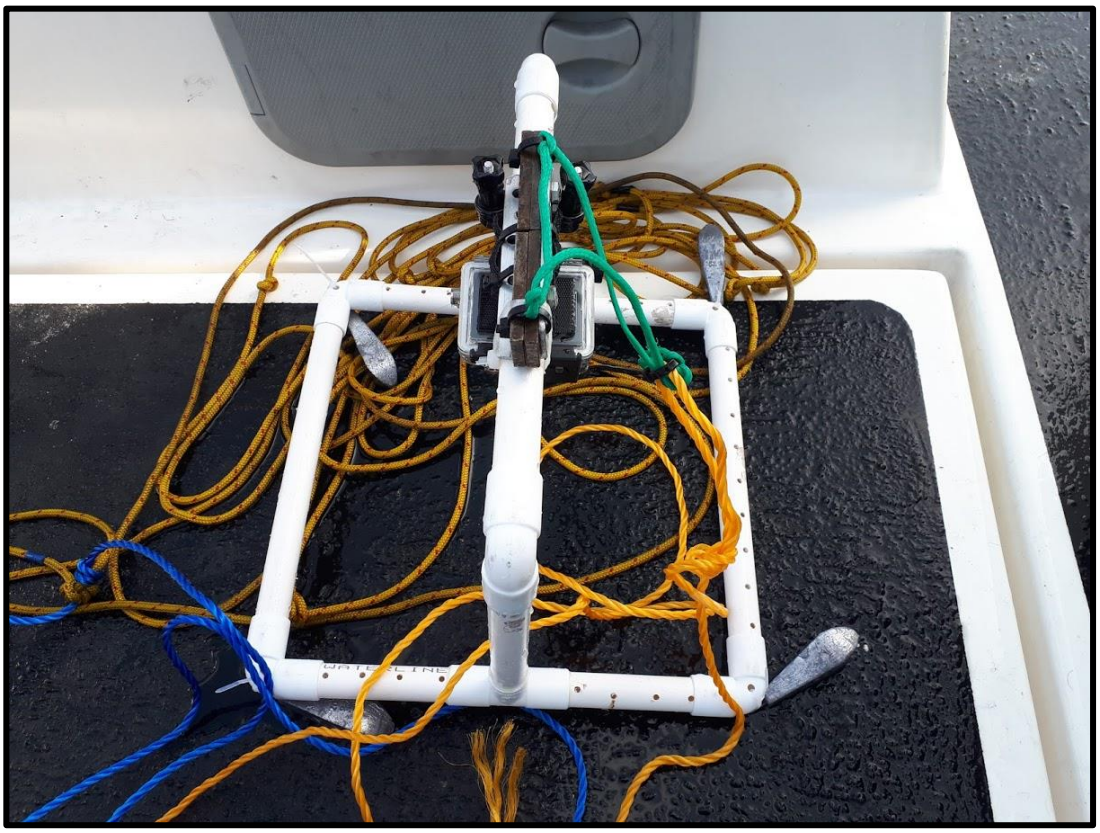

Fig. S5.1. Drop down GoPro camera rig attached to ~25 m of line.

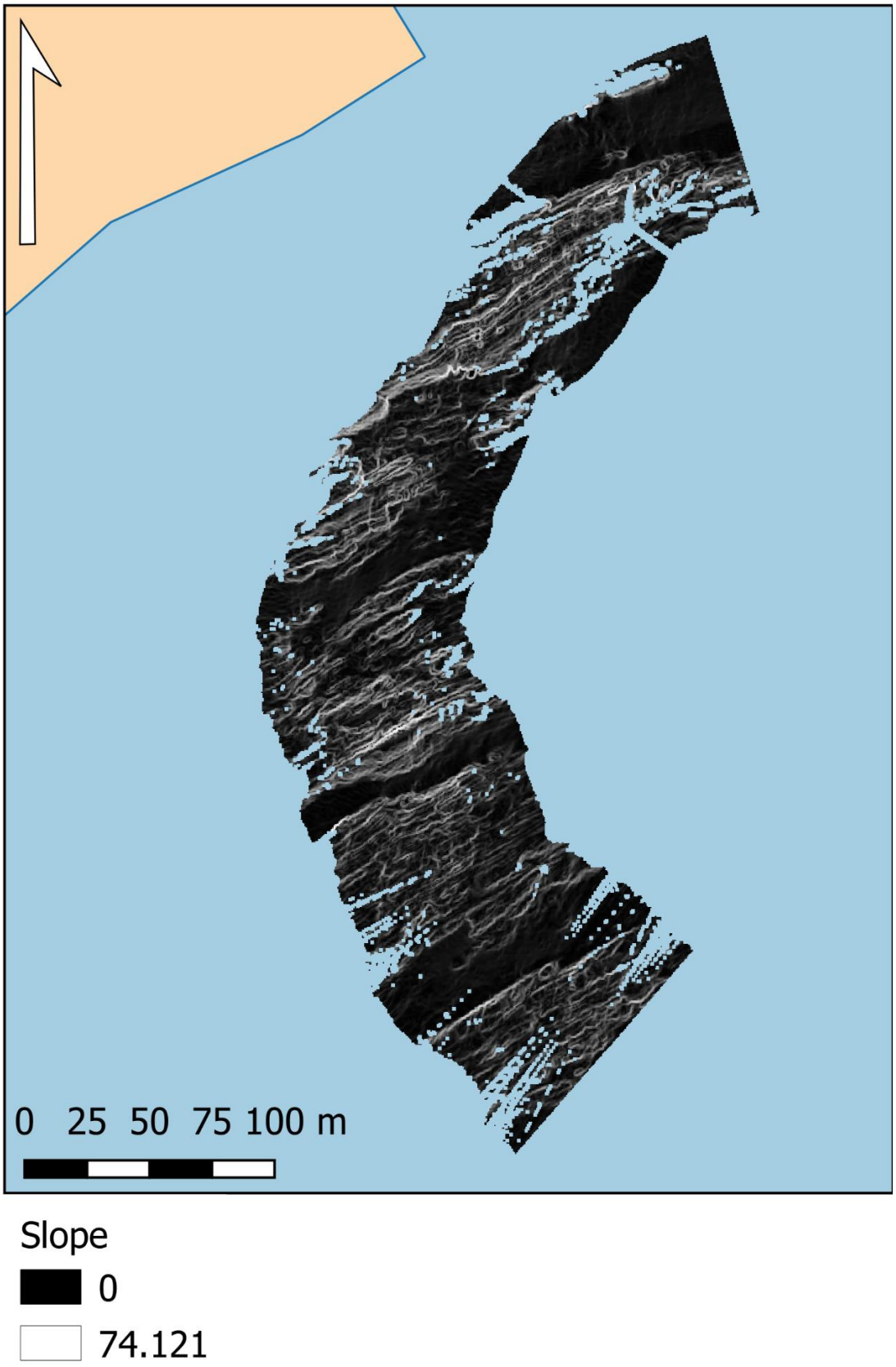

Fig. S5.2. Slope map created from 200 kHz Multibeam dataset collected in Roaringwater Bay (Co.Cork) in August 2019. Higher values indicate steep slopes which can be used to infer the presence of rocky reefs. Low values represent relatively flat sediment substratum.

A1. Developing a methodology for extracting a macroalgae only layer

During the course of this research, additional work was conducted to develop a relatively simple and low-cost methodology for extracting the distribution of canopy-forming brown macroalgal species. Object-based image analysis (OBIA) was selected as the classification method as it is available on free-to-use software, such as SAGA, and thus represents a lower-cost analysis solution than some pixel-based classifiers available through software such as ENVI. The rapid isolation of macroalgae distribution from other habitats including substratum and terrestrial vegetation allows for the classification of features (*e.g.* species) within the macroalgal zone of distribution to be conducted without the potential for misclassification with non-macroalgal habitats.

A1.1. OBIA methodology

ArcGIS Pro was used to classify drone multispectral imagery collected from Doleen Pier, near An Cheathrú Rua. The following methodology outlined herein is specific to the workflow used in ArcGIS and may be different depending on the software used. A subset of the multispectral image was used to develop the methodology owing to the limited computer processing power available.

A1.1.1. Segment mean shift

Images are segment into groups of 'super-pixels' based upon similar spectral characteristics. Varying levels of spectral and spatial detail can be set depending on the desired image output. Having a higher level of spectral detail (values range from 1-20) can be useful for classifying features that similar spectral properties, and lower levels of spectral detail will create a more spectrally homogenous output. Spatial detail, also occurring over a range of 1-20, will need to be finer when looking at a spatially heterogenous scene where features (*i.e.* macroalgal species) are occurring in mixed assemblages, allowing these finer details to be recorded. Conversely, having a coarser spatial resolution will produce a more homogenous result, for example, if the research objective was to identify spectrally distinct macroalgal groups rather than spectrally similar macroalgal species.

Both spectral and spatial detail were set to 10 to homogenise and spectral and spatial variance within the macroalgal distribution zone but still ensure that it was distinguishable from substratum and terrestrial habitats. Smoothing the data in this way removes random scattered pixels (Comaniciu *et al.*, 2002) to create a homogenous output.

A1.1.2. Creation of training samples

To proceed with the segmentation process, training samples need to be collected. These should be representative of the desired classes. In this case five classes were chosen, seaweed, vegetation, rock, light sediment and dark sediment. Training samples are a collection of pixels (or in this case segments) that define the range of colour associated with a class. For some classifiers, such as Maximum Likelihood Classifier (MLC), there needs to be a statistically significant number of samples, equating to a minimum of 20 samples per class.

The segmented multispectral image was used to collect training samples for each of the classes. A minimum of 20 segments were selected for each class with larger classes, such as seaweed, containing nearly 100 training areas and smaller one, such as vegetation, containing just over 20. Training sample creation is done through the Image Classification tool. The Select Segment function was used as the reference dataset is a segmented layer. Once all samples have been collected for each class the result is then exported as a .xml and .shp file. This training file is now used in the next step of the process to calculate the analytical information associated with the segmented layer.

A1.1.3. Training Support Vector Machine classifier (SVM)

SVM is a supervised non-parametric classification method (Mountrakis *et al*., 2010) that is suitable for classifying a segmented raster input. SVM's are well suited to handling smaller training sets than other classification methods such as Maximum Likelihood (MLC) (Mantero *et al*., 2005). SVM is a linear classifier which aims to find the optimal hyperplane for linearly separable patterns, in this case, separating out the dataset into predefined classes (Mountrakis *et al*., 2010). Hyperplane refers to a plane in multi-dimensional space that separates data points from two classes (Huang *et al*., 2002). Rather than assigning a class based on the distance between class spectral means SVM identifies the hyperplane that separates out the two classes (Heumann, 2011).

The segmented multispectral image along with training samples are inputted into the classifier which then outputs a classifier definition file (.ecd). The resulting file computes each segment attribute, as defined by the training samples and is subsequently using in a separate classification tool. The SVM classifier is suitable for the current dataset as it requires fewer training samples and does not require them to be normally distributed. This is useful for datasets where different cover categories vary greatly in size, for example the area covered by seaweed is much larger than that covered by terrestrial vegetation.

A1.1.4. Compute Segment Attributes

This function computes the attributes for every segment that occurs in the segmented raster, it is an optional step that can be performed. There are a range of different attributes that can be computed. The default options are colour, count, compactness and rectangularity, with other attributes including mean, standard deviation and segment size. This tool outputs an attribute table which allows for further, optional, analysis of the data.

A1.1.5. Classification

Based upon the .ecd file the Classify Raster tool then classifies the image. The type of classification performed is determined by the properties of the .ecd file, in this case SVM is the classifier.

A1.1.6. Accuracy Assessment

Assessing classification accuracy involves comparing the classified image to a reference dataset. Random points were created from the reference data and then compared to points of the same location in the classified data using a confusion matrix.

The confusion matrix calculates the user's accuracy and producer's accuracy for each category along with a final kappa index. The kappa accuracy ranges from 0 to 1 with 1 being 100 percent classification accuracy. The Users Accuracy, or errors of commission/ type 1 error, shows pixels that have been incorrectly classified as a known class when they should be something else. Producer's accuracy, or errors of omission/type 2 error, is where pixels of a known class are identified as something else.

A1.1.7. Preliminary results

The final classified image can be seen in **Fig. A1.1**. The kappa coefficient (0.879947) indicates a good overall classification accuracy for the subset multispectral image (**Tab. A1.1**). There was some misclassification between sediment and rock and areas where fragmented seaweed and sediment/rock have been confused with one another. All classes show good errors of omission and commission (> 0.80) indicating that each class has been accurately classified.

Tab. A1.1 Confusion matrix.

Class	Seaweed	Vegetation	Rock	Sed_L	Sed_D	Total	U_Accuracy	Kappa
Seaweed	288	0	22	16	27	353	0.815864023	0
Vegetation	0	267	0	0	0	267	1	0
Rock	0	13	252	0	25	290	0.868965517	0
Sediment_Light	8	0	19	282	0	309	0.912621359	0
Sediment_Dark	4	0	6	2	248	260	0.953846154	0
Total	300	280	299	300	300	1479	0	0
P_Accuracy	0.96	0.954	0.843	0.94	0.827	0	0.903989182	0
Kappa	0	0	0	0	0	0	0	0.879947

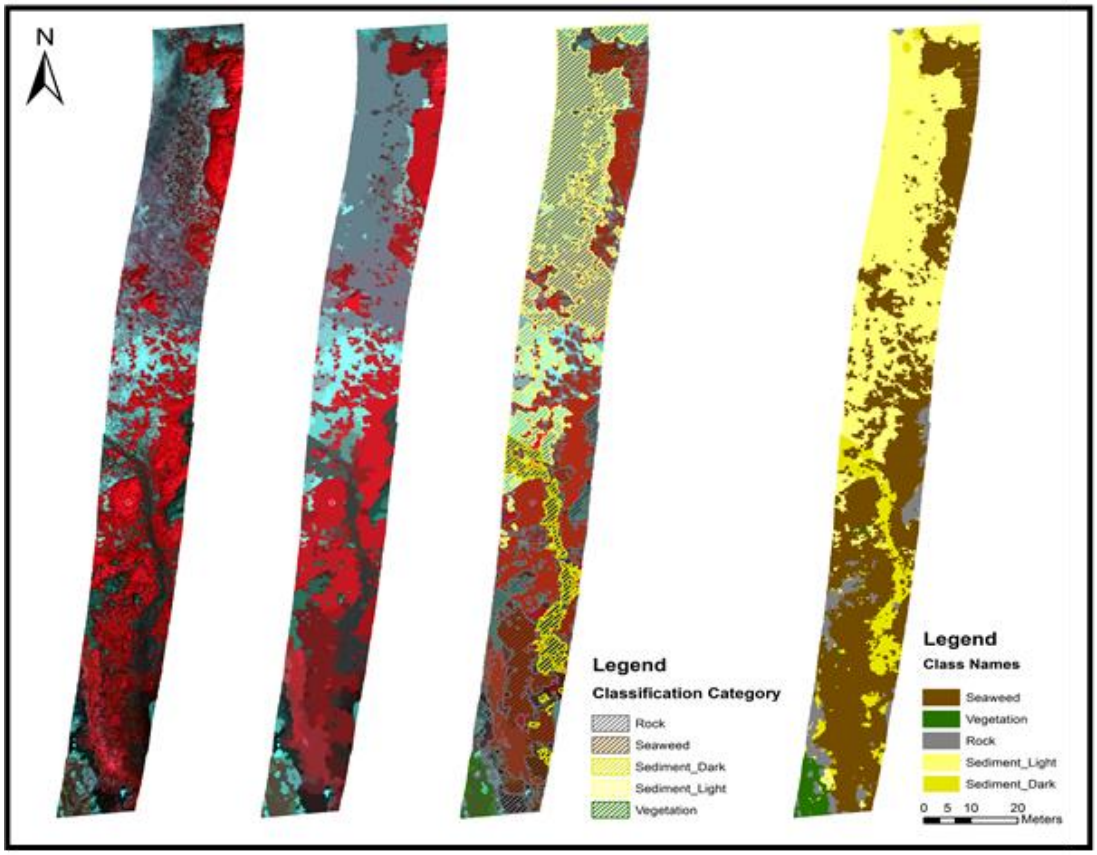

Fig. A1.1 Image segmentation steps on a subsection of multispectral data. From left to right: original multispectral image, segmented multispectral image, selection of training classes and final classification.

A1.1.8. Extrapolation of method to whole site

Based upon these encouraging results the same process was then repeated for the entire site. First the water was manually masked out. This was done to remove potential confusion of spectra caused by submerged seaweed and shallower water. Some rock was also removed using this process. The Segmentation and Classification workflow in ArcGIS Pro was then used to classify the seaweed. After initially running the segmentation workflow on strips of data, the multispectral mosaic was gridded into four cells. Attempts were made to process the entire scene at once, but this was processing intensive and no desirable output could be achieved. The scene was instead split into four cells which were each analysed independently before being stitched back together. Three broad categories were chosen for the classification, seaweed, substrate (rock and sediment) and terrestrial vegetation. The output segmented rasters were used to collect training samples from. The output of this is shown in **Fig. A1.2** and demonstrates the feasibility of this method for larger areas.

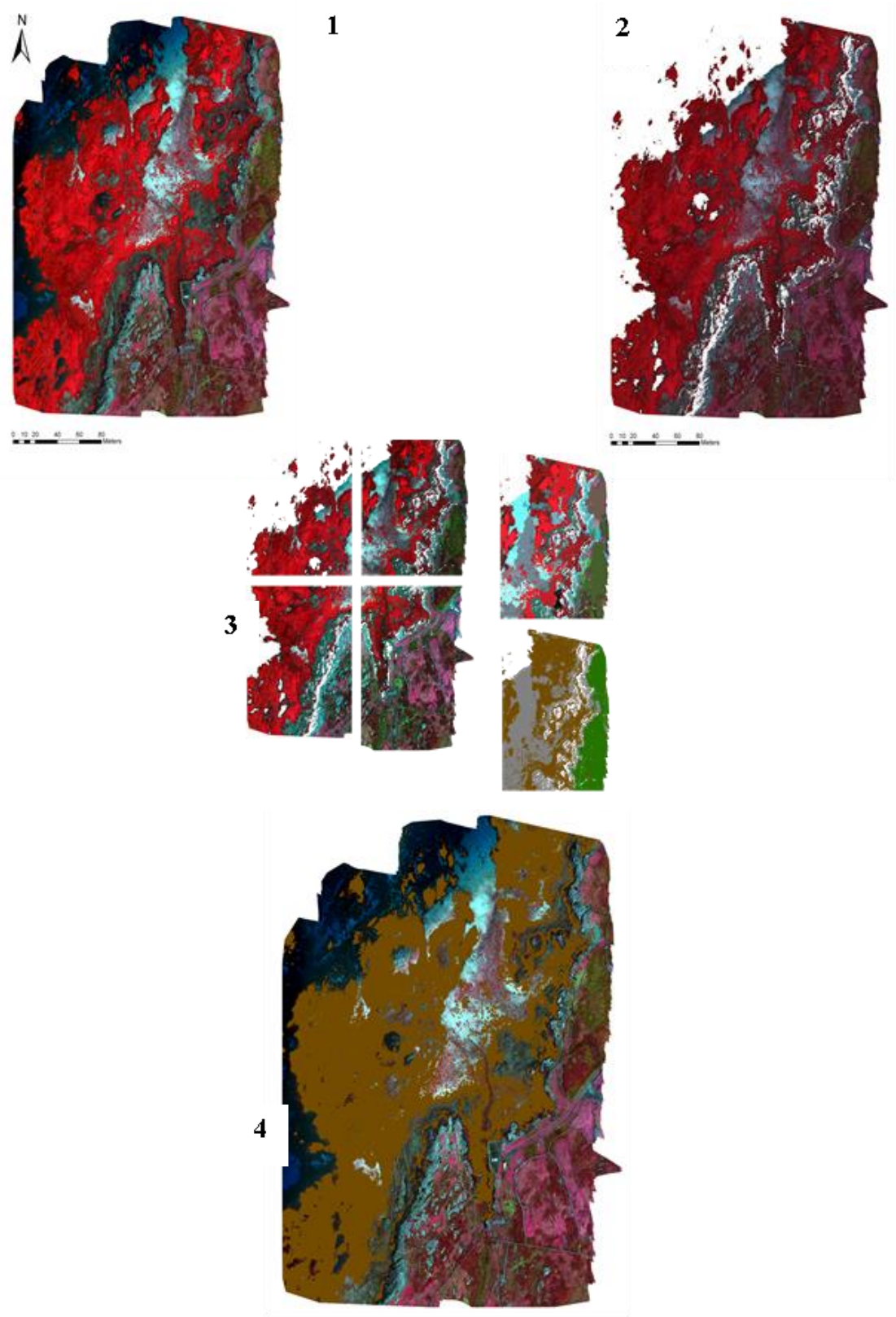

Fig. A1.2 Segmentation workflow for the entire site (Carraroe) using multispectral data.

A2. Biomass and species diversity sampling within Kilkieran Bay

During the summer of 2016, seven different sites within Kilkieran Bay were sampled to collect data on the wet weight biomass of *A. nodosum* and to record the species diversity and average percent cover of macroalgal species occurring within the *A. nodosum* zone of distribution. Morphometric data on stipe density and frond length were also collected for *A. nodosum*. High resolution *in-situ* biological sampling can be used to ground-truth remote sensing data.

At each site four transects were set from the upper zone of *A. nodosum* distribution to the lower. Five $1m^2$ quadrats were then set evenly along the transect with one at the start and one at the end. The quadrat size was chosen because smaller sizes may miss important species and may not sufficiently sample the distribution of large macroalgal species such as *A. nodosum* (Gonor & Kemp, 1978). Images of each quadrat were taken using a GoPro Hero 4+ camera and were later analysed for dominant canopy forming species and the area that each covered using the image analysis software ImageJ. Quadrats one, three and five were, due to tide constraints, subsequently sampled for the wet weight biomass of *A. nodosum* by removing all individuals whose were attached, via a holdfast, within the quadrat and immediately weighing them. **Fig. A2.1** shows the location of each study site along with the biomass of *A. nodosum* at each site. The aerial survey conducted in the summer of 2016 collected RGB imagery of the coastline. Where these images overlapped with our study sites, we were able to produce a series of maps showing the species diversity and percentage cover along each of the transects within the study sites (**Figs A2.2 – A2.6**). **Tab. A2.1** shows the site averages for *A. nodosum* morphometric data along with wet weight biomass (kg/m^2).

Tab. A2.1 Average percentage cover (%), frond length (cm), stipe density ($/m^2$) and wet weight biomass (kg/m^2) of *Ascophyllum nodosum* from the seven sites sampled during summer 2016.

Site	Average % cover	Average frond (cm)	Average stipe density	Average biomass (kg)
Baile Lar	73.3	67.6	31.7	11.5
Carraroe North	33.4	54.6	23.4	6.3
Cuan Na Luinge	40.1	62.1	29.5	7.3
Criminagh	41.9	77.4	38.5	6.2
Hooker	45	84.7	17.4	3.5
Sean Bhaile	53	76.4	40.1	7.9
Tiernee Pier	58.1	55	31.6	2.9

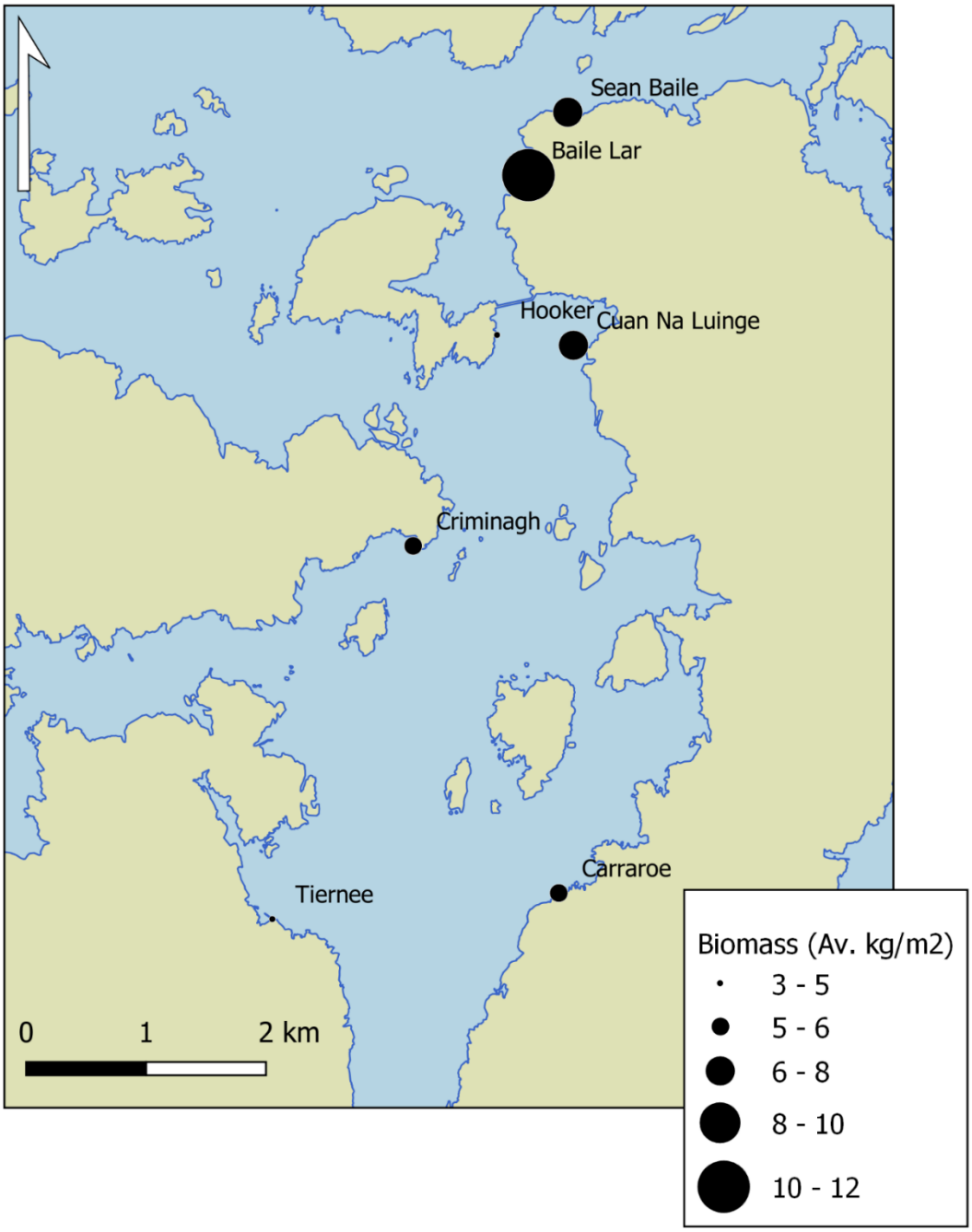

Fig. A2.1. Map showing the spatial variation in average biomass (kg/m^2) of *A. nodosum* within Kilkieran Bay using field data collected from 2016. Biomass data was averaged from 12 1 m^2 quadrats spaced along four transects within the *A. nodosum* zone of distribution. Values are in wet weight.

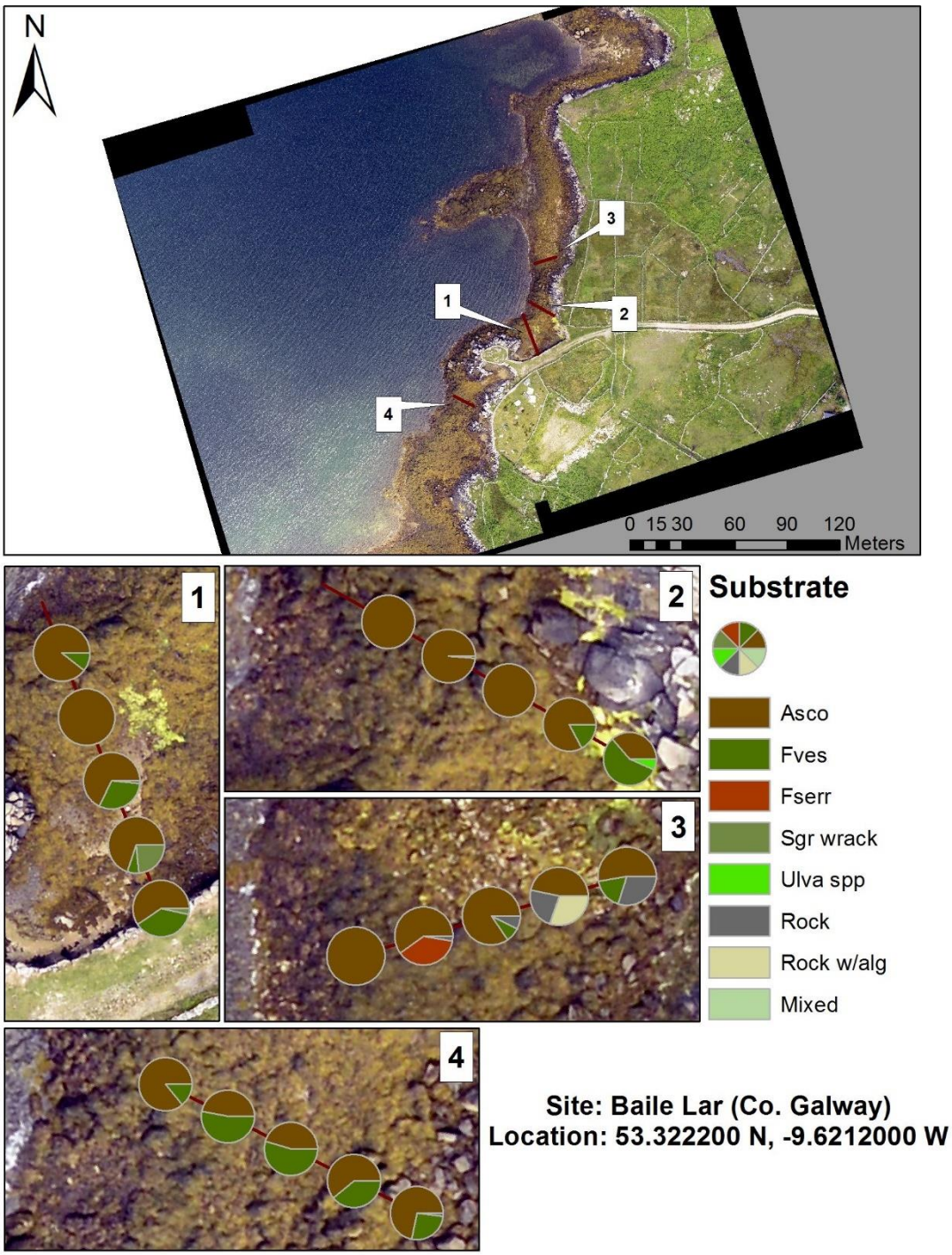

Fig. A2.2. Species diversity and percentage cover in 20 quadrats sampled across 4 transects in Baile Lar. *A. nodosum* (Asco), *F. vesiculosus* (Fves), *F. serratus* (Fserr), seagrass wrack (Sgr wrack), green seaweed (Ulva spp.), Rock, Rock w/alg (rock with algae), Mixed (Mixed sediment).

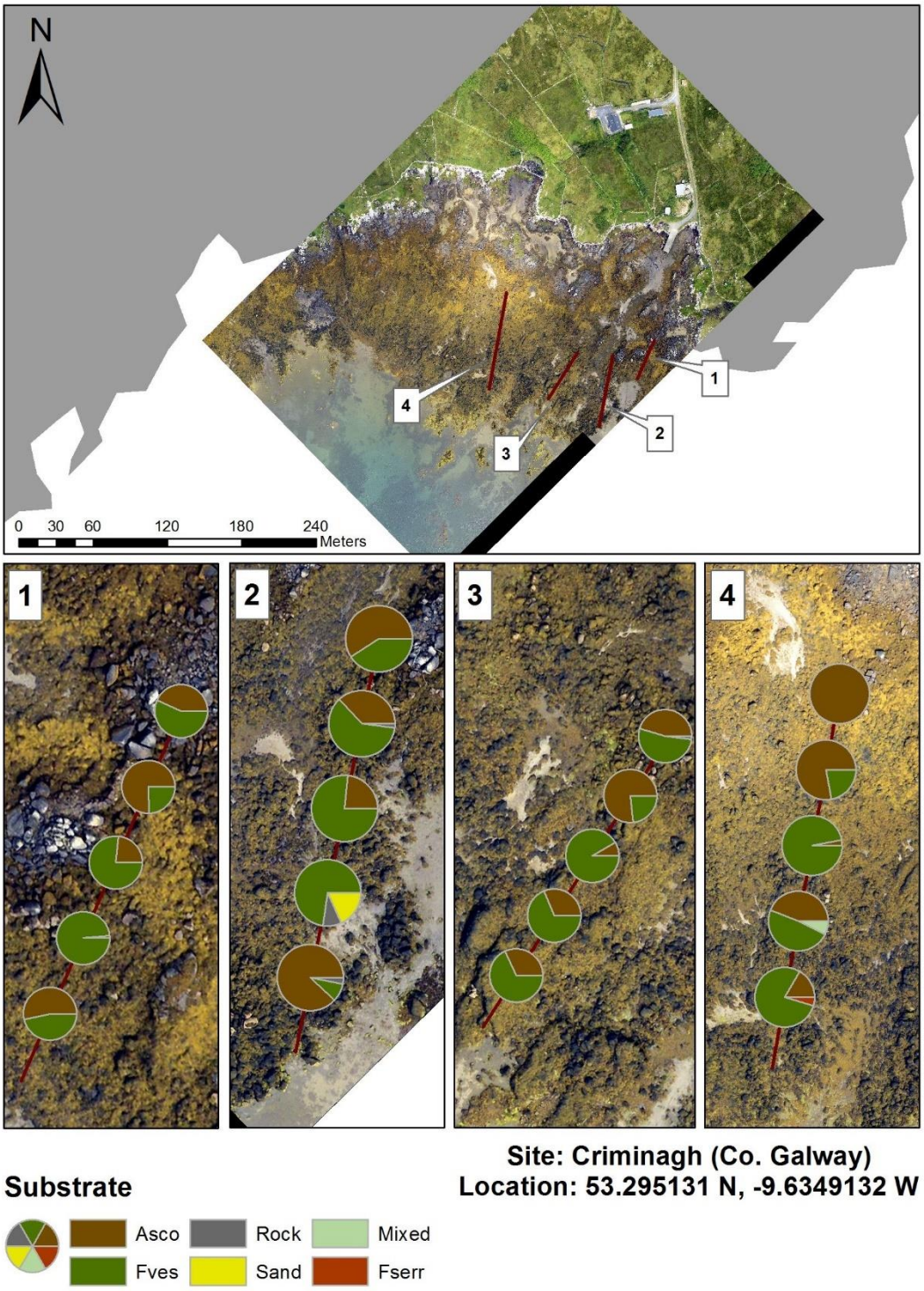

Fig. A2.3. Species diversity and percentage cover in 20 quadrats sampled across 4 transects in Criminagh. *A. nodosum* (Asco), *F. vesiculosus* (Fves), *F. serratus* (Fserr), Rock, Sand, Mixed (Mixed sediment).

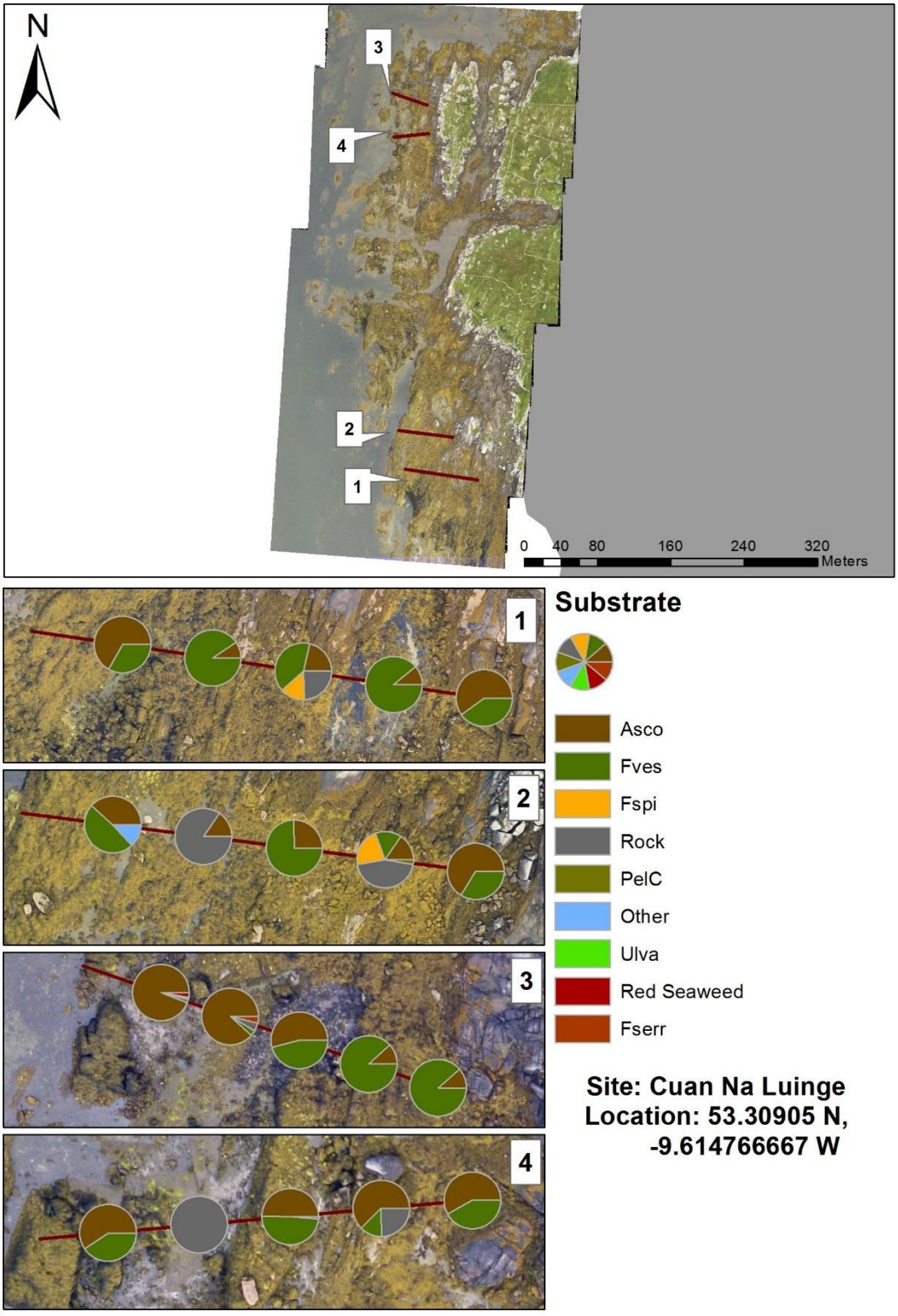

Fig. A2.4. Species diversity and percentage cover in 20 quadrats sampled across 4 transects in Cuan Na Luinge. *A. nodosum* (Asco), *F. vesiculosus* (Fves), *F. serratus* (Fserr), *F. spiralis* (Fspi), green seaweed (Ulva spp.), Rock, *P. canaliculata* (PelC), Unidentified seaweed (Other), unidentified red seaweed (Red seaweed).

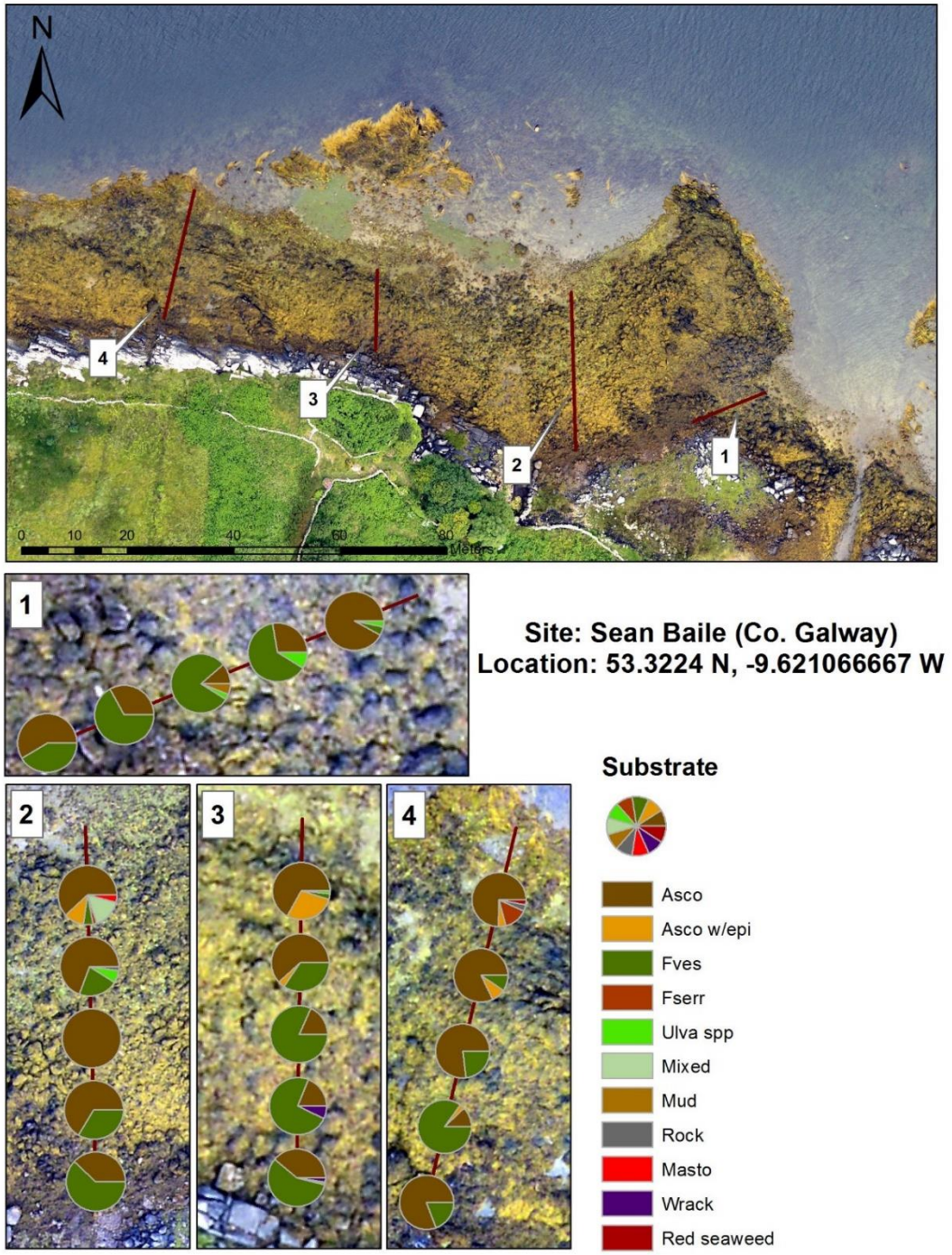

Fig. A2.5. Species diversity and percentage cover in 20 quadrats sampled across 4 transects in Sean Baile. *A. nodosum* (Asco), *A. nodosum* with epiphytes (Asco w/epi), *F. vesiculosus* (Fves), *F. serratus* (Fserr), green seaweed (Ulva spp.), Rock, Mixed (Mixed sediment), Mud, Seaweed wrack (Wrack), *M. stellatus* (Masto), Unidentified red seaweed (Red seaweed).

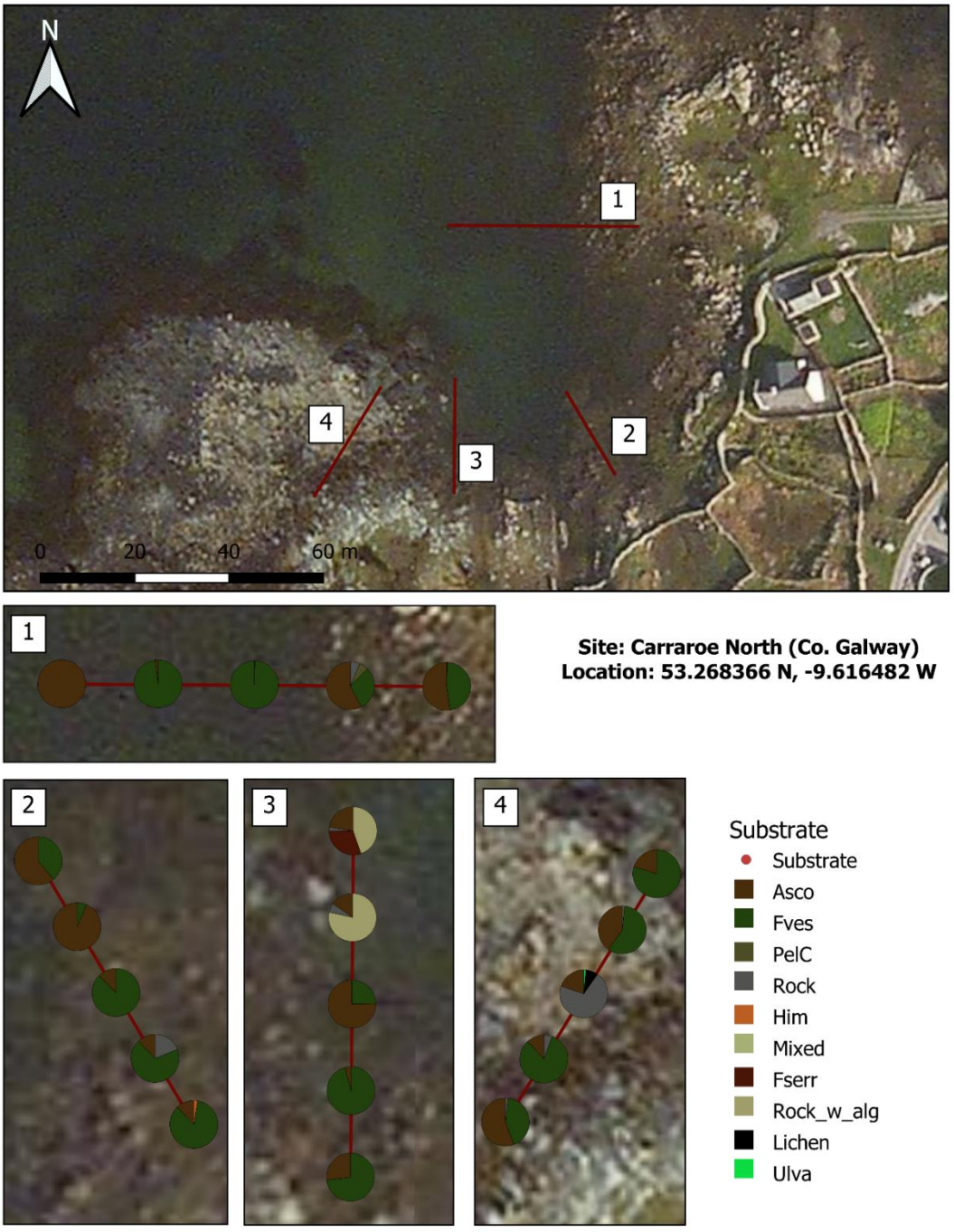

Fig. A2.6. Species diversity and percentage cover in 20 quadrats sampled across 4 transects in Carraroe. *A. nodosum* (Asco), *F. vesiculosus* (Fves), *F. serratus* (Fserr), Unidentified lichen species (Lichen), green seaweed (Ulva spp.), Rock, Rock w/alg (rock with algae), Mixed sediment (Mixed), *P. canaliculata* (PelC). Satellite imagery used as the background as no aerial imagery covered this site.

“Araf deg mae mynd ymhell”

- Welsh proverb